DEPOSITIONAL BEHAVIOR OF COHESIVE SEDIMENTS

By

ASHISH JAYANT MEHTA

A DISSERTATION PRESENTED TO THE GRADUATE COUNCIL OF
THE UNIVERSITY OF FLORIDA IN PARTIAL
FULFILLMENT OF THE REQUIREMENTS FOR THE DEGREE OF
DOCTOR OF PHILOSOPHY

UNIVERSITY OF FLORIDA
1973

ACKNOWLEDGMENT

The author wishes to express his sincere appreciation to Dr. E. Partheniades, Chairman of his Supervisory Committee, for his guidance and encouragement throughout the period during which the present study was conducted. The author would like to thank the other members of his committee: Dr. R. G. Dean and Dr. B. A. Christensen of the Department of Civil and Coastal Engineering, and Dr. G. M. Griffin of the Department of Geology, for their helpful suggestions and assistance in clarifying various aspects of the subject matter.

Thanks are due to Professors R. P. Hoyer and Roger Nava of the University of Zulia in Maracaibo, Venezuela, for their assistance in providing sediment samples from the Maracaibo Channel. Sincere thanks are also due to Dr. R. B. Krone of the Department of Civil Engineering, University of California at Davis, for his help in providing sediment samples from the San Francisco Bay.

Thanks go to the staff of Coastal Engineering Laboratory and Mr. Peter Bush for help in installing the basic equipment. The author would like to thank Mr. Bruce Ripy for doing the mineralogical analysis of the sediments and Mr. Shailesh Bhende for drafting the figures. Mrs. Karen Walker's patience in typing the dissertation is especially acknowledged.

The author's deepest appreciation goes to his wife, Chetana, without whose presence and support he would not have been able to undertake the present work.

The present study has been conducted as a part of a major research project entitled "Deposition of Fine Sediments in Turbulent

Flows," supported currently by the National Science Foundation under Grant No. GK-31259. This support is sincerely and gratefully acknowledged.

TABLE OF CONTENTS

TABLE OF CONTENTS (Continued)

TABLE OF CONTENTS (Continued)

LIST OF FIGURES

LIST OF FIGURES (Continued)

LIST OF FIGURES (Continued)

LIST OF FIGURES (Continued)

NOMENCLATURE

a	elevation of lowest sample tap
a'	empirical coefficient in the exponential relation between W_s' and time
A	cross-section of idealized estuary
$\mathring{A}$	Ångström unit
$\tilde{A}$	area of ring as well as false bottom
A_1	coefficient in the exponential solution for $\overline{T}$
b	annular channel width
B	width of idealized estuary
C	instantaneous suspended sediment concentration either with respect to time of deposition or with respect to time scale of turbulence
C'	fluctuating component of sediment concentration
C_1	constant of integration
$\overline{C}$	time-averaged component of sediment concentration
C_a	suspended sediment concentration at $y = a$
C_D	drag coefficient for drag exerted on a settling floc
C_L	lift coefficient
C_R	reference concentration in measurements of Etter and Hoyer
C_o	initial suspended sediment concentration
C_τ	drag coefficient in near-bed zone
C_{eq}	equilibrium concentration
C^*	fraction of depositable concentration deposited at time t
C^{**}	fraction of depositable concentration in suspension at time t
C_1^{**}	value of C^{**} at time t_1
C_{eq}^*	relative equilibrium concentration

C_{eq}^{**}	degree of deposition
d	depth of flow measured from channel bottom
d'	depth of flow measured from bed surface
d_s	floc diameter
D_L	dispersion coefficient
$f(\tau_b)$	function of τ_b
F	gage factor
F''	cohesive force at sediment bed
g	acceleration due to gravity
k	coefficient of frictional resistance
k_1	depth from channel bottom to $y = \xi$
k_2	coefficient relating depth-averaged concentration to near-bed concentration
k_s	bed roughness
K	dimensionless parameter in relation between W_s and d_s
K_1	empirical coefficient in Krone's measurement
K_2	coefficient in Krone's measurements
$\tilde{K}$	coefficient in measurements of Etter and Hoyer
ℓ	basal order of diffraction
ℓ_b	near-bed zone thickness
L	instantaneous lift force
L'	fluctuating component of lift force
$\bar{L}$	time-averaged component of lift force
$\tilde{L}$	length of an element before application of stress
L_ℓ	lower limit for fluctuation of L
L_u	upper limit for fluctuation of L
m	empirical coefficient in the exponential relation between W_s and time

m'	coefficient in hypergeometric equation
M	mean of a normal distribution
n	number of data points or estuarial segments
n'	coefficient in hypergeometric equation
$\tilde{p}$	pressure in fluid
p	cumulative probability
p_1	pressure at inner wall of annular channel
p_2	pressure at outer wall of annular channel
p_e	probability of erosion
p_d	probability of deposition
P_r	probability
P	cumulative probability for normal distribution
P_m	measured cumulative probability
P_t	computed cumulative probability for normal distribution
q'	coefficient in hypergeometric equation
r	radial distance
r'	radius of largest idealized spherical floc
r_1	radius of the inner wall of annular channel
r_2	radius of the outer wall of annular channel
R	resistance
$\tilde{R}$	source or sink term
R_d	sink term in diffusion equation
R_e	source term in diffusion equation
t	time after beginning of deposition
t_{50}	geometric mean of the plot of C^* versus t
t_1	value of time beyond which W_s' decreases exponentially with time

T	upper integral limit in the logarithmic-normal distribution of C^* versus t/t_{50}
T_1	tidal period
$\bar{T}$	t-dependent solution of diffusion equation
u	flow velocity corresponding to x or θ corrdinate
u_*	friction velocity
u'	fluctuating component of u
$\bar{u}$	time-mean component of u
u_m	depth-averaged flow velocity
u_p	velocity measured by propeller probe
u_t	instantaneous velocity above a floc
v	flow velocity in y direction
v'	fluctuating component of v
$\bar{v}$	time-mean component of v
w	dummy variable
W	buoyant weight of floc
$\tilde{W}$	metric weight
W_s	terminal settling velocity of floc
W_s'	apparent settling velocity of floc
x	coordinate in the direction of flow
x'	independent variable in hypergeometric equation
x''	logarithmic-normally distributed variable
x''_{50}	geometric mean of x''
x_a	normally distributed variable
y	vertical coordinate
y_o	virtual origin of logarithmic velocity profile

y_a upper integral limit in the logarithmic-normal distribution of C^*_{eq} versus $(\tau^*_b - 1)$

y_m a particular value of y coordinate

$\overline{Y}$ y-dependent solution of diffusion equation

z coordinate transverse to the flow

Greek Letters

α constant of integration

α_o coefficient relating ℓ_b to d_s

α_1 area shape factor

α_2 volume shape factor

α_3 coefficient in the expression for W'_s

γ specific weight of water

γ_s specific weight of floc

δ laminar boundary layer thickness

Δ dimensionless laminar boundary layer thickness

$\Delta\tilde{L}$ change in the element of length $\tilde{L}$

ΔM small increment in M

$\Delta\tilde{p}$ pressure difference $p_2 - p_1$ between outer and inner walls of annular channel

Δr difference in radii $r_2 - r_1$ between outer and inner walls of annular channel

ΔR small change in resistance R

$\Delta r'$ thickness of floc surface roughness

Δt small time interval

ΔV linear differential velocity between ring and channel

Δx control volume dimension in flow direction

$\Delta\sigma$	small increment in σ
ε	vertical eddy diffusivity independent of y
ε_x	eddy diffusivity in x direction
ε_y	eddy diffusivity in y direction
ε_z	eddy diffusivity in z direction
η	ratio of L' to $\overline{L}$
η'	water surface elevation in idealized estuary
η_d	limit of η for probability of deposition
η_e	limit of η for probability of erosion
θ	angular polar coordinate
κ	Karman constant
μ	micron
ν	kinematic viscosity of water
ξ	finite control volume boundary elevation above bed surface
ρ	density of water
ρ'	density of suspension
σ	standard deviation of a logarithmic-normal distribution
σ'	applied stress
σ_1	standard deviation of the logarithmic-normal relationship between C^*_{eq} and $(\tau^*_b - 1)$
σ_2	standard deviation of logarithmic-normal relationship between C^* and t
τ	shear stress at the boundary of the laminar flow field in Krone's experiments
τ_b	mean bed shear stress
τ_{bi}	instantaneous bed shear stress

τ_{be}	critical shear stress for erosion in experiments of Partheniades
τ_{bf}	bed shear stress measured by false bottom
τ_{bmax}	maximum bed shear stress corresponding to near-complete suspension of sediment
τ_{bmin}	minimum bed shear stress below which entire suspended sediment eventually deposits
τ_{bf}	bed shear stress measured by velocity probe
τ_b^*	dimensionless bed shear stress τ_b/τ_{bmin}
τ_c	critical bed shear stress for deposition according to Krone
τ_{ch}	mean shear stress on channel boundaries
τ_i	local instantaneous shear stress
τ_{max}	floc shear strength
τ_r	ring shear stress
$(\tau_b^* - 1)_{50}$	geometric mean of the logarithmic-normal relationship between C_{eq}^* and $(\tau_b^* - 1)$
$\phi(\eta)$	frequency distribution
ω	flow velocity in z direction
ω'	fluctuating component of ω
$\bar{\omega}$	time-mean component of ω
Ω	angular velocity
Ω_o	angular velocity of ring or channel
Ω_m	angular velocity at $y = y_m$

Abstract of Dissertation Presented to the
Graduate Council of the University of Florida in Partial Fulfillment
of the Requirements for the Degree of Doctor of Philosophy

DEPOSITIONAL BEHAVIOR OF COHESIVE SEDIMENTS

By

Ashish Jayant Mehta

March, 1973

Chairman: Professor Emmanuel Partheniades
Major Department: Civil and Coastal Engineering

The depositional properties of flocculated fine cohesive sediments in a turbulent flow field have been investigated. The experiments have been conducted in a special apparatus consisting of a system of an annular channel containing the sediment suspension, and an annular ring positioned within the channel, and in contact with the water surface. A simultaneous rotation of the two components in opposite directions and at properly selected speeds eliminates the secondary currents and generates a uniform turbulent flow field free from any floc-disrupting elements.

For a given suspension and flow condition, the time-concentration relationship indicates an initial period of deposition, after which the suspended sediment concentration reaches a steady state value, C_{eq}, defined as equilibrium concentration. It is found that the ratio $C^*_{eq} = C_{eq}/C_o$, where C_o is the sediment concentration at the beginning of deposition, varies solely with the bed shear stress, τ_b. This

variation of C^*_{eq} with τ_b, and consequently of $C^{**}_{eq} = 1 - C^*_{eq}$ defined as the degree of deposition, is according to a logarithmic-normal law. It is further found that the degree of deposition, for any given suspension, is characterized by the minimum bed shear stress, τ_{bmin}, below which C^*_{eq} is zero, i.e., below which the entire amount of initially suspended sediment eventually deposits. Finally, it is shown that when the ambient water quality is constant, the cation exchange capacity of the sediment, which is representative of the physico-chemical properties of the sediment, correlates with τ_{bmin}, and therefore ultimately characterizes the degree of deposition.

A law describing the rates of deposition has been obtained. This law gives the deposited fraction of the depositable portion of the sediment as a logarithmic-normal function of time. For a given suspension, the standard deviation and the mean of this functional relationship are found to depend on the bed shear stress τ_b, depth of flow, and initial concentration, C_o. Using a sediment continuity principle, it is further shown that the apparent settling velocities of the flocs also depend on the same parameters.

Reanalyzed data on the deposition of sediments from the San Francisco Bay and the Maracaibo estuary in Venezuela indicate a good agreement with the results derived from measurements in the annular apparatus.

CHAPTER 1

INTRODUCTION

1.1 Problem of Deposition

In recent years the investigation of fundamental laws governing the transport of fine cohesive sediments has been emphasized, as a result of the need to control erosion and shoaling of such material in rivers, canals, harbors and navigable waterways. Shoaling due to deposition of fine grained sediments is especially an important problem in estuaries and estuarine channels, where the presence of relatively high salinity and low flow velocities results in the settlement of flocculated sediments carried by the flow. The sediment may be derived from upstream river sources, or it may be brought into the estuary from the ocean entrance by upstream saline currents near the channel bottom (Partheniades, 1971).

When the sediment load is heavy, dredging becomes a necessary albeit expensive operation. For example, the dredging maintenance of harbors and navigable channels within the San Francisco Bay alone amounts to an annual expenditure of more than two million dollars (Krone, 1962). According to the Corps of Engineers, U. S. Army (1963), the total volume of sediment dredged annually from major harbors and tidal waterways in the United States is well over fifty million cubic yards at a total cost well in excess of thirteen million dollars. The maintenance of major estuarial waterways in other countries amounts to similar figures in terms of sediment volume and expenditure. For instance, about thirteen million cubic yards of wet

mud are dredged annually from the navigable channel in the Maracaibo estuary in Venezuela at a cost exceeding five million dollars (Partheniades, 1966), and an estimated volume of three million cubic yards is dredged from the Thames River estuary in England (Partheniades, 1964).

Often, the presence of fine sediments in flows has a beneficial rather than an adverse effect. For example, according to the Task Committee on Preparation of Sediment Manual, Committee on Sedimentation of the Hydraulics Division (1972), fine sediment carried in some irrigation water is beneficial in sealing the canal or lateral, and if carried through the canal, may contribute to the improvement of the fertility of the croplands. For instance in countries like India, sediments rich in organic matter derived from river floods have maintained the productive fertility of the fields for centuries. It is noteworthy that in such a situation, the problem is one of keeping the sediment from shoaling, even at the lowest flow velocities, so that the canals themselves do not get clogged, and yet are able to carry the sediment through.

Recently, Krone (1966) has shown that suspended sediment affects the growth of certain photosensitive algae in estuaries. He found that the growth of these algae is inhibited by insufficient light penetration. Thus, water free of sediment permits a different pattern of light absorption in water, and will produce a different environment for algae, than the same estuary carrying a suspended sediment load. For this problem, therefore, the control of suspended sediment load is of considerable interest.

1.2 Approaches to the Problem

In contrast to the more basic approach pursued in recent times, earlier studies since early nineteenth century, which were based on a large number of field and laboratory measurements, attempted to derive empirical expressions related to the erosion and deposition of sediments for designing of stable channels. These studies have been well summarized by Leliavsky (1959). The obvious disadvantages of using such expressions is that they provide no information on the mechanics of the physical processes involved, and therefore are of a limited utility, since they can only be used for conditions similar to the ones on which they themselves are based.

The desirability of relating sediment transport to flow parameters and sediment characteristics has led to fundamental studies on the hydrodynamic interaction of flow and sediment, mainly in the past three decades. Based on phenomenological theories of turbulence, semitheoretical expressions have been developed, supplemented by some experimentally estimated "universal" constants. One of the well-known and widely accepted theories is the bed load function theory formulated by Einstein (1950). For such theories, although a dependence on empirical data is unavoidable because of the complexity of sediment transport, the fundamental functional relationships between the variables involved are based on the laws of mechanics, the empirical information being used only for the evaluation of certain constants in these relationships. Unfortunately, the applicability of these theories is generally limited to granular cohensionless beds consisting of sand and gravel, and for alluvial channels in equilibrium.

1.3 Nature of Fine Sediments

The predominant constituents of fine cohesive sediments are silt and clay, with particles ranging in size from a minute fraction of a micron up to several microns. In contrast to a cohesionless or coarse sediment, a basic characteristic of a fine sediment is that the effect of interparticle physicochemical forces is much more important in controlling its hydrodynamic behavior than the submerged weights of its individual particles. Some of these forces are attractive, while others are of a repulsive nature. Their resultant effect is either repulsive or attractive depending on the types of ions adsorbed on the particle surface and also on the ions in the ambient aquatic medium. When the net forces are repulsive, the particles remain in a dispersed or peptized state (van Olphen, 1963), so that the finer particles may indefinitely remain in a state of suspension either due to a slight turbulence, or even due to Brownian motion. On the other hand, when the net interparticle forces are attractive, the particles tend to aggregate themselves into flocs, whose dimensions, and consequently settling velocities, often are orders of magnitude higher than those of the individual particles. This phenomenon of flocculation is the primary cause of shoaling in estuaries (Partheniades, 1971). An investigation of the depositional behavior of fine cohesive sediment is essentially therefore a study of the settling properties of sediment flocs.

In a flocculated suspension, where a floc rather than an individual particle is the settling unit, the floc size distribution is contingent not only upon the physicochemical properties of the sediment,

but also on the flow conditions themselves. This is the main cause of the relatively much more complex depositional behavior of cohesive sediments as compared to that of cohesionless sediments. This fact often has not been recognized by some investigators. For example, Owen (1971) attempted to observe the effect of turbulence on the settling velocities of suspended flocs, from samples of flocculated suspensions collected in a special instrument at various locations in the Thames estuary. The collecting apparatus essentially consisted of a tube pivotted near its center, and so balanced that it could remain horizontal in water and hang vertically in air. Samples were collected by automatically closing the ends of the tube while in water. It was then pulled out of water and the settling velocities were measured in the vertically held tube by the conventional method of sample withdrawal at various times. Owen found that the settling velocities thus obtained were up to ten times greater than if the same suspension were tested in the laboratory by standard methods. The results of tests using such an instrument however are questionable, since the floc characteristics strongly depend on the flow conditions. Therefore observing the settling of flocs under quiescent conditions in the tube, even almost immediately after they have been removed from the turbulent flow field, is not likely to produce comparable results.

The dearth of sufficient knowledge on the settling behavior of flocs of fine cohesive sediments has been a limiting factor in its application to transport processes. For example, Gole, Tarapore and Brahme (1971) have developed an interesting method for predicting the siltation load in harbor channels, based on a sediment continuity

principle. However, it is noteworthy that since the continuity equation involves the settling velocities of flocs, and since these were not known as functions of the flow parameters, they had to be computed for quiescent conditions, and for certain estimates of the floc diameter. Such approximations often tend to attenuate the validity of the results.

Shubinski and Krone (1970) have proposed a commendable mathematical model to predict suspended sediment concentrations in estuarine systems. In the model, they have used an empirical law of deposition derived from measurements by Krone (1962). Results of the present experimental analysis have indicated, however, that Krone's measurements may have a limited applicability. The work of Harrison and Owen (1971), in which an expression for computing the rate of siltation in a channel across an estuary is developed, is also limited by the use of the same law of deposition obtained by Krone.

1.4 Present Study

In a deposition study, it is necessary to identify both the flow variables as well as the physicochemical parameters that determine the behavior of cohesive sediments. Using a given type of fine sediment in a water of given quality, the physicochemical properties of the sediment suspension may be kept constant, so that the depositional behavior of the sediment can be related to identifiable flow variables. Then, using different sediment types, and also varying the water quality, these flow variables can be correlated with parameters that represent the physicochemical properties of the various suspensions tested. A study of this nature is described and discussed in the

present experimental work, which utilizes a specially designed annular rotating channel to measure the rates of deposition of various cohesive sediment suspensions. The subject matter is presented in the following sequence.

Chapter 2 begins with background information on the physico-chemical and mineralogical aspects of fine sediments. There, the important process of flocculation is also discussed. Previous investigations on erosion and deposition are next described, and, lastly, the objectives of the present investigation are stated.

In Chapter 3, the annular rotating apparatus is described along with accessory equipment, followed by procedures for the measurements and calibration of the equipment.

In Chapter 4, the results of the investigation are described and discussed in detail. Comparison with measurements of other investigations is also included therein.

Chapter 5 summarizes the conclusions derived from the results. Some suggestions for related future research are also presented.

Finally, in Appendices A through E, material which is supplementary to the main subject matter is included.

CHAPTER 2

SCOPE OF PRESENT INVESTIGATION

2.1 Properties of Fine Cohesive Sediments

2.1.1 Classification

Fine cohesive sediment particles essentially have high specific surface areas (surface area per unit weight) in comparison with the relatively larger cohesionless particles such as sand, and tend to exhibit cohesion, or tendency to stick together, by virtue of the physicochemical surface forces which exist between them. For example, a quartz sphere of 1 mm diameter has a specific surface area of nearly 0.0023 m^2/gm, whereas van Olphen (1963) has calculated the specific surface area of a sodium substituted montmorillonite to be approximately 750 m^2/gm. As a consequence of these large specific surface areas, the physicochemical forces acting on the fine particle surfaces are often orders of magnitude higher than the gravitational forces, as indicated by Terzaghi and Peck (1967). If, for instance, a cube of quartz with a volume of 1 cm^3 were subdivided into smaller ones with sides of 1 micron, then the ratio of gravitational force to the physicochemical force would decrease by a factor of 10^{-4}. These surface forces therefore largely determine many of the properties of the fine sediments.

The nature of these physicochemical forces depends on many factors, important among which are particle size, shape, and the crystal-chemical nature of the material itself. As a result, any classification of a fine sediment in terms of one of these factors alone is not sufficient to describe all the properties of the sediment.

The most common method of classification used by engineers and geologists is based on particle size, and although by no means completely descriptive, it is adequate for a preliminary or a general description.

In Fig. 3.1.13, the size distributions of the three different types of cohesive sediments shown are classified according to the M.I.T. system of classification (Terzaghi and Peck, 1967). In general, particles in silt and clay size range are expected to exhibit cohesion, with the degree of cohesion depending among other factors, on the type of the sedimentary material.

2.1.2 Composition

A cohesive sediment may be termed clay material, which according to Grim (1968) is "any fine grained, natural, earthy argillaceous material." Clay material itself contains clay minerals and non-clay minerals. While the non-clay minerals include substances such as calcite, dolomite, large flakes of mica, pyrite, feldspar, gibbsite and others, the term clay minerals refers specifically to a certain small number of hydrous aluminum silicates called clays in general, which are largely present in size fractions smaller than 1 or 2 microns. Now in the M.I.T. classification, the size range less than 2 microns is referred to as clay fraction. However, from a mineralogical point of view, this size range contains both clay minerals as well as non-clay minerals, the latter also being present in sizes less than 2 microns. For example, many clay materials contain extremely fine iron oxide or hydroxide, which acts as a pigment.

In addition to clay and non-clay minerals, clay materials often

contain varying amounts of organic matter. In general, organic matter occurs in clay materials in several ways. For instance, it may be present as discrete particles of wood, leaf matter, spores, etc. It may also be present as organic molecules on the surface of the clay mineral particles, or it may be intercalated between layers of clay minerals. The discrete particles may be present in any size from large visible chunks, to particles of colloidal size which act as pigments. These pigments often tend to impart a greyish or black appearance to the sediment.

Clay materials often contain water-soluble salts, such as chlorides and sulfates of alkalies and alkaline earths, which may have been entrained at the time of accumulation, or may have developed subsequently as a consequence of geological weathering and other alteration processes. Exchangeable cations and anions are also present on the clay particle surfaces in an adsorbed state.

In addition to the above, cohesive sediments dredged from rivers and estuaries may contain small and large shells, woody remains, a host of industrial and other pollutants, and different kinds of bacteria and other forms of organisms.

2.1.3 Structural Aspects

Essentially, clay minerals are hydrous silicates of aluminum and/or iron and magnesium. Structurally, there are two fundamental building units for the crystalline clay structure (Grim, 1968).

One is a silica tetrahedral unit. It consists of four oxygens in a tetrahedral configuration enclosing a silicon atom. The tetrahedra

are combined in a sheet structure so that the oxygens of the bases of the tetrahedra are in a common plane, and each oxygen is shared by two tetrahedra.

The second is an octahedral unit. It consists of four oxygen atoms plus two hydroxyl (OH) groups in an octahedral configuration enclosing an aluminum, iron or magnesium cation. The octahedral units are combined into a sheet structure with each anion shared by two units. The sheet may be viewed as two layers of densely packed oxygens and/or hydroxyls, with the cation in octahedral coordination.

The above two units combine to give several types of clay minerals, of which three basic types important to the present investigation are described below.

a. Kaolinite: Its structural unit is composed of an aluminum octahedral layer with a superimposed inverted tetrahedral layer such that the tips of the tetrahedra and one of the hydroxyl layers of the octahedral sheet form a common plane. Successive structural units are held together by van der Waals attractive forces. Inasmuch as the individual units are nearly neutral electrically, it is difficult for water molecules or cations to penetrate between the units. Kaolinite particles have plate-like forms with well-defined hexagonal boundaries.

b. Montmorillonite: The structural unit is made up of two tetrahedral layers with their tips pointing towards each other, and with an octahedral sheet in between. The oxygens of the tetrahedral tips are shared with the oxygens of the octahedral layer, so that the three layers form a single structural unit. Part of the silicon of the tetrahedral layer is typically replaced by aluminum or other cations of lower valence, and also, part of the aluminum of the octahedral layer is

typically substituted by magnesium. As a consequence, the unit assumes a net negative charge, which results in the attraction of exchangeable cations (exchange cations) between the units. The ion-dipole bond that results holds the negative dipolar units together but rather weakly; therefore, water molecules (dipoles) can penetrate between the units in addition to the exchangeable cations, leading to the well-known swelling properties characteristic of montmorillonite.

Electron micrographs of montmorillonite show broad undulating mosaic sheets that when disturbed and dispersed break easily into irregular fluffy masses of extremely small often flake-like particles.

c. Illite: The structural unit is similar to that of montmorillonite, except that there is a significantly greater substitution of silicon by lower valence cations, especially aluminum. This substitution leaves a net negative charge deficiency within the structural lattice that is considerably greater than montmorillonite. This charge is almost always compensated by the potassium ion, which fits into the structural cavity of the oxygen rings almost perfectly. This ion is relatively firmly intercalated in the basal planes between the units, forming a bond that resists the intrusion of water molecules and other exchangeable ions between the units. As a result, the mineral does not swell measurably.

Electron micrographs of illite show small, poorly defined flakes commonly grouped together in irregular aggregates.

Some of the clay minerals not mentioned above include dickite, nacrite and anauxite, which are similar to kaolinite. It should be noted that montmorillonite is in fact a name given to the

most important member of a group of clay minerals referred to lately by the name of smectites (Grim, 1968). Two other important members are nontronite (iron substituted) and saponite (magnesium substituted). Illite has several polymorphic forms. Halloysite, chlorite and vermiculite are also relatively important clay minerals. They are essentially made up of the same two basic tetrahedral and octahedral units. Sepiolite, palygorskite and attapulgite minerals are fibrous in nature and are structurally distinct from the above described minerals. They are also relatively less abundant. Finally, in nature one finds a range of certain mixed layer minerals which consist of ordered to disordered stacks comprised of two or more of the above described minerals together.

2.1.4 Interparticle Forces

Two types of interparticle forces which are important in the phenomenon of flocculation to be discussed in Section 2.1.6 are described in the sequel.

a. van der Waals Forces: The attractive force between fine particles is attributed to the van der Waals electrochemical attraction forces between all atoms of one particle and all atoms of another particle. The total attractive force between the particles is the sum of the forces between all atom pairs, and the magnitude of this total force depends on the size and shape of the particle, but does not depend on the ambient water quality or its salt content (van Olphen, 1963). These forces are strong at short range, but fall inversely with the seventh power of separation for small spheres, and with the square or cube of the distance for parallel plates.

b. Electric Surface Forces: There are a number of attractive, and particularly repulsive forces generated by electric charges on the particles. The following two causes of the presence of these charges are of interest.

Imperfections within the interior of the crystal lattice may be the cause of a net positive or net negative lattice charge. More commonly, as in clay suspensions in water, the net particle charge is created by the preferential adsorption of certain specific ions on the particle surface. The magnitude of the total charge on a particle of course depends on the type of adsorbing material as well as on the availability of certain ions in the ambient medium. Such ions are called peptizing ions (van Olphen, 1963).

2.1.5 The Double Layer

Whatever the origin of the surface electric charges, any charged particle in an ion containing aquatic medium will attract ions of opposite charges called counter-ions, to compensate its own electric charge. At the same time, the counter-ions tend to diffuse away from the particle surface because of their thermal activity, since such a diffusion takes place from a zone of high ionic concentration to one of lower ionic concentration. Thus, a clay particle idealized by a thin plate will be surrounded on either side by a diffused layer of counter-ions, whose positions will be determined by the balance between their electrostatic attraction and thermal activity. This layer known as "double layer" and the particle together are electrically neutral. This double layer significantly determines the properties of clays in suspension.

2.1.6 Flocculation

Flocculation, or aggregation of fine sediments in saline waters, is a well-known phenomenon. The importance of flocculation to estuarial sediment transport lies in the associated changes in the character of the suspended particles. These changes strongly affect the transport of the suspended sediment itself.

Flocculation of sediment particles occurs as a result of cohesion between particles brought sufficiently close together, and for this to happen, particle collisions are essential. Collisions themselves are caused by Brownian motion of the suspended particles, by the shear flow and by the differential settling velocities of the suspended particles or flocs (Krone, 1962). Now cohesion results from the predominance of attractive van der Waals forces. These forces are strong at short range, but as was mentioned in Section 2.1.4, they decay rapidly with distance. Thus, whether colliding particles cohere depends on whether the short range attractive forces dominate the repulsive electric forces created by the double layer of counter-ions. Ordinarily, when no salt is present, a sediment suspension remains in a dispersed or peptized state because, under such a condition, the influence of the repulsive forces extends beyond that at which the attractive forces are significant. In this case, the double layer of counter-ions surrounding each particle is in a given state of equilibrium, due to the attractive particle surface forces, and the opposing tendency of the counter-ions to diffuse away from their high concentration near the particle surface. However, when salt is added to the suspension, the increase in the ambient medium of the concentration of ions with

charge of the same sign as that on the counter-ions, results in a reduction in the diffusive tendency of the counter-ions, since this tendency decreases with decreasing magnitude of the counter-ionic concentration gradient. As a consequence, a new state of equilibrium is established, with the double layer closer to the particle surface. If the amount of salt added is sufficient, the thickness of the double layer will be depressed to an extent such that the attractive forces will prevail over a longer distance compared to the repulsive forces, causing a cohesion of particles, when they are brought sufficiently close together by collisions.

In estuarial waters, the kinds of dissolved salts present are determined largely by the composition of ocean water, and only at high river flows the composition of the river water is of significance. Since the relative abundance of the constituent salts is nearly constant, the variables affecting flocculation are the salt concentration and the mineral type. For example, in the San Francisco Bay, where the minerals appear to be well-mixed, flocculation of Bay mud depends only on salinity (Krone, 1962).

2.1.7 Cation Exchange Capacity

Clay minerals have the property of adsorbing certain anions and cations and retaining them in an exchangeable state, i.e., these ions are exchangeable for other anions or cations by treatment with such ions in a water solution. This exchange capacity is determined under neutral conditions (pH = 7) in terms of milliequivalents per hundred grams of the clay mineral. Thus, for example, one equivalent

of Na^+ expressed as Na_2O would be a combining weight of 31, and 1 milli-equivalent per hundred gram would be equal to 0.031% Na_2O (Grim, 1968).

The cation exchange capacity (CEC) is an important property of clay minerals, and in a cohesive sediment it is largely restricted to the clay size fraction. As such it depends on the mineral type and is independent of the ambient medium. There are three causes of the CEC, which are discussed below.

a. Broken bonds around the edges of the clay structural unit give rise to unsatisfied charges, which are balanced by adsorbed cations. These broken bonds tend to be on the edges rather than cleavage planes of the particles, and they are the primary cause of CEC in kaolinite and illite minerals.

b. Substitutions in the lattice structure result in unbalanced charges. Exchangeable cations resulting from lattice substitutions are found mostly on the basal cleavage planes of the clay minerals. Thus, in smectites, for example, 80% of the CEC results from this cause.

c. The hydrogens of the exposed hydroxyls in the structure may be replaced by exchangeable cations.

The CEC of a mineral strongly depends on its chemical pretreatment. Particle size and temperature also affect the CEC. Such materials as iron oxide and sulfur compounds tend to cover the sites to be occupied by exchangeable ions and thereby reduce the CEC.

2.1.8 Origin and Occurrence of Clays

Clays are formed from rock-forming material by weathering and other geological alteration processes. The type of clay formed depends

on the parent rock material, but also depends to a significant extent on the conditions under which alteration takes place. Thus, for example, an acidic environment is conducive to the formation of kaolinite. Another important factor is the presence or absence of certain ions. If, for instance, alkali, alkaline earths and calcium are absent, kaolinite will be formed. This happens, for example, under conditions of heavy rainfall and sufficient capacity for the soil to allow a downward percolation of the water and the salts, thus leaching the soil of ions. The presence of such ions as iron and magnesium favors the formation of smectites, while if potassium is present, illite is the result.

On the surface of earth, kaolinite, smectites, illites and chlorites are abundant clay minerals, followed by halloysite and vermiculite, while sepiolite, palygorskite and attapulgite minerals are comparatively rare.

2.2 Review of Basic Investigations

2.2.1 Erosion

An extensive literature review of empirical measurements, field studies and laboratory research on the erosion of cohesive soils is made by Partheniades (1971). Only the basic research aspect, which is within the scope of the present study, is briefly reviewed here.

Fundamental laboratory research has been concentrated on two classes of cohesive soils, namely medium to high strength consolidated clays, and soft cohesive soils ranging from freshly deposited mud to low strength older deposits.

a. Erosion of consolidated and compacted clays: Dunn (1959) tried to experimentally correlate the shear strength of different clays measured with a vane shear test apparatus, and the measured critical tractive force. This tractive force was created by a water jet impinging on the bottom of a container, part of which was occupied by the surface of a clay sample. The critical point was arbitrarily defined as the shear stress which caused erosion to cloud the water carried to the surface continuously.

Smerdon and Beasley (1959) tried to correlate the tractive force at failure with plasticity index, dispersion ratio and mean particle size, using an open flume. The point of bed failure was arbitrarily defined as "the tractive force at which the bed material was in general movement."

Moore and Masch (1962) and Epsey (1963) also attempted to devise a small-scale testing apparatus for determining the scouring resistance of cohesive soils. The first two investigators used a method employing a submerged jet in a manner similar to that of Dunn. Epsey used a system of rotating coaxial cylinders with the inner stationary cylinder composed of the clay samples. Neither of these two investigations showed conclusive results, and no correlations with soil parameters were attempted. Erosion took place by the removal of relatively large chunks of the sample.

In general, as indicated above, basic work on erosion has concentrated on the correlation of some "critical" velocity or shear stress, with the indices defining clay properties. Some of these correlations are based on small-scale scour tests. The definitions of critical shear stress and of the point of bed failure have been

arbitrary and based entirely on visual observation and judgment of the experimentor. It is therefore difficult to utilize such information to predict the stability of channels subject to high flow rates for short time periods, or to predict the erosion depth of a channel at constant flow rate during its expected life. Further, the effects of suspended sediment concentration on erosion or the conditions under which eroded material may redeposit were not studied by the above investigators.

Grissinger (1966) studied the effects of bulk density, water temperature, antecedent water, type and orientation of clay mineral, aging and percent clay on erodibility under constant flow conditions. Instead of an arbitrary critical shear stress, the determination of erodibility was given in terms of mass erosion rates (Partheniades and Paaswell, 1970). Grissinger found that all the above variables have an effect on the erosion rates. This, in fact, points out the difficulty in an arbitrary assignment of existing soil parameters as representative indices for erosion studies. Indices such as percent clay, plasticity index and dispersion ratio are in effect secondary indices which reflect the primary physicochemical forces which essentially control the soil properties.

b. Erosion of soft clay deposits: This research phase was aimed at an understanding of the details of mechanical interaction between the clay particles and water, the discovery of important flow parameters and soil properties controlling the initiation and rates of erosion, and the establishment of relationships between these properties and parameters. These studies, coupled with similar investigations on the depositional behavior of fine cohesive sediment suspensions, to be

discussed in Section 2.2.2 have thrown a considerable light on the hydrodynamic interaction between fine sediments and turbulent flows.

Partheniades (1965) conducted investigations on the erosion and deposition of a cohesive sediment in an open flume with recirculating water at ocean salinity and constant depth of flow. The sediment used was composed of nearly equal amounts of silt and clay, with traces of sand and some organic matter dredged from the San Francisco Bay. This sediment, commonly known as Bay mud, is described in Section 3.1.3. The original purpose of the study was to investigate the influences of shear stress, suspended sediment concentration and shear strength of the bed on erosion rates, and to study in a more general way the deposition of the sediment at different flow velocities. The depositional aspect is discussed in Section 2.2.2.

Two types of beds were tested. The first was remolded at field moisture of about 110%. The ultimate remolded shear strength was about 20 psf, and the strength at yield point was about 11 psf. The second bed was flocculated and deposited in the flume directly from suspension at very low flow velocity. Two experimental series were run on the first bed and one on the second. The ratio of strengths of the dense to the flocculated bed measured by a special device was of the order of 100:1. The following important conclusions were reached.

The minimum velocity or shear stress at which erosion was first observed was about the same for both beds. The minimum scouring

shear stress was of the order of 0.0020 psf. For these two series, the rates of erosion were found to be independent of the macroscopic bed shear strength.

In all but one run, erosion took place by removal of individual clay particles and clay clusters. This type of erosion may be referred to as surface erosion. In contrast, the kind of erosion that was observed by investigators in experiments described previously in this section took place by removal of relatively large chunks of the soil, and may be referred to as mass erosion. Mass erosion occurs when the flow-induced forces on the bed cause shear stresses which may exceed the soil strength along some plane below the soil surface. Such a failure is of little practical significance since it goes far beyond the desirable design stability conditions.

The erosion rates depended strongly on the increase of average bed shear stress past a threshold value. It was observed that eroding shear stresses varied widely starting from 0.002 psf. Partheniades therefore concluded that the term "critical" in fact depends on the particular rate, which is why any designated critical shear stress based on observed mass scouring may differ from observer to observer even for the same soil.

During the process of erosion the time-concentration relationship was linear, suggesting constant erosion rates independent of suspended sediment concentration.

A mechanistic model was developed to explain the observed erosion phenomena, and an expression, giving the erosion rates in terms

of known or measurable quantities representing the flow condition and soil properties, was derived. This expression had as an underlying assumption the Gaussian or normal distribution of time varying shear and lift forces. Christensen (1965) has pointed out that based on experiments by El-Samni (1949) it appears that the instantaneous velocity fluctuations rather than the shear stresses follow a normal distribution. On the basis of this interpretation he rederived the expression giving the erosion rate and presented it in a dimensionless form.

An important conclusion derived from the above experiments is that erosion of cohesive sediments is controlled by the bed shear stress. Moreover, any designation of a shear stress as critical should indicate either the stress at which erosion just begins, or the stress that would cause a particular erosion rate, or the stress that would be expected to cause a maximum estimated depth or erosion.

It was shown that the soil shear strength is not the only property governing erosion. For low strength clays, no definite correlation has been found between strength and erodibility. For medium to high strength clays, the resistance to erosion seems to increase with increasing strength, although no well-defined empirical relationship has been developed. As a large number of physicochemical factors control erosion, attention should be paid to duplicate in a model test the natural conditions as far as possible.

2.2.2 Deposition

It is pointed out in Appendix D, that as a result of the

complex behavior of depositing sediment flocs in a turbulent flow field, the boundary conditions that are required to integrate the sediment continuity equation are not known, and therefore an analytic solution describing the rates of deposition is difficult to formulate. As a consequence, studies on the depositional behavior of cohesive sediments have mainly been of experimental nature.

Early experimental studies connected with a systematic investigation of the depositional behavior were performed in recirculating open flumes. Krone (1962) conducted an important series of experiments on the measurement of deposition rates of Bay mud from the San Francisco Bay, described in Section 3.1.3. He used a 100 ft. long and 3 ft. wide flume, and essentially correlated his results with the bed shear stress.

For sediment concentrations less than 300 ppm, his measurements indicated an exponential decrease in the suspended concentration with time, which he explained in the following manner: Since his measurements were made at relatively low flow velocities at which all the sediment eventually deposits, he assumed that under these conditions, the particle-bed collision frequency is independent of the flow velocity. Considering p_d as the probability of a particle or a floc sticking to the bed, continuity for the amount of sediment may be expressed as

$$\frac{dC}{dt} = - \frac{p_d W_s C}{d} \qquad (2.2\text{-}1)$$

where C is the suspended sediment concentration at time t, d is the total depth of flow, and W_s is the near-bed settling velocity of the

particles, so that $W_s C$ is the flux of the particles approaching the bed. Then, assuming W_s to be independent of C and t, integration of Eq. (2.2-1) yields

$$\frac{C}{C_o} = \exp\left[\frac{-p_d W_s}{d} t\right] \qquad (2.2\text{-}2)$$

where C_o is the concentration at $t = 0$. According to Krone, p_d depends on the bed shear stress τ_b, and can be expressed as

$$p_d = 1 - \frac{\tau_b}{\tau_c} \qquad (2.2\text{-}3)$$

where τ_c is the critical shear stress above which no particle can stick to the bed; this is by virtue of τ_c being that shear stress above which no deposition can take place, while at lower stresses, all sediment must eventually deposit. From experimental measurements below 300 ppm, $\tau_c = 0.6$ dynes/cm^2 and $W_s = 6.6 \times 10^{-4}$ cm/sec. were obtained.

For concentrations between 300 ppm and 10000 ppm, a logarithmic relationship was derived:

$$\log C = - K_2 \log t + \text{constant} \qquad (2.2\text{-}4)$$

where K_2 was found to be approximated by the expression

$$K_2 = \frac{103}{d}\left[1 - \frac{\tau_b}{\tau_c}\right] \qquad (2.2\text{-}5)$$

For this concentration range, τ_c was found to be equal to 0.78 dynes/cm^2. This higher value of τ_c for higher concentrations as compared to those

below 300 ppm was mainly attributed to the observation that at higher concentrations, larger flocs are formed due to the greater number of interparticle collisions.

For high concentrations in excess of 10000 ppm, Krone found the relationship

$$\log C = - K_1 \log t + \text{constant} \qquad (2.2\text{-}6)$$

which is similar to Eq. (2.2-4) and where K_1 is an empirical coefficient.

The different depositional behaviors in the three concentration ranges were attributed to three modes of settling. For very low concentrations, i.e., less than about 300 ppm, the particles or the flocs settle more or less independently, without any significant mutual interference. For intermediate concentrations between 300 ppm and 10000 ppm there is an increasing amount of interference due to increased interparticle collisions, with the result that larger flocs are able to form, causing a faster rate of deposition. Finally for concentrations above 10000 ppm the suspension assumes a form of a continuous network called "fluid mud," with water escaping upward between the network spaces due to settling. This type of settling is called "hindered settling," and Krone suggested that this type of settling is the cause of lower deposition rates at very high sediment concentrations.

Krone made a deposition test in which he labeled part of the sediment with radioactive gold-198, and observed that the labeled sediment showed a higher deposition rate than the total sediment;

from which he concluded that during deposition, an interchange between suspended and deposited sediment takes place. This conclusion has been contradicted by Partheniades (1962).

Inasmuch as the floc size is controlled by the local shear within the flow, Krone conducted an experiment using two concentric cylinders to determine a relationship between floc size and shear stress, under laminar conditions. The shearing rates were varied by inserting stationary cylinders of diameters ranging from 0.5 cm to 2.25 cm inside an outer cylinder of 5.8 cm diameter, which rotated at a speed of 28 rpm. Now internal shearing can both promote floc growth and limit its size, since up to a certain limit, interparticle collisions have the dominating effect of increasing floc size, while above that limit, shear may exceed the shear strength of the flocs and begin disrupting them. Krone therefore reasoned that the flocs should approach a maximum limiting size under each condition of sustained shearing. The floc size was determined by taking photographs with the help of a strobe light. The results of the experiments showed an inverse relationship between the maximum floc diameter and shear stress at the inner cylinder down to a shear stress of 0.06 dynes/cm^2. Below this limit, the floc size increased rapidly with decreasing shear stress. This inverse relationship agrees with a theoretically derived expression

$$r' = \left[\frac{16}{3\pi} (\Delta r')\tau_{max}\right] \frac{1}{\tau} \qquad (2.2\text{-}7)$$

where r' is the radius of the largest idealized spherical floc and τ is the shear at the boundary of the laminar shear field. The terms $\Delta r'$ and

τ_{max} refer to the thickness of the floc surface roughness and to the floc shear strength, respectively, which are assumed to be properties of the sediment only. Krone assumed a value of 2 microns for $\Delta r'$ and calculated the shear strength of the Bay mud flocs as 2.7 dynes/cm^2.

The deposition tests of Partheniades (1965) on the Bay mud were adjunct to his erosion studies described in the previous section. He nevertheless made some important observations. In a given test, after each velocity reduction a sudden concentration drop occurred, whereas at constant flow conditions, after a period of relatively rapid deposition, the suspended sediment eventually approached an apparent "equilibrium value." It was noted that two deposition runs, one of high and one of low initial concentration, resulted in nearly the same ratio of the apparent "equilibrium concentration" to initial concentration C_o, at the beginning of the run. From this observation he concluded that for a given flow condition, a constant proportion of the total suspended cohesive material (silt and clay) is always carried in suspension. This implies that the equilibrium concentration is due to the amount of material available of a size equal to or less than the maximum size the flow can support, and that it does not represent the total sediment carrying capacity of the flow.

Partheniades also observed in his deposition tests that by reducing the flow velocity from 0.81 to 0.58 ft/sec, negligible deposition took place. However, by reducing the velocity further from 0.58 to 0.47 ft./sec, the suspended sediment concentration decreased from 5500 ppm to a very low value, and it appeared that if

given sufficient time, all the remaining suspended material would settle out. He estimated the "critical" velocity below which all the sediment must eventually deposit to be approximately 0.50 ft./sec. Since this velocity was lower than the observed minimum scouring velocity of 0.70 to 0.80 ft./sec for the same material, he reasoned that for the range of concentrations studied, simultaneous erosion and deposition did not take place, i.e., interchange between the bed particles and suspended particles did not occur.

It is interesting to obtain an approximate estimate of the critical shear stress corresponding to the critical velocity of 0.50 ft./sec obtained by Partheniades, and to compare it with τ_c of Krone's measurements, which also essentially is the critical shear stress for complete sediment deposition. Partheniades made several measurements of mean flow velocities and corresponding bed shear stresses; the latter being computed from the slope of the energy grade line, which in turn was obtained by measuring the downstream drop in the water surface elevation in the flume. The measurements are plotted in Fig. 2.2.1, which nearly fall on a straight line on a log-log plot, with a slope of 1.94. When the same data points are plotted on a Moody friction factor diagram for pipes (which involves multiplying the hydraulic radius of the flume by a factor of 4 to obtain the corresponding equivalent pipe diameter), all except two points consistently fall in the near-fully rough to fully rough flow regime, and they indicate an average bed roughness of 0.0015 ft. This observation is also consistent with the near square law which describes the straight line of Fig. 2.2.1. When

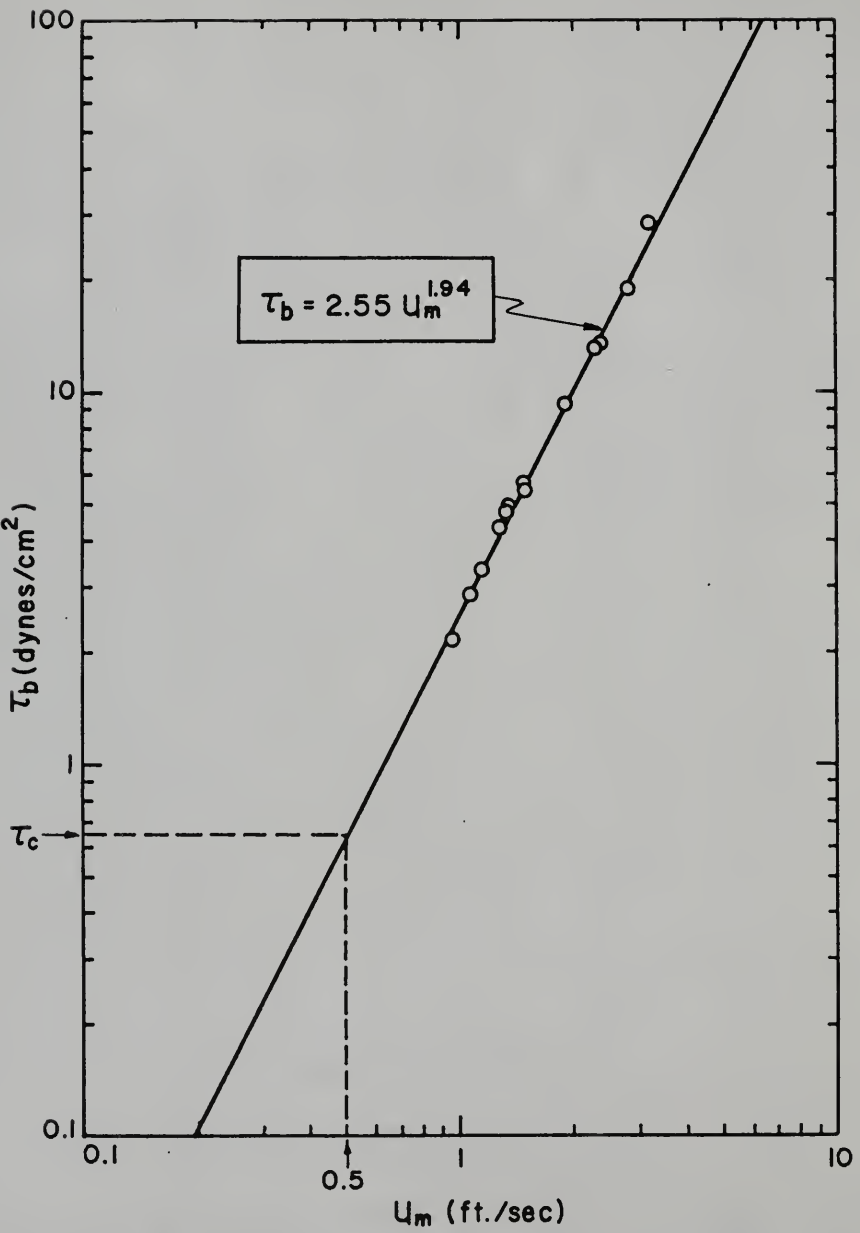

Fig. 2.2.1. Depth-averaged Velocity u_m Versus Bed Shear Stress τ_b from Measurements of Partheniades.

this straight line is extrapolated to lower shear stresses, the value of the critical shear stress at the critical velocity of 0.50 ft./sec is observed to be 0.65 dynes/cm^2. This value is consistent with Krone's 0.60-0.78 dynes/cm^2. Now as noted, Partheniades observed that the minimum scouring velocities were of the order of 0.70 to 0.80 ft./sec, which are significantly higher than the critical velocity of 0.50 ft./sec for the complete deposition of the same sediment in suspension. Based on these scouring velocities, the corresponding critical shear stresses for erosion are observed from Fig. 2.2.1 to be 1.25 to 1.65 dynes/cm^2. Hence, the ratios of the critical stress for erosion to that for deposition are 1.92 and 2.54, respectively.

It is noteworthy that since Krone's deposition measurements were carried at shear stresses below the critical shear stress for deposition, he did not observe the phenomenon associated with the equilibrium concentration in his experiments.

Etter and Hoyer (Partheniades, Kennedy, Etter and Hoyer, 1966) conducted deposition experiments in salt water at the University of Zulia in Maracaibo, Venezuela. The sediment, referred here as Maracaibo sediment, came from the Bay of Tablazo, and is described in Section 3.1.3. Four runs were conducted in which the suspended sediment attained a concentration of less than 300 ppm. In all cases, an exponential decrease of the suspended concentration was observed for data below 200 to 300 ppm, but not for higher concentrations. They obtained the relationship

$$\frac{C}{C_R} = \exp[-\tilde{K}t] \qquad (2.2\text{-}8)$$

where C_R is not the initial concentration of the run, but rather is a reference concentration corresponding to the time at which the straight line slope $-\tilde{K}$ begins on the plot. Etter and Hoyer were unable to correlate the exponent $\tilde{K}$ with the bed shear stress.

Rosillon and Volkenborn (1964) also studied the depositional behavior of the Maracaibo sediment. They noted that the deposition rates varied significantly with depth. Also, they found that increasing the initial concentration increased the rate of deposition throughout a given run. In two of their runs, the suspended sediment concentration apparently reached an equilibrium value. An examination of their data, however, reveals that many of their runs were not carried out for long enough periods to determine whether equilibrium concentrations would be attained, and this fact limited the possibility of a systematic analysis of their measurements.

In addition to the deposition runs, they studied the deposition of the sediment in still water of varying salinity. In determining the effect of salinity on a sediment with an initial concentration of 3000 ppm, they observed that flocculation of the sediment particles increases with increasing salinity up to nearly 15000 ppm, above which salinity has no further effect on flocculation. This observation is in agreement with that of Krone (1962).

The various studies described above were able to isolate some of the important factors affecting the depositional behavior of cohesive sediments. These are bed shear stress and turbulent structure

above the bed, type of sediment and ionic constitution of the ambient water including salinity, depth of flow, and the initial sediment concentration. The geometry of the flume and the return pipes are also significant insofar as they influence flocculation through the effect of local shear stresses. However, since the number of variables involved is large, none of the above investigations can be considered as exhaustive in terms of analyzing the effects of each of these variables over wide ranges of values. One of the causes of a dearth of experimental data is due to the long time periods required to complete a deposition run. In many cases, even after several hundred hours of operation, complete deposition was not achieved, even at relatively low flow velocities. This problem is characteristic of straight flumes, in which the process of deposition is slow as a result of the suspended sediment having to pass through the return pipes. The high shears acting in these pipes by virtue of their relatively small cross-sections causes a disruption of the sediment flocs into smaller units, so that when this sediment reappears at the upstream end of the flume, it is completely resuspended and with relatively smaller floc sizes, with the result that deposition of the sediment is retarded. Often two other limiting factors in the operation of straight flumes are the rather narrow range of possible flow rates, and the relatively large amount of total sediment required to run the experiments.

In order to overcome the difficulties inherent in a straight flume, a special apparatus was designed at M.I.T. Its main components were an annular channel with inner and outer diameters of 28-3/8 in.

and 36 in., respectively, for containing the sediment suspension, and an annular ring positioned within the channel and in contact with the water surface. A simultaneous rotation of the ring and channel in opposite directions generated a turbulent flow field. The advantages of this apparatus in comparison with a conventional straight flume are as follows: (1) The flow is uniform at every section, and is free from any floc-disrupting elements such as pump blades, return pipes and diffusers. (2) The apparatus can be instrumented so that the average shear stresses acting on the ring and on the channel boundaries can be readily evaluated. (3) The equipment permits a quick and precise variation of the flow parameters over a wide range of values. (4) Due to its relatively small volume, a large number of tests with different fluids, sediment types and concentrations can be performed inexpensively, and in much shorter periods of time as compared to a straight flume. (5) The entire apparatus occupies a relatively small area.

The effect of rotation-induced secondary currents on the uniformity of deposition was practically eliminated by properly adjusting the speeds of the ring and channel for a uniform sediment deposition across the width of the channel. For these particular speeds, the bed shear stress distribution across the channel width was found to be almost uniform (Partheniades, Cross and Ayora, 1968). The details of the instrument and its operation are described by Partheniades et al. (1966) and Etter et al. (1968). A commercial kaolinite clay was used as the sediment with a grain size distribution from a fraction of a micron up to nearly fifty microns. Inasmuch as

the experiments were concentrated on the role of flow variables in deposition, the type of sediment and the ambient water quality were kept constant. The results of the investigation are summarized below.

1. For a given flow confining geometry, sediment type and flow conditions, the suspended sediment concentration reaches, after a period of relatively rapid deposition, a constant value C_{eq}, defined previously as equilibrium concentration. This equilibrium concentration is a constant fraction of the initial concentration C_o; i.e., the ratio C_{eq}/C_o is independent of C_o and is a function of the flow conditions only. This implies that each flow can maintain in suspension a constant percentage of a given initial amount of sediment.

2. The ratio C_{eq}/C_o for various depths depends on the bed shear stress, according to a logarithmic-normal relationship (Partheniades, Cross and Ayora, 1968). For the particular sediment and geometry of the annular channel, this relationship was found to be

$$\frac{C_{eq}}{C_o} = \frac{1}{0.49\sqrt{2\pi}} \int_{-\infty}^{\log\Delta P_\omega} \exp\{-\frac{1}{0.48}[\log\Delta P_\omega - 1.764]^2\} d(\log\Delta P_\omega) \quad (2.2\text{-}9)$$

where

$$\Delta P_\omega = \log(2.38 \times 10^4 \times \tau_b^{0.834} - 65) \quad (2.2\text{-}10)$$

in which the average bed shear stress τ_b is expressed in psf.

3. The initiation and rates of erosion of cohesive sediments have also been found to depend strongly on the bed shear stress, as observed by Partheniades (1965). Moreover, the stresses at which

erosion begins for a given sediment are considerably higher than the stresses at which the same sediment is suspension deposits entirely. This observation is in complete agreement with field observations in irrigation canals (Partheniades and Paaswell, 1970).

4. The conclusions cited so far reveal that the aspects related to the erosion and deposition of cohesive sediments are different from those of a coarse sediment. The constancy of the relative equilibrium concentration C_{eq}/C_o for constant flow conditions is a fundamental depositional characteristic of cohesive sediments. It has been well established that in flows over a movable cohesionless bed there is a simultaneous deposition and erosion of particles. A constant concentration of sediment in such flows is attained when the number of particles eroded is equal to the number of particles deposited per unit bed area, per unit time. If the suspended load is suddenly increased by an additional amount of sediment of similar composition to the one already in suspension, the concentration will eventually drop to its original equilibrium value, and the fluxes of erosion and deposition will again become equal. The constant value of C_{eq}/C_o independent of C_o in the case of fine sediments suggests that interchange of bed and suspended material does not take place. Such an interchange is also excluded by virtue of conclusion 3. Moreover, experiments in the rotating channel in which the suspended sediment at equilibrium concentration was gradually flushed out have directly confirmed this conclusion (Partheniades, Cross and Ayora, 1968). The constant equilibrium concentration of sediments in suspension does not therefore represent

the level of saturation of the sediment-carrying capacity of the flow. It rather appears to represent the fraction of the sediment with weak enough interparticle bonds, such that the settling flocs of that part of the sediment cannot resist the high disruptive shear stresses near the bed. The part of sediment which can form flocs large enough to settle on the bed and with sufficiently strong bonds to resist breaking and resuspension, deposits permanently without being resuspended.

5. The ratio C_{eq}/C_o ceases to be a unique function of the average bed shear stress for any speed combination other than the one resulting in a uniform deposition. This suggests that the rotation-induced unbalanced secondary currents in the annular channel also control the equilibrium concentration.

6. Mechanical analysis has revealed that at equilibrium concentration, the suspended sediment contains the entire particle size range of the original sediment (Partheniades et al., 1966). From this observation, it has been concluded that the degree of flocculation and the strength of the interparticle bonds play a dominant role in the deposition process rather than the particle size, and that there is little correlation between the particle size and the intensity of interparticle forces.

7. Limited data from experiments showed that the deposition rates are also strongly controlled by the bed shear stress. The following two tentative expressions were developed for the instantaneous concentration C by two different approaches (Partheniades, Cross and Ayora, 1968):

$$C = C_o f(\tau_b) t^{-2.14}\ 10^{-6}\ \tau_b^{-1.84} \qquad (2.2\text{-}11)$$

and

$$\frac{C_o - C}{C_o - C_{eq}} = -0.592 + 0.135 \log C_o + 0.455 \log t \qquad (2.2\text{-}12)$$

where t is in minutes and τ_b is in psf, and $f(\tau_b)$ is a function of τ_b. Differentiating Eq. (2.2-12) with respect to time, the following equation for the rate of deposition is obtained:

$$\frac{dC}{dt} = -\frac{0.198}{t} C_o \left[1 - \frac{C_{eq}}{C_o}\right] \qquad (2.2\text{-}13)$$

In Eq. (2.2-13) the effect of the shear stress τ_b exists implicitly through C_{eq}/C_o.

2.3 Objectives of Present Investigation

In the preceding section it was noted that the annular rotating apparatus used at M.I.T. was a convenient and efficient means to study, under controlled conditions, the depositional behavior of fine cohesive sediments. A similar apparatus, described in Section 3.1 was therefore used in the present investigation, with the following specific objectives.

1. A study of the effects of flow parameters on the rates of deposition of flocculated sediments under turbulent flow conditions, and derivation of quantitative relationships describing these effects. Limited measurements at M.I.T. discussed in the previous section had indicated that the bed shear stress, flow depth and the initial sediment concentration were some of the important variables involved.

2. Verify and generalize the logarithmic-normal law relating the equilibrium concentration to the bed shear stress as determined by the M.I.T. experiments.

3. Inasmuch as accurate values of the bed shear stresses are required, it was decided to measure them with the help of a false annular channel bottom. This false bottom would be instrumented so that it would directly measure the stresses acting on it. Velocity profiles would also be measured to supplement these shear stress measurements.

4. Once objectives 1 and 2 were met, it would then be possible to test more than one sediment, and thereby investigate the effects of the physicochemical properties of the sediments on the depositional behavior. Particular attention would be given to obtaining suitable and readily measurable parameters representing the physicochemical properties of the sediments, and relating the hydrodynamic behavior of a sediment in terms of these parameters.

5. A comparison of the experimental laws describing the depositional behavior with results of earlier investigations described in the previous section. A comparison with the data obtained in straight flumes would especially reflect on the merit of using the special annular rotating apparatus for testing cohesive sediment suspensions.

6. To attempt to elucidate the nature of the depositional process, in terms of a physical model. Since the behavior of sediment flocs is rather complex by virtue of their dependence both on the hydrodynamic as well as physicochemical forces, such a model would

essentially have to be based on certain simplifying assumptions related to sediment continuity, the nature of the physicochemical forces, the physical boundary conditions and the structure of turbulence.

CHAPTER 3

EXPERIMENTAL EQUIPMENT AND PROCEDURE

3.1 Experimental Equipment

3.1.1 Basic Apparatus

The components of the basic experimental equipment, consisting essentially of a system of a rotating ring and an annular channel are described in the following paragraphs. It is similar in principle to the one designed by Partheniades et al. (1966) at M.I.T., but is of twice the size (in linear dimensions) of the latter. The components are:

a. An annular channel, shown in Fig. 3.1.1, which is 8 in. wide, 18 in. deep and 30 in. in mean radius, and is made of 3/8 in. thick fiberglass. Four 3 x 2 in. plexiglass windows are provided every 90° in the lower part of its outer wall for visual observation. Lateral rigidity is provided by top and bottom horizontal flanges as well as by vertical stiffeners, also made of 3/8 in. thick fiberglass. The interior of the channel is smooth, without any obstructions that might impede the flow, and is coated with a white oil based paint.

b. An annular 1/4 in. thick plexiglass ring of the same mean radius as the channel, but with a slightly smaller width of 7-3/4 in., described in Fig. 3.1.2. The ring can be positioned within the channel, at any given height, with a clearance of 1/8 in. between its edges and the channel walls, so that it can rotate freely while in contact with the water surface. A plexiglass reinforcing member

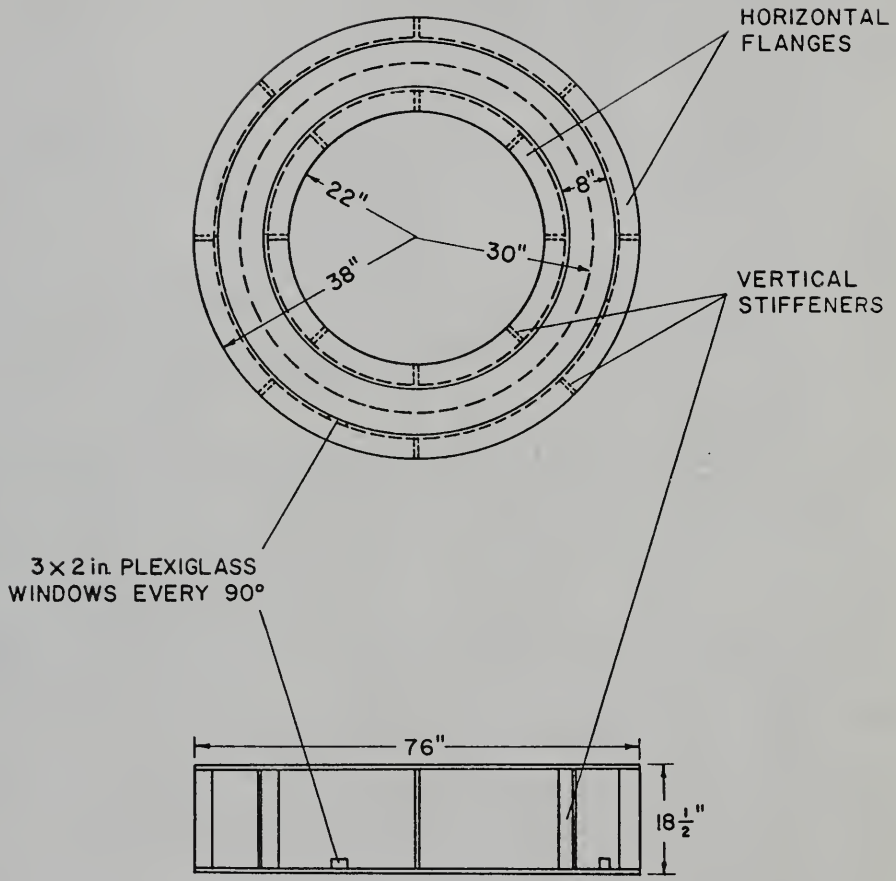

Fig. 3.1.1. Schematic Views of Annular Channel.

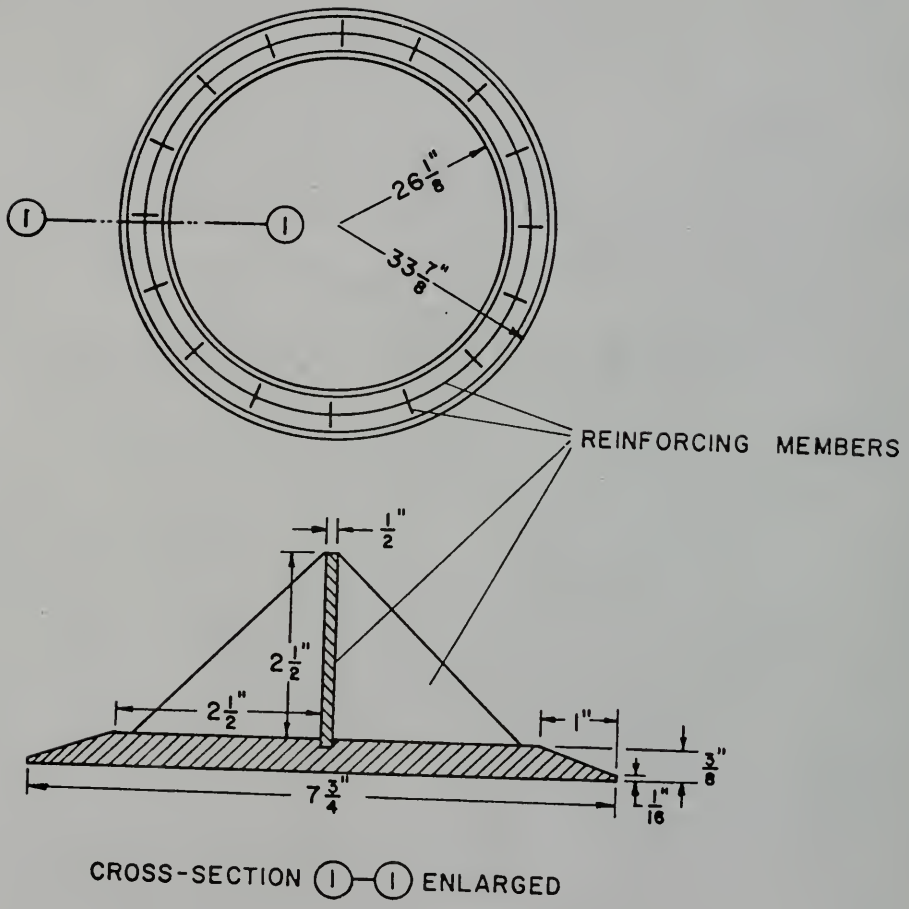

Fig. 3.1.2. Schematic Views of Annular Ring.

has been glued at the center of the ring, forming a T-shaped cross-section, to minimize deflection between the supports.

c. Two concentric steel shafts, as depicted in the schematic diagram of the entire assembly, shown in Fig. 3.1.3. The 3 in. diameter hollow outer shaft, which rotates the channel, is supported by the two indicated 1/2 in. thick, 18 in. equilateral triangular plates, through ball bearings. The 1 in. diameter inner shaft, which supports and turns the ring, is also supported by ball bearings, inside the hollow outer shaft.

d. A steel turntable, made essentially from octagonally positioned I-beams, with a circular plate in the middle, as shown in Fig. 3.1.5. The turntable is attached to the outer shaft, and the channel is bolted to the turntable, with a 5/8 in. chip board in between for a uniform support.

e. A ring support made of four 29-1/2 in. long, 2 in. wide and 1/4 in. thick radial steel arms shown in Fig. 3.1.3 as well as in Fig. 3.1.4, which is a top view of the assembly, showing some essential details. The arms themselves are attached to the 1 in. diameter inner shaft by an arrangement indicated in detail in Fig. 3.1.6. The ring is suspended from the radial arms by four 20-1/2 in. long, 3 in. wide and 0.025 in. thick flexible stainless steel blades, through clamping fixtures also indicated in Fig. 3.1.6. The lower end of each blade is rigidly bolted to the ring and to the plexiglass reinforcing member attached to the ring by two aluminum plates and angle brackets.

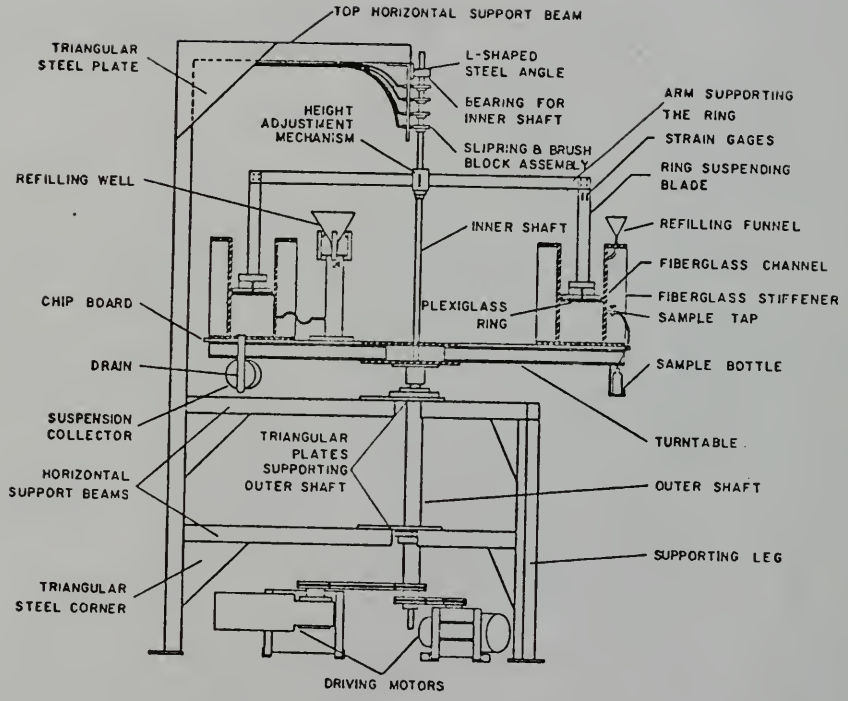

Fig. 3.1.3. Schematic View of Annular Ring and Channel Assembly.

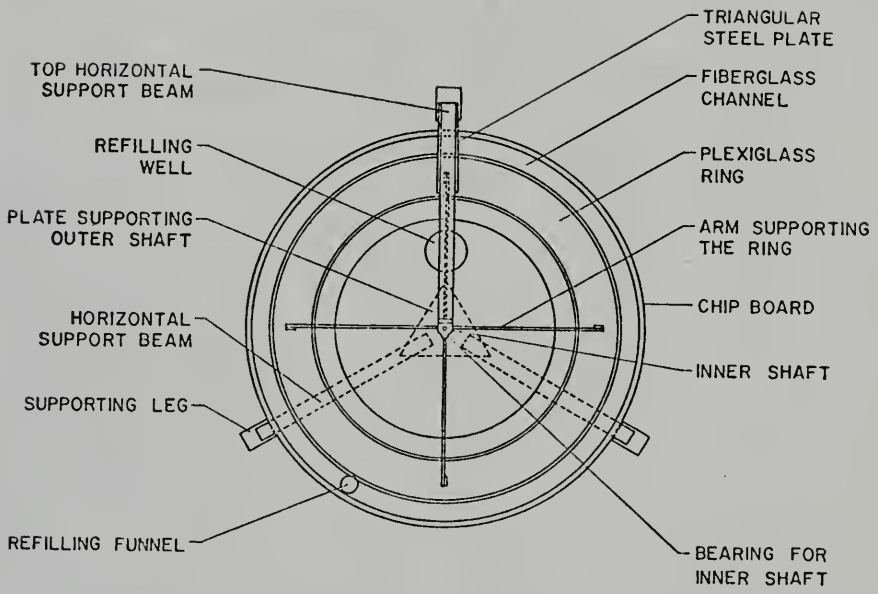

Fig. 3.1.4. Top View of Ring and Channel Assembly.

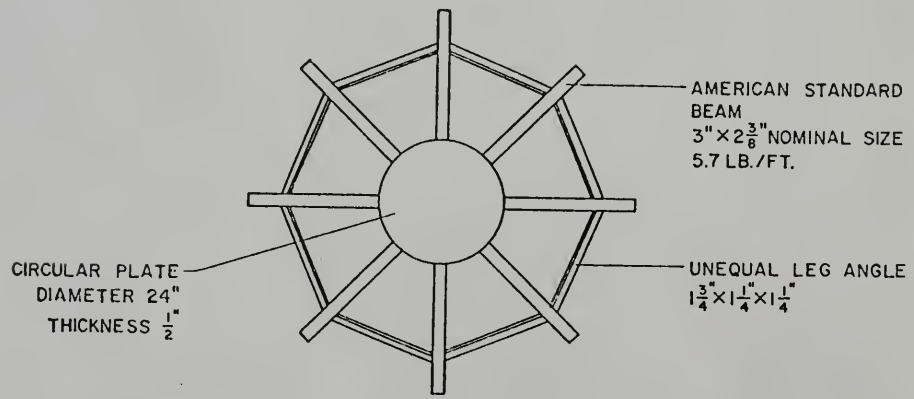

Fig. 3.1.5. Steel Turn-table.

f. A vertical height adjustment mechanism as shown in Fig. 3.1.6. This mechanism is designed with coarse and fine adjustment devices, to position the ring to touch the water surface for any given depth of flow. It consists of two components, the first of which is a steel collar fitting closely to the inner shaft. The collar slides on the shaft to the desired height, and is locked into position by a set screw which fits into countersunk cavities, spaced 1 in. apart vertically on the inner shaft. The collar is thus used for a coarse adjustment. The second, outer component, is attached to the four radial steel arms, and is threaded onto the steel collar. A lock nut, which also threads over the inner collar, is used to lock the outer component in any position, and is used for a fine height adjustment.

g. The support structure shown in Fig. 3.1.3. It is made from 3 x 3 in. square steel beams. These beams are hollow, with 1/4 in. thick walls. The three legs of the structure are placed 120° apart. The legs are securely bolted to the concrete floor, to provide the necessary rigidity to the structure. This support structure holds the outer hollow shaft through the triangular plates and ball bearings mentioned previously. Two horizontal support frames, each made of three 3 x 3 in. square and 34 in. long beams radially placed 120° apart as indicated in Fig. 3.1.4, and located at heights of 24 in. and 48 in. from the floor, are welded at the center to the triangular plates. 1/4 in. thick, triangular steel corners with base lengths of 14 in. are used to weld the frame beams and the legs together. One of the legs is extended to a total

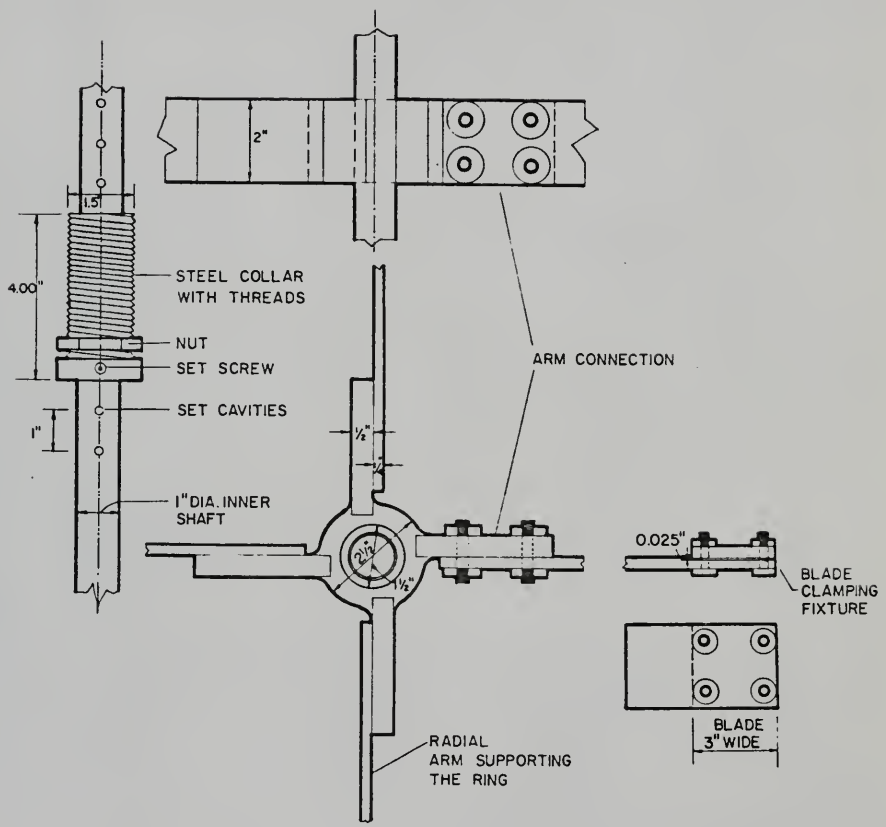

Fig. 3.1.6. Height Adjustment Mechanism Including Radial Arm and Blade Connections.

height of 150 in., and a horizontal 37 in. long 3 x 3 in. steel beam is connected to it at the top by bolts through two 1/4 in. thick and 28 in. base length triangular steel plates. This horizontal beam is used to hold the inner shaft in place through an L-shaped steel angle and a bearing, as indicated at the top of Fig. 3.1.3.

3.1.2 Accessory Equipment

Auxiliary equipment attached to the basic system described in Section 3.1.1, as well as special equipment used in the experimental work, is described in this section.

a. Four SR-4 type FAP-50-12-S9 temperature compensated strain gages, each with 120 ohm resistance and 2.1 gage factor were attached two on each side, of one of the blades supporting the ring, 1-1/2 in. below the top of the blade, for the measurement of the shear stress transmitted by the ring to the flow. For specifications and instructions for the use of these strain gages, refer to Strain Gage Bulletin (1967). A B.L.H. Portable Digital Strain Indicator Model 120C was used to measure the strain directly in a digital microinches per inch readout. For specifications on the indicator, see Strain Instruments Catalog (1968). The circuit diagram and procedure for the measurements is given in Section 3.2.3.

The electrical connection between the gages and the indicator had to pass through a set of four copper slip rings and carbon brush blocks shown in Fig. 3.1.3. These were designed at the Coastal Engineering Laboratory, and were able to function well, as long as the ring surfaces were periodically cleaned of carbon deposits.

b. An annular false bottom was designed for a direct measurement of the bed shear stress. It is made of 1/8 in. thick plexiglass, and has the same dimensions as the annular ring, i.e., it has a mean radius of 30 in. and a width of 7-3/4 in. Fig. 3.1.7 shows a schematic representation of the false bottom and plexiglass support used to position the former in the channel. Three such supports were designed and positioned every 120° in the channel, between plexiglass blocks glued on the channel bottom, with one of the supports instrumented with strain gages for shear measurement. Stiffeners are attached below the false bottom to keep it from flexing. Essentially, the false bottom is held in place by three 3-3/4 in. long and 2 in. wide blades made from a 0.004 in. stainless steel shim material. These blades are securely clamped between the false bottom and the support base by the indicated fixtures. The elevation of the false bottom is 5 in. above the channel bottom. Since plexiglass is slightly denser than water, with a specific gravity of 1.05, to avoid buckling of the blades due to the submerged weight of the false bottom, six 6-1/2 x 5 in. pieces of 1/2 in. thick styrofoam were glued underneath the false bottom to provide a sufficient upward buoyant force to balance its submerged weight. To adjust the number and size of the styrofoam pieces, the false bottom was placed in a large tank containing water, and styrofoam pieces of various sizes were introduced underneath the false bottom until it became almost neutrally buoyant.

The bed shear is measured by the bending strain produced in two SR-4 type FAP-50-12-S9 temperature compensated strain gages,

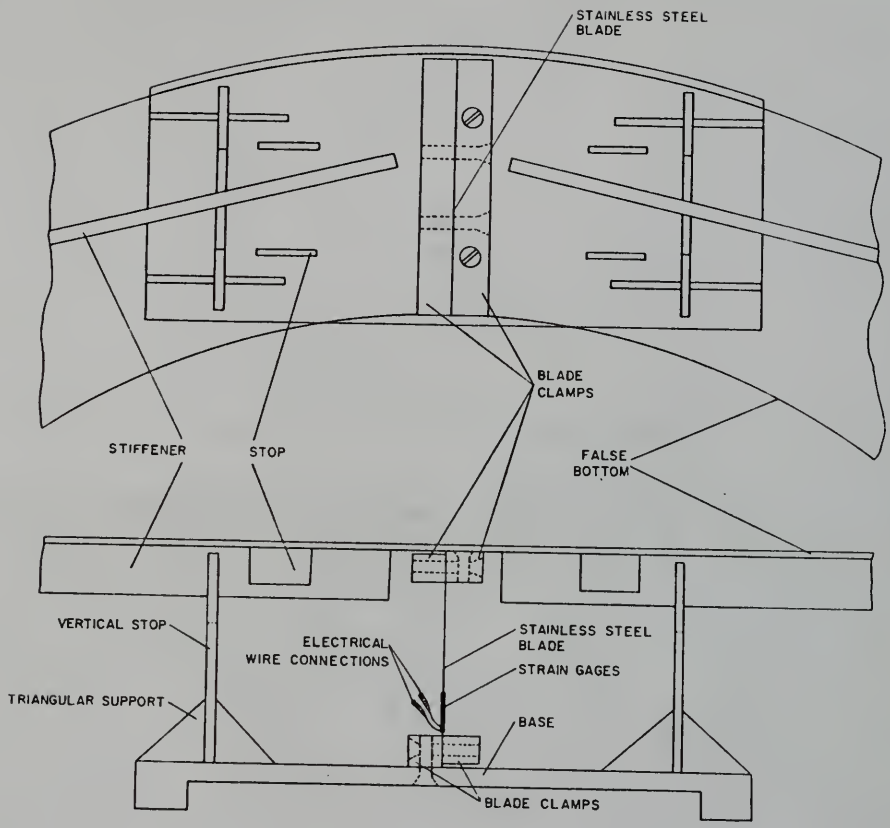

Fig. 3.1.7. Support for Annular Plexiglass False Bottom.

one on each side, on one of the blades, as shown in Fig. 3.1.7. The bending of the blade itself is due to the shear exerted on the false bottom by the flow above. In order to stop the flow below the false bottom, three vertical plexiglass partitions were positioned, half way between each support and below the false bottom. Stops shown in Fig. 3.1.7 are provided to keep the blades from bending more than 3/4 in. from its mean position either way, so that the elastic limit of the shim material is not exceeded. Since the strain gages were operating underwater, a thorough waterproofing was required. This was achieved by coating the gages with Dow Corning 3140 RTV Coating. Even on the two blades on which gages were not installed, the same coating was applied similarly to keep the bending characteristics of the three blades as similar as possible. Silicone grease was additionally applied on the blades for further protection against penetration by water.

c. Sampling equipment for sediment concentration includes four sample taps, at mean elevations of 1-9/16, 5, 8-3/4 and 12-1/8 in. from the bottom of the channel. Vinyl tubes attached to the taps lead to four 250 ml polyethylene sample bottles placed on a plexiglass stand attached below the chip board supporting the channel, as shown in Fig. 3.1.3. Due to the convenient locations of the taps and the bottles, it was possible to withdraw samples from the taps, as well as remove and replace the sample bottles while the channel was in motion.

A Millipore filtration apparatus was used for collecting the sediment from the samples taken through the taps. The equipment

consists of a Millipore vacuum-pressure pump, which provides a vacuum up to 27 in. Hg, a Pyrex filter holder with a stainless steel screen, a 1 liter capacity filtering flask, a 10 ml pipette, and type HA MF-Millipore filters with a mean pore size of 0.45 micron.

The pore size of 0.45 micron is about twice the diameter of the upper limit of a fine or colloidal clay particle, as given by the M.I.T. classification system, which is in the neighborhood of 0.20 micron, as indicated by Terzaghi and Peck (1967). Since clay particles always appear in a flocculated state in the samples, even the colloid-sized particles, if present, will be retained on the filter.

Water lost due to sample withdrawals was replaced through a refilling funnel shown in Fig. 3.1.3. A refilling well, also shown in Fig. 3.1.3, was designed for replenishing water lost by evaporation during long periods of several hours between sample withdrawals. The funnel over the well was filled with water, and it was allowed to drip into the well at a rate adjusted by trial and error to be equal to the mean rate of evaporation. Since the well is connected to the channel by a rubber tubing, water lost from the channel was thus replenished. It was later found, however, that under the controlled temperature conditions in the room where the experiments were conducted, evaporation of water was not sufficient to warrant the use of the well.

.d. In order to thoroughly mix the sediment with water before introducing it into the channel, a Hamilton Beach mixer with a large glass bowl was employed. Another mixer was constructed in the laboratory for mixing the sediment within the channel. This mixer consists

basically of a steel rod with three blades for mixing at one end, and with the other end attached to an electric drill gun which rotates the rod at a high speed. The mixer can be clamped on to the frame of the ring-channel assembly such that it can continue mixing while the channel is rotating. This way, a thorough mixing of all the sediment is achieved.

e. A Kent Miniflow Velocity Kit was used to measure velocities in the channel. This kit contains a D.C. velocity indicator with two 10 mm propeller probes, Nos. 265-3 and 265-4, together covering a range of velocity from 2 cm/sec to 300 cm/sec. An additional 4 mm probe with a velocity range from 1 in./sec to 30 in./sec was used to measure velocities close to the bottom surface.

f. Two Louis Allis 1 Hp forward and reverse motors were used to drive the ring and channel, separately. The attached tachometers are electrically connected to two Louis Allis Saber 3100 controllers for adjusting the speeds of the ring and the channel. Pulleys of 5-1/4 in. diameter on the inner and outer shafts are connected to those on the motors by belts, as shown in Fig. 3.1.3.

g. A 1 KHz square wave generator was designed for the measurement of bed shear stress through the false bottom. The output of the measured values was read on a Triplett Auto Polarity Micro Power V-O-M Model 602 on which A.C. voltage as low as 0.01 volt can be read on a linear scale.

h. A CL-277 B Soiltest hydrometer was purchased for measuring the particle size distributions of the various cohesive sediments. It has a specific gravity range of 0.995 to 1.038 with divisions of 0.001.

i. A drain and a polyethylene suspension collecting bottle are provided for collecting large quantities of the sediment suspension, while the channel is in motion. This is done in order that the particle size distribution of that portion of the sediment which is in suspension may be determined. The drain itself consists of two concentric steel pipes with the inner 1 in. O.D. pipe sealed at the upper end, and with two 1/2 in. diameter holes in its side, 1 in. below the upper end. The lower end of the inner pipe is connected to a vinyl tubing, the other end of which goes into the suspension collector. The inner pipe closely fits inside the outer pipe, but slides freely with the help of silicone grease. This way, water-tightness is maintained. Ordinarily, the top of the inner pipe stays flush with the channel bottom, so that no water can go through the drain. If a collection of the suspension is required, the inner pipe can be pushed upward, causing the suspension to flow through the two side holes into the collector. Pulling it back to the original position stops the flow. In this way, any required amount of suspension can be collected.

j. For the static calibration of the ring and the false bottom, as described in Section 3.2.3, two special types of plexiglass brackets were designed. These can be clamped on to the channel flanges. Pulleys are provided on these brackets, so that metric weights on small metallic pans can be hung from these pulleys, using nylon threads, with one of their ends attached to the pan and the other to the ring or the false bottom. In this way, torques of known values can be applied. The bracket used for the static calibration of the false

bottom is shown on the left of Fig. 3.1.8, while on the right, the one used for the calibration of the ring is shown.

Fig. 3.1.9 is a photograph of the complete annular channel and ring assembly. The air conditioner at the top right of the picture was used to control the room temperature, and maintain it at approximately 20°C. Below the air conditioner, one of the two Louis Allis Saber 3100 speed controllers is visible. On the assembly itself, the channel, its flanges and windows, ring arms and blades, supporting structure, driving motors, refilling funnel, sample taps and bottles and the drain and suspension collector are visible. At the top of the inner shaft, four slip rings can be observed.

Fig. 3.1.10(a) shows a closer view of the channel with the ring in operational position. Part of the refilling well also can be observed. In Fig. 3.1.10(b), the plexiglass false bottom is shown on four roller type supports. This arrangement was found inadequate because it could not keep the false bottom from flexing, nor could it prevent it from displacing vertically, due to the hydrodynamic lift exerted on it by the flow. As a result, the arrangement was changed to that described earlier in this section.

Fig. 3.1.11(a) shows the driving motors, pulleys and belts. The motor on the right drives the inner shaft, while the one almost perpendicular to the photograph is connected to the outer shaft. Fig. 3.1.11(b) shows the building that housed the experimental equipment. It has now been extended to include other additional experimental facilities.

Fig. 3.1.12 shows a schematic plan view of the arrangement of experimental equipment within the building shown in Fig. 3.1.11(b).

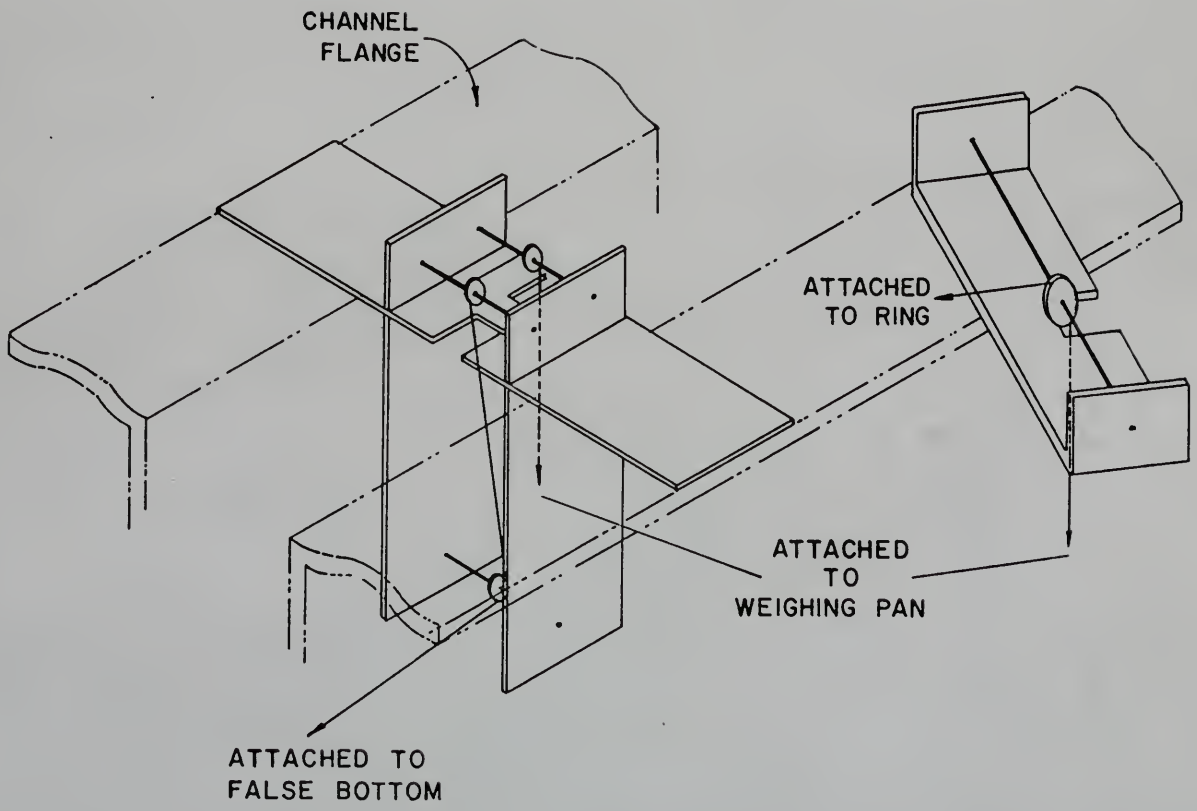

Fig. 3.1.8. Brackets for Static Calibrations of Shear Stresses on False Bottom and on Ring.

Fig. 3.1.9. Annular Channel and Ring Assembly.

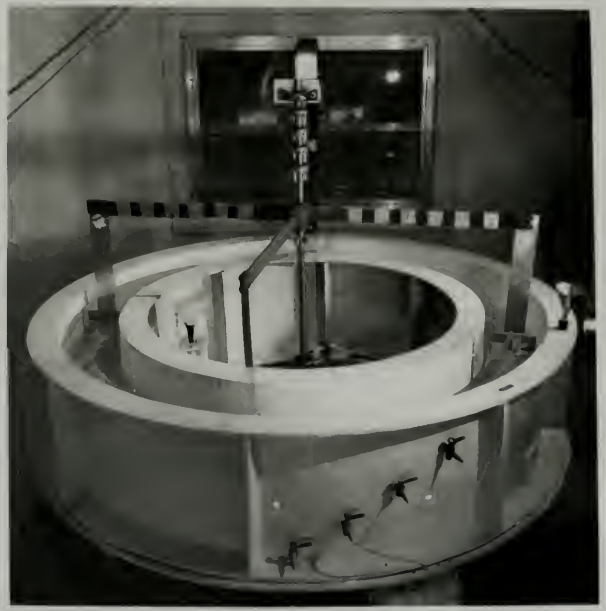

(a)

(b)

Fig. 3.1.10. (a) Annular Channel with Ring in Operational Position
(b) Annular False Bottom on Supports.

(a)

(b)

Fig. 3.1.11. (a) Motors Driving Inner and Outer Shafts
(b) Housing for Experimental Equipment.

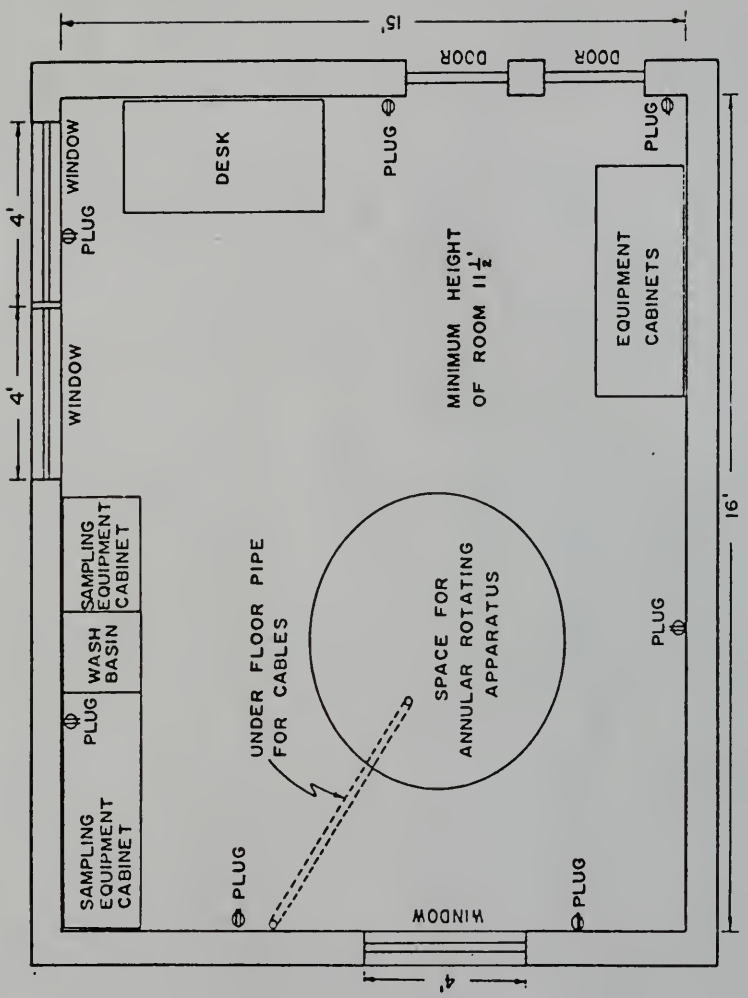

Fig. 3.1.12. Arrangement of Experimental Equipment.

3.1.3 Sedimentary Material

a. Kaolinite: The kaolinite clay used in the deposition experiments was supplied by R. T. Vanderbilt Company of New York. Part of the following information on the clay is taken from the Technical Data Sheet (1970) provided by the company.

The trade name for the particular kaolinite clay used is Peerless No. 2. It is a light cream-colored secondary kaolin which is non-abrasive and non-alkaline, is compatible with commonly used wetting and dispersing agents, and it immediately flocculates in distilled water. It is mined in Bath, South Carolina by Dixie Clay Company, by the open pit method. The clay is air dried in sheds and passed through a rotary kiln. It is ground in a Raymond mill and air separated. Table 3.1.1 gives its chemical composition.

TABLE 3.1.1

Constituent	SiO_2	Al_2O_3	Fe_2O_3	TiO_2	CaO	MgO	Na_2O	K_2O	Loss on Ignition
% by Weight	44.99	39.95	0.34	0.73	trace	trace	0.12	0.10	13.82

Fig. 3.1.13 shows the particle size distribution as measured by Partheniades et al. (1966). It is observed that 66% by weight of the material is in the clay size range, and 34% in the silt range.

X-ray diffraction pattern with copper (Cu) Kα radiation of the bulk material is shown in Fig. 3.1.14. Since a sediment slide was used, the basal (00ℓ) reflections are intense. The material appears to

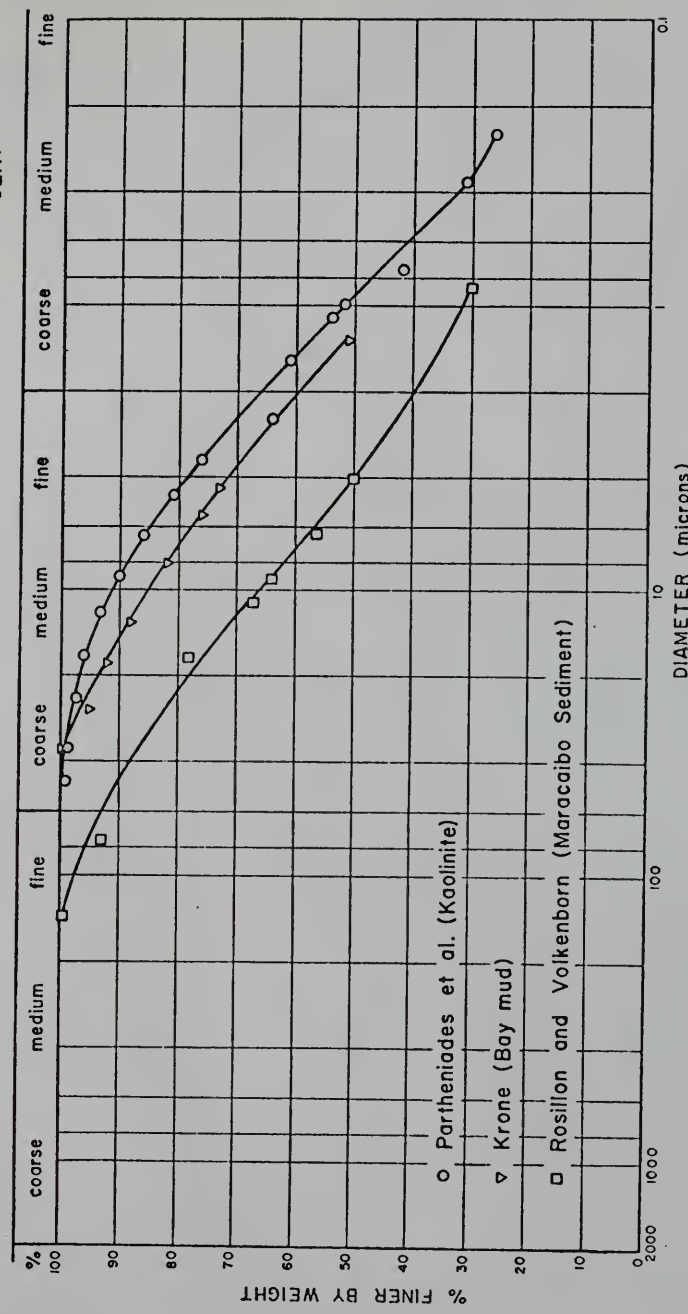

Fig. 3.1.13. Particle Size Distributions for Three Types of Fine Cohesive Sediments.

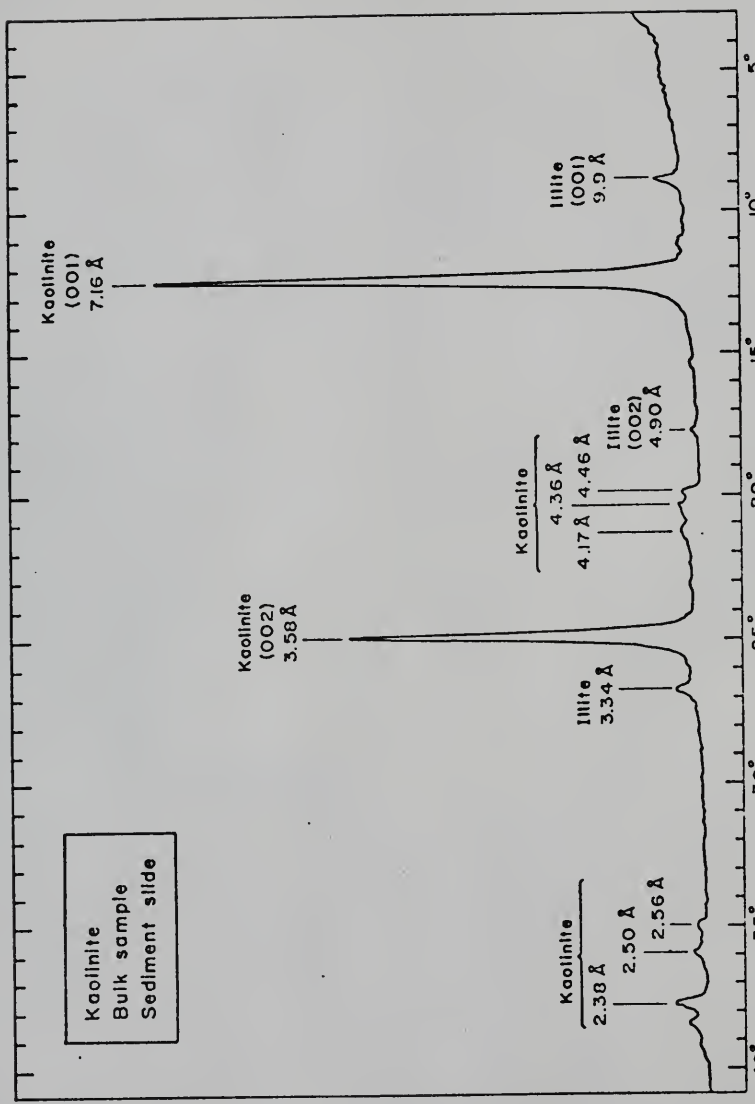

Fig. 3.1.14. X-ray Diffraction Pattern for Kaolinite for Bulk Sample.

consist almost entirely of kaolinite with a very small amount of illite, as indicated by the peak intensities.

The cation exchange capacity of the material was found to be 77 milliequivalents per hundred grams of the material. This high value is not representative of the CEC of kaolinite, which should be approximately in the range of 3 to 15 milliequivalents per hundred grams, according to Grim (1968). Even after almost complete salt removal from the material, as checked by the silver nitrate test, similar high values of the CEC were obtained. This high value is therefore attributed to a possible chemical pretreatment of the commercial material, which could significantly alter its CEC (Grim, 1968). Such a pretreatment would also account for the tendency of the material to flocculate even in distilled water.

For the material free of sodium chloride, a pH of 5.1 was determined, indicating an acidic nature.

b. Bay mud: Part of the following description of the Bay mud, dredged from the Mare Island Strait of San Francisco Bay, is obtained from studies by Krone (1962).

Differential thermal analysis (DTA) and X-ray diffraction measurements of the sediment show that the predominant clay mineral constituent is montmorillonite, followed by illite, kaolinite, halloysite and chlorite. Among the non-clay materials, quartz, organic matter and iron flocs are present. Some structural iron is also present, due to the replacement of aluminum by iron in illite.

Suspended, or recently deposited, Bay mud has a light brown color, while sediment from a depth of a few centimeters below the surface has a color ranging from light grey to black. When a sample of wet dredged sediment was placed in a large glass cylinder and thoroughly stirred in water, a color change from dark grey to brown took place. When allowed to stand, the color slowly changed back to greenish grey and finally back to dark grey. These color changes take place due to the following reasons: in the dark grey sediment iron is present as ferrous sulfide. When stirred, ferrous sulfide is easily oxidized, due to aeration, to ferric hydroxide, which imparts a brownish color to the sediment. If allowed to stand, bacterial reduction first changes ferric iron to ferrous iron which is greenish, and then finally back to ferrous sulfide.

Particle size distribution of the Bay mud is shown in Fig. 3.1.13. It is seen that 60% by weight of the sediment is in the clay range, and the remaining in silt range. Comparison with the curve for kaolinite shows that there is relatively more silt in Bay mud than in kaolinite.

Fig. 3.1.15 shows an X-ray diffraction pattern of a sediment slide of the less than 62 micron fraction (silt and clay) of the Bay mud. The pattern confirms Krone's observations, with an additional peak for orthoclase feldspar at 3.19 Å.

In Fig. 3.1.16, the pattern corresponds to a less than 2 micron fraction (clay) of a sediment slide treated with ethylene glycol, which has shifted the montmorillonite peak to 17 Å. A chlorite (001) peak at 14.2 Å is therefore observed clearly.

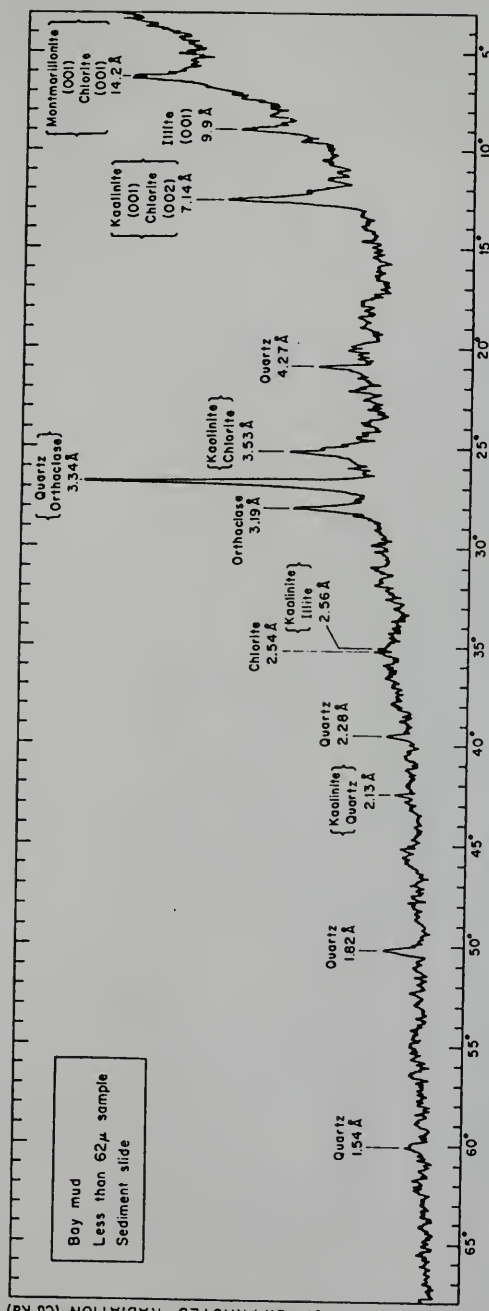

Fig. 3.1.15. X-ray Diffraction Pattern for Bay Mud for Less than 62 Micron Fraction.

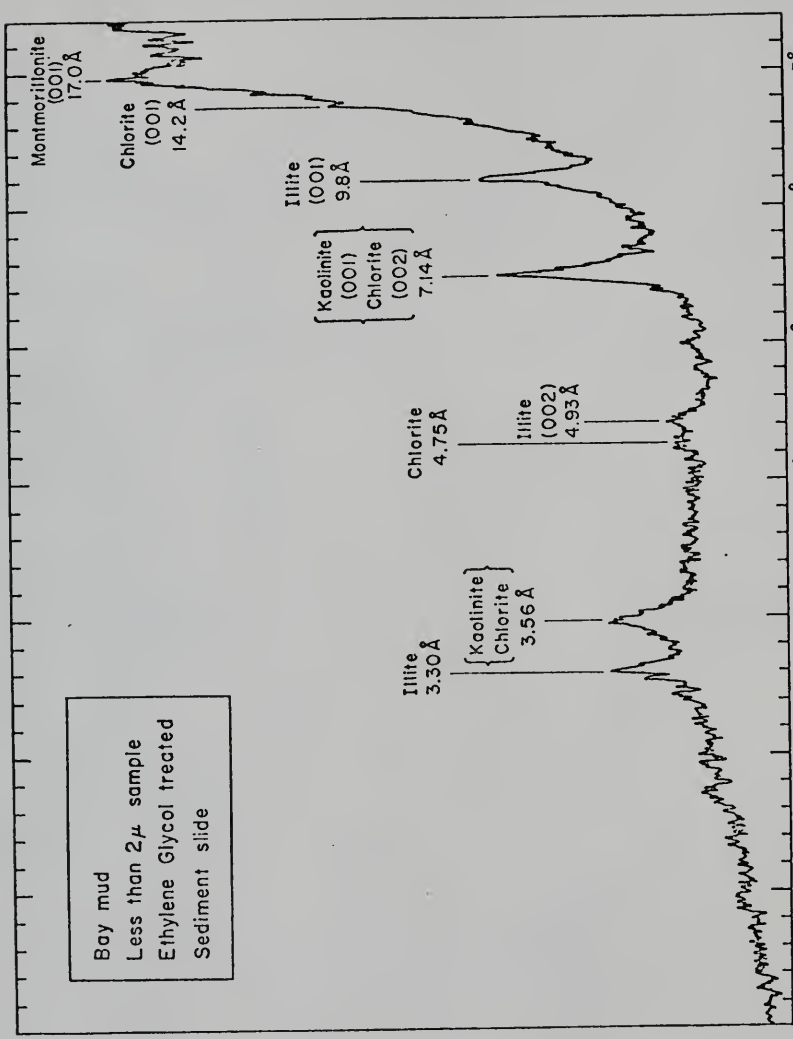

Fig. 3.1.16. X-ray Diffraction Pattern for Bay Mud for Less than 2 Micron Fraction.

The cation exchange capacity was found to be 24 milliequivalents per hundred grams of the material, and this value is in agreement with values ranging from 18.7 to 30 milliequivalents per hundred grams obtained by Krone (1957).

c. Maracaibo Sediment: The Maracaibo sediment was not studied for its depositional behavior in the annular channel. However, results of Rosillon and Volkenborn (1964), who used the sediment in depositional studies carried out in a straight flume, have been reanalyzed and compared with those using kaolinite and Bay mud in Section 4.2.3. For that reason, three samples of the sediment from the Inner Maracaibo Channel were analyzed in the Geology Department of the University of Florida, for their particle size distribution, clay mineral and non-clay mineral content and the cation exchange capacity. This analysis is included in Appendix C.

Fig. 3.1.13 shows the particle size distribution of the sediment used by Rosillon and Volkenborn. Approximately 7% by weight of the material is fine sand, 53% is silt and 40% is in the clay range.

3.2 Experimental Procedure

3.2.1 Calibration of Speed Controllers

The Louis Allis Saber 3100 speed controllers required calibration, since the meters provided on them did not read the speeds of the ring and the channel directly in rpm. Calibration was therefore carried out by actual rpm measurements for the ring and the channel using a stopwatch, for given different settings on the meters.

Fig. 3.2.1 shows the calibration curves for the ring and the channel.

3.2.2 Determination of Operational Speeds

The rotational motion of the channel and the ring induces a secondary motion in the radial direction, in addition to the main flow in the tangential direction. The following explanation for the mechanism which generates this secondary motion is taken from the report by Partheniades et al. (1966), in which the same phenomenon occurring in the smaller annular channel used at M.I.T. is described.

Consider the ring-channel system sealed off and filled with water completely, with a hydrostatic pressure distribution, i.e., at the ring $\tilde{p} = 0$, as indicated in Fig. 3.2.2(a). Now consider a simultaneous rotation of the ring and the channel at the same angular speed Ω. After a sufficient length of time, at steady state, a rigid body rotation will be established. The tangential velocity u at any point with a radius r is then given by

$$u = \Omega r \tag{3.2-1}$$

and from the equation of motion in the r-direction (Bird, Stewart and Lightfoot, 1960) one obtains

$$\frac{1}{\rho}\frac{\partial \tilde{p}}{\partial r} = \frac{u^2}{r} = r\Omega^2 \tag{3.2-2}$$

where ρ is the density of water. Or, expressing the pressure gradient as a total derivative

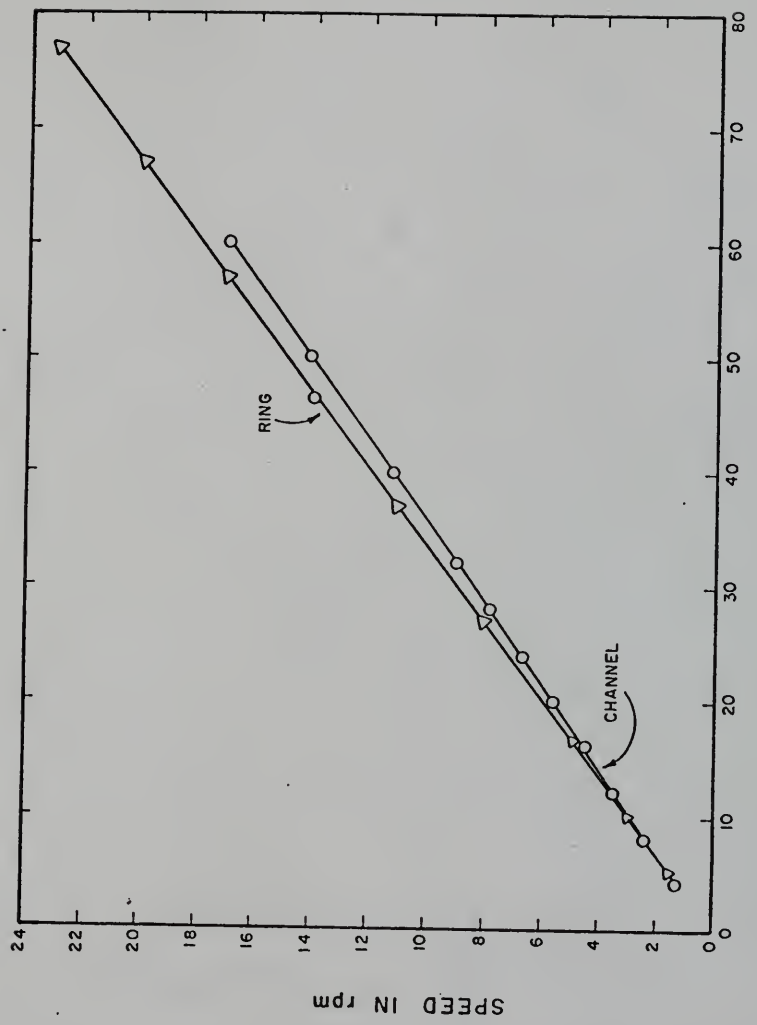

Fig. 3.2.1. Speed Calibration Curves for Ring and Channel.

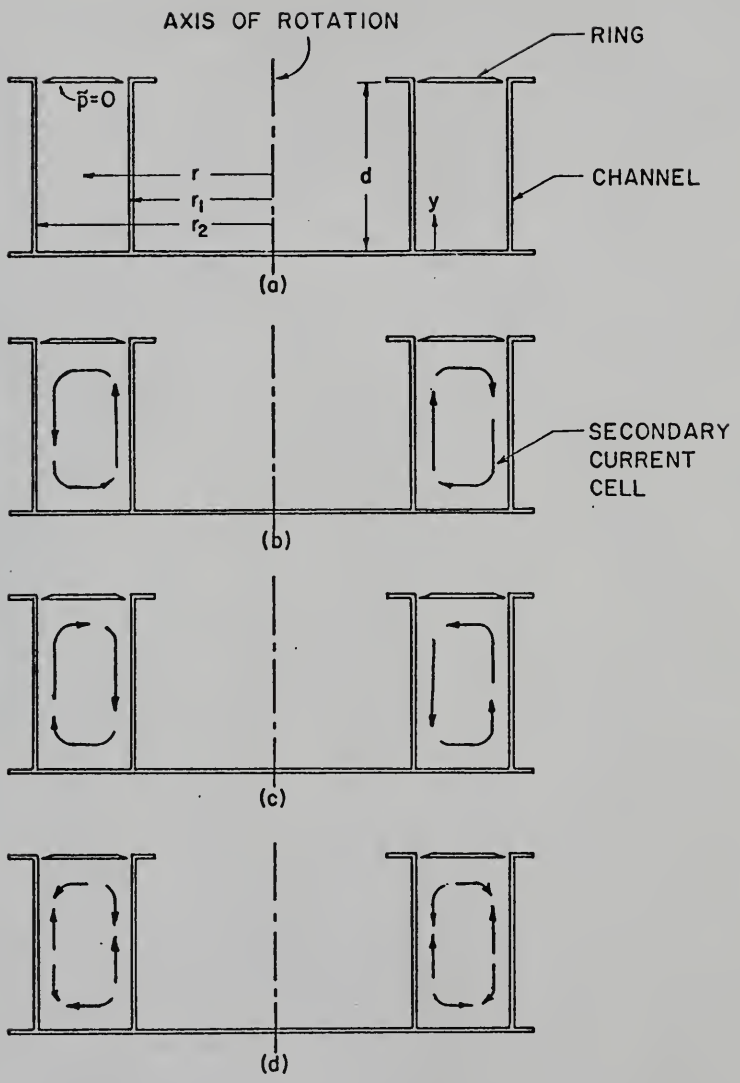

Fig. 3.2.2. Secondary Cells in Ring-Channel System
(a) Solid Body Rotation
(b) Ring Only Rotating
(c) Channel Only Rotating
(d) Ring and Channel Rotating at Operational Speeds.

$$\frac{d\tilde{p}}{dr} = \rho r\Omega^2 \tag{3.2-3}$$

Integrating Eq. (3.2-3) gives

$$\tilde{p} = \frac{\rho r^2\Omega^2}{2} + C_1 \tag{3.2-4}$$

where C_1 is a constant. The pressure difference Δp between the outside and inside walls becomes

$$\Delta\tilde{p} = p_2 - p_1 = \frac{\rho\Omega^2}{2}(r_2^2 - r_1^2) \tag{3.2-5}$$

Now the y-component of the equation of motion gives

$$\frac{\partial\tilde{p}}{\partial y} = -\rho g \tag{3.2-6}$$

which implies a hydrostatic pressure distribution. In the case of solid body rotation, there is no secondary flow, since at any cylindrical surface (corresponding to r = const.), the velocity u is constant at any level, so that the centrifugal force on every fluid element is exactly counter-balanced by the net pressure force acting on the element.

Now with reference to the notation of Fig. 3.2.2, the following cases arise:

Case a: Ring only rotating with an angular velocity Ω_o. In this case, Ω varies from Ω_o at the ring to zero at the channel bottom. The pressure difference between the outside and inside wall is the same according to Eq. (3.2-5) for any elevation, since the pressure varies

hydrostatically with depth. This pressure difference corresponds to a speed Ω_m at $y = y_m$, such that

$$\frac{d\tilde{p}}{dr} = \rho r\Omega_m^2 \tag{3.2-7}$$

Now for $y_m < y \leq d$, $\Omega > \Omega_m$ and

$$\frac{d\tilde{p}}{dr} < \rho r\Omega^2 \tag{3.2-8}$$

or

$$d\tilde{p} < \rho r\Omega^2 dr \tag{3.2-9}$$

Hence the existing pressure is not adequate to balance the centrifugal force, and as a result the fluid particles move radially outward. For $0 \leq y < y_m$, $\Omega < \Omega_m$ and

$$d\tilde{p} > \rho r\Omega^2 dr \tag{3.2-10}$$

which means that there is an excess of pressure force over the centrifugal force, which causes the fluid particles to move radially inward. The resultant effect of these two situations above and below $y = y_m$ is that a counterclockwise secondary circulatory motion is set up in the channel, as shown in Fig. 3.2.2(b).

Case b: Channel only rotating with an angular speed Ω_o. By a similar argument as in case a, it can easily be shown that in this situation, a clockwise secondary current is set up, as indicated in Fig. 3.2.2(c).

Secondary currents such as those described above also occur in pipes and flumes, when bends are present. Schlichting (1968) discusses secondary flows in pipes of circular as well as non-circular

cross sections. In describing flow through a curved circular pipe, he indicates that a secondary flow arises because of the fact that particles near the flow axis which have higher velocities are acted upon by a larger centrifugal force than the slower particles near the walls. This leads to a secondary current directed outward in the center, and inward, toward the center of curvature, near the wall.

Secondary currents are also present in straight flumes, where the velocities at the corners are comparatively very large, which is because the fluid flows towards the corner, along the bisectrix of the angle, and then outward in both directions. Thus the secondary flows continuously transport momentum from the middle region to the corners, and generate high velocities there. Such flows are undesirable because they tend to complicate a nearly two-dimensional flow pattern into a three-dimensional one, which is difficult to interprete analytically.

In order to minimize the effect of secondary currents on the uniformity of sediment deposition across the width of the channel, the ring and the channel are rotated simultaneously in opposite directions. This motion sets up two circulatory currents in opposite directions, since both near the ring and near the channel bottom, the fluid particles tend to move outward, as shown in Fig. 3.2.2(d). Now if the speed of the ring is sufficiently higher than that of the channel, the vertical momentum of the downcoming particles could be high enough to build adequate pressure, in order to compensate the excess centrifugal force near the bottom, and thus eliminate the

secondary circulation there. Then, a fairly uniform deposition of suspended sediment could be expected to take place. The ring, which has a smaller area of contact with the water surface than the channel, would apparently have to rotate faster than the channel, to produce a secondary circulation cell of the magnitude equal to that produced by the channel. Correspondingly, as the distance between the ring and the channel bottom, i.e., the depth, increases, the relative speed of the ring would have to become greater with respect to that of the channel.

In order to determine the ratio of speeds at which the effect of the secondary current is minimized, plastic beads of 3/8 in. mean diameter, and of 1.04 specific gravity were introduced to simulate sediment motion. These beads, very close to the specific gravity of water, were easily moved by the induced shear flow at the bottom, and were extremely sensitive to the secondary currents. Rotating the ring alone caused the beads to move toward the inside wall of the channel, as predicted by the current pattern of Fig. 3.2.2(b). Similarly, rotating only the channel moved the beads toward the outside wall, as predicted by the current pattern of Fig. 3.2.2(c). Thus the presence of two secondary cells of currents cancelling each other at the bottom could be detected when various ratios of the ring and channel speeds caused the beads to remain at the center of the channel. This position of the beads was then chosen as the criterion for minimum secondary current effect.

For a more refined measurement of the ring-channel speed ratios corresponding to minimum secondary current effect, kaolinite

sediment itself was introduced into the channel. Since preliminary values of these ratios were already available from the tests using beads, in a given test, the ring and channel were rotated at speeds corresponding to a known ratio, and after several hours during which the initially suspended sediment was allowed to deposit, the system was gently brought to a stop. Then after any remaining small fraction of the total sediment settled out, thus freeing the water of any turbidity, the sediment bed depth across the width of the channel was measured. This was done with the help of a point gage with vernier scale. If these measurements showed that the bed was too thick near the inner wall of the channel, the test was carried out again with a slightly lower ring speed. On the other hand, if the bed was found to be too thick near the outer wall of the channel, the test was performed with a slightly higher ring speed. This way, by trial and error adjustments, it was possible to accurately determine the ring-channel speed ratios corresponding to a uniform sediment deposition across the width of the channel. Bed depth measurements are discussed in Appendix A. After several measurements at various ring-channel speed ratios, or speed combinations, and at different flow depths, it was found that in measurements using beads, the ring was rotating faster than the required speed for a uniform sediment deposition, and that in all cases its speed had to be reduced by 9.5%. This discrepancy between the values obtained by using beads and those obtained using the sediment is attributed to the fact that while the mean radius of the beads is 3/16 in., the effective mean radius of the sediment flocs is probably not more than a few hundred microns. Therefore, since the relative

strengths of the secondary currents due to the ring and the channel are expected to vary with the distance from the bottom of the channel, the beads, with their relatively large size, are acted upon by secondary currents of different strengths than those acting on the comparatively small sediment flocs. This results in a difference between the ratios of ring-channel speeds for a minimal secondary effect, which requires the beads on the one hand and the sediment on the other to remain uniformly distributed. Essentially therefore, the beads were too large for accurately simulating sediment motion.

The ring-channel speed combination is herein referred to as "operational speed." Fig. 3.2.3 shows the operational speeds for flow depths ranging from 2 in. to 14 in. The measurements corresponding to the slowest operational speeds correspond to a channel speed of 1.35 rpm. Below this value, it was difficult to move the beads with the prevailing shear stresses. The straight line corresponding to depth d = 0 in. is of course the one for which the ring and channel speeds are equal, since at zero depth, both of them have the same area of contact. Also, it is clearly observed that as pointed out earlier, as the depth increases for a constant channel speed, the ring has to be rotated with increasing speed to maintain a minimal secondary flow effect. In all the experiments, the plot of Fig. 3.2.3 was used to obtain the ring speed, for a given channel speed and depth of flow.

3.2.3 Calibration of Equipment for Shear Stress Measurements

For the determination of the bed shear stress in the channel,

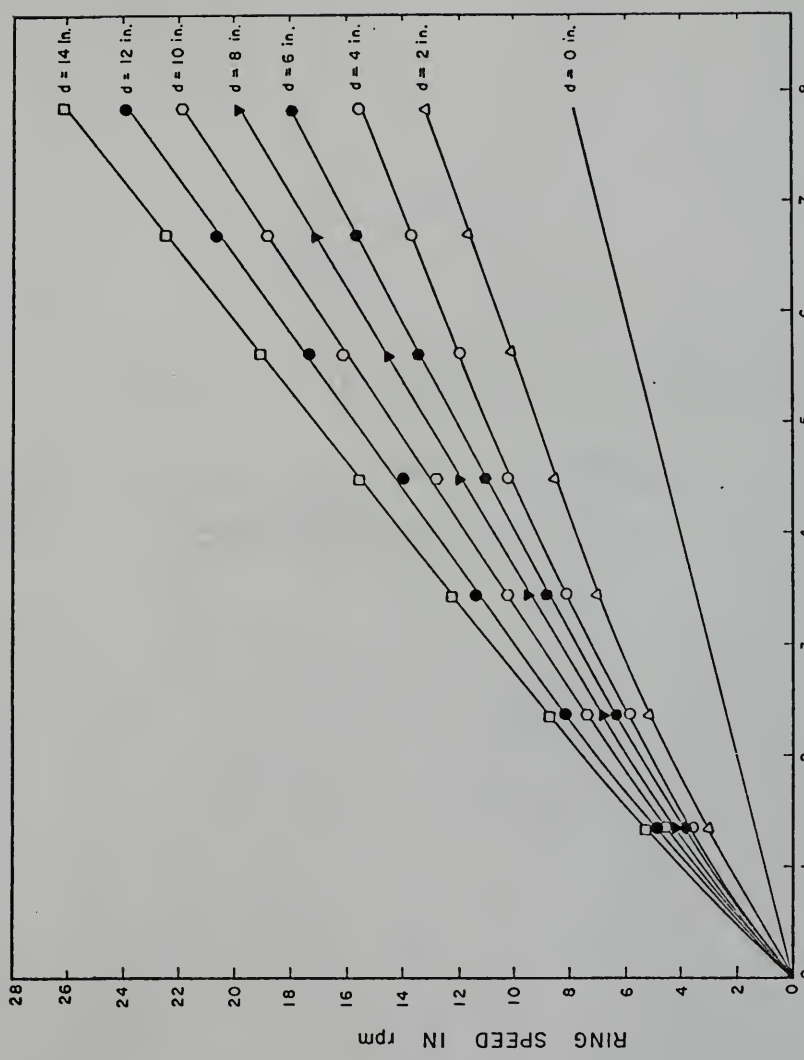

Fig. 3.2.3. Operational Speeds for Ring and Channel.

an important variable in the depositional process as indicated by previous investigations, both the ring shear stress, as well as the shear stress on the false bottom were measured; the former for an indirect estimation of the bed shear stress, and the latter for a direct measurement of the same. The results of these measurements are discussed in Sections 4.1.1 and 4.1.2. For these measurements, it was necessary to calibrate the readout scales on the measuring instruments in terms of the shear stress itself. Thus in the case of the ring shear stress measurement, a calibration curve was required to convert the microinch per inch strain readout on the strain indicator to shear stress in dynes per square centimeter. Similarly, in the case of bed shear stress measurement by the false bottom, the voltage readout on the voltmeter was required to be converted to the corresponding shear stress value. In both cases, this was done by the simple method of static calibration, as described below.

a. The location of the SR-4 strain gages on the stainless steel blade instrumented to measure the ring shear stress is indicated in Fig. 3.2.4(a). The two gages on each side are connected in series, such that the two pairs constitute the two arms of a four-arm Wheatstone bridge circuit. The other two arms, the required power supply and the strain readout meter are included in the strain indicator, so that the general arrangement is as shown in Fig. 3.2.4(b).

The strain σ' produced in a strain gage is defined as

$$\sigma' = \frac{\Delta \tilde{L}}{\tilde{L}} \qquad (3.2\text{-}11)$$

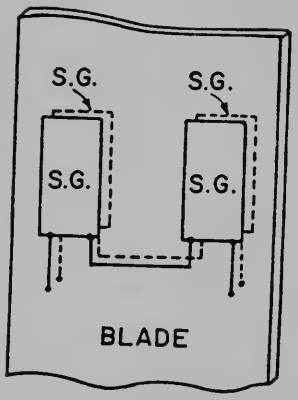

(a)

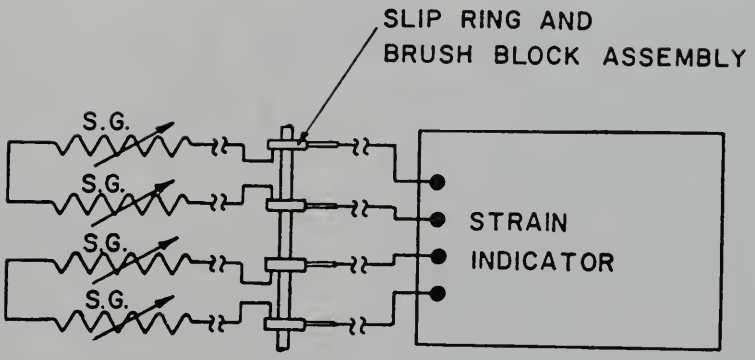

(b)

Fig. 3.2.4. (a) Location of Strain Gages
(b) Circuit for Strain Measurement.

where $\tilde{L}$ is the initial length of the gage and $\Delta\tilde{L}$ is the small change in length produced by the bending of the gage. If R is the initial resistance of the gage, then the change ΔR in its value is related to ΔL by a dimensionless expression

$$F = \frac{\Delta R/R}{\Delta\tilde{L}/\tilde{L}} = \frac{\Delta R/R}{\sigma} \tag{3.2-12}$$

or

$$\sigma' = \left(\frac{1}{FR} \right) \Delta R \tag{3.2-13}$$

where F is called the gage factor and is a known constant for a given gage (F = 2.1 in the present case). Therefore, since R for the given number of gages used in the circuit is also known, σ' is obtained for any R, according to Eq. (3.2-13).

The circuit was arranged according to Fig. 3.2.4 and the gage factor F = 2.1 was set on the dial provided on the strain indicator. Two brackets with pulleys such as the one shown on the right of Fig. 3.1.8 were positioned 180° apart, by clamping them to the channel flanges. The ring itself was positioned at an elevation such that a horizontal tangential force could be applied to it, with the help of the nylon threads clipped on to the ring's reinforcing member. The threads were passed over the pulleys on the brackets and their ends were tied to small metal weighing pans, as suggested in Fig. 3.1.8, so that metric weights could be placed on them.

The purpose of the tangentially applied force is to simulate the shear caused by rotating the ring in contact with the water surface. The shear force is evenly, or near evenly, distributed over the surface

of contact. Its resultant moment may be represented by a pair of vectors opposite in sense and tangential to the center line of the ring at points 180° apart from each other, as shown in Fig. 3.2.5. A couple is thus formed. Now each of these vectors is equal in magnitude to one-half the product of the average shear stress on the ring, and the ring area. Thus, when a weight $\tilde{W}$ is applied to each of the two points, the simulated shear stress on the ring is

$$\tau_r = \frac{2\tilde{W}}{\tilde{A}} \tag{3.2-14}$$

where $\tilde{A}$ is the surface area of the ring. Now since $\tilde{A} = 9740\ cm^2$, therefore

$$\tau_r = 0.202\tilde{W}\ dynes/cm^2 \tag{3.2-15}$$

where $\tilde{W}$ is expressed grams. In the procedure therefore identical metric weights of increasing magnitude were placed on the pans, and the corresponding σ' in microinches per inch was recorded after each addition of a weight, and after adjusting the strain indicator for a null balance of the bridge. Similarly, values of σ' were recorded when the load in the pans was gradually reduced. This way, for each $\tilde{W}$, σ' was known and the corresponding value of the ring shear stress τ_r was obtained from Eq. (3.2-15). The calibration curve thus obtained is shown in Fig. 3.2.6.

b. For the static calibration of the false bottom, a procedure similar to the one described above was employed. The circuit of Fig. 3.2.4, however, could not be used in this case, because a set of four additional slip rings and brush blocks would have been required on the inner shaft to transmit the electrical signal between the strain

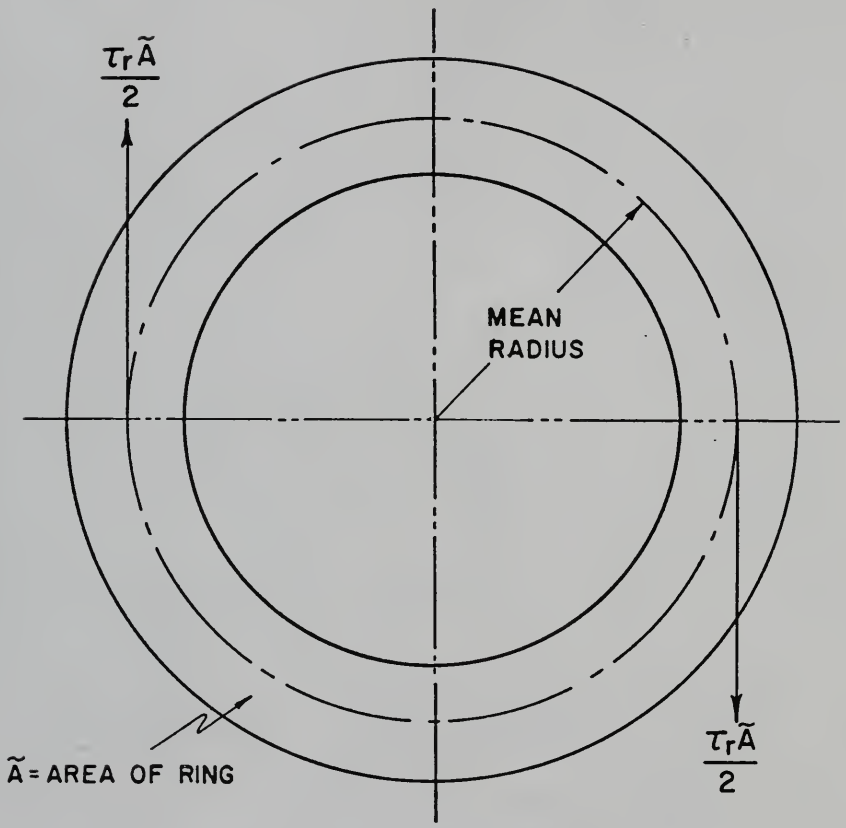

Fig. 3.2.5. Schematic Representation of Resultant Moment on Ring as well as False Bottom.

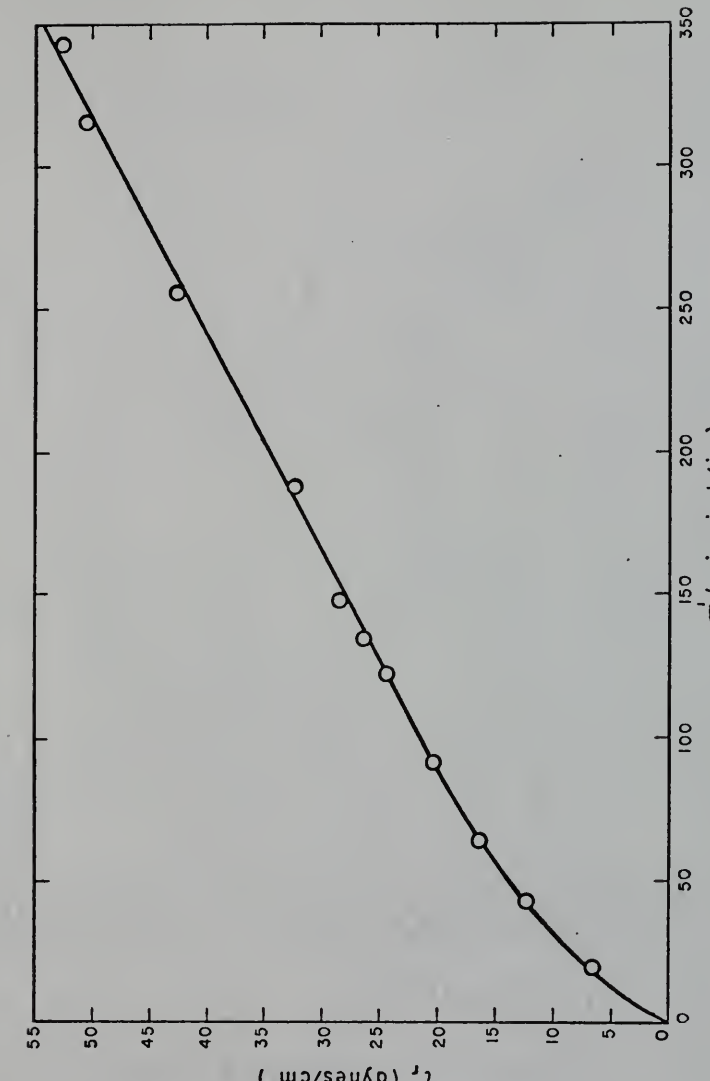

Fig. 3.2.6. Static Calibration of Ring.

gages on the support blade of the false bottom within the channel (see Section 3.1.2 for a description), and the existing set of slip rings on the inner shaft. This is essentially the case because the inner shaft and the channel rotate independently of each other. Initially, the additional required set of slip rings were in fact installed on the inner shaft for this purpose, but the simultaneous operation of two sets of slip rings introduced a significant noise in the measurements, so that this method had to be abandoned.

The alternate circuit, which did not involve the use of any slip rings, is shown in Fig. 3.2.7(b). It is also a four-arm Wheatstone bridge arrangement with two of its arms consisting of the two strain gages attached to one of the support blades of the false bottom. The other two arms each with a fixed resistance of 1 kiloohm, the potentiometer, the 1 KHz square wave generator and a signal amplifier were all included in a 7-1/2 x 5 x 3 in. metal box. The output was read on a Triplett voltmeter described in Section 3.1.2. The electrical wires connecting the strain gages to the metal box were passed through a small hole drilled in the outer wall of the channel, and the hole was sealed with a rubber cement to prevent water leak. The metal box and the voltmeter were installed beside the outer wall of the channel, on the lower flange, and were held in place by plexiglass brackets glued to the channel. This way, the dial on the voltmeter could be read from outside, and since the channel did not have to be rotated at too high a speed during the tests, the voltmeter dial could be read without difficulty, when the channel was in motion.

The arrangement of the two strain gages on the support blade

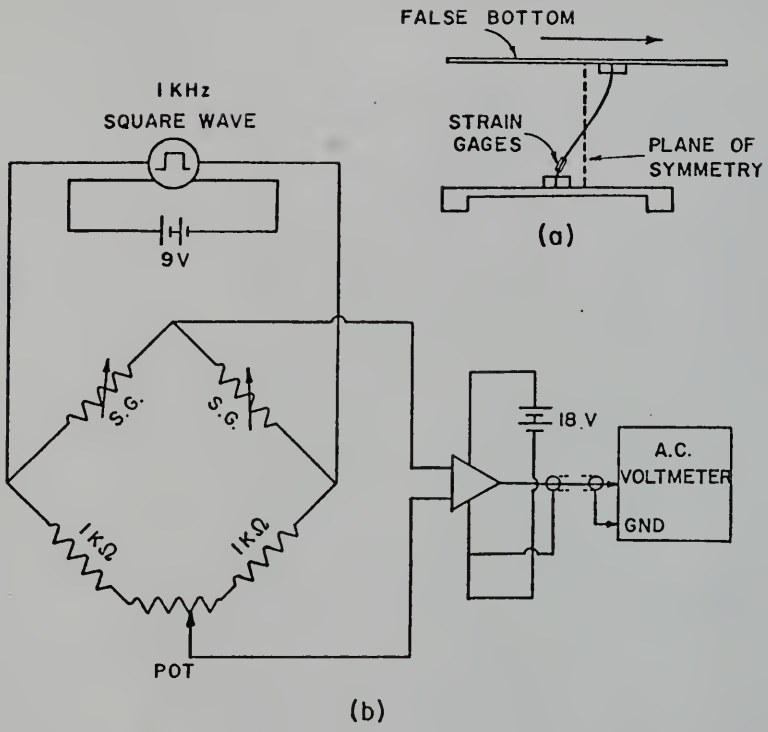

Fig. 3.2.7. (a) Bending of Blade Supporting False Bottom
(b) Circuit for Measurement of Strain Produced by Shear Stress on False Bottom.

is indicated in Fig. 3.2.7(a). Since the bending of the blade due to the shear on the false bottom is symmetrical by virtue of its position about a plane perpendicular to the false bottom, the highest bending moments are expected to occur near the clamped ends of the blade. For this reason the gages, one on each side, were centered and located as near the lower end of the blade as possible.

In the procedure for calibration, the channel was filled with water just enough to submerge the false bottom, and the special brackets shown on the left of Fig. 3.1.8 were positioned as shown and clamped there to the channel flange 180° apart from each other. The potentiometer in the metal box was used to zero the voltmeter reading, for the zero load condition. Loads were then applied as described in the procedure for the calibration of the annular ring, and a calibration curve was thus obtained between the voltmeter reading and the bed shear stress τ_b. Fig. 3.2.8 shows the calibration curve.

3.2.4 Calibration of Velocity Probes

Velocity profiles in the channel were determined with the help of Kent Miniflow Velocity Kit described in Section 3.1.2. For the velocity measurements, only the 10 mm probe No. 265-3 and the smaller 4 mm probe were used. A calibration curve for converting the D.C. indicator reading into linear velocity in cm/sec, for the 10 mm probe, was provided by the company, and is shown in Fig. 3.2.9. The two curves correspond to gains of 1 and 5 provided on the indicator.

For the 4 mm probe, since a calibration curve was not provided, it was calibrated according to the following procedure. A 3/4 in.

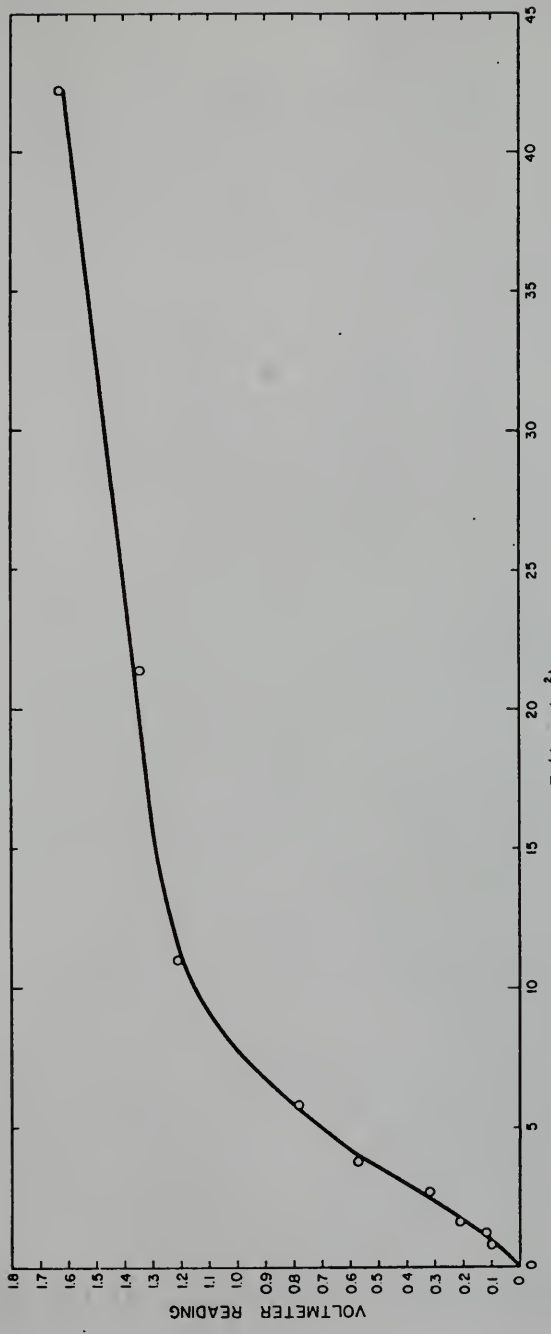

Fig. 3.2.8. Static Calibration of False Bottom.

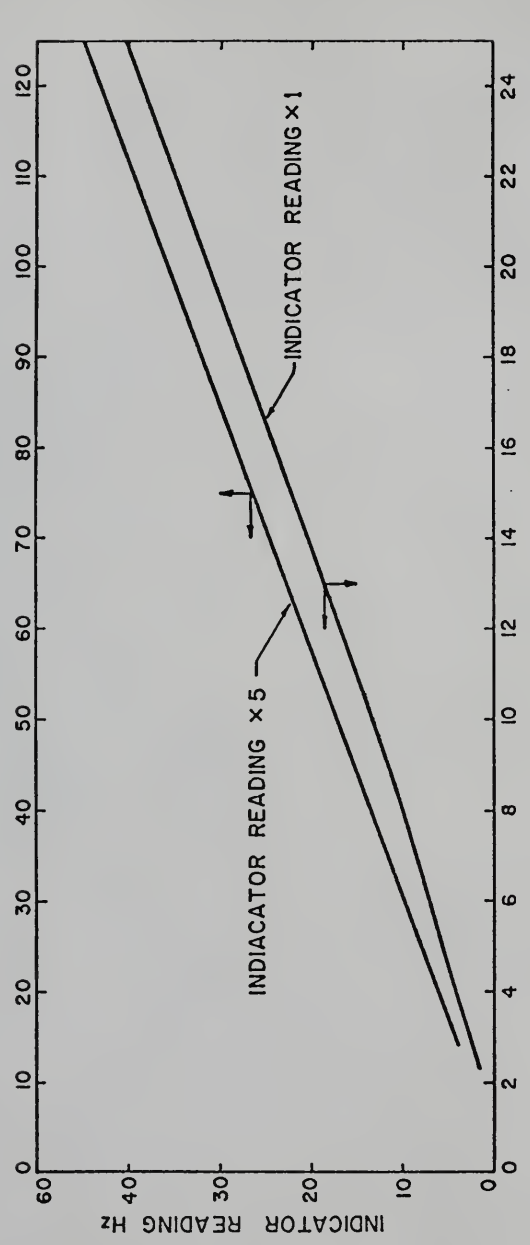

Fig. 3.2.9. Calibration Curves for 10 mm Velocity Probe.

diameter hole was made in the annular plexiglass ring, to insert the probe, and a plexiglass support stand was glued on that location to rigidly hold the probe in position at any elevation. A scale was provided on the stand and the probe elevation could be read by a pointed pin clipped on the probe, with the pin head touching the scale. The D.C. indicator itself was mounted on a bracket clamped to one of the radial steel arms supporting the ring. This way both the probe and the indicator could be rotated with the ring assembly. The scale on the indicator could be read without difficulty even when the ring was in motion. The 4 mm probe was suspended through the hole in the ring, such that its propeller was three or four inches below the water surface in the channel, which was filled to a depth of approximately eight inches. Then, while the ring was held stationary, the channel was allowed to rotate at a constant speed until a steady state was established, and the water inside moved together with the channel in a solid body rotation. This establishment of a solid body motion could be ascertained from the pointer on the indicator scale, when it no longer shifted with time. Then the angular speed of the channel was measured in rpm by a stopwatch. Now since the probe was located at the mean radius of 30 in. from the channel center, the linear velocity could be obtained from rpm by the expression

$$\text{Linear Velocity (cm/sec)} = 7.98 \times \text{speed in rpm} \qquad (3.2\text{-}16)$$

Measurements were taken at several different channel speeds. The resultant calibration curve for velocity u_p measured by the probe

is shown in Fig. 3.2.10. It should be pointed out that at comparatively high rotational speeds of the channel, the turbulent wake created behind the probe is likely to affect the velocity measured by the probe, if this wake is as long as the mean circumference of the channel, since the probe was located at the mean radius. At lower speeds, the wake will have a shorter length, since the turbulent energy associated with it will be smaller. A comparison of the velocity measured by the 4 mm probe and the 10 mm probe at selected elevations, when both the ring and the channel were rotating, showed a good agreement. This indicated that the effect of wake in the calibration of the 4 mm probe was not significant for the measured range of velocity.

3.2.5 Preparation of Sediment Suspension

a. Kaolinite Suspension: In order to prepare a kaolinite suspension in water of a given concentration, the desired amount of sediment was weighed and added to the bowl of the Hamilton Beach mixer described in Section 3.1.2, with enough water added to make a mixable slurry. The sediment was thoroughly mixed for about 5 min and was then added to the water in the channel. The annular ring was then raised as high as possible, and the electric mixer, also described in Section 3.1.2, was clamped to the supporting frame of the apparatus with its stirring blades at about mid-depth and centered between the walls of the channel. The high speed mixer was then operated for nearly 5 min while the channel was rotated simultaneously to disperse the sediment particles throughout the channel. The mixer was then removed and the ring lowered to the desired elevation, and additional

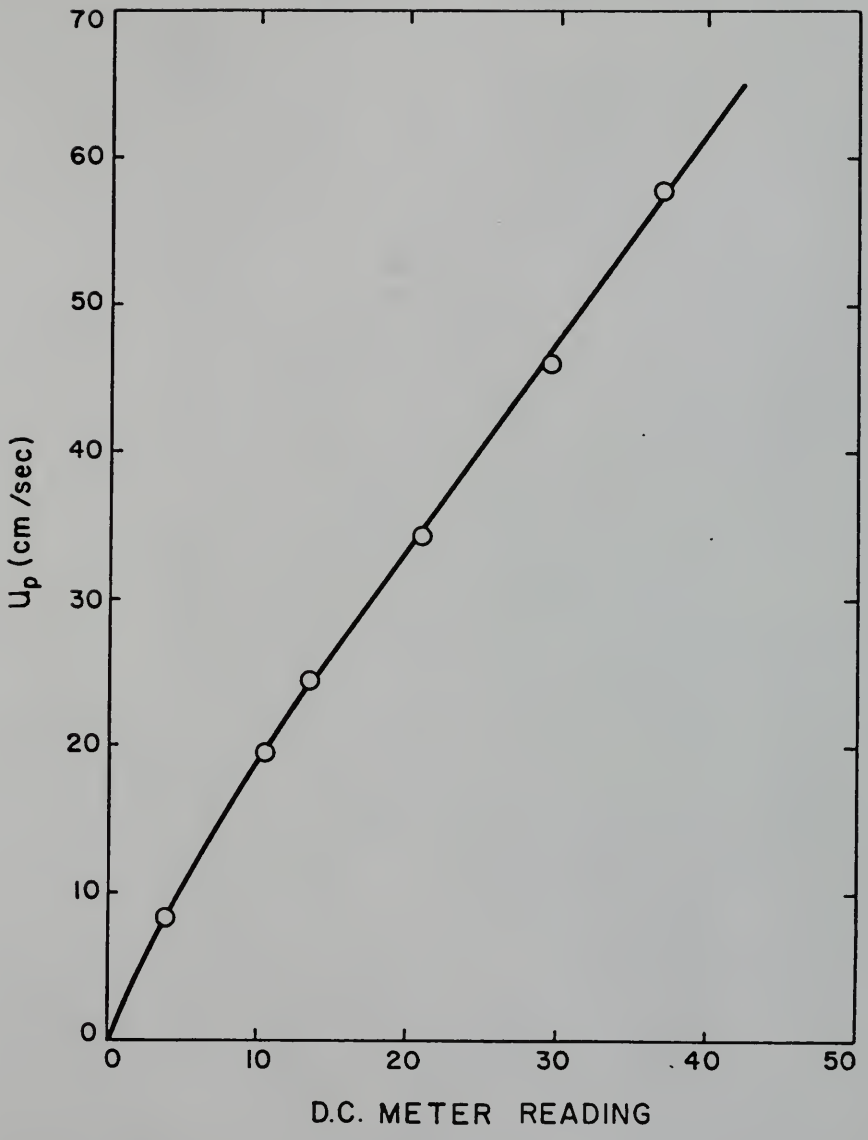

Fig. 3.2.10. Calibration Curve for 4 mm Velocity Probe.

water added to the channel, until the entire lower surface of the ring touched the water surface.

b. Bay Mud Suspension: The Bay mud samples used were stored in polyethylene bottles and submerged in water, since if the mud is dried for weighing purposes and then dispersed in water again, the process of dispersion is not complete, and consequently, its depositional properties are altered, as indicated by Krone (1962). Therefore, wet mud itself was weighed and added to the channel for obtaining a mud suspension. The bulk weight of the wet mud was found to contain nearly 33% solids. Therefore, to make a suspension of a given approximate concentration, wet mud of nearly three times the required dry weight was added to water in the channel. The remaining procedure is the same as that described for the kaolinite suspension.

3.2.6 Sample Extraction and Concentration Measurement

Sampling equipment including taps and bottles is described in Section 3.1.2. The samples had to be withdrawn necessarily while the ring and the channel were in motion. Each time a sample was withdrawn, the volume removed was replaced by clear water through the refilling funnel. The average sample volume was 50 ml, and the volume of the channel filled to the minimum used depth of 6 in. is 148000 ml. Therefore, since the maximum number of samples removed in a given run did not exceed 20, the total replacement of clear water amounted to 0.7% of the total volume of water within the channel, which is an insignificant quantity. After nearly every sample withdrawal, an equal volume of water was replenished through the refilling

funnel, so that the entire surface of the ring was in contact with water at all times.

The withdrawn samples were stored in numbered glass bottles with plastic caps. The Millipore equipment described in Section 3.1.2 was used for filtering the samples. 10 to 30 ml of the samples, depending on their sediment concentration, were filtered and the filter papers with the filtered wet sediment were placed on watch glasses and dried in an oven for 1/2 hour at 105°C. The dried samples were placed in a desiccator containing silica gel as a demoisturizer, cooled, and then weighed in a single-pan electronic digital balance which was accurate up to four decimal places. Knowing the sample volume used and the weight of the dry sediment, the concentration was then calculated in parts per million (ppm).

3.2.7 Procedure for Deposition Tests

To begin a test for time-concentration measurements at a given operational speed, initial sediment concentration and depth of flow, the ring and channel were rotated at high speeds to insure a complete suspension of the sediment. At these high speeds, two sediment samples were withdrawn to obtain a mean of the initial suspended concentration. The speeds were then lowered within 10 sec to the operational speed values, at which point a stopwatch began registering the time of deposition. The first sample was then withdrawn usually at 30 sec.

During the test runs, water temperature was noted three or four times from a thermometer placed in a beaker full of water. The

room temperature was maintained at around 20°C with the help of a heater and an air-conditioner.

CHAPTER 4

RESULTS OF INVESTIGATION

4.1 Preliminary Measurements

4.1.1 Indirect Bed Shear Stress Measurement

The measurement of the ring shear stress τ_r in dynes/cm^2, for each value of the differential linear velocity ΔV in cm/sec between the ring and the channel (calculated at the point of mean radius of 30 in.) was carried out for two situations. In the first, the ring alone was rotated, while in the second, the ring and channel were rotated simultaneously at various operational speeds. However, the two situations are essentially similar when viewed in terms of the relationship between ΔV and τ_r, since the unbalanced secondary currents in the first case do not affect the results, as they generate a shear stress which is perpendicular to τ_r. Figs. 4.1.1(a) and (b) confirm this observation, where a careful observation indicates that while for comparatively low ΔV values, the data points show relatively greater scattering, no systematic effect of depth of flow on the measurements can be observed, within the limits of experimental error. The data points for depths varying from 4 to 12 in. are described by the single equation

$$\tau_r = 0.134(\Delta V)^{1.14} \qquad (4.1\text{-}1)$$

Now a balance of shear forces on the ring and on the channel boundaries gives

$$\tau_{ch} \cdot (2d + b) = \tau_r \cdot b \qquad (4.1\text{-}2)$$

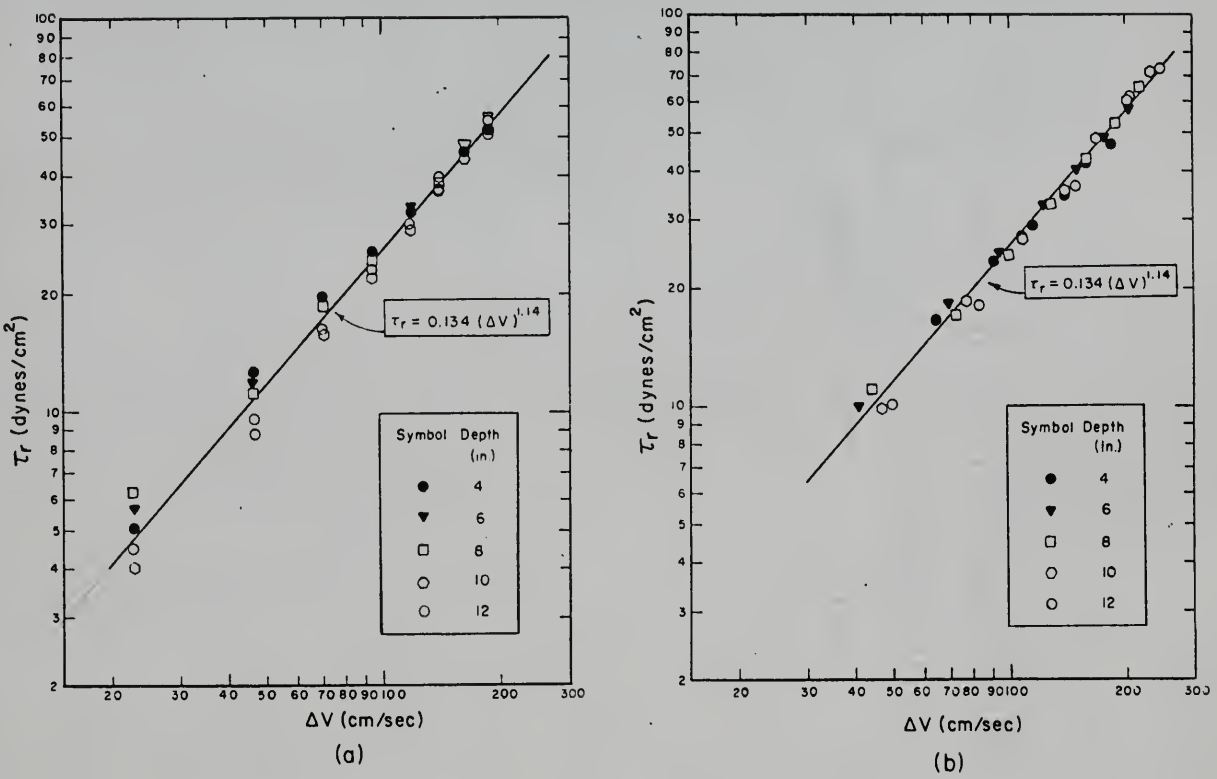

Fig. 4.1.1. (a) Ring Shear Stress τ_r Versus Differential Linear Velocity ΔV for Ring Only Rotating
(b) Ring Shear Stress τ_r Versus Differential Linear Velocity ΔV for Ring and Channel Rotating Simultaneously.

where τ_{ch} is the average shear stress on the channel boundaries, d is the depth and b is the width of the channel. Substituting Eq. (4.1-2) into Eq. (4.1-1) gives

$$\tau_{ch} = 0.134 \frac{(\Delta V)^{1.14}}{1 + 2\left(\frac{d}{b}\right)} \qquad (4.1\text{-}3)$$

Next, in order to obtain a relationship between the bed shear stress τ_b and ΔV, it is necessary to know the relation of τ_b to τ_{ch}. Such a relationship was obtained by Preston tube measurements of bed shear stress in the annular channel at M.I.T. (Partheniades, Cross and Ayora, 1968). Since for operational speeds the shear stress at the channel bottom was found to be almost uniform across the channel width, measurement taken at the centerline of the channel was considered to be representative of the average bed shear stress τ_b. The expression obtained was

$$\tau_b = 0.258(\tau_{ch})^{1.2} \qquad (4.1\text{-}4)$$

where the shear stresses are expressed in dynes/cm^2. Assuming the validity of Eq. (4.1-4) for the present larger but similar channel, substitution into Eq. (4.1-3) gives

$$\tau_b = 0.0231\left[\frac{(\Delta V)^{1.14}}{1 + 2\left(\frac{d}{b}\right)}\right]^{1.2} \qquad (4.1\text{-}5)$$

Eq. (4.1-5) may be used to calculate τ_b in dynes/cm^2 for a given ΔV in cm/sec, and given d/b ratio.

4.1.2 Direct Bed Shear Stress Measurements

Initially, the experimental results on the equilibrium concentration and the deposition rates were correlated with bed shear stresses obtained from Eq. (4.1-5). However, this equation: (1) is based on an indirect method for obtaining the bed shear stress through Eqs. (4.1-1) and (4.1-2), (2) employs an empirical expression (Eq. (4.1-4)) derived from measurement in another apparatus, (3) assumes that a Preston tube correctly measures shear stresses near the bed, and (4) assumes that measurements taken at the centerline of the channel represent the average shear stress on the bed. Since these aspects of Eq. (4.1-5) make its applicability somewhat questionable, a direct method of obtaining bed shear stress by the false bottom, described in Section 3.1.2, was employed. The procedure for false bottom calibration is given in Section 3.2.3. The measurements carried out at depths of 6, 9 and 12 in. and for various operational values of the differential linear velocities ΔV are plotted in Fig. 4.1.2. On the log-log plot, the data points appear to indicate the following relationships:

For 6 in. depth

$$\tau_b = 0.022(\Delta V)^{1.15} \qquad (4.1\text{-}6)$$

For 9 in. depth

$$\tau_b = 0.010(\Delta V)^{1.27} \qquad (4.1\text{-}7)$$

For 12 in. depth

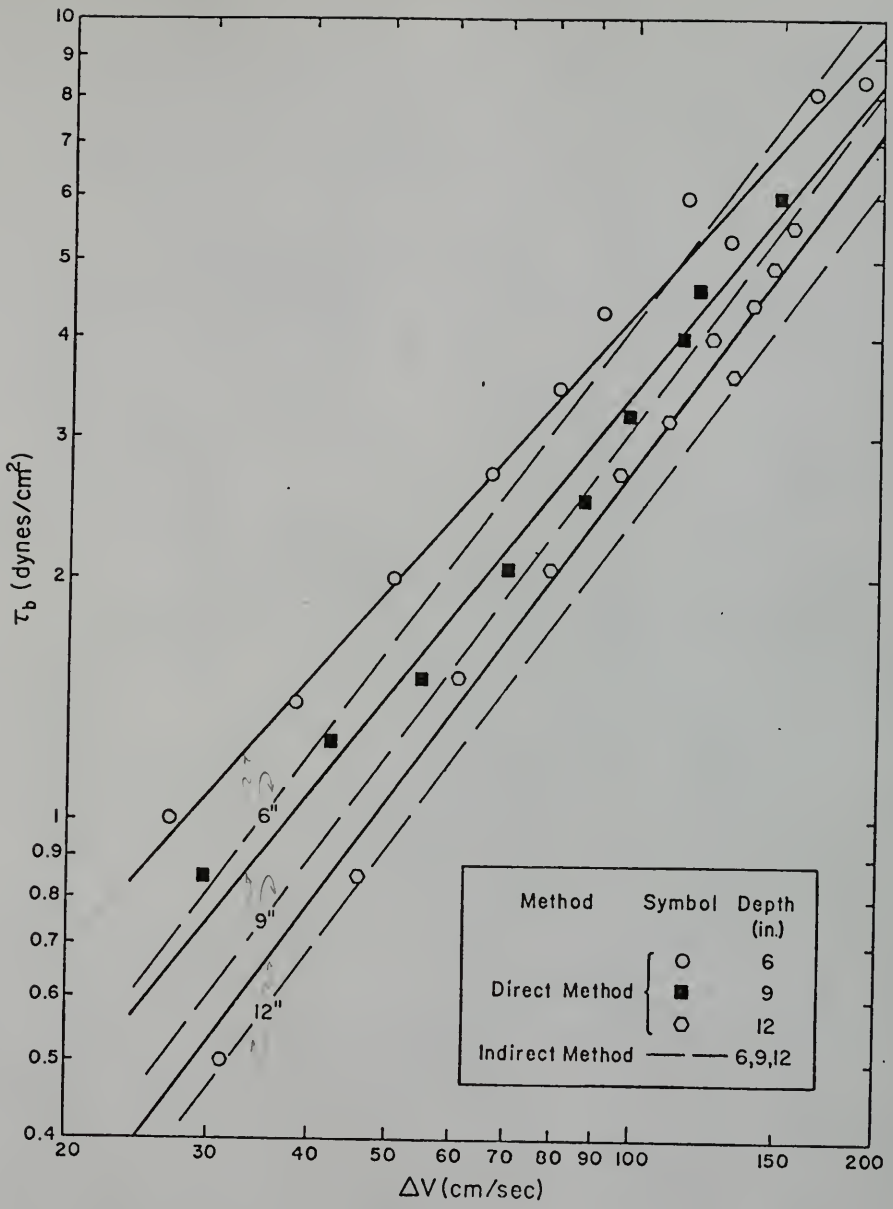

Fig. 4.1.2. Direct and Indirect Measurement of Bed Shear Stress τ_b Versus Differential Linear Velocity ΔV.

$$\tau_b = 0.005(\Delta V)^{1.37} \qquad (4.1\text{-}8)$$

where τ_b is in dynes/cm^2 and ΔV is in cm/sec. These relationships may be compared with Eq. (4.1-5), which is also plotted in Fig. 4.1.2 for 6, 9 and 12 in. depths. The similarity in the trends appears to attest to the validity of assumptions inherent in Eq. (4.1-5). However, direct measurements, which are more reliable, give somewhat higher shear stress values for all depths, below a ΔV of nearly 110 cm/sec. The same trend exists for 9 and 12 in. depths, above this value of ΔV, but for 6 in. depth, the trend is reversed, i.e., direct measurements give somewhat lower shear stress values compared to those obtained from Eq. (4.1-5).

In all deposition measurements use was made of Eqs. (4.1-6), (4.1-7) and (4.1-8) in computing the bed shear stresses.

4.1.3 Velocity Profiles

The calibration procedure for the velocity probes is given in Section 3.2.4. Velocity profiles measured for depths of 6-1/4 in. and 9 in. are given in Figs. 4.1.3 and 4.1.4, respectively, for indicated values of ΔV. Since the probes were attached to the ring, they measured velocities u_p relative to a zero velocity at the ring surface. In order therefore to obtain flow velocities u relative to a zero velocity at the channel bottom, as plotted in Figs. 4.1.3 and 4.1.4, the following conversion was used:

$$u = \Delta V - u_p \qquad (4.1\text{-}9)$$

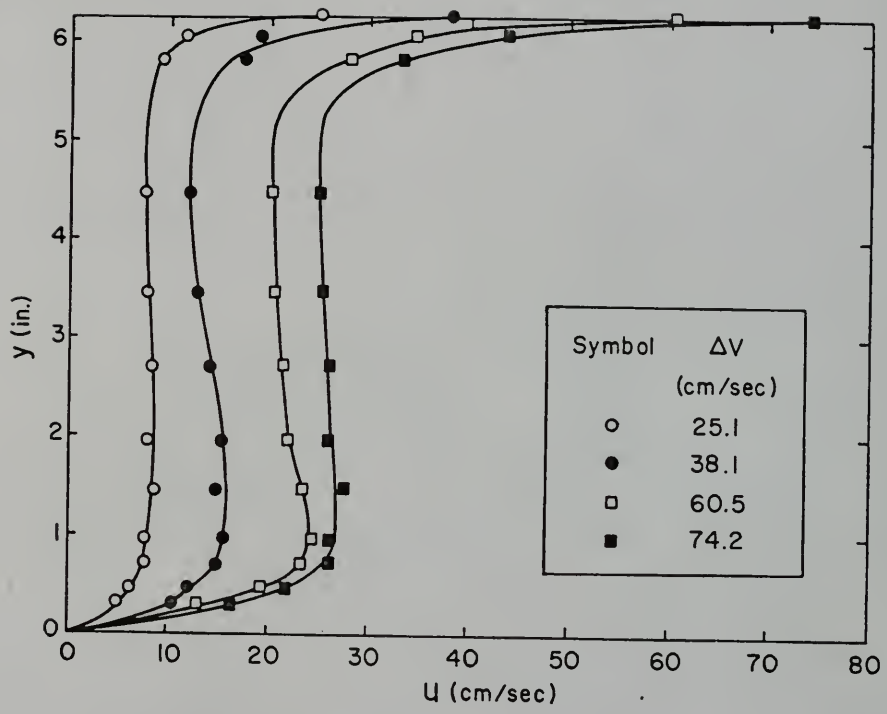

Fig. 4.1.3. Velocity Profiles for 6-1/4 in. Depth.

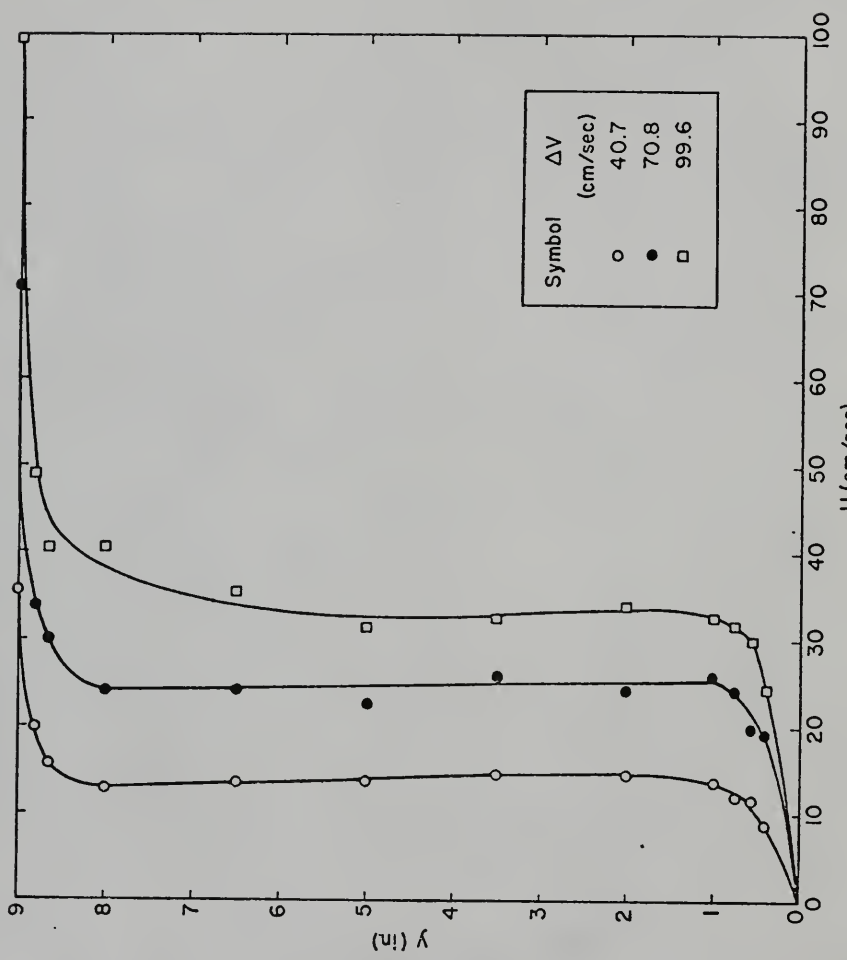

Fig. 4.1.4. Velocity Profiles for 9 in. Depth.

Velocity profiles could not be measured with sediment in suspension, because of the difficulties associated with using miniature propeller probes in sediment laden flows due to the interference of sediment particles.

Profiles for both depths resemble turbulent Couette flows (Schlichting, 1968), but unlike the latter, the measured profiles are not symmetrical about a horizontal plane at mid-depth, primarily because they are affected by the drag on the channel walls. Thus, for a given ΔV, the shear on the ring is higher than that on the channel bottom, according to Eq. (4.1-2). This is clearly observed from the profiles, in which the velocity gradients appear to be steeper near the ring as compared to those near the bottom. Another significant feature of these profiles is that they exhibit a relatively large middle zone of almost zero velocity gradient, which corresponds to a condition of a nearly homogeneous structure of turbulence in this zone. For measurements at 6-1/4 in. depth as well as 9 in. depth, this zone appears nearly one inch below the ring and one inch above the channel bottom. Such a condition implies that the total mean shear stress acting in this region is close to zero. It appears that the flow geometry, the highly turbulent condition, and particularly the secondary currents, though compensated in a gross sense, are the factors that effectively produce such a core of homogeneous turbulence.

Velocity profiles close to the bottom tend to indicate a logarithmic law similar to that in open channels. As examples, two of the profiles for 6-1/4 in. depth (and ΔV of 25.1 and 38.1 cm/sec) are plotted in Fig. 4.1.5 for y less than 1-1/2 in. The profiles

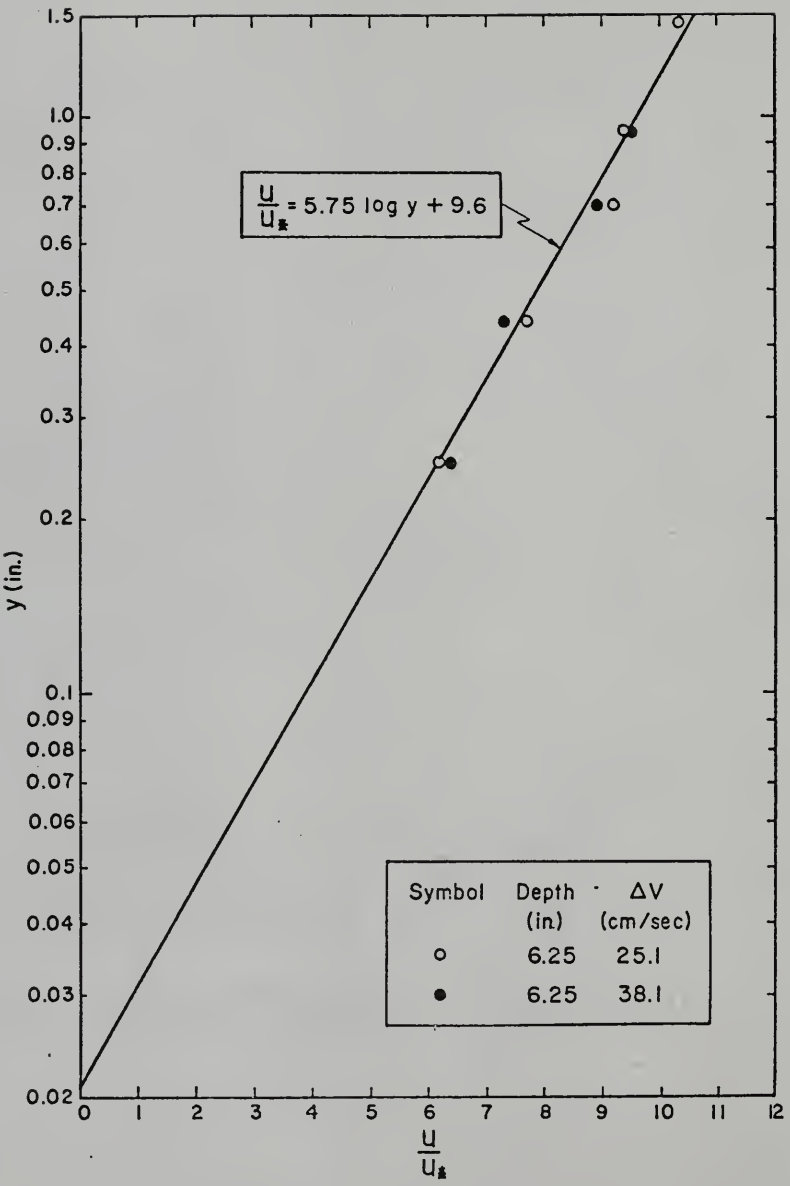

Fig. 4.1.5. Near-bed Velocity Profiles.

appear to correspond to a fully rough flow condition (rather than a smooth one) given by the general expression

$$\frac{u}{u_*} = \frac{1}{\kappa} \ln \frac{y}{y_o} \qquad (4.1\text{-}10)$$

with $\kappa = 0.40$, and the virtual origin of the profile $y_o = 0.021$ in. In Table 4.1.1, bed shear stresses τ_{bv} obtained from u_* values for these profiles are compared with τ_{bf} obtained by the false bottom. It is observed from the last column of Table 4.1.1 that the shear stresses obtained from the velocity profiles do not agree well with those measured by the false bottom. One of the reasons for this is that there are no velocity measurements close enough to the bed to provide sufficiently accurate values of u_* and y_o. Accurate measurements close to the bottom were not possible because of the limitation imposed by the relatively large diameters of the propellers of the probes and because these had to be attached to the ring rather than the channel bottom, which made it necessary to keep them slightly above the bottom to prevent them from rubbing against the bottom surface.

TABLE 4.1.1

Depth (in.)	ΔV (cm/sec)	u_* (cm/sec)	τ_{bv} (from vel. profile) (dynes/cm^2)	τ_{bf} (from false bottom) (dynes/cm^2)	$\frac{\tau_{bv} - \tau_{bf}}{\tau_{bf}} \times 100$
6-1/4	25.1	0.82	0.67	0.89	-25
6-1/4	38.1	1.65	2.71	1.43	+90

Fig. 4.1.6 is a plot of depth-averaged velocities u_m corresponding to the profiles of Figs. 4.1.3 and 4.1.4, plotted against the corresponding bed shear stresses measured by the false bottom. These average velocities were obtained from area measurements by a planimeter. It is noteworthy that the data points indicate a straight line relationship on the log-log plot, describing the law

$$\tau_b = 0.126\ u_m^{0.94} \qquad (4.1\text{-}11)$$

4.2 Deposition Measurements

4.2.1 Degree of Deposition

Initial extensive measurements on the rates of deposition were carried out using the commercial kaolinite described in Section 3.1.3, in distilled water, in which it readily flocculates. The primary purpose of these measurements was to investigate the hydrodynamic interaction between the settling flocs and the flow variables, by keeping the sediment type and water quality constant. Flow depths of 6, 9 and 12 in. were used. A few measurements were also taken at a depth of 13 in., primarily for ascertaining the nature of the depth-concentration profiles, which are described and discussed in Section 4.2.4. The initial suspended sediment concentration C_o was varied from nearly 1000 to 26000 ppm, while the bed shear stress τ_b was varied from approximately 0.40 to 11 dynes/cm^2.

Fig. 4.2.1 shows a set of time-concentration runs for a depth of 6 in. and C_o of 1005 ppm, for various values of ΔV and the corresponding τ_b values, as shown in the inset. Here, the ratio C/C_o,

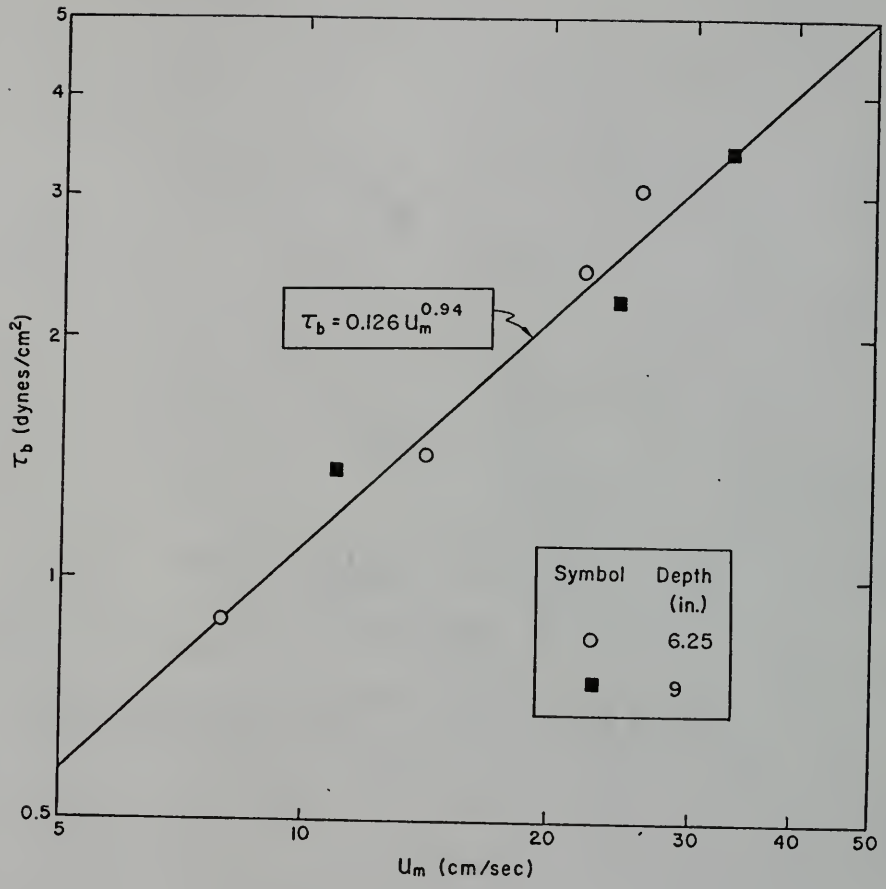

Fig. 4.1.6. Bed Shear Stress τ_b as Function of Depth-averaged Velocity u_m.

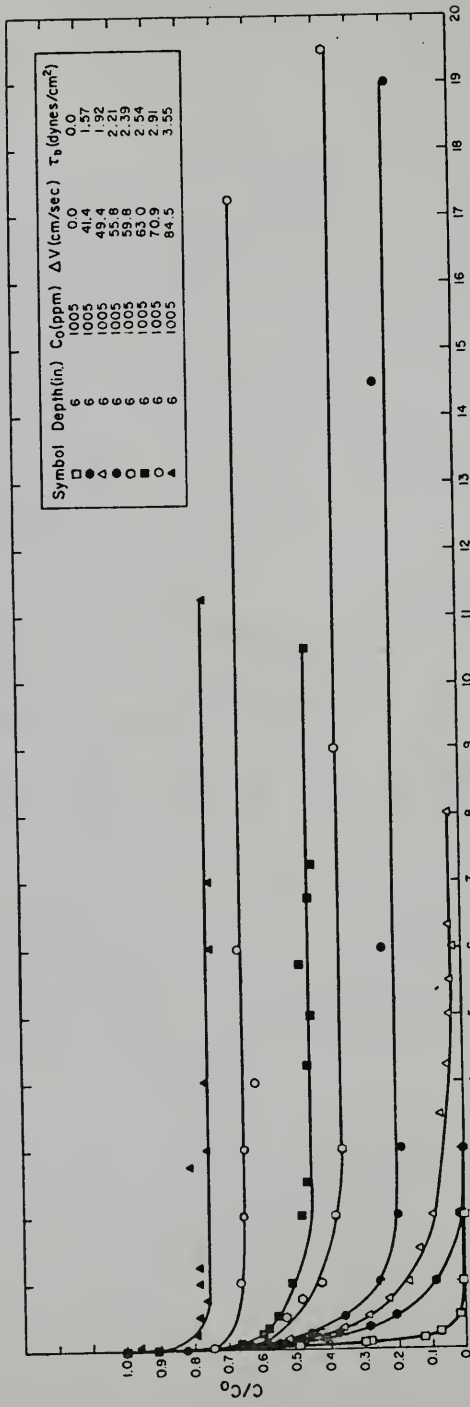

Fig. 4.2.1. Ratio C/C_o of Instantaneous to Initial Suspended Concentration Versus Time t for Kaolinite in Distilled Water.

where C is the suspended sediment concentration at time t is plotted against t in hours. The most interesting feature of these curves is that depending on the value of τ_b, the suspended sediment concentration reaches, after a relatively short transient period of deposition, a certain steady state value referred previously as equilibrium concentration.

In Fig. 4.2.2, the ratio C_{eq}/C_o, where C_{eq} is the equilibrium concentration, is plotted against the bed shear stress τ_b, for all the measurements similar to those of Fig. 4.2.1 taken at depths and ranges of C_o indicated in the inset. The data points appear to fall randomly about the indicated mean curve, which clearly suggests a unique dependence of C_{eq}/C_o on τ_b, and confirms the same observation made at M.I.T. by Partheniades, Cross and Ayora (1968), and also from the preliminary measurements made in the present annular apparatus by Partheniades and Mehta (1971). The curve of Fig. 4.2.2 also indicates the existence of a distinct minimum shear stress τ_{bmin}, below which no equilibrium concentration can exist, i.e., below which all the sediment must eventually deposit. For the measurements shown, $\tau_{bmin} = 1.80$ dynes/cm^2. It should be noted that the ratio C_{eq}/C_o may be referred to as "relative equilibrium concentration," while the ratio $(C_o - C_{eq})/C_o$, which represents the fraction of deposited sediment, may be called "the degree of deposition" (Mehta and Partheniades, 1973).

In Fig. 4.2.3, where $C^*_{eq} = C_{eq}/C_o$ and $\tau^*_b = \tau_b/\tau_{bmin}$, the data of Fig. 4.2.2 are plotted on logarithmic-normal coordinates. Here, the data points fall randomly about a straight line, which may

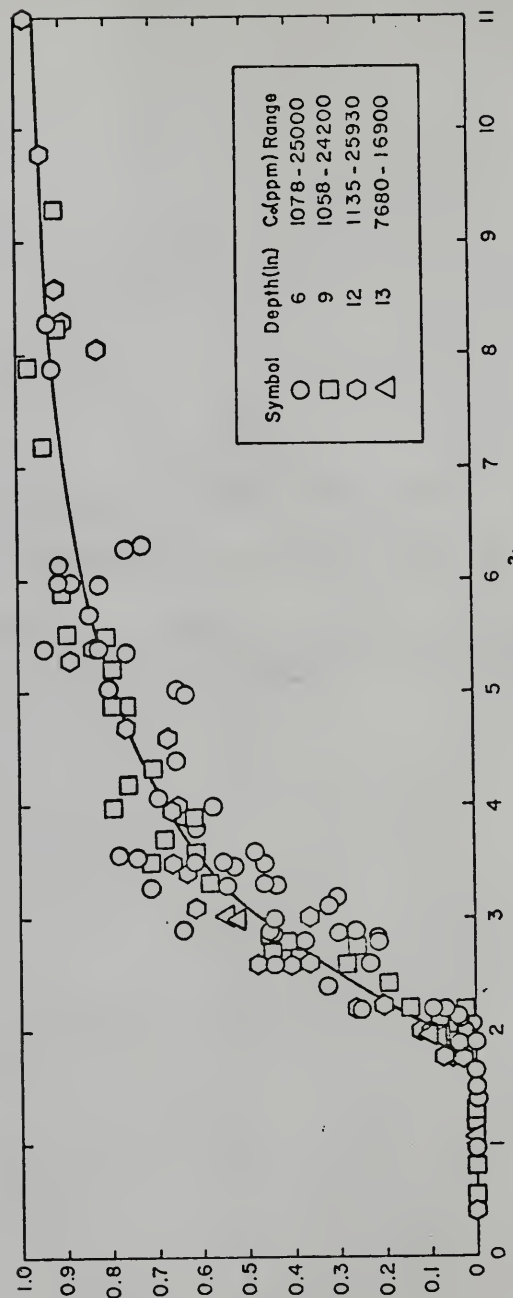

Fig. 4.2.2. Ratio of Equilibrium to Initial Concentration C_{eq}/C_o Versus Bed Shear Stress τ_b.

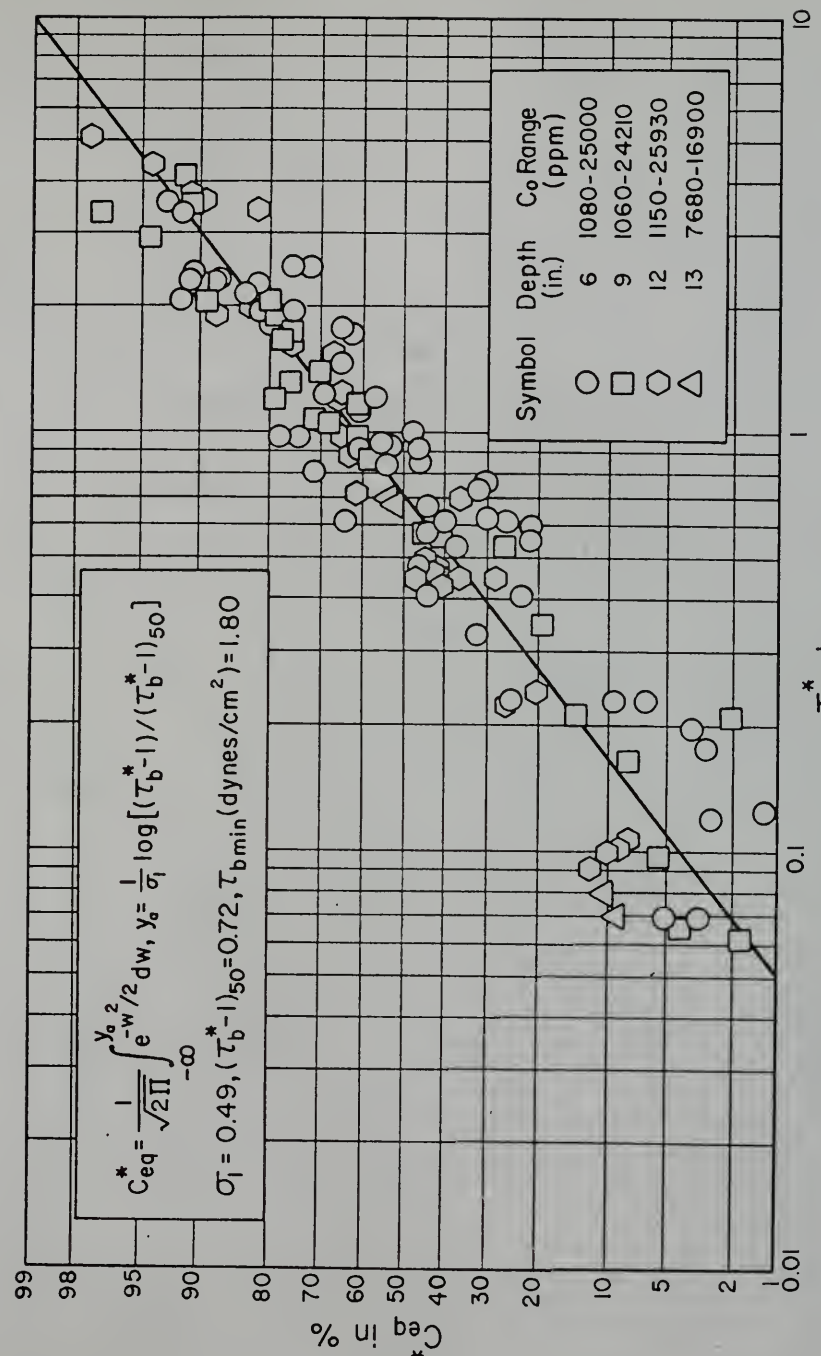

Fig. 4.2.3. Relative Equilibrium Concentration C^*_{eq} in Percent Against Bed Shear Stress Parameter $\tau^*_b - 1$.

be expressed as:

$$C^*_{eq} = \frac{1}{\sqrt{2\pi}} \int_{-\infty}^{y_a} e^{-w^2/2}\, dw \qquad (4.2\text{-}1)$$

where

$$y_a = \frac{1}{\sigma_1} \log[(\tau_b^* - 1)/(\tau_b^* - 1)_{50}] \qquad (4.2\text{-}2)$$

Here, σ_1 is the standard deviation, $(\tau_b^* - 1)_{50}$ is the geometric mean of the logarithmic-normal relationship and w is a dummy variable. For the data of Fig. 4.2.3, $\sigma_1 = 0.49$ and $(\tau_b^* - 1)_{50} = 0.72$. Corresponding to C^*_{eq} expressed by Eqs. (4.2-1) and (4.2-2), the degree of deposition, which may be designated by the symbol $C^{**}_{eq} = 1 - C^*_{eq}$, is also specified by the same equations. It must be pointed out that the straight line of Fig. 4.2.3 which corresponds to these given values of σ_1 and $(\tau_b^* - 1)_{50}$, was fitted to the data points by the method of least squares described in Appendix B.

In order to investigate the effect of physicochemical properties of different suspensions on the relative equilibrium concentration, two other types of sediments were tested, both in water at approximately 34000 ppm salt concentration, which is close to ocean salinity. One was the Bay mud described in Section 3.1.3, and the other was a mixture of 50% Bay mud and 50% kaolinite. The purpose of using such a mixture of two sediments was twofold. The first was to find out if such a mixture would behave as a single type of sediment with its own characteristic properties, or whether it would indicate, to some degree, the properties of the sediments it

was composed of. The second was to determine, in the event that it showed its own characteristic properties, its degree of deposition, and to compare it with that of its constituents. In Fig. 4.2.4, the data points for the Bay mud suspension (Series D at a depth of 6 in. and C_o = 3180 ppm) and the 50/50 mixture of Bay mud and kaolinite (Series C at a depth of 6 in. and C_o = 6360 ppm) appear to indicate linear relationships on the logarithmic-normal plot. These straight lines are very nearly parallel to the dashed line corresponding to the straight line of Fig. 4.2.3 for the kaolinite suspension. Thus all the lines appear to be characterized by a single value of the standard deviation $\sigma_1 = 0.49$, although the values of τ_{bmin} and $(\tau_b^* - 1)_{50}$ are different, as indicated in the inset. The results of Fig. 4.2.4 also indicate that the 50/50 mixture behaves as a unique sediment, with the degree of deposition characteristics that are intermediate between those of its constituents, i.e., kaolinite and Bay mud.

If the data of Fig. 4.2.4 are normalized with respect to the respective geometric means $(\tau_b^* - 1)_{50}$, the parallel lines of Fig. 4.2.3 must collapse into a single line. This is clearly observed from Fig. 4.2.5, in which several additional measurements from the annular apparatus are included, along with some reanalyzed data from previous experimental investigations. These additional measurements confirm the observation that a single value of $\sigma_1 = 0.49$ characterizes the data obtained by testing several different types of cohesive sediments. Values of τ_{bmin} and $(\tau_b^* - 1)_{50}$ for the various suspensions are as indicated. Here, Series A (at a depth of 6 in. and C_o = 6140 ppm) and

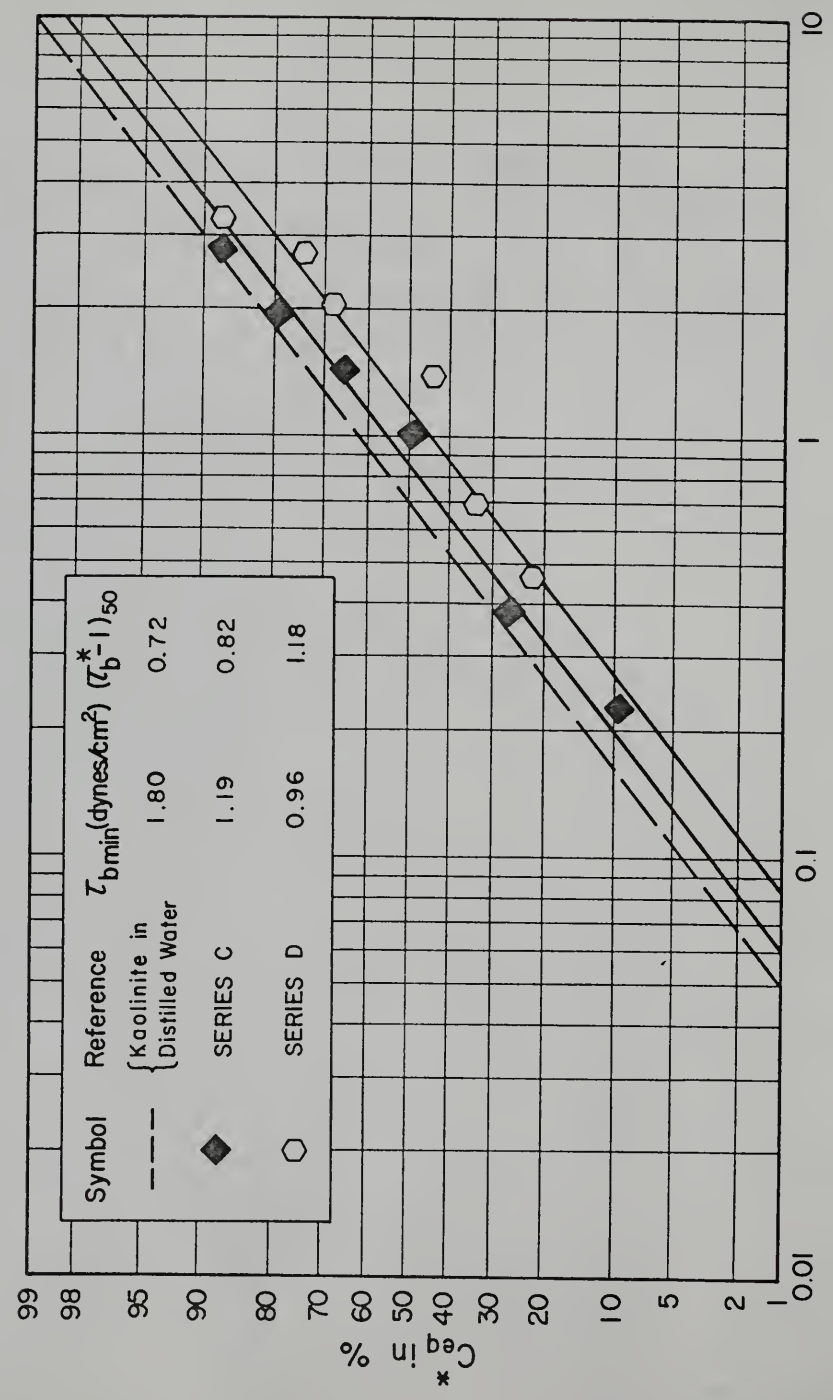

Fig. 4.2.4. Relative Equilibrium Concentration C_{eq}^* in Percent Versus $\tau_b^* - 1$ for Three Different Suspensions.

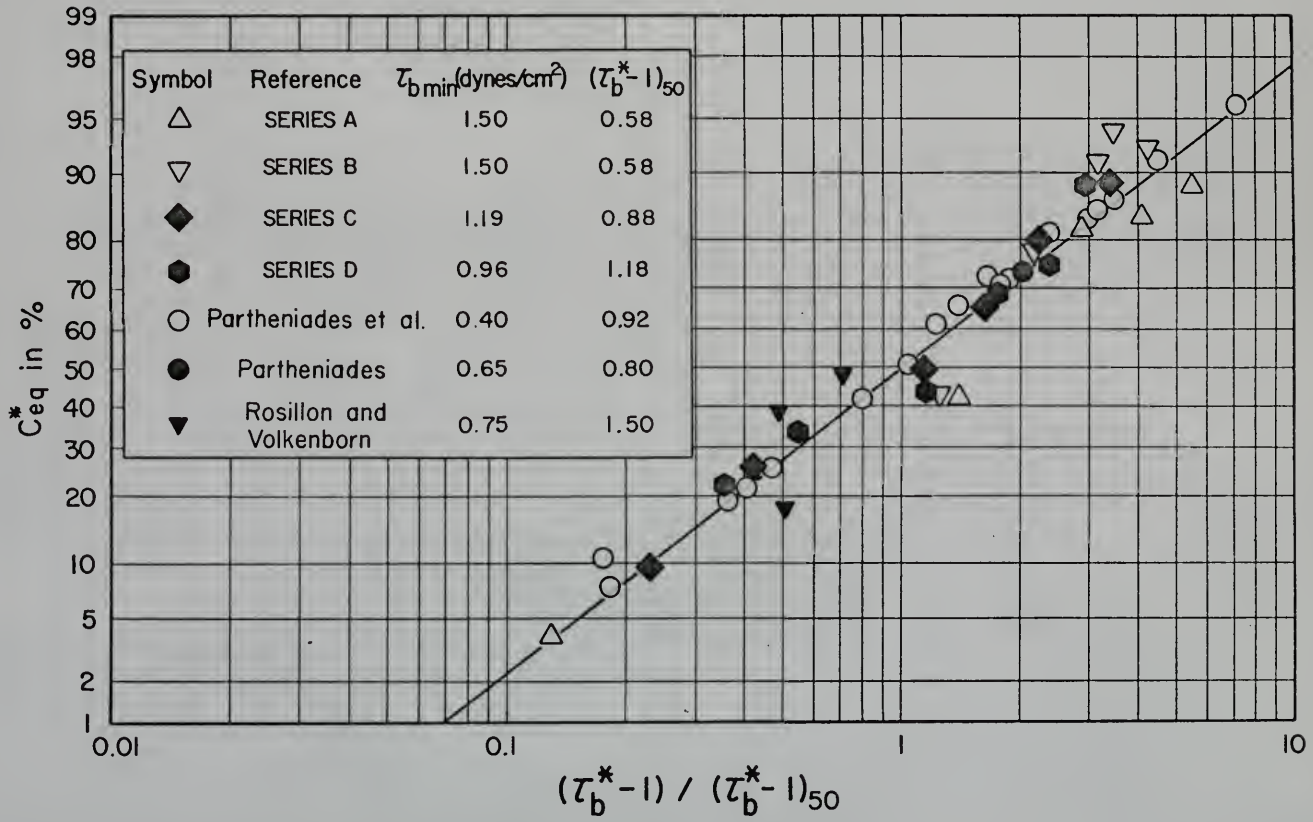

Fig. 4.2.5. Relative Equilibrium Concentration C^*_{eq} in Percent Against Bed Shear Stress Parameter $(\tau_b^* - 1)/(\tau_b^* - 1)_{50}$.

Series B (at a depth of 9 in. and C_o = 10270 ppm) correspond to measurements using kaolinite in salt water in the annular apparatus. Measurements of Partheniades et al. (1968) are for kaolinite in distilled water in the similar but smaller annular apparatus at M.I.T., described in Section 2.2.2. The single point of Partheniades (1965) is from experiments also mentioned in Section 2.2.2, using Bay mud in salt water in a straight flume. The value of $\tau_{bmin} = 0.65$ dynes/cm^2 for this measurement is obtained from Fig. 2.2.1. Finally, the data of Rosillon and Volkenborn (1964) were obtained from the Maracaibo sediment described in Section 3.1.3, also in a straight flume and in salt water.

For measurements taken in salt water, which correspond to an ambient water environment of constant quality, the parameters $(\tau_b^* - 1)_{50}$, and the bed shear stress τ_{b50} corresponding to $C_{eq}^* = 0.50$, for the different sediment suspensions are plotted against τ_{bmin} in Fig. 4.2.6. Parameters for the single data point of Partheniades (1965) are not included because a single point is not sufficient to obtain a representative value of $(\tau_b^* - 1)_{50}$. The curves of Fig. 4.2.6 show that $(\tau_b^* - 1)_{50}$ and τ_{b50} correlate with τ_{bmin}. Of course, τ_{b50} is related to $(\tau_b^* - 1)_{50}$, since

$$\tau_{b50} = [(\tau_b^* - 1)_{50} + 1]\tau_{bmin} \qquad (4.2\text{-}3)$$

The rather remarkably generalized law of Fig. 4.2.5 requires some elaboration. The parameter τ_{bmin} is indicative of the smallest floc size formed in a given sediment suspension. For example, for a suspension of kaolinite in salt water (Series A and B), $\tau_{bmin} = 1.50$

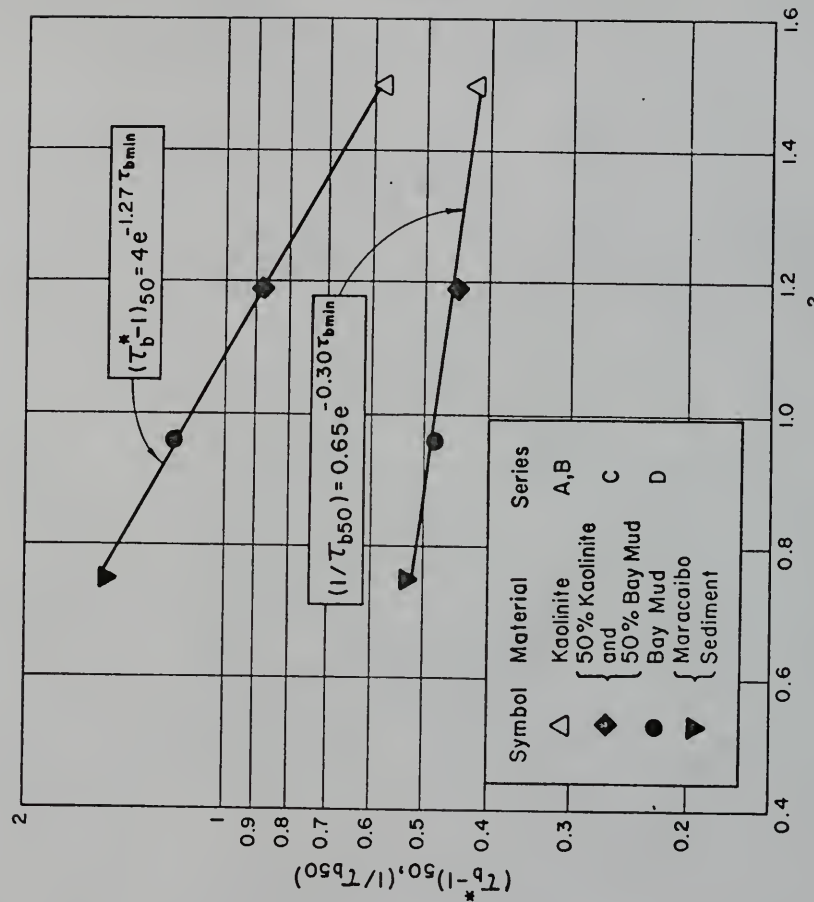

Fig. 4.2.6. Relationships Between τ_{bmin}, $(\tau_b^* - 1)_{50}$ and τ_{b50}.

dynes/cm^2, and for a suspension of Bay mud in salt water (Series D), τ_{bmin} = 0.96 dynes/cm^2, which implies that the smallest flocs of Bay mud are smaller than those of kaolinite, under the test conditions. Correspondingly, when the flocs in general are smaller, the bed shear stress required to maintain a given relative equilibrium concentration C^*_{eq} must be lower, as indicated by the parameter τ_{b50}, which has a lower value (2.09 dynes/cm^2) for the Bay mud suspension than for the kaolinite suspension (2.37 dynes/cm^2). This explains the trend of increasing τ_{b50} with increasing τ_{bmin} observed in Fig. 4.2.6, and also, as a consequence, the trend of decreasing $(\tau^*_b - 1)_{50}$ with increasing τ_{bmin}, by virtue of the relationship of Eq. (4.2-3), between $(\tau^*_b - 1)_{50}$ and τ_{b50}.

Fig. 4.2.5 shows that irrespective of the values of τ_{bmin} and $(\tau^*_b - 1)_{50}$, C^*_{eq} or equivalently the degree of deposition C^{**}_{eq} is uniquely determined by the parameter $(\tau^*_b - 1)/(\tau^*_b - 1)_{50}$. In practical terms this observation implies that the need to experimentally measure the equilibrium concentration at several bed shear stresses in order to determine the nature of the relationship between these two variables is eliminated, and only $_{bmin}$ is required to be determined, since, according to Fig. 4.2.6, τ_{bmin} alone is sufficient to define the degree of deposition.

It is noteworthy that since the variable y_a of Eq. (4.2-2) is normally distributed according to Eq. (4.2-1), from the table of normal probability integral (Dwight, 1965), one may obtain:

$$y_a\Big|_{C^*_{eq}=0.01} = \frac{1}{\sigma_1} \log[(\tau_b^* - 1)/(\tau_b^* - 1)_{50}]_1 = -2.33 \qquad (4.2\text{-}4)$$

and

$$y_a\Big|_{C^*_{eq}=0.99} = \frac{1}{\sigma_1} \log[(\tau_b^* - 1)/(\tau_b^* - 1)_{50}]_{99} = 2.33 \qquad (4.2\text{-}5)$$

so that for $\sigma_1 = 0.49$,

$$[(\tau_b^* - 1)/(\tau_b^* - 1)_{50}]_1 = 0.07 \qquad (4.2\text{-}6)$$

and

$$[(\tau_b^* - 1)/(\tau_b^* - 1)_{50}]_{99} = 13.9 \qquad (4.2\text{-}7)$$

Therefore, considering $C^*_{eq} = 0.01$ as the point of near-complete deposition and $C^*_{eq} = 0.99$ as the point of near-complete suspension of the sediment, it is observed that correspondingly, the degree of deposition C^{**}_{eq} varies from near-unity to near-zero value over a range of the variable $(\tau_b^* - 1)/(\tau_b^* - 1)_{50}$ from 0.07 to 13.9, which is a ratio of 1:199. This important observation precludes the existence of a single "critical" shear stress below which all the sediment deposits completely and above which all the sediment remains entirely in suspension, as suggested by Krone (1962).

When the ambient water quality is constant, it would seem reasonable that the physicochemical characteristics of different sediment suspensions could be described in terms of parameters that are representative of the physicochemical properties of the sediments themselves. Thus, in the case of salt water suspensions at sea water salinity, if the effect of relatively small amounts of ionic

constituents other than sodium and chloride ions, that might be derived from impurities present in the sediments themselves, are assumed to be insignificant, then the water quality of each of the tested sediment suspensions may be considered as invariant. One parameter that is characteristic of certain physicochemical properties of the sediment particles themselves, under such a condition of constant ambient environment, is the catio exchange capacity (CEC) described in Section 2.1.8, which is a measure of the cation adsorbing capacity of clay minerals. This adsorptive capacity is in turn indicative of the physicochemical forces that act on the surfaces and cleavage planes of clay particles, and therefore it may be considered as a measure of the interparticle forces that bind the clay particles together into flocs.

In Fig. 4.2.7, the parameters $(\tau_b^* - 1)_{50}$ and τ_{bmin} are plotted against the respective cation exchange capacities of the sediments. Here, the CEC of the 50/50 mixture of kaolinite and Bay mud is obtained as the mean of the CEC of kaolinite and of Bay mud. It may be observed that the data points for Bay mud, the 50/50 mixture and for kaolinite vary almost linearly with the CEC. The trend of increasing τ_{bmin} with CEC may be explained in terms of increasing strength of interparticle forces with increasing CEC, with the consequent formation of larger flocs, which in turn implies larger τ_{bmin} value, as mentioned previously. The same reasoning of course applies for the corresponding decreasing trend of $(\tau_b^* - 1)_{50}$ with the CEC, since $(\tau_b^* - 1)_{50}$ decreases with increasing τ_{bmin}, according to the relationship described in Fig. 4.2.6. The data from the Maracaibo

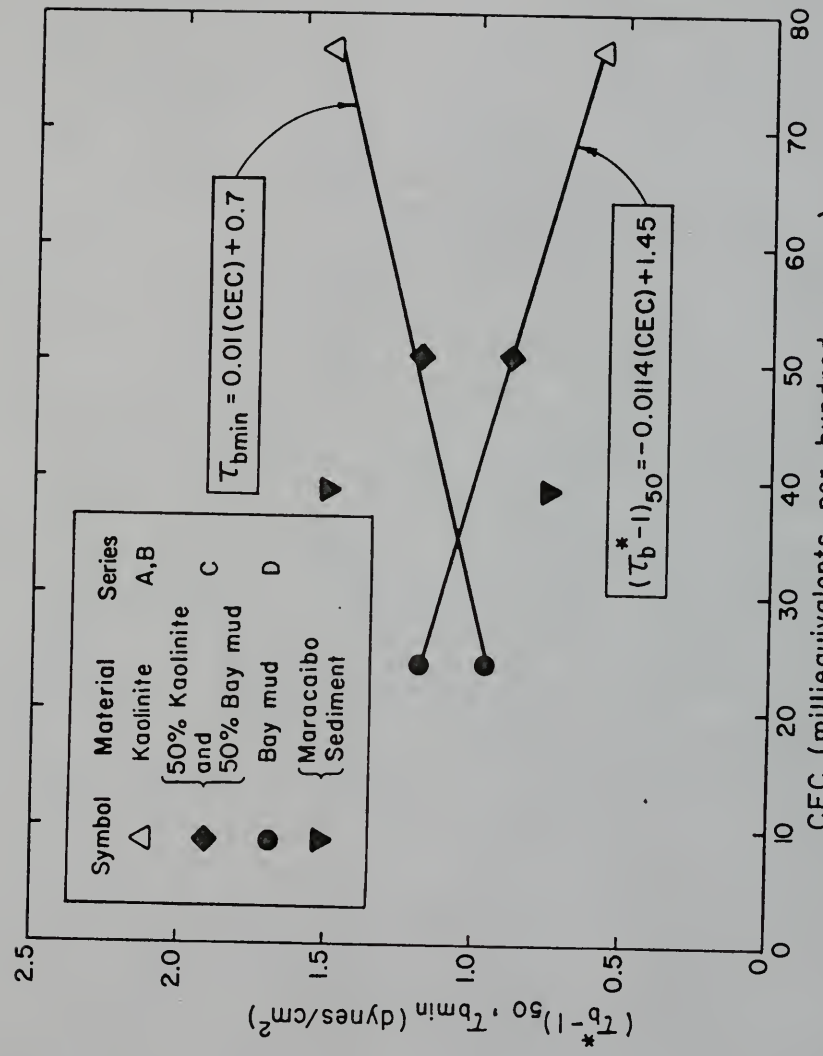

Fig. 4.2.7. Relationships Between $(\tau_b^* - 1)_{50}$, τ_{bmin} and Cation Exchange Capacity (CEC).

sediment tests do not agree with the other three, for which several reasons may be cited. One important difference lies in the fact that this sediment was tested in a straight flume, so that the results derived from it may not be quantitatively comparable with those obtained in the annular rotating apparatus, even though an apparent agreement is observed in Fig. 4.2.6. Moreover, the relatively small number of data points used to obtain values of $(\tau_b^* - 1)_{50}$ and τ_{bmin} for this sediment may not be large enough to give representative values of these parameters. Further, the value of CEC used for the sediment was obtained from samples (Appendix C) which were different from those used in the tests. It should be stressed that the CEC is mainly a property of clay minerals as was mentioned in Section 2.1.8, while the X-ray diffraction pattern of the less than 62 micron fraction shown in Fig. C.3 in Appendix C indicates that the predominant constituents of Maracaibo sediment are such non-clay minerals as quartz and calcite. Thus, the significance of CEC to correlate the data in such a case may be attenuated.

The measured CEC of 77 milliequivalents per hundred grams for kaolinite used in Fig. 4.2.7 is not in the normal range of 3 to 15 milliequivalents per hundred grams as mentioned in Section 3.1.3, for probable reasons noted therein. If, therefore, a mean value of 9 milliequivalents per hundred grams is used in the present case, the data of Fig. 4.2.7 may be replotted as in Fig. 4.2.8, which shows a relationship between all the four sets of data points. However, since an assumed value of CEC for kaolinite is used, the nature of this relationship must be considered as tentative.

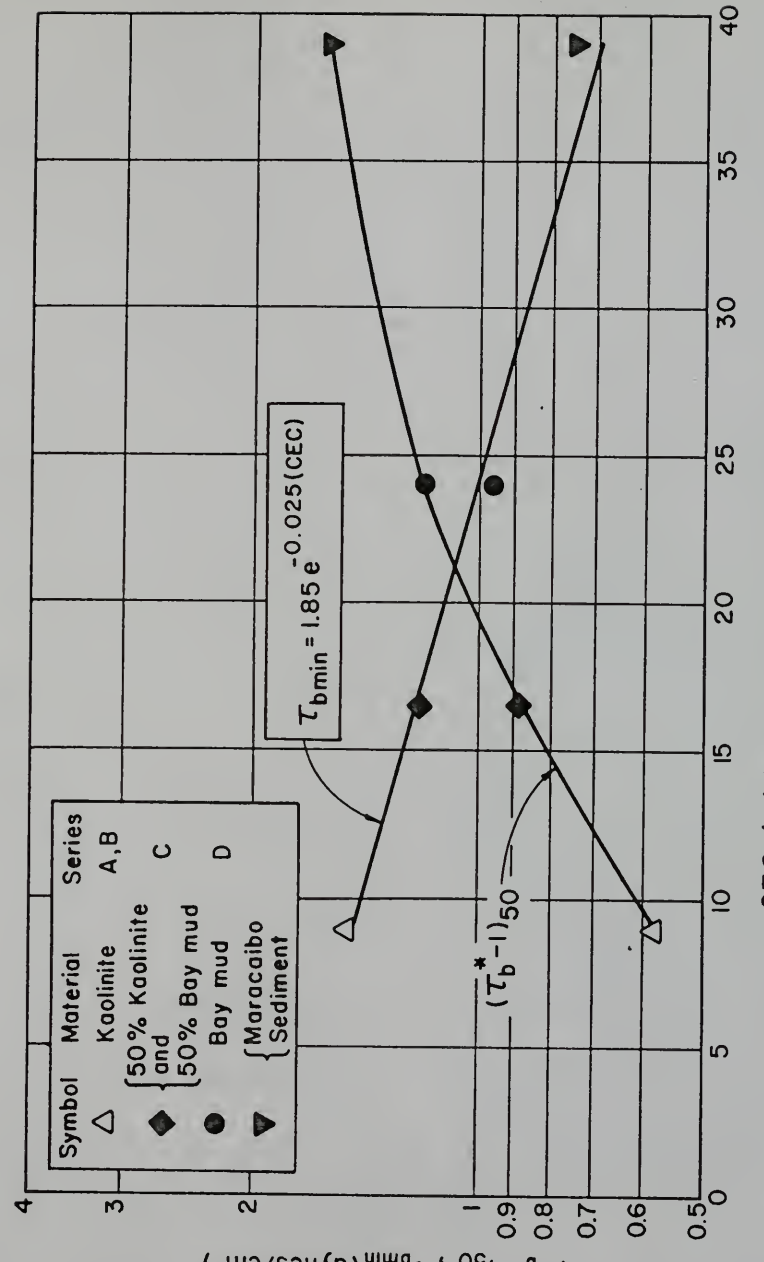

Fig. 4.2.8. Relationships Between $(\tau_b^* - 1)_{50}$, τ_{bmin} and Cation Exchange Capacity (CEC).

4.2.2 Deposition Rates

a. Rates in Distilled Water: As noted previously, the measurement of rates of deposition using kaolinite in distilled water was to ensure that the sediment and its ambient environment remained unchanged, so that the deposition measurements could throw light on the hydrodynamic interaction of sediment and flow in such a situation. Now since the equilibrium concentration C_{eq} indicates, for a particular flow condition, that fraction of the total initial concentration C_o which does not deposit, the fraction $(C_o - C)/(C_o - C_{eq})$ represents the fraction of the depositable sediment deposited at any given time. Correspondingly, the fraction $(C - C_{eq})/(C_o - C_{eq})$ is the fraction of depositable sediment which is in suspension at any given time. If the first fraction is designated by the symbol C^* and the second by C^{**} then clearly, since $C^{**} = 1 - C^*$, as the suspended sediment concentration C varies from its initial value of C_o to the final value of C_{eq} (which may or may not be zero depending on whether τ_b^* is less or greater than unity), the value of C^* changes from zero to unity, and correspondingly C^{**} varies from unity to zero.

In Figs. 4.2.9 through 4.2.27, the deposition rates are plotted on logarithmic-normal coordinates, in terms of C^* in percent as a function of the parameter t/t_{50}, where t is the time from the beginning of deposition, and t_{50} is the time corresponding to $C^* = 50\%$. Values of C_o, flow depth, τ_b^* and t_{50} for each of the runs are given in the insets. In Figs. 4.2.9 through 4.2.23, all runs, except one in Fig. 4.2.9, are for τ_b^* greater than unity, whereas in Figs. 4.2.24 through 4.2.27, the runs correspond to τ_b^* less than unity.

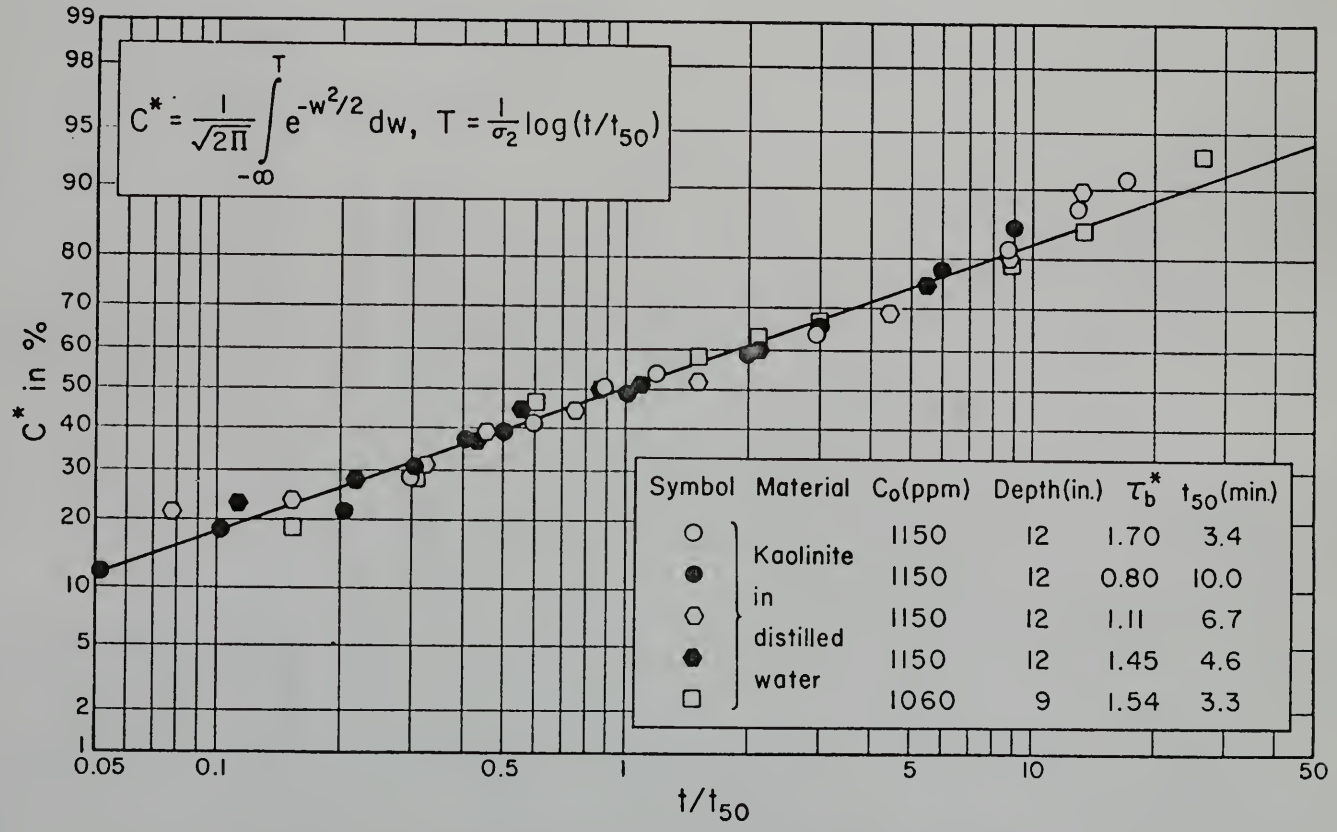

Fig. 4.2.9. Fraction of Depositable Sediment Concentration C^* Deposited at Time t, in Percent, Versus Time Parameter t/t_{50}, for Kaolinite in Distilled Water.

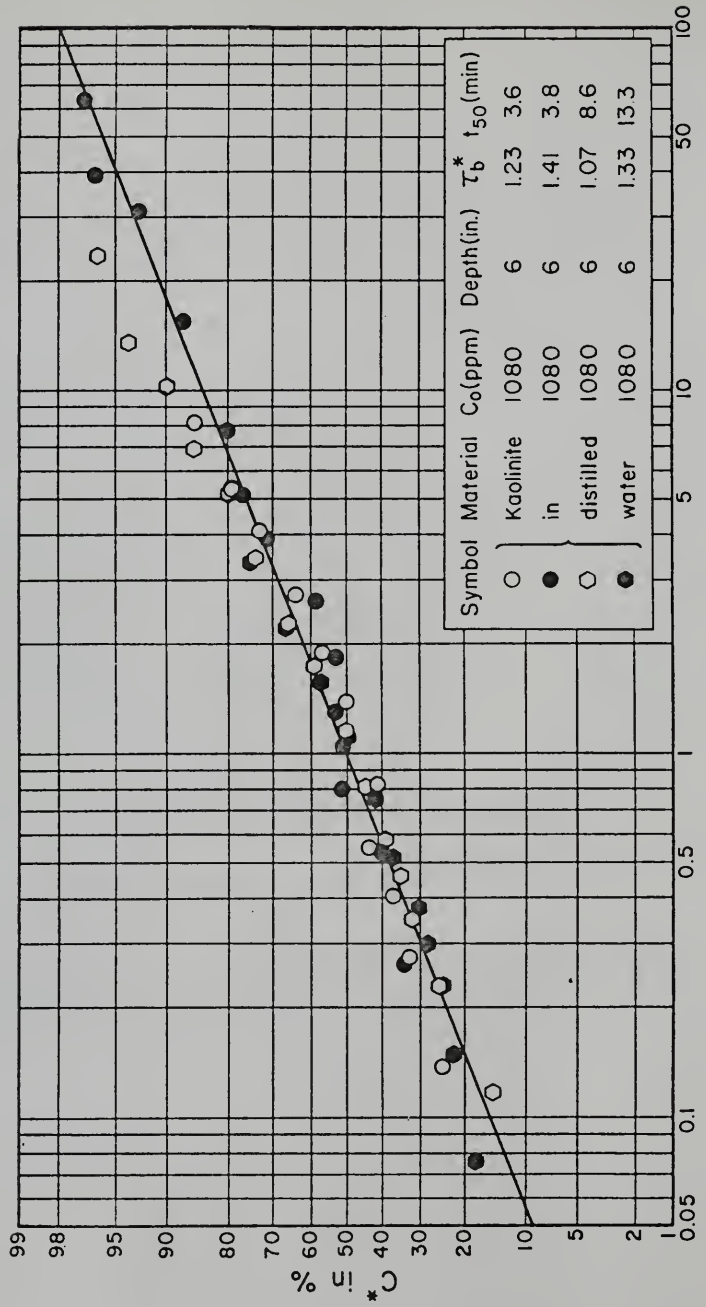

Fig. 4.2.10. C^* in Percent Versus t/t_{50} for Kaolinite in Distilled Water.

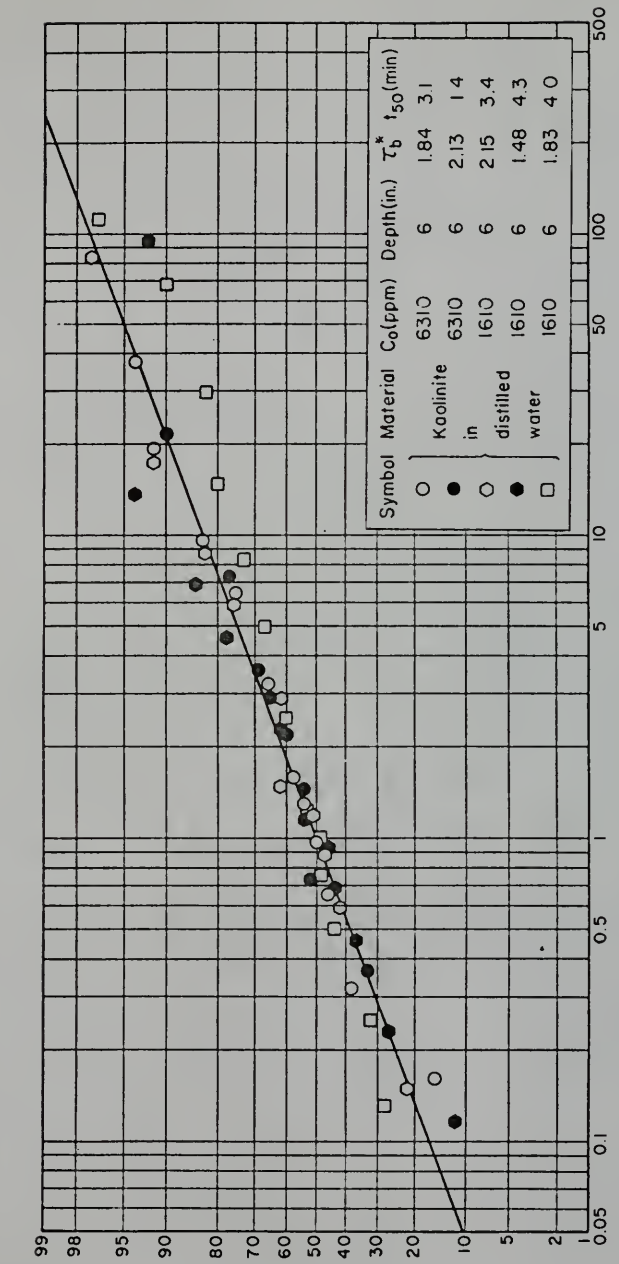

Fig. 4.2.11. C^* in Percent Versus t/t_{50} for Kaolinite in Distilled Water.

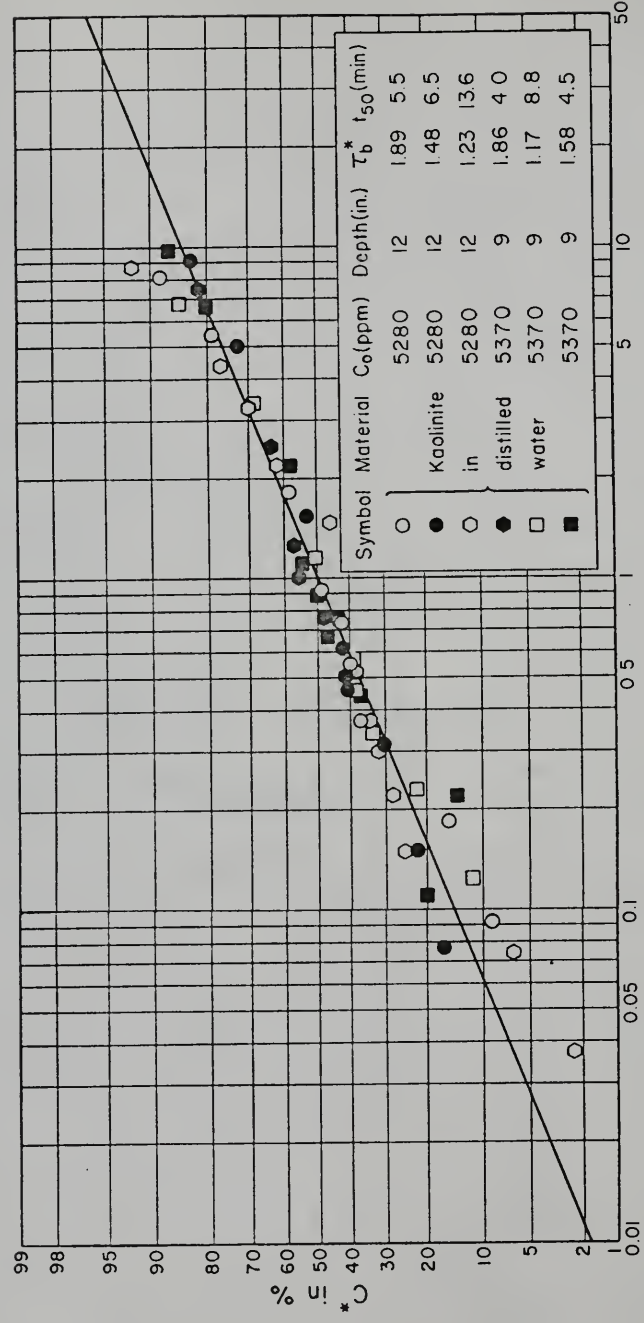

Fig. 4.2.12. C^* in Percent Versus t/t_{50} for Kaolinite in Distilled Water.

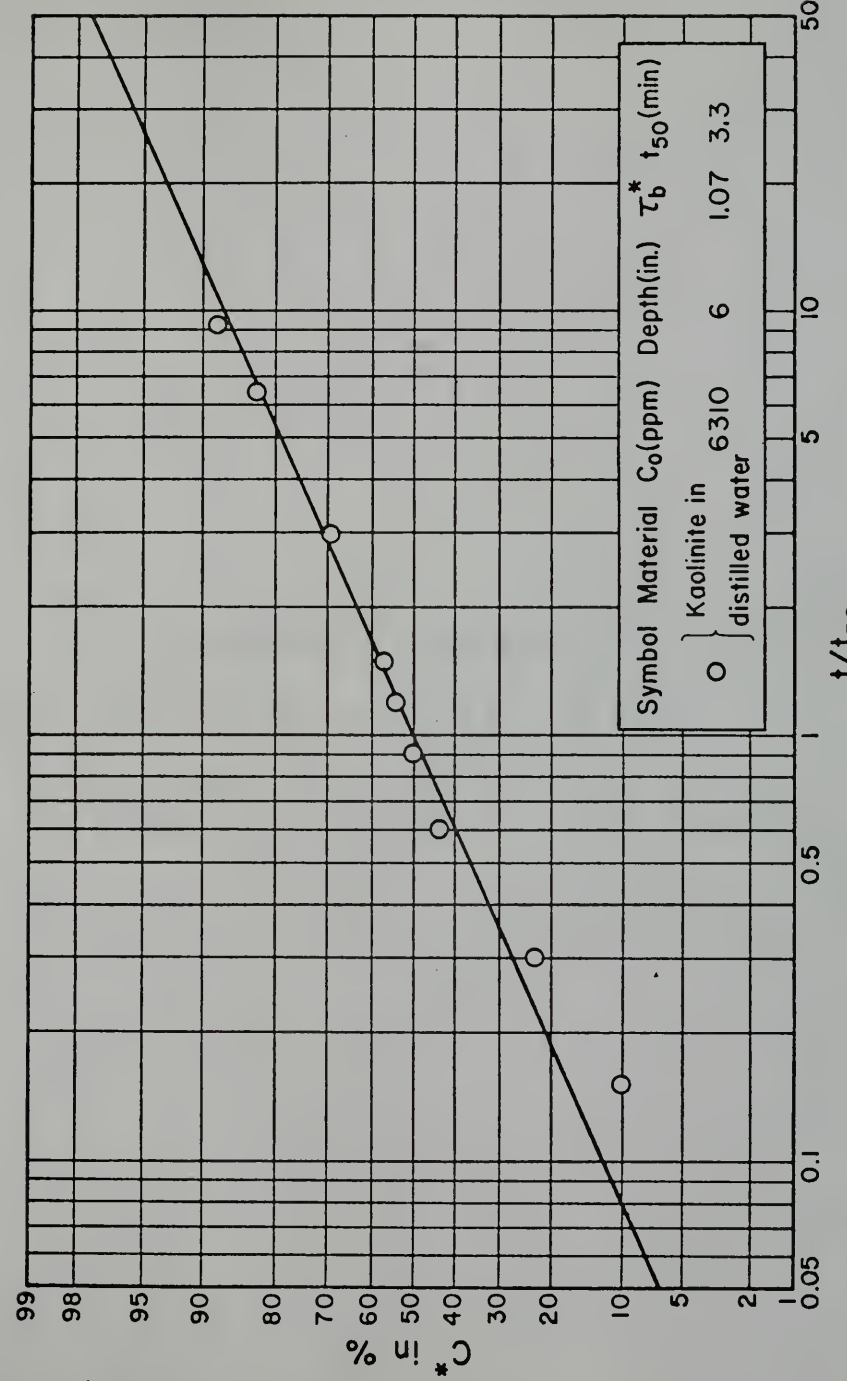

Fig. 4.2.13. C^* in Percent Versus t/t_{50} for Kaolinite in Distilled Water.

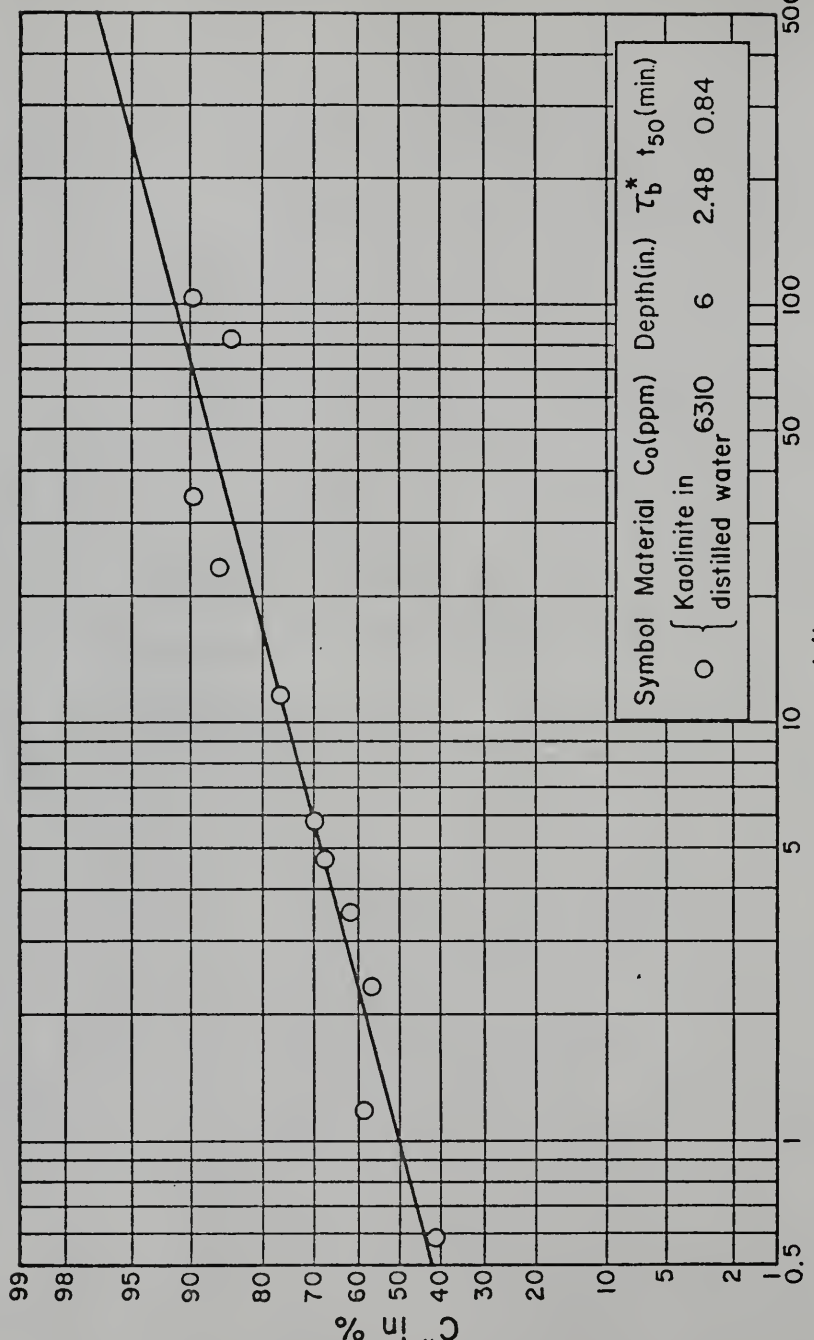

Fig. 4.2.14. C^* in Percent Versus t/t_{50} for Kaolinite in Distilled Water.

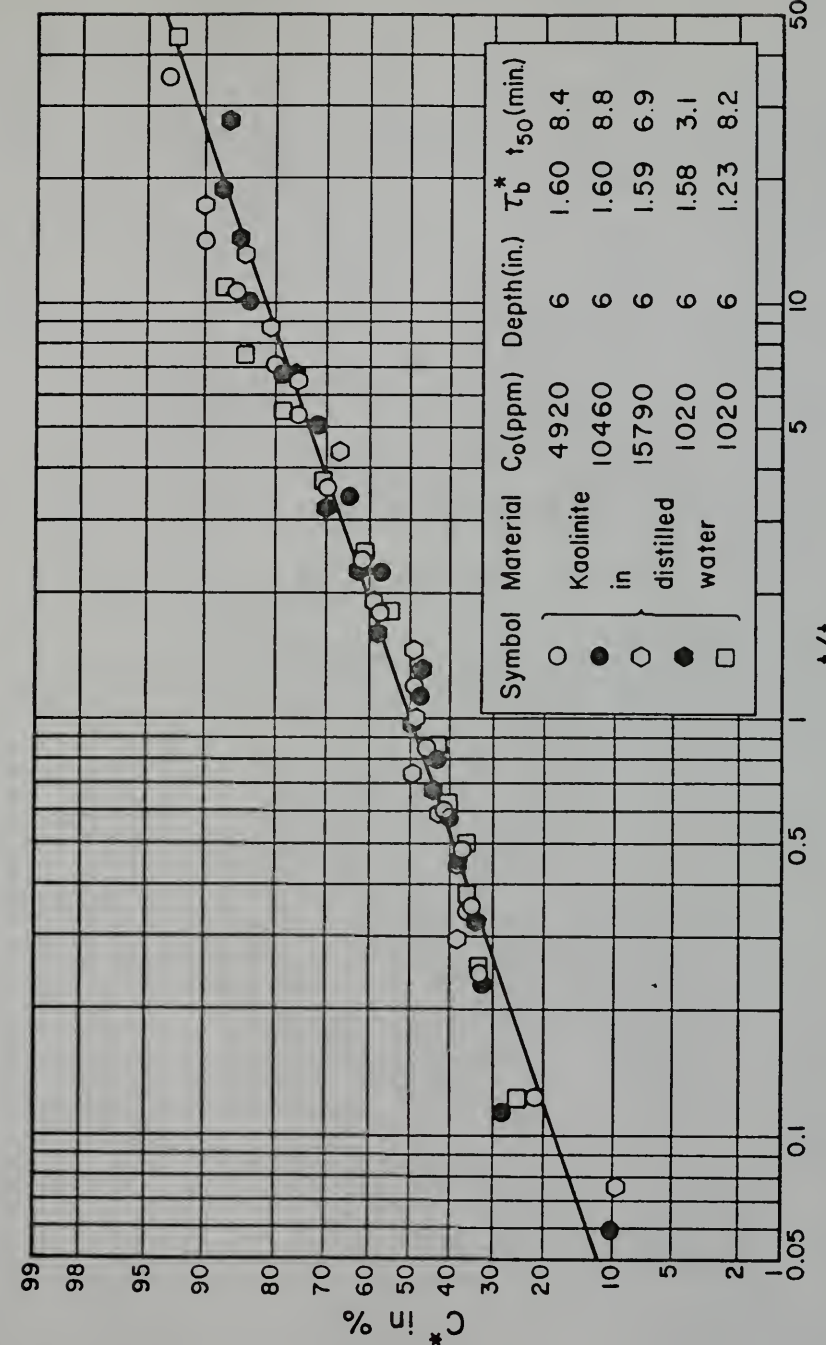

Fig. 4.2.15. C^* in Percent Versus t/t_{50} for Kaolinite in Distilled Water.

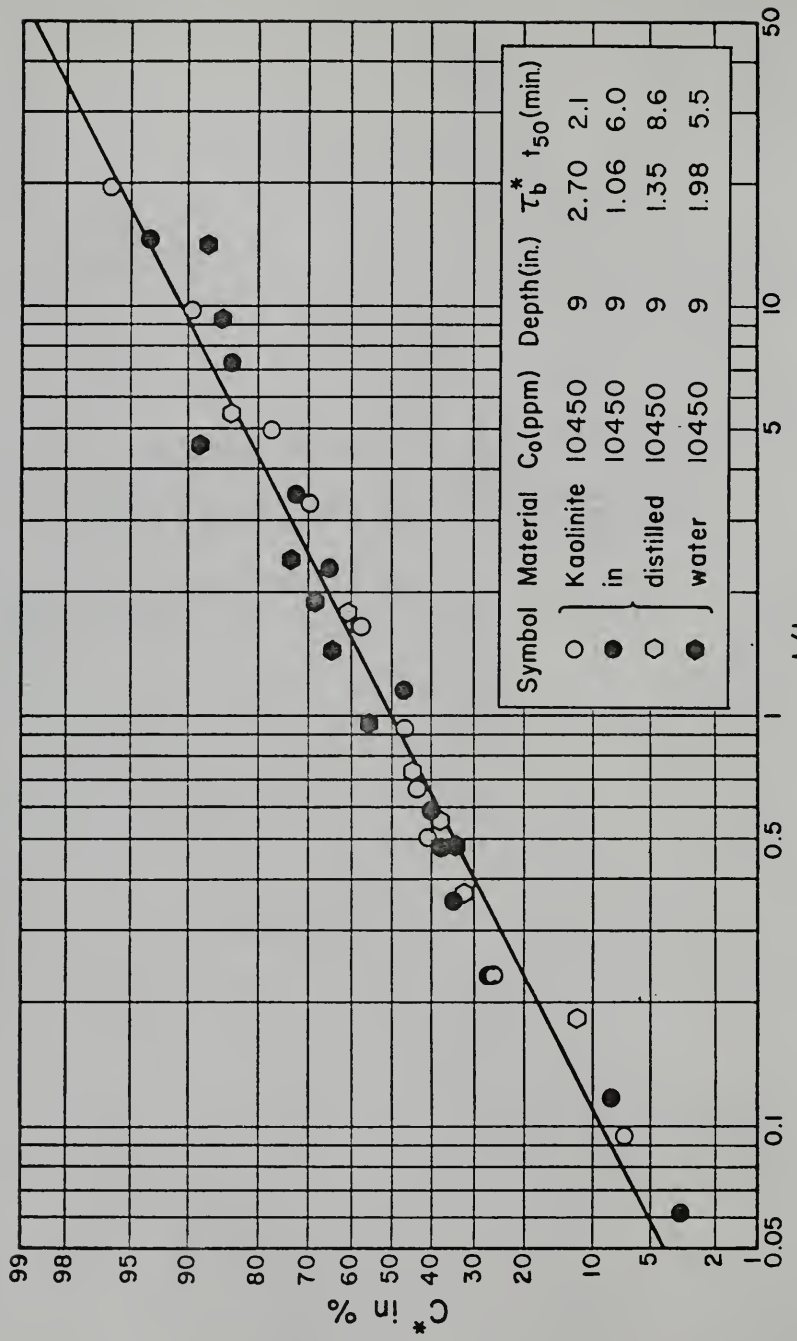

Fig. 4.2.16. C^* in Percent Versus t/t_{50} for Kaolinite in Distilled Water.

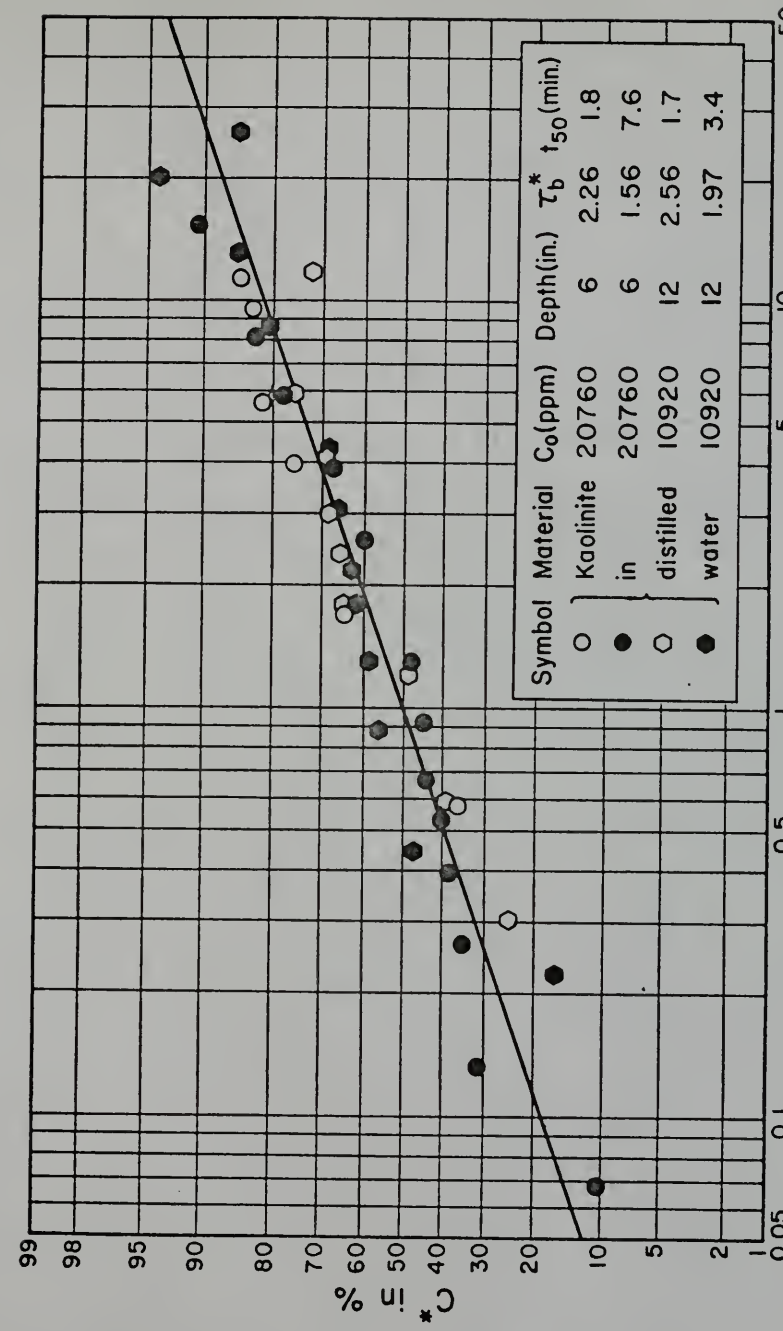

Fig. 4.2.17. C^* in Percent Versus t/t_{50} for Kaolinite in Distilled Water.

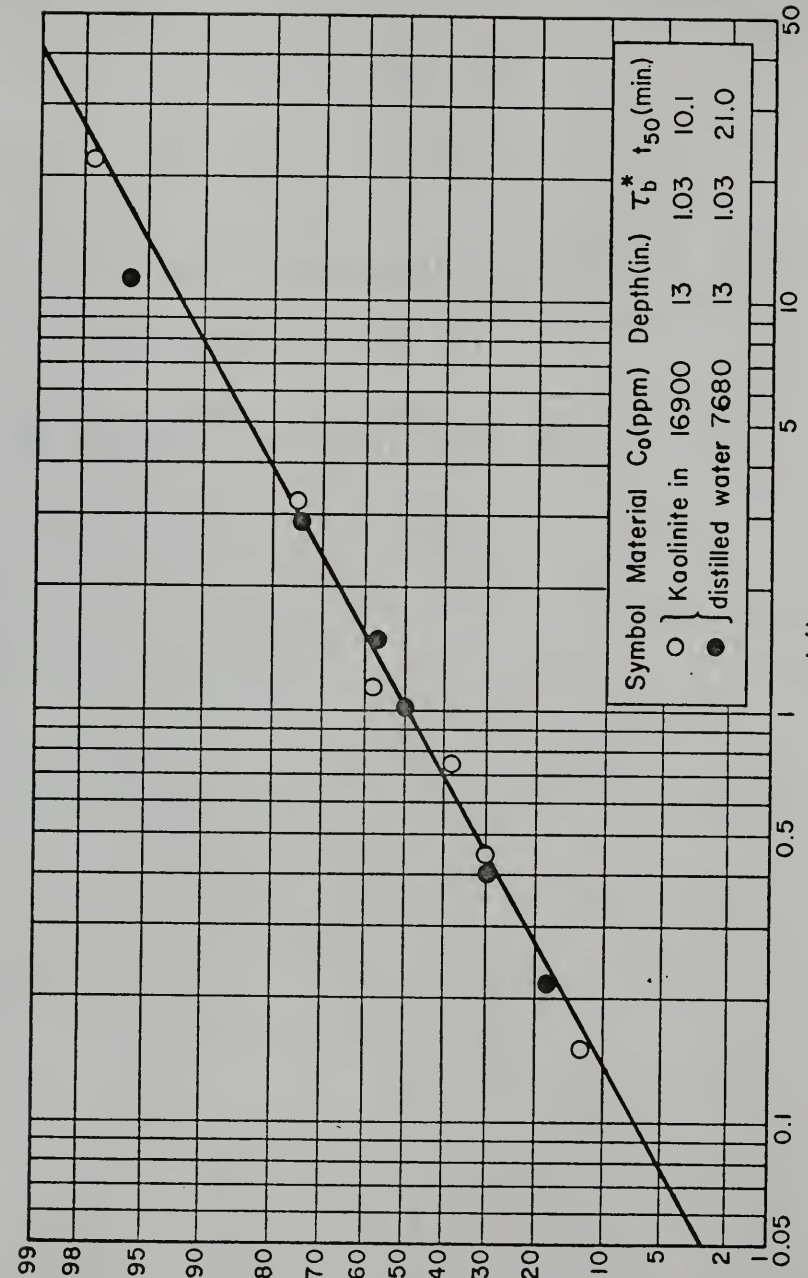

Fig. 4.2.18. C^* in Percent Versus t/t_{50} for Kaolinite in Distilled Water.

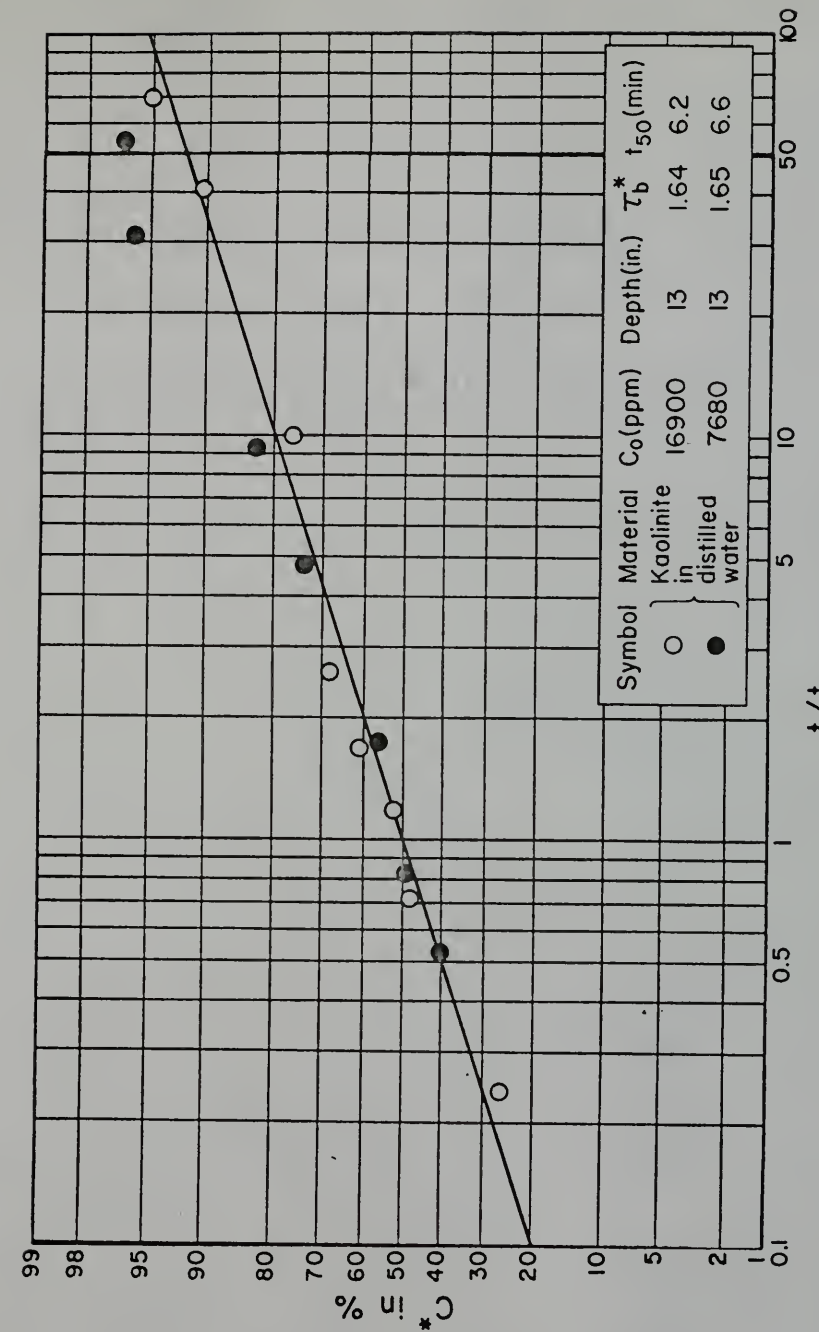

Fig. 4.2.19. C^* in Percent Versus t/t_{50} for Kaolinite in Distilled Water.

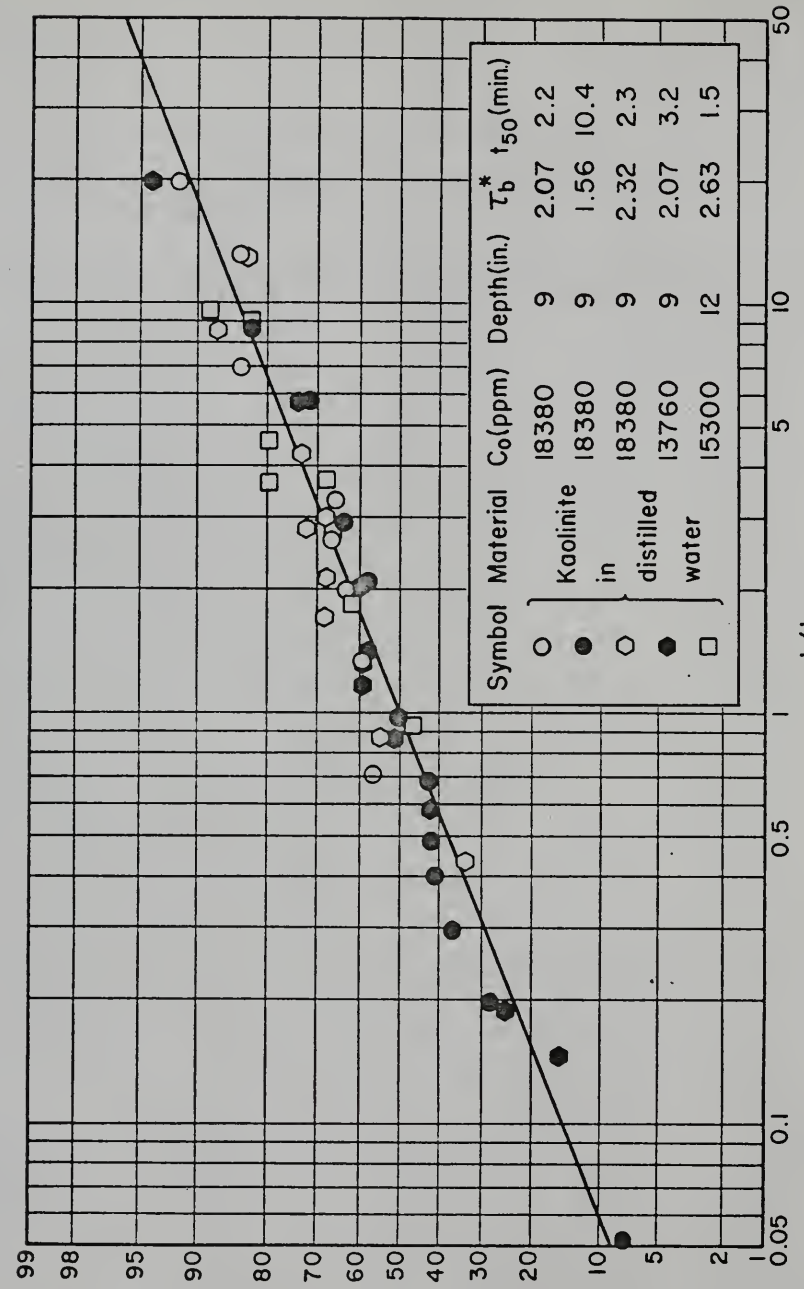

Fig. 4.2.20. C^* in Percent Versus t/t_{50} for Kaolinite in Distilled Water.

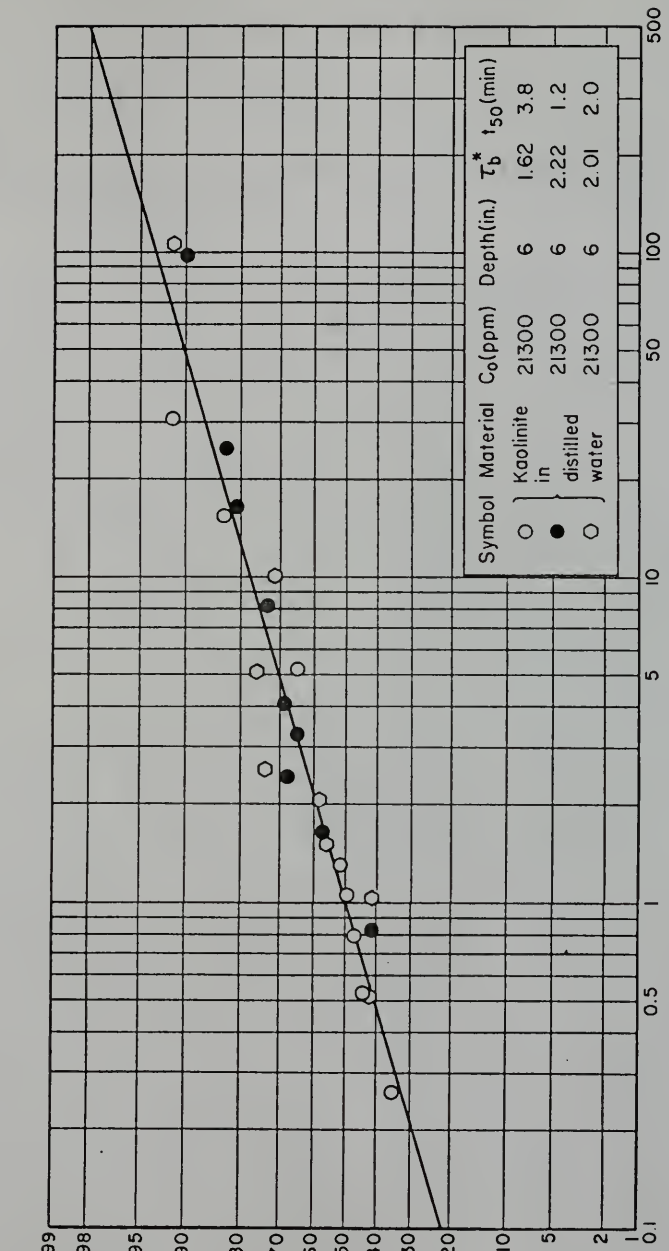

Fig. 4.2.21. C^* in Percent Versus t/t_{50} for Kaolinite in Distilled Water.

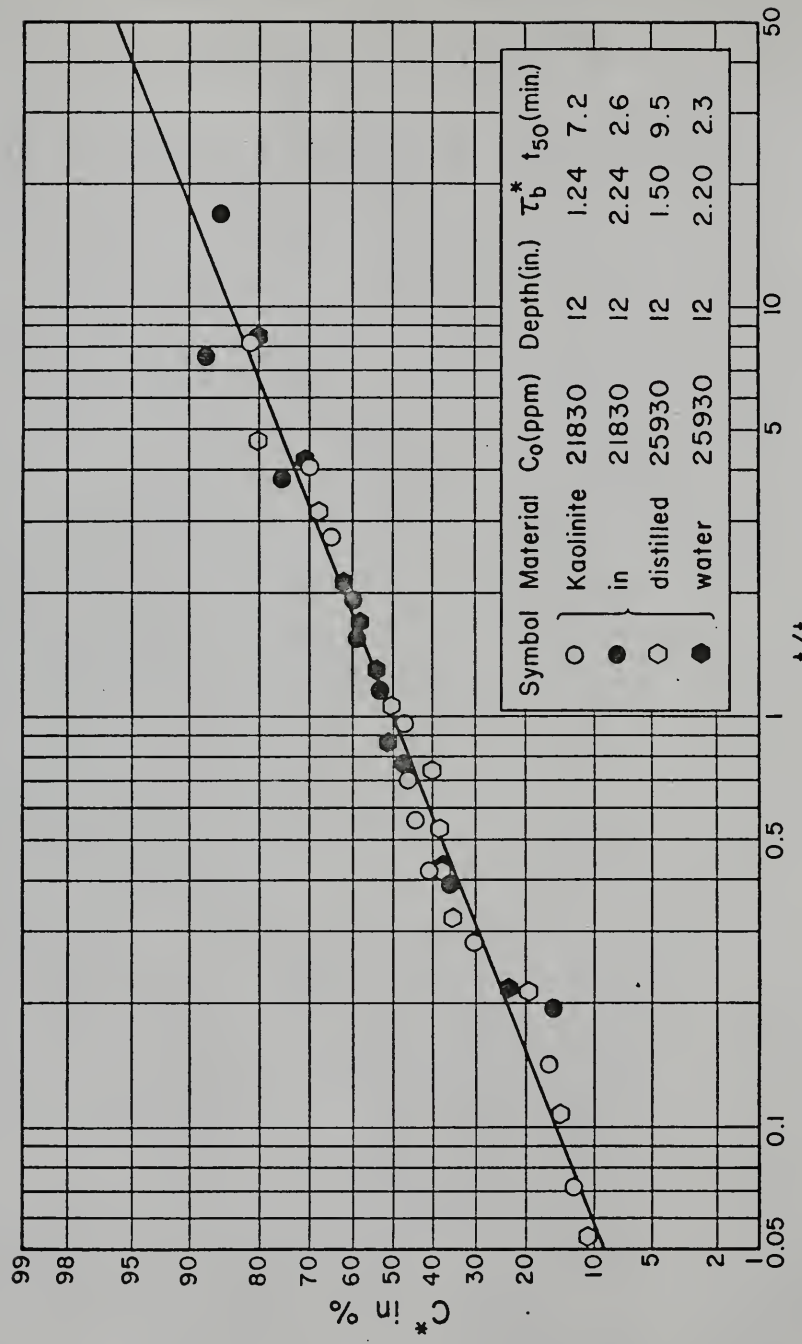

Fig. 4.2.22. C^* in Percent Versus t/t_{50} for Kaolinite in Distilled Water.

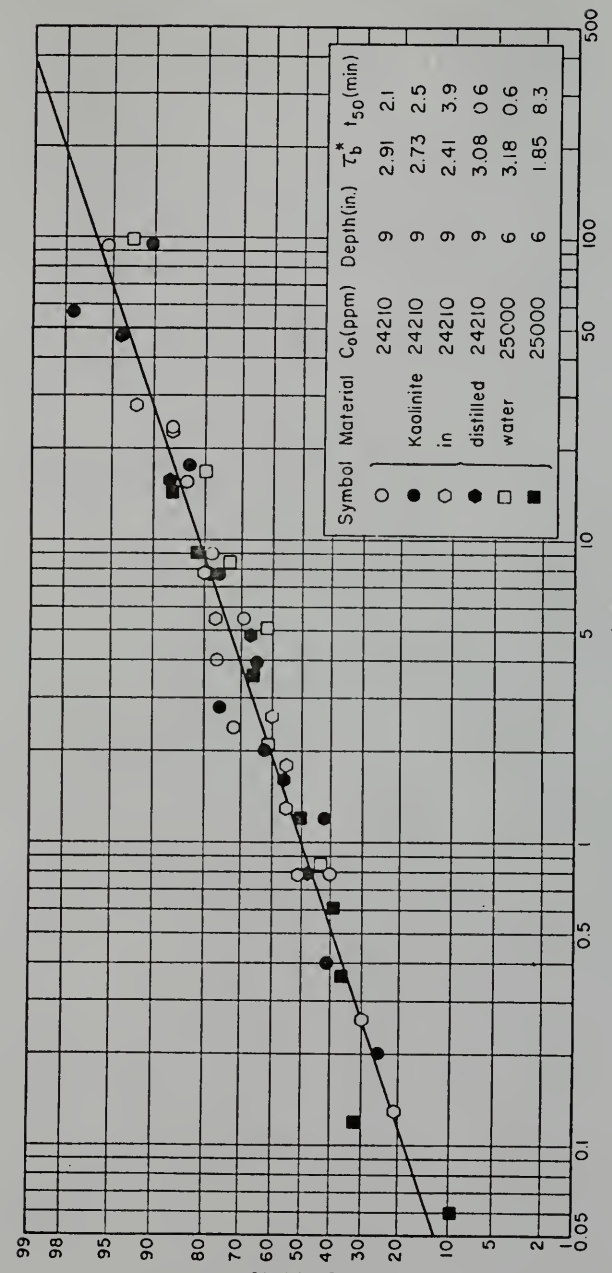

Fig. 4.2.23. C^* in Percent Versus t/t_{50} for Kaolinite in Distilled Water.

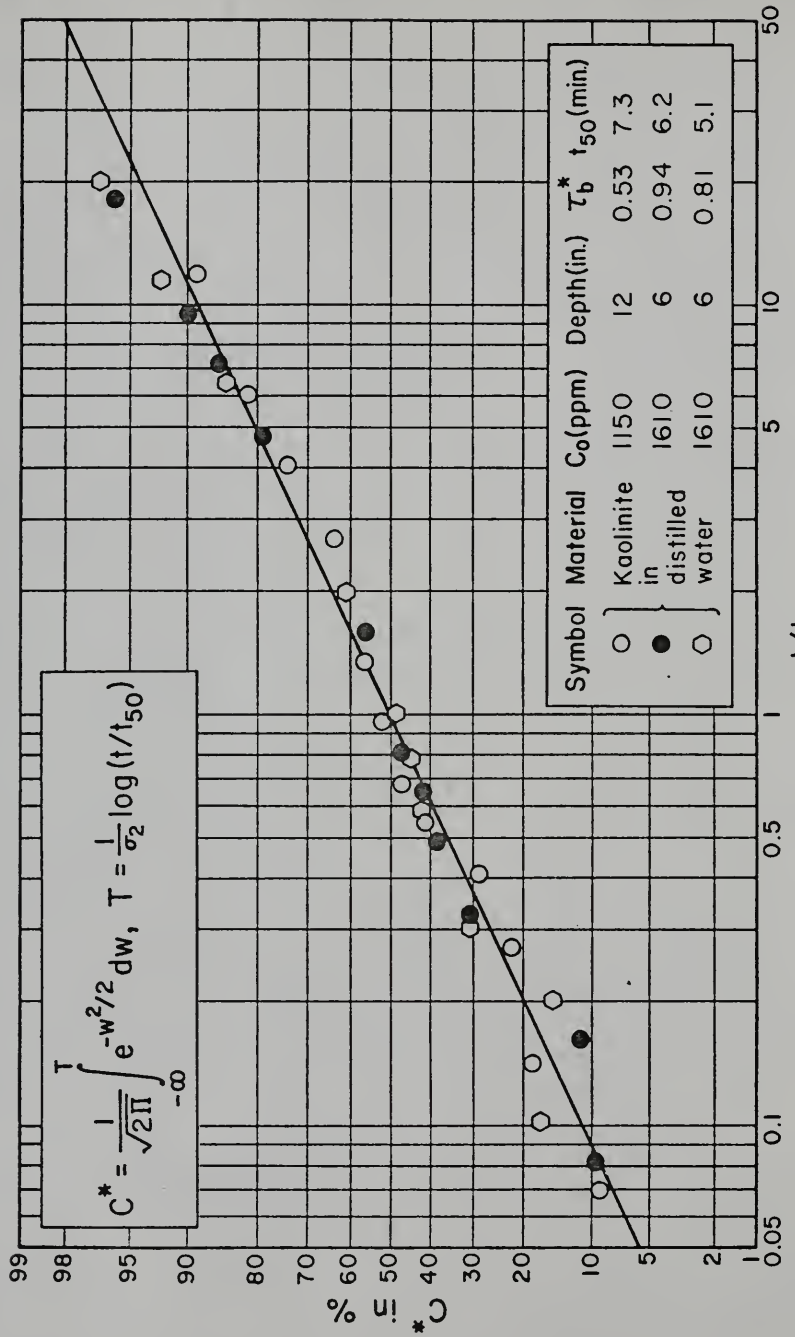

Fig. 4.2.24. C^* in Percent Versus t/t_{50} for Kaolinite in Distilled Water.

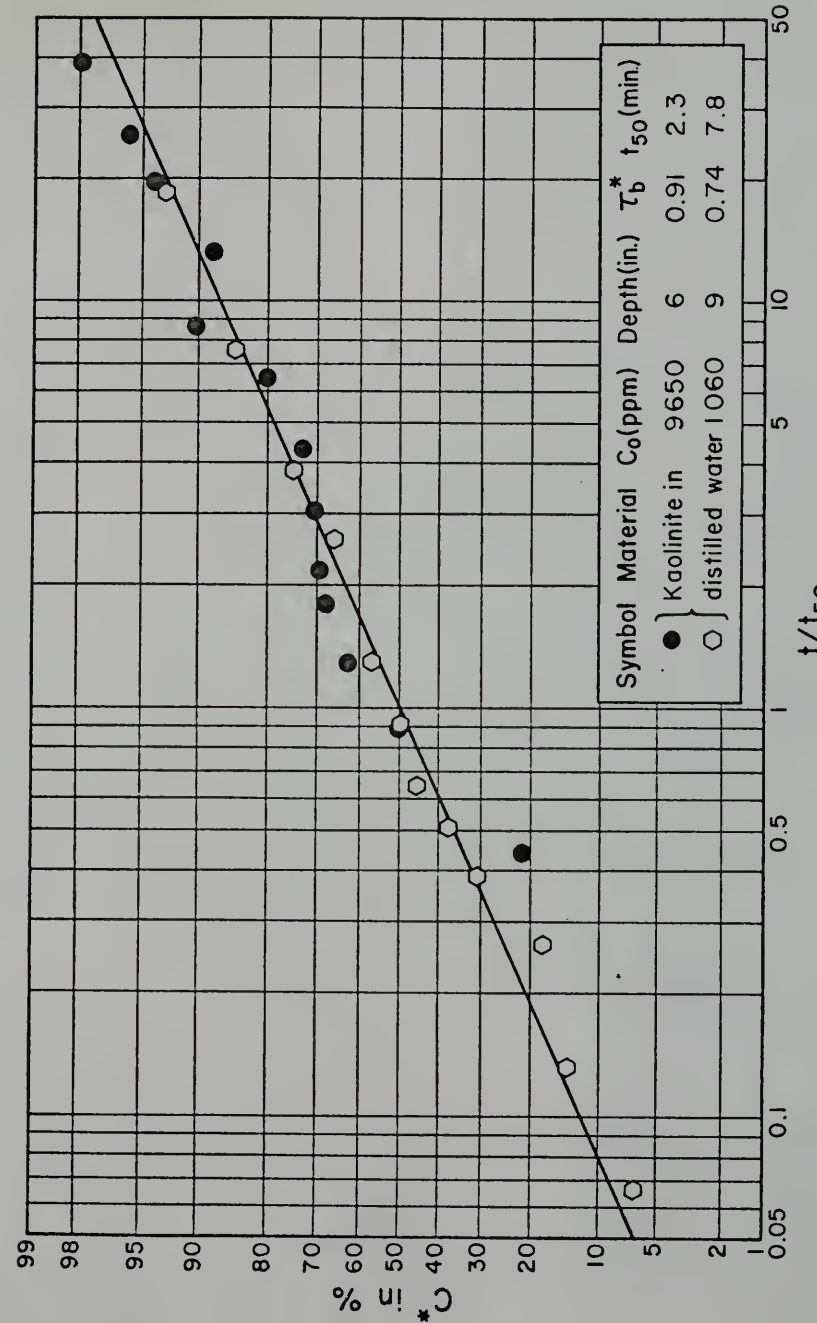

Fig. 4.2.25. C^* in Percent Versus t/t_{50} for Kaolinite in Distilled Water.

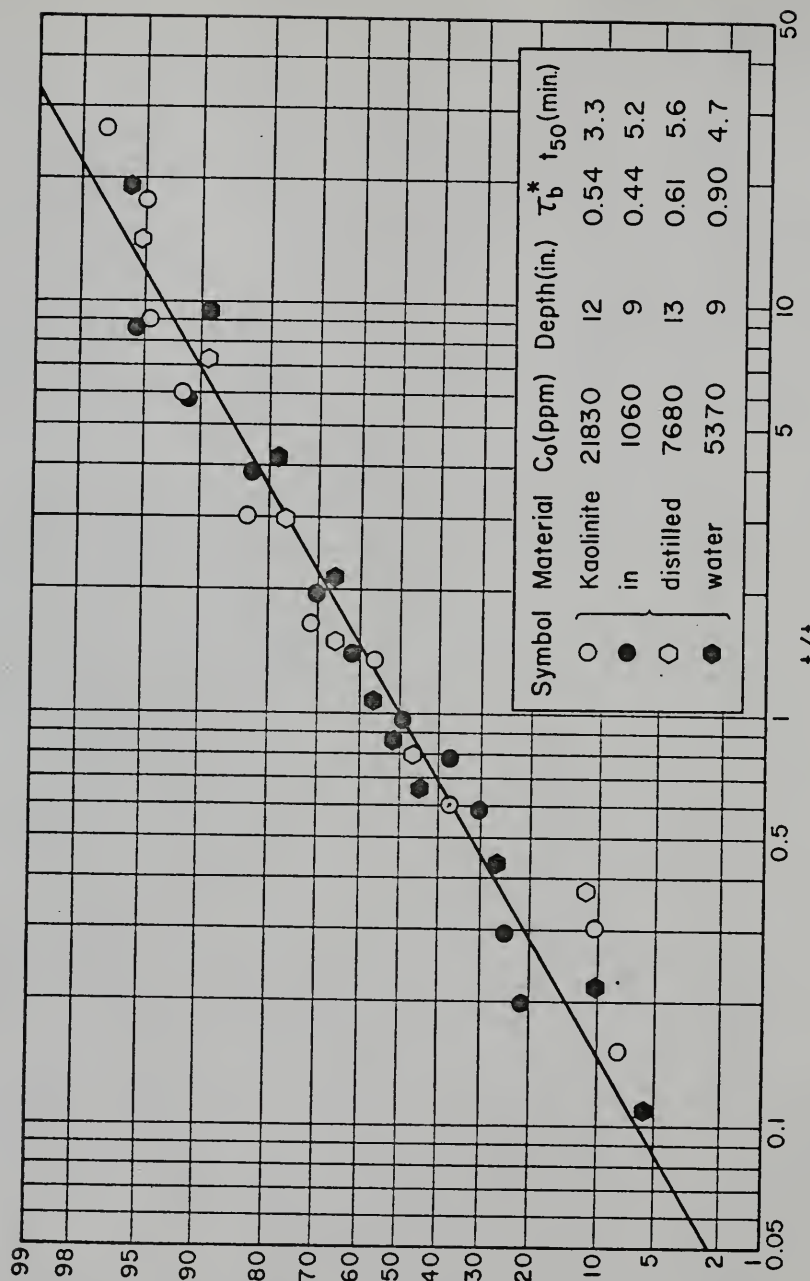

Fig. 4.2.26. C^* in Percent Versus t/t_{50} for Kaolinite in Distilled Water.

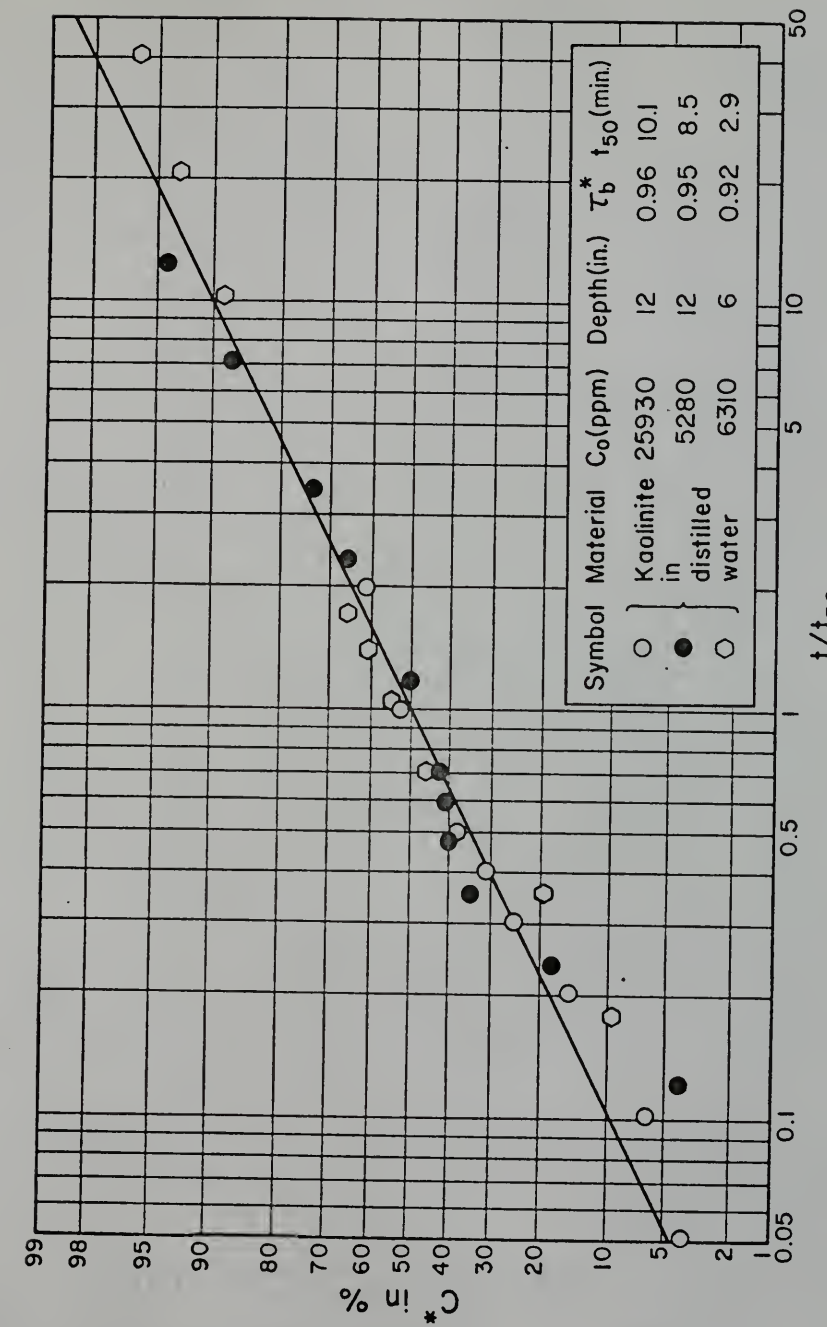

Fig. 4.2.27. C^* in Percent Versus t/t_{50} for Kaolinite in Distilled Water.

These runs in general indicate a logarithmic-normal law which may be expressed as

$$C^* = \frac{1}{\sqrt{2\pi}} \int_{-\infty}^{T} e^{-w^2/2} dw \qquad (4.2\text{-}8)$$

where

$$T = \frac{1}{\sigma_2} \log[t/t_{50}] \qquad (4.2\text{-}9)$$

Here, σ_2 is the standard deviation, t_{50} is the geometric mean and w is a dummy variable. In terms of the error function, Eq. (4.2-8) may be alternatively expressed as

$$C^* = \frac{1}{2} + \frac{1}{2} \operatorname{erf}(T/\sqrt{2}) \qquad (4.2\text{-}10)$$

and consequently,

$$C^{**} = \frac{1}{2} \operatorname{erfc}(T/\sqrt{2}) \qquad (4.2\text{-}11)$$

where by definition

$$\operatorname{erfc}(T/\sqrt{2}) = 1 - \operatorname{erf}(T/\sqrt{2}) \qquad (4.2\text{-}12)$$

The time-rates corresponding to C^* and C^{**} may be derived from Eqs. (4.2-10) and (4.2-11), respectively, as

$$\frac{dC^*}{dt} = \frac{0.434}{\sqrt{2\pi}\,\sigma_2} e^{-T^2/2} \frac{1}{t} \qquad (4.2\text{-}13)$$

and

$$\frac{dC^{**}}{dt} = -\frac{0.434}{\sqrt{2\pi}\,\sigma_2} e^{-T^2/2} \frac{1}{t} \qquad (4.2\text{-}14)$$

Values of σ_2 and t_{50} for each of the runs were obtained by the method of least squares described in Appendix B. Although σ_2 values vary from run to run, those runs with values close to each other have been

plotted together in Figs. 4.2.9 through 4.2.27, to emphasize the generality of the logarithmic-normal law.

With reference to Fig. 4.2.9, for the run corresponding to τ_b^* of 0.80, the first recorded value of C^* is 11.6% at t/t_{50} of 0.05. Since the value of t_{50} for this run is 10 min, this value of C^* corresponds to a measurement at a time t of 1/2 min after the beginning of deposition. This indicates that at 1/2 min, 11.6% of the depositable concentration has already been deposited. As a result, the segment of the line for C^* less than this value is absent from the plot. Since in no case was the first measurement taken earlier than approximately 1/2 min after the beginning of deposition, segments of data for values of C^* lower than those measured at 1/2 min are absent from all the plots. Another feature that should be noted is the absence in many cases of data points for C^* greater than approximately 95%. This is because there usually was a period of several hours of night time between the last but one and the last measurement, with the result that the deposition of the last few percents of the depositable material was often not recorded.

A comparison of data for τ_b^* greater than unity with that less than unity indicates that the former in general indicate a better agreement with the logarithmic-normal law than the latter. Moreover, in both cases, the upper and the lower ends of the straight lines show relatively greater deviations and/or scattering of data as compared to the middle zone, which must at least in part be attributed to errors in the measurements. For the upper end, this error in measurement is due either to small differences in $C - C_{eq}$, when τ_b^*

is greater than unity, or it is due to the relatively small values of C close to zero, when τ_b^* is less than unity. Measurements at the lower ends of the straight lines indicate deviations partly because they are sensitive to changes in the abscissa. Thus, as it took nearly 10 to 15 seconds to withdraw a sample, an error was often introduced in specifying the exact mean time corresponding to a given sample withdrawal, particularly in the first minute or two after the beginning of deposition. Another source of error, especially for the relatively low flow velocities corresponding to τ_b^* less than unity, was due to the sudden lowering of the speeds of the ring and the channel at the beginning of deposition, in order for the initially completely suspended material to begin depositing. The relatively high initial momentum associated with the flow in such a situation would keep the suspended material from depositing for a short length of time until the momentum was sufficiently reduced by boundary friction. This caused an error in the measurement of the time of deposition, since this time was always measured from the moment at which the ring and the channel speeds were lowered to their predetermined operational values.

In Figs. 4.2.28 through 4.2.32, plots are shown for deposition runs for cases where significant deviations from the logarithmic-normal law are observed. The runs in Fig. 4.2.28 through 4.2.30 correspond to relatively low values of τ_b^*, with the highest being 0.76. In all three cases, relatively large portions of the curves may still be approximated by a logarithmic-normal relationship. Comparing the data of Fig. 4.2.28 with those of Fig. 4.2.29, it may be

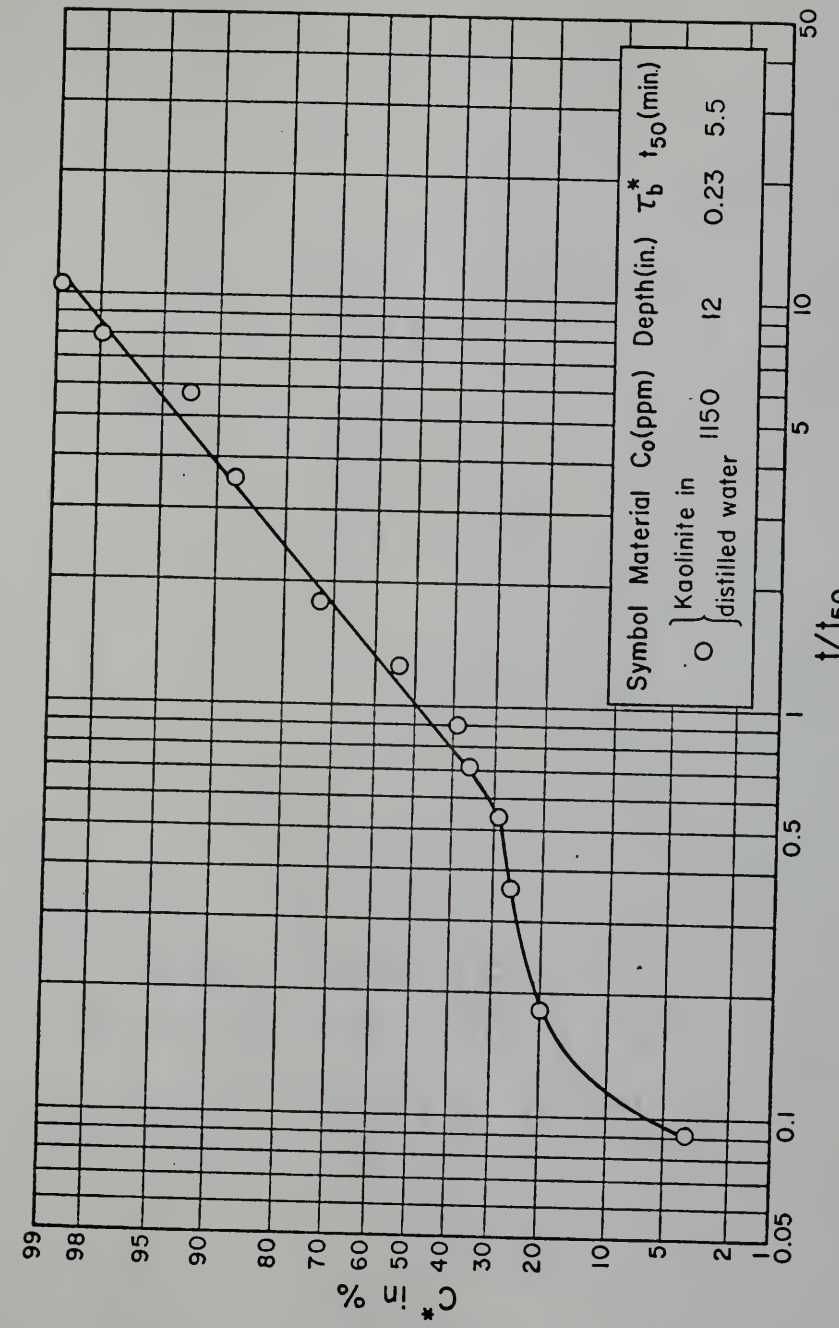

Fig. 4.2.28. C^* in Percent Versus t/t_{50} for Kaolinite in Distilled Water.

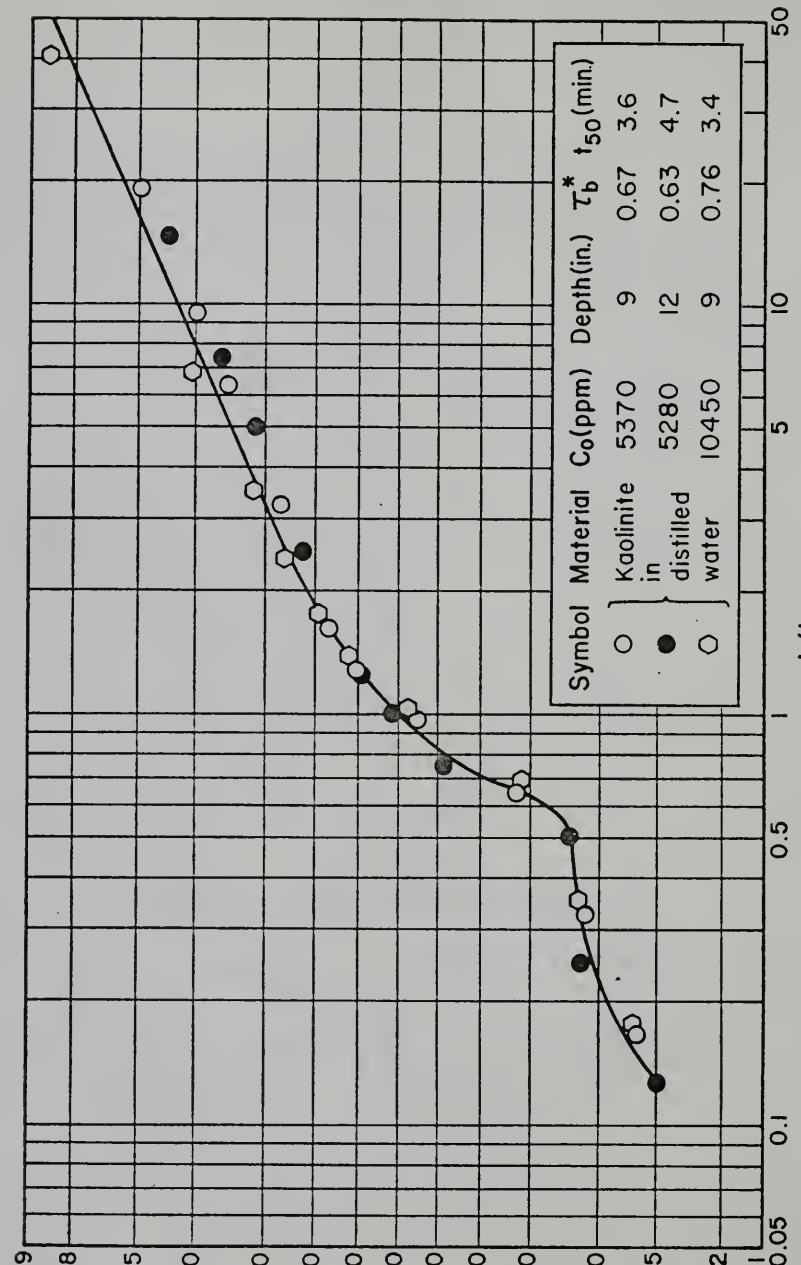

Fig. 4.2.29. C^* in Percent Versus t/t_{50} for Kaolinite in Distilled Water.

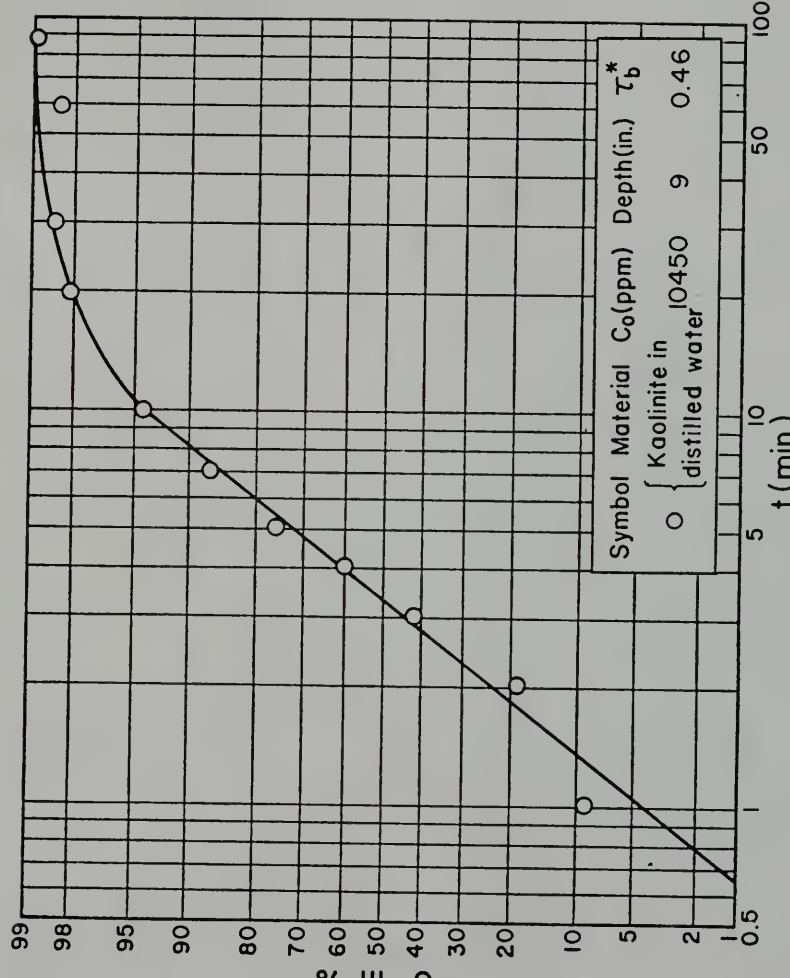

Fig. 4.2.30. Fraction of Depositable Sediment Concentration C^* Deposited at Time t, in Percent, Versus Time t for Kaolinite in Distilled Water.

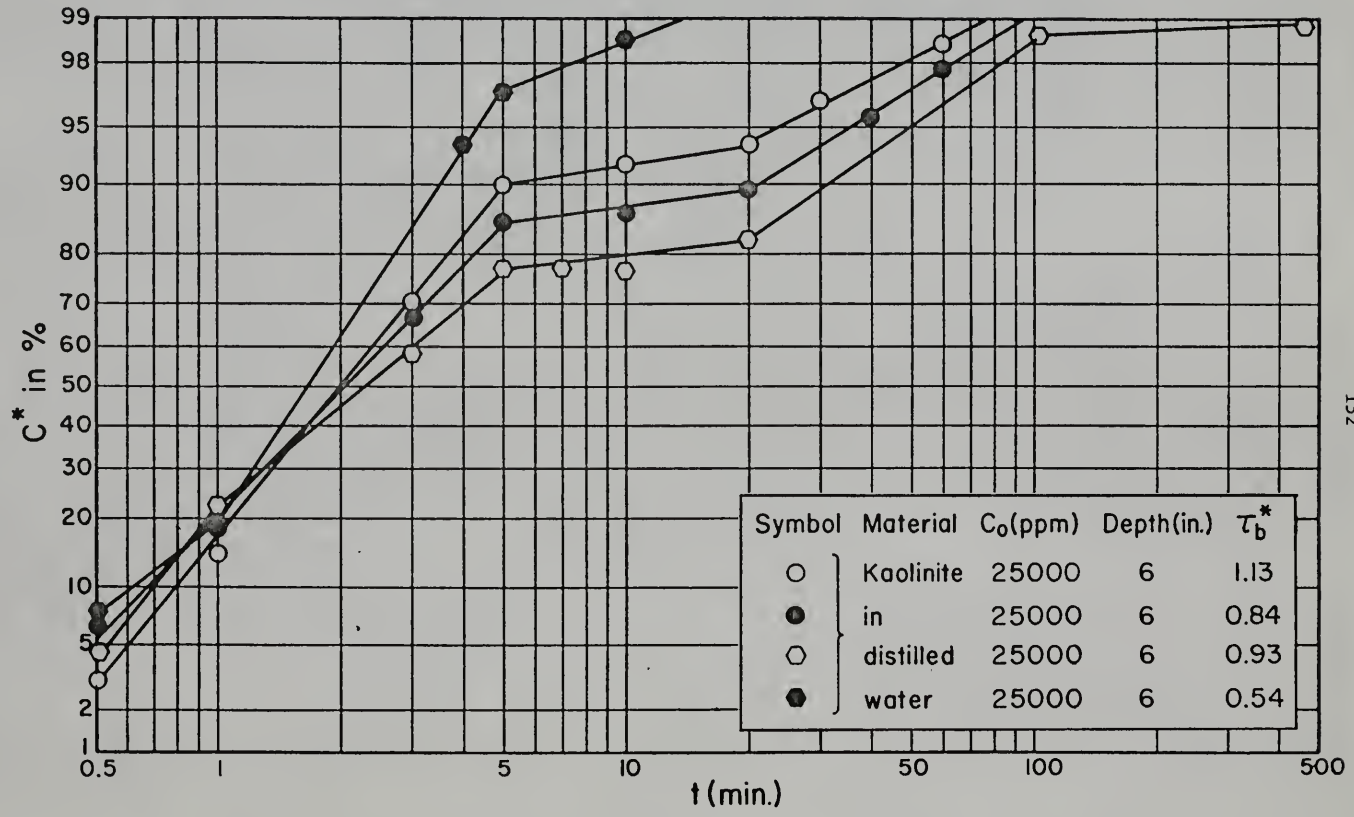

Fig. 4.2.31. C^* in Percent Versus Time t for Kaolinite in Distilled Water.

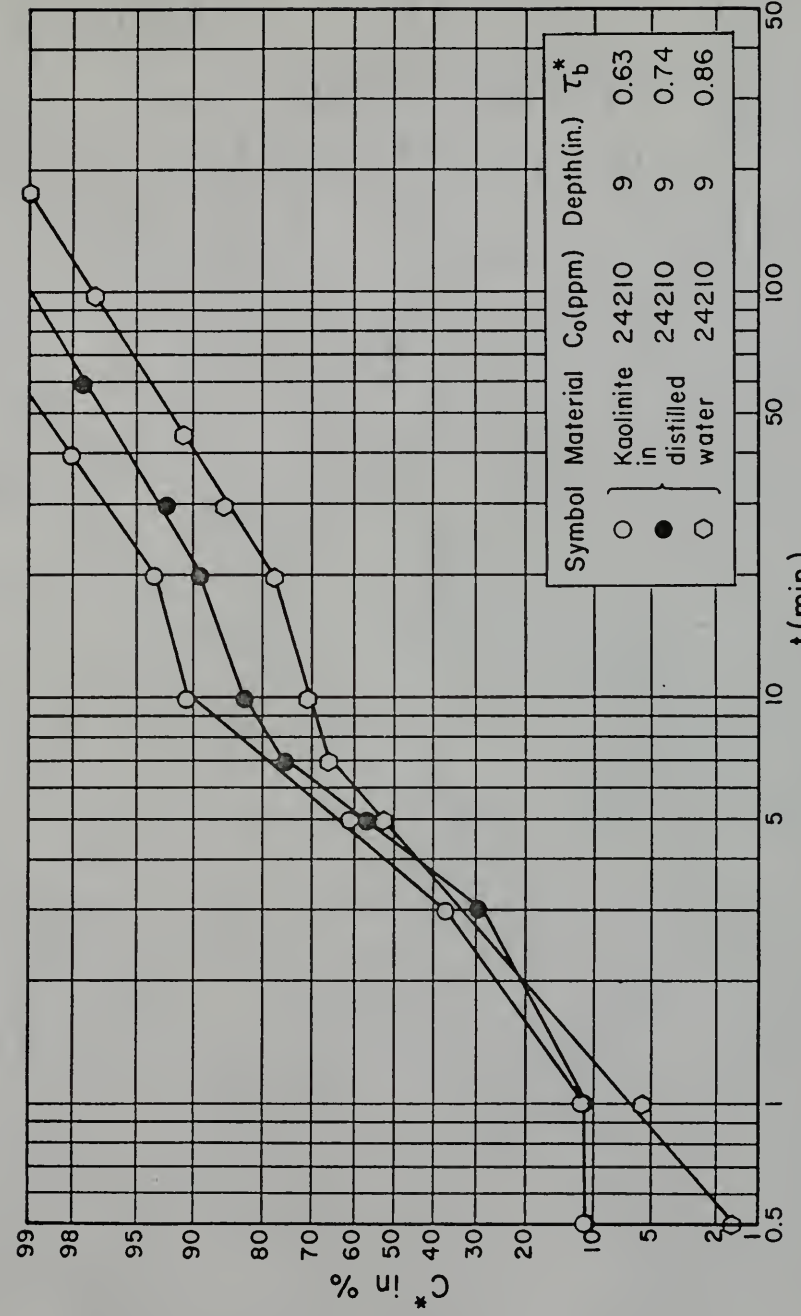

Fig. 4.2.32. c^* in Percent Versus Time t for Kaolinite in Distilled Water.

observed that in both cases the deviations are significant only in the initial phase of deposition. However, although the three runs of Fig. 4.2.29, with similar τ_b^* values indicate similarity in trends, the data of Fig. 4.2.28, which correspond to a τ_b^* which is lower than those of Fig. 4.2.28 by almost a factor of three, indicate a different trend in the deviation from the logarithmic-normal law. Values of σ_2 and t_{50} computed for the curves of Figs. 4.2.28 and 4.2.29 must be considered to be tentative. Comparing the runs of Fig. 4.2.29 with those in Figs. 4.2.24, 4.2.25 and 4.2.26 which correspond to τ_b^* less than 0.76, it may be observed that the pattern of deviations from the logarithmic-normal law is not obvious, inasmuch as some runs indicate closer agreement with this law than others. However, the data of Fig. 4.2.28 show that for τ_b^* as low as 0.23, significant portions of the plots may be described by the logarithmic-normal law. Comparison of data for natural sediments described in Section 4.2.3 confirms this observation. Thus in Fig. 4.2.44, a run for $\tau_b^* = 0.14$, for the Maracaibo sediment, follows the logarithmic-normal law.

For the data of Fig. 4.2.30, σ_2 or t_{50} are not computed. Here, the logarithmic-normal law is observed to hold up to C^* of almost 95%, and it is followed by a segment with a significantly lower rate of deposition.

In Figs. 4.2.31 and 4.2.32, deposition data are shown for C_o of 25000 and 24210 ppm, at depths of 6 and 9 in., respectively. Here, except for one case, τ_b^* values are less than unity. A characteristic feature of these data is that the initial segments of the curves indicate rapid rates of deposition, followed by curves

suggesting significantly lower rates of settling. In Fig. 4.2.31, this initial portion of rapid deposition in each case corresponds to nearly the first five minutes of deposition, during which period, depending on τ_b^*, with its value decreasing from 1.13 to 0.54, anywhere between 77 to 97% of the material is deposited at a rate which may be approximated by the logarithmic-normal law. In Fig. 4.2.32, this portion of rapid deposition in each case extends from 7 to 10 min, but in general it does not suggest the logarithmic-normal law. Such a phenomenon of rapid deposition, which essentially involves the settling of large sediment flocs at low bed shear stresses and high initial concentrations, may be defined as "mass deposition," and may be viewed as the counterpart in the deposition process, of the phenomenon of mass erosion described by Partheniades (1965), in which large chunks of flocculated bed material are eroded at relatively high bed shear stresses. It is noteworthy that for the 12 in. depth, the run for τ_b^* of 0.96 in Fig. 4.2.27 suggests that in that particular case, even though C_o is 25930 ppm, the logarithmic-normal law describes the rate of deposition reasonably well. Moreover, Figs. 4.2.22 and 4.2.23 show that for 6, 9 and 12 in. depths and respective C_o values of 25000, 24210 and 25930 ppm, the logarithmic-normal behavior is valid for τ_b^* values well above unity.

In view of the variability of the observed depositional behavior for initial concentrations of the order of 25000 ppm, it may be concluded that at these high concentrations, the logarithmic-normal law for τ_b^* less than unity must be used with caution, whereas for τ_b^* greater than unity, it may be reasonable to assume its validity.

The rates of deposition of a given sediment suspension appear to vary with the bed shear stress, depth and initial concentration. Therefore, where the logarithmic-normal law holds, the standard deviation σ_2 and the geometric mean t_{50}, which characterize the rates according to Eqs. (4.2-13) and (4.2-14), are also expected to depend on the same variables. Moreover, the dependence of σ_2 and t_{50} on these variables is also expected to vary with the properties of the sediment as well as with the ambient environment.

In Figs. 4.2.33 through 4.2.38, values of σ_2 and log t_{50} are plotted against τ_b^* for the indicated depths and initial concentrations, corresponding to the data plotted in Figs. 4.2.9 through 4.2.29. It should be pointed out that the effect of bed shear stress, depth and initial concentration on the rates must be described in terms of the combined effect of σ_2 and t_{50} on the rates. The experimental results have however shown that in general for τ_b^* less than unity, the effect of σ_2 is similar to the effect of t_{50}, whereas for τ_b^* increasing above unity, the effect of t_{50} becomes relatively more pronounced, inasmuch as variation in σ_2 values becomes relatively less significant. In the following paragraphs therefore the effects on rates are described primarily in terms of variation of t_{50} with bed shear stress, depth and initial concentration.

It may be observed from the plots of log t_{50} versus τ_b^* that, in general, for each given depth and initial concentration, and for a τ_b^* smaller than a particular value, log t_{50} increases with increasing τ_b^*, whereas for τ_b^* greater than this particular value, log t_{50} begins to decrease with increasing τ_b^*. According to Eqs. (4.2-9) and (4.2-13),

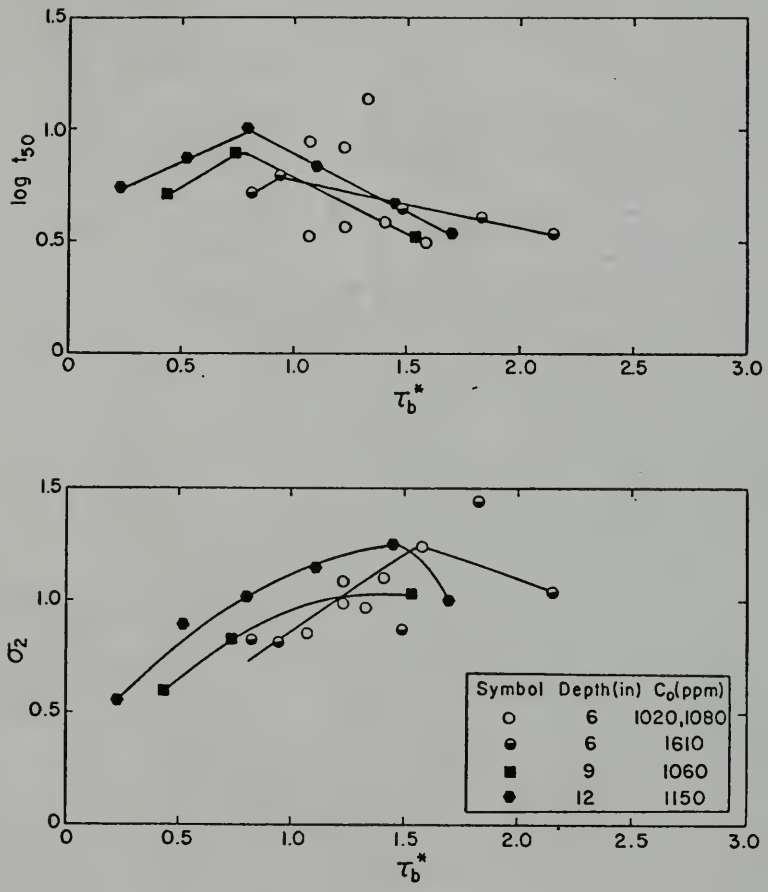

Fig. 4.2.33. Log t_{50} and σ_2 Versus τ_b^* for Kaolinite in Distilled Water.

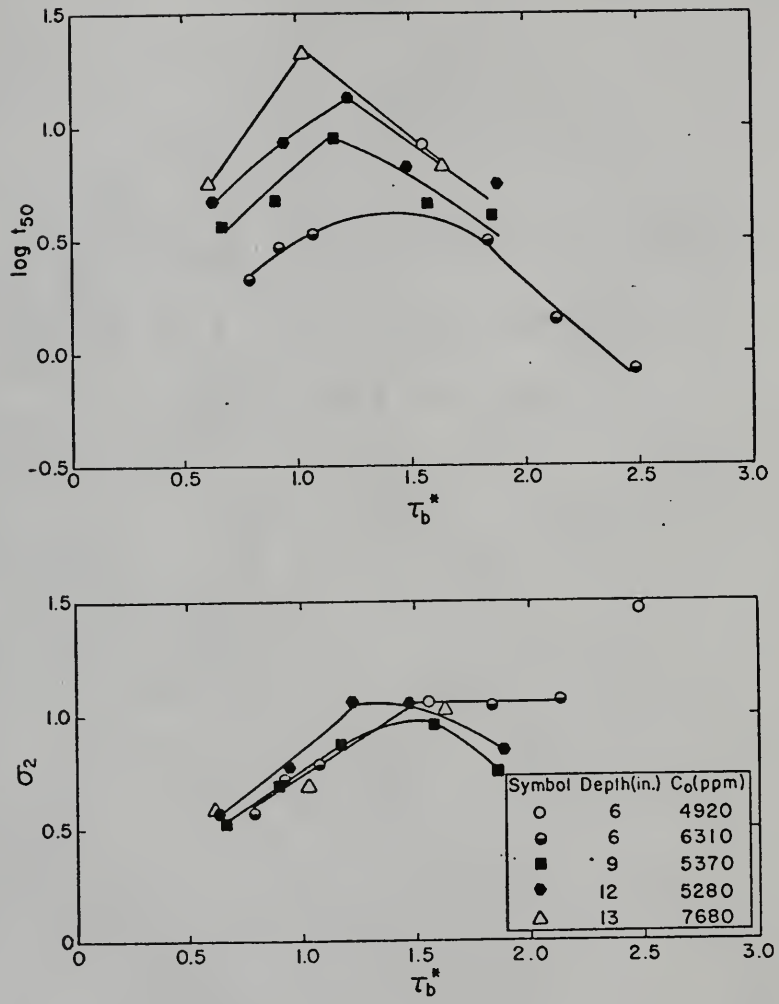

Fig. 4.2.34. Log t_{50} and σ_2 Versus τ_b^* for Kaolinite in Distilled Water.

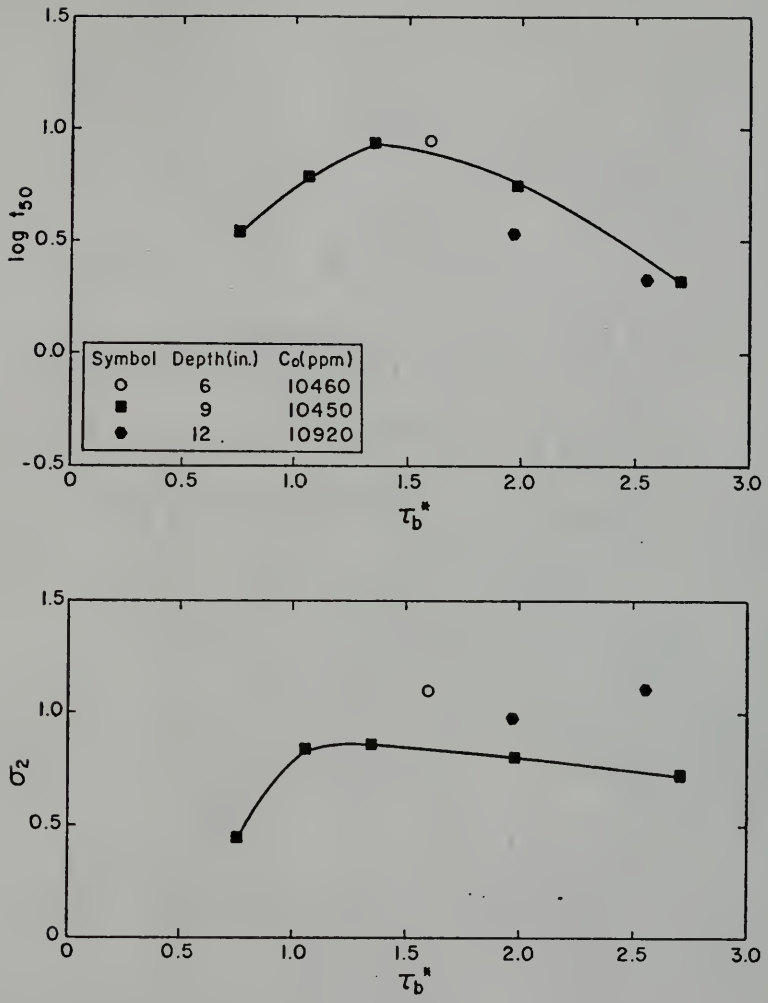

Fig. 4.2.35. Log t_{50} and σ_2 Versus τ_b^* for Kaolinite in Distilled Water.

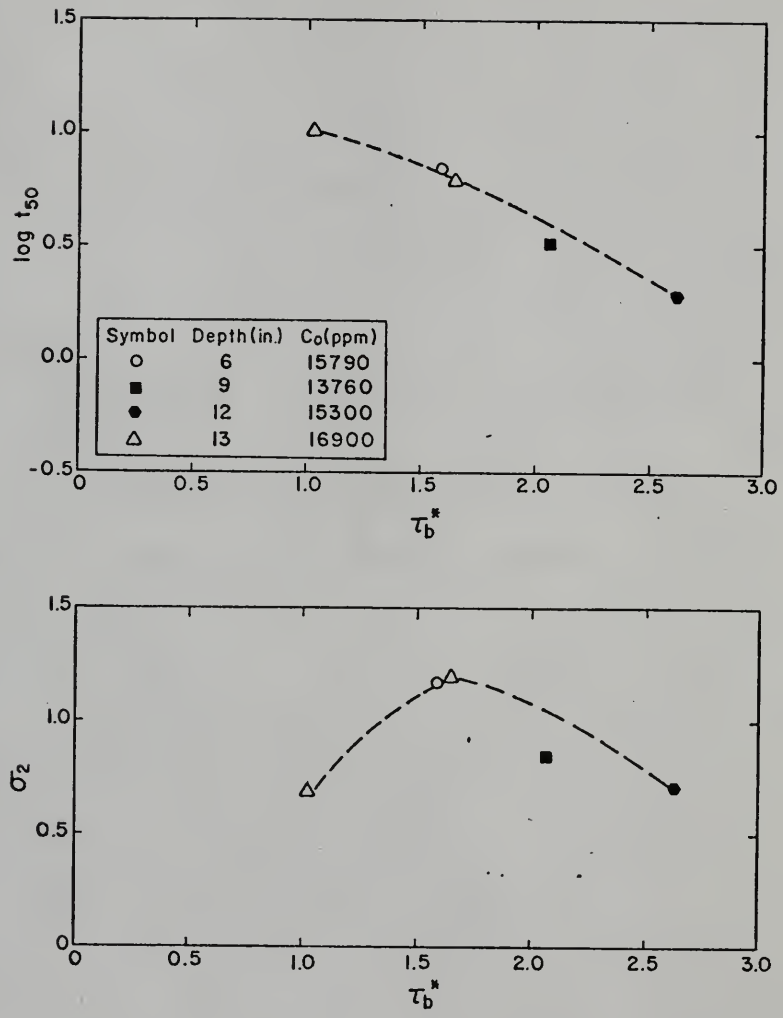

Fig. 4.2.36. Log t_{50} and σ_2 Versus τ_b^* for Kaolinite in Distilled Water.

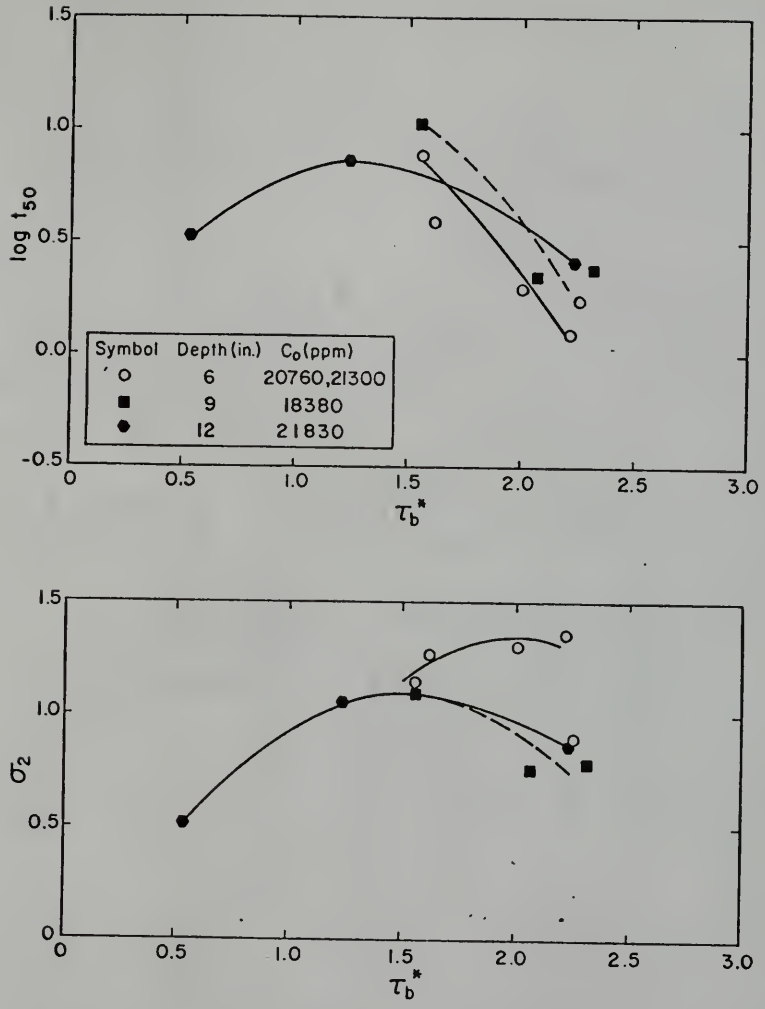

Fig. 4.2.37. Log t_{50} and σ_2 Versus τ_b^* for Kaolinite in Distilled Water.

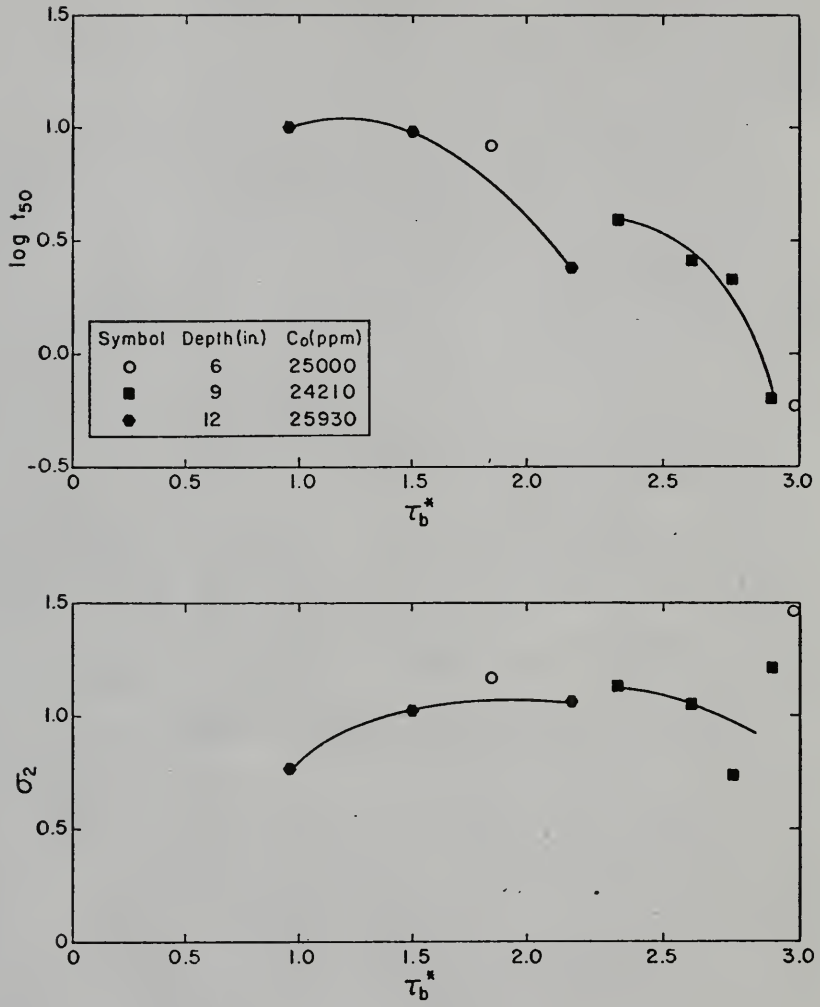

Fig. 4.2.38. Log t_{50} and σ_2 Versus τ_b^* for Kaolinite in Distilled Water.

the value of τ_b^* at which log t_{50} has its highest value corresponds to the slowest rate of deposition. It may be noted that since this peak value of log t_{50} does not occur in any of the cases for τ_b^* less than unity, the rates of deposition in all cases decrease as τ_b^* approaches unity from values below unity.

Because of the scarcity of data for C_o of approximately 10000 ppm and higher, and the scattering of data points especially for the 6 in. depth, it would be premature to make general quantitative conclusions regarding the effect of depth and C_o on log t_{50}. However, it may be observed from Figs. 4.2.33 and 4.2.34 that for a given τ_b^* less than unity and at a given C_o, increasing the depth of flow increases log t_{50}, or decreases the rate of deposition. This observation is in agreement with that of Krone (1962), whose results as expressed by Eqs. (2.2-1) through (2.2-6) indicate a similar qualitative effect of depth.

The effect of C_o on the rates in general is such that increasing C_o for a given depth of flow and τ_b^* increases log t_{50}, which corresponds to a decreasing rate of deposition. This is observed by comparing the curves of Figs. 4.2.33, 4.2.34, and 4.2.37 for 6 in. depth, the curves of Figs. 4.2.33, 4.2.34, 4.2.35 and 4.2.38 for 9 in. depth, and finally, the curves of Figs. 4.2.33, 4.2.34, 4.2.37 and 4.2.38 for 12 in. depth. Krone (1962) has noted that this effect of concentration on the rates is due to the fact that as the suspended sediment concentration increases, the flocs are brought closer together, with the result that they ultimately

tend to form a continuous network-like configuration, through the pores of which water must escape upward, for the flocculated material to deposit. Settling is thus hindered and the rates are correspondingly lowered.

The behavior of σ_2 as a function of τ_b^* also appears to indicate peaks corresponding to highest σ_2 values, or lowest rates of deposition, by virtue of Eq. (4.2-13), for a given τ_b^* and C_o. From the data of Figs. 4.2.33 and 4.2.34, it appears that the peaks do not in general coincide with the corresponding peaks of log t_{50} at the same τ_b^* values. As for the effect of C_o on the curves, the trends are not distinct, and in general, the effect of increasing C_o is much less significant than that observed in the variation of log t_{50} with τ_b^*.

For τ_b^* less than unity, the effect of depth is such that increasing the depth increases σ_2, or decreases the rate, as observed in Figs. 4.2.33 and 4.2.34. This characteristic is in agreement with the similar behavior suggested by the variation of log t_{50} with depth.

It is noteworthy that in Figs. 4.2.33, 4.2.34 and 4.2.37, for τ_b^* approximately greater than unity, the trend of data points for 6 in. depth is observed to be somewhat different from that exhibited at 9 and 12 in. depths. In Fig. 4.2.33, the exact nature of this trend is somewhat obscured by the scattering of values. However, the behavior of σ_2 with τ_b^* in Fig. 4.2.34 for the 6 in. depth appears to be distinctly different from that corresponding to 9 and 12 in. depths. It is observed there that after approaching a peak value, while σ_2 begins to decrease with increasing τ_b^* for 9 and 12 in. depths,

its value becomes nearly independent of τ_b^* for the 6 in. depth. Similarly in Fig. 4.2.37, the data for 6 in. depth appear to describe a different behavior of σ_2 with τ_b^* as compared to the other depths. However, in view of the lack of sufficient experimental evidence, any explanation for this effect at present would at best be somewhat speculative.

b. Rates in Salt Water: Deposition rates in salt water at nearly 34000 ppm salinity, for kaolinite, are given in Figs. 4.2.39 through 4.2.42. The data of Fig. 4.2.39 at 6 in. depth and C_o of 6140 ppm (Series A), and for τ_b^* greater than unity indicate that on the average, for C^* ranging from 6% to 92%, the straight line corresponding to the logarithmic-normal law represents the observed behavior. Fig. 4.2.40, which is for τ_b^* less than unity, also suggests the same law.

In Figs. 4.2.41 and 4.2.42, the rates are described for a depth of 9 in. and C_o of 10270 ppm (Series B). The data in Fig. 4.2.41 are for τ_b^* greater than unity, and these agree well with the logarithmic-normal law. In Fig. 4.2.42, which is for τ_b^* less than unity, it can be observed that after an initial short period of almost negligible deposition, the sediment deposits according to the logarithmic-normal law. It should be pointed out that the τ_b^* values for the described runs are 0.53 and 0.31, and that at corresponding low values for kaolinite in distilled water, significant deviations from the logarithmic-normal law are observed. The probable explanation for the observed behavior of negligible deposition in the beginning lies in the previously made remark that the imparted

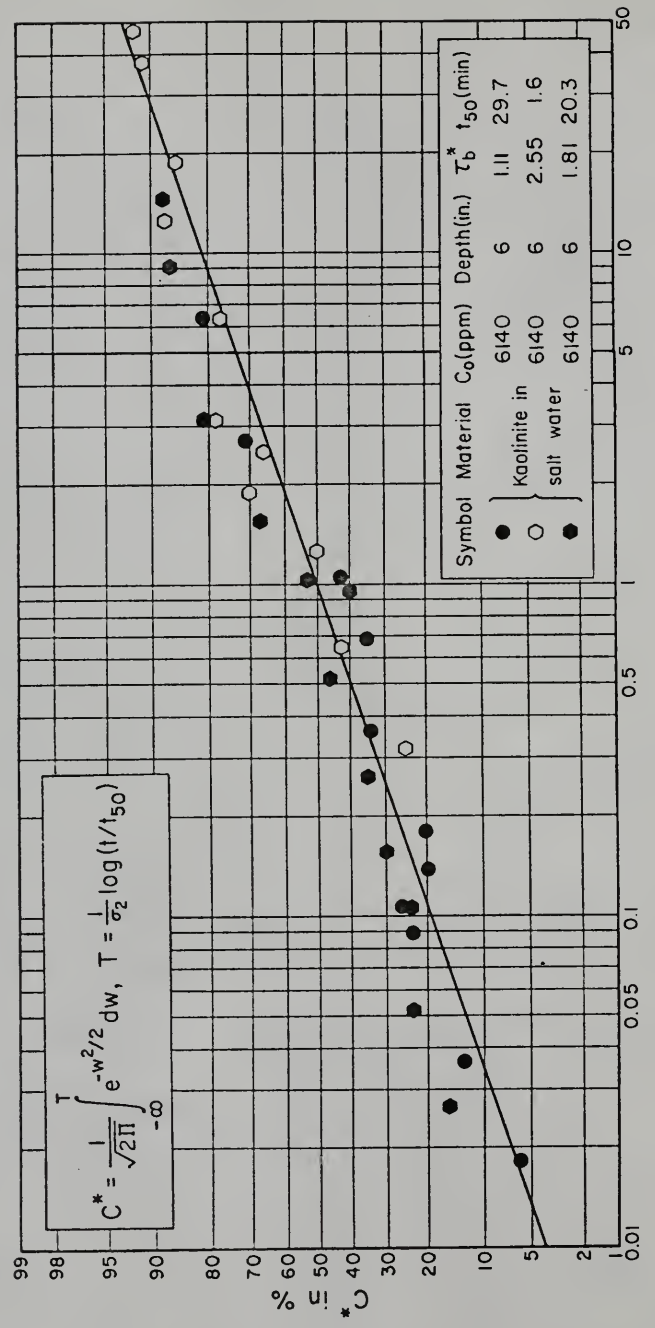

Fig. 4.2.39. Fraction of Depositable Sediment Concentration C^* Deposited at Time t, in Percent, Versus Time Parameter t/t_{50} for Kaolinite in Salt Water.

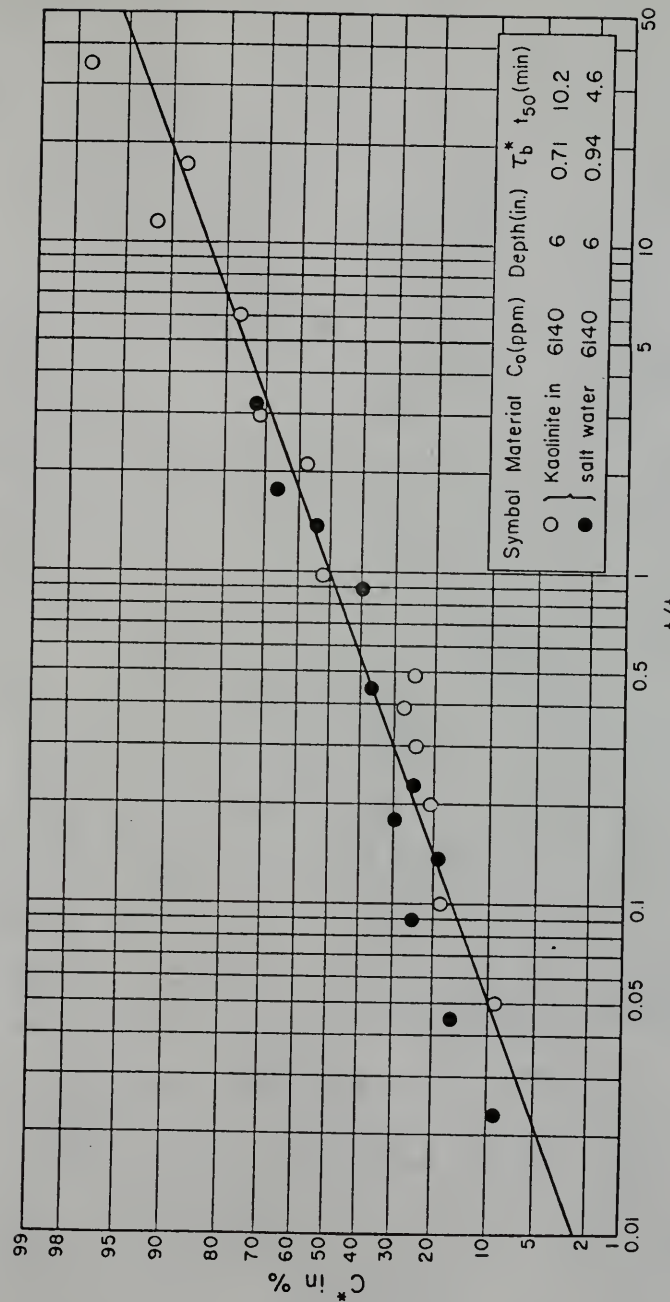

Fig. 4.2.40. c^* in Percent Versus t/t_{50} for Kaolinite in Salt Water.

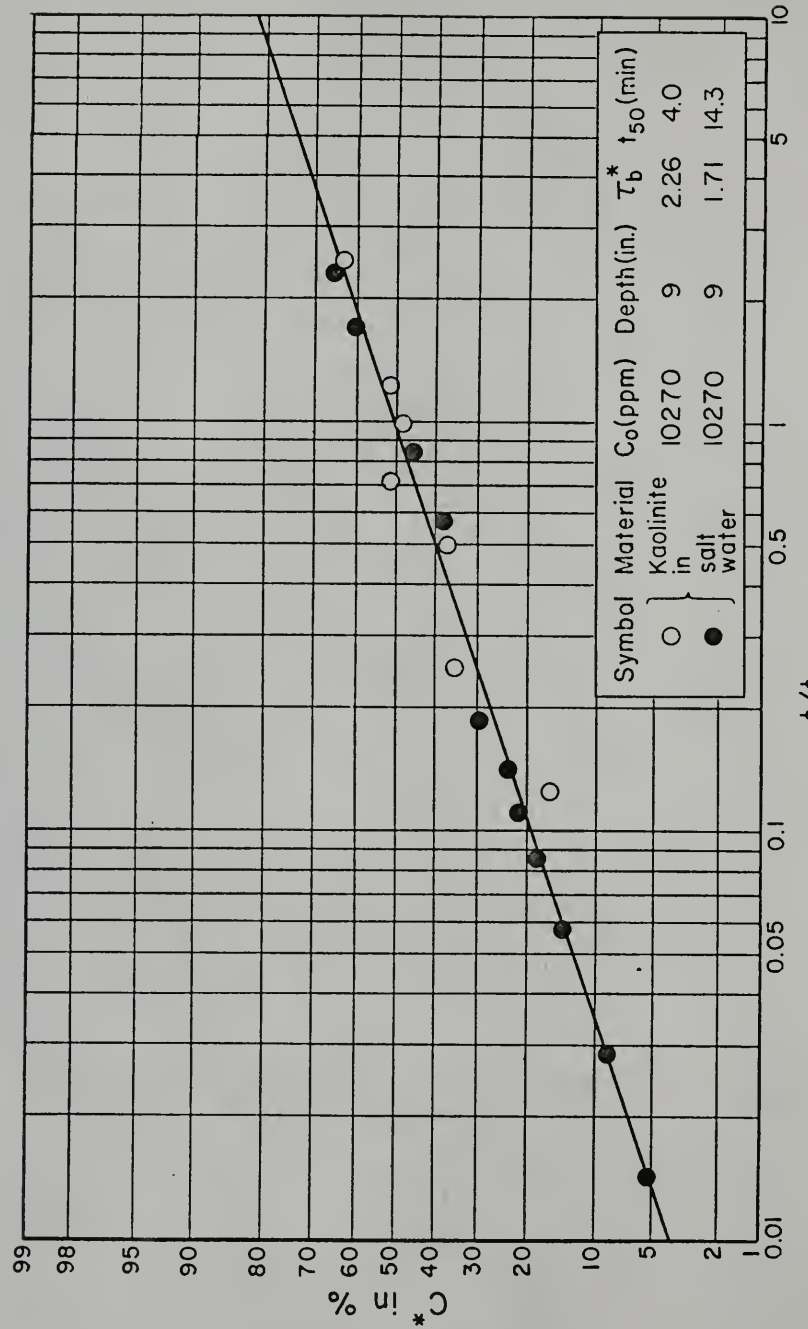

Fig. 4.2.41. c^* in Percent Versus t/t_{50} for Kaolinite in Salt Water.

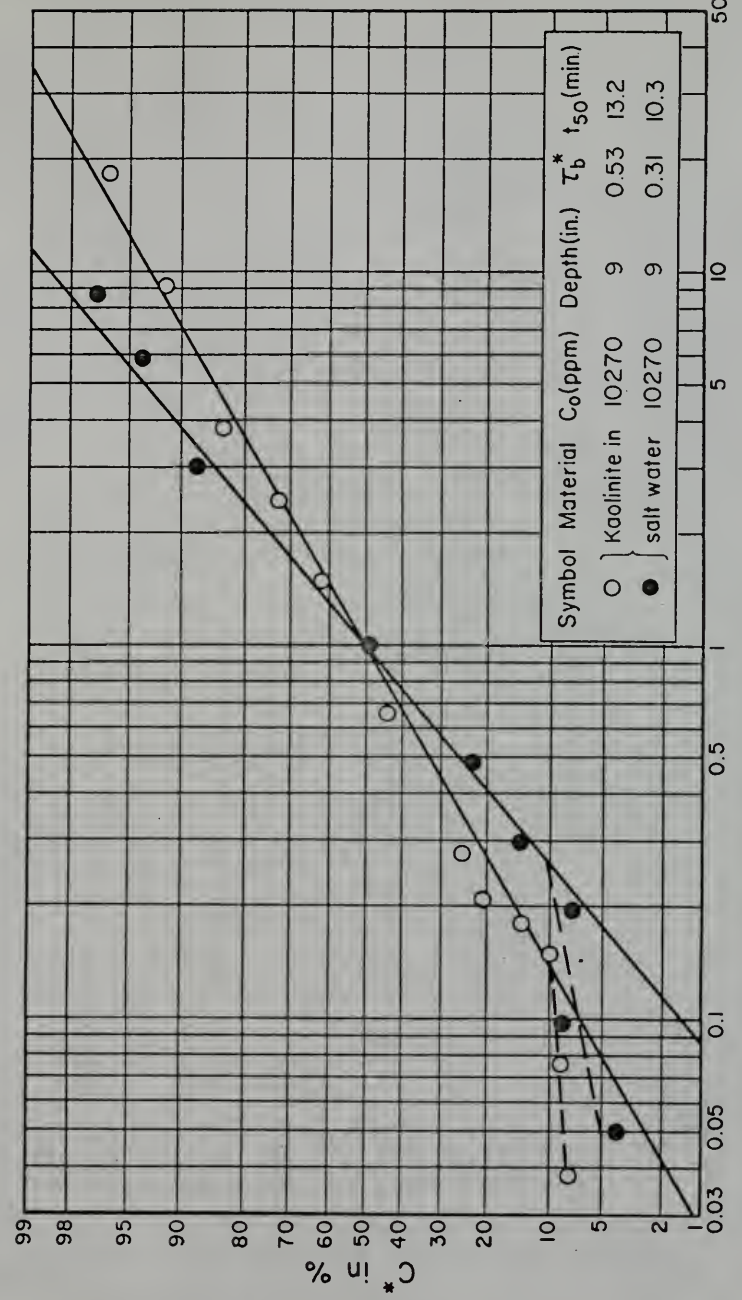

Fig. 4.2.42. c^* in Percent Versus t/t_{50} for Kaolinite in Salt Water.

high momentum to the fluid at the time of the sudden lowering of the ring and channel speeds, at the beginning of the deposition process, is likely to keep the material in suspension from depositing for a short period until the momentum is sufficiently reduced by boundary friction. This, it was noted is especially true in cases where the flow velocity, and consequently, the bed shear stress have relatively low values. Further, such an effect is likely to be more significant for the kaolinite suspension in salt water as compared to distilled water, since as described below, the flocs in the former case are smaller and therefore have lower settling velocities than in the latter case. They may therefore be kept in suspension at relatively lower speeds than the speeds required to keep the larger flocs in distilled water in suspension.

Fig. 4.2.43 shows σ_2 and log t_{50} plotted against τ_b^*, corresponding to the data of Figs. 4.2.39 through 4.2.42. The general qualitative trends for the two curves are similar to those discussed for kaolinite in distilled water. It should however be noted that the two sets of curves both for log t_{50} and σ_2 cannot strictly be compared with each other in terms of the effect of depth or of C_o on the curves, because both the depth and C_o are different in the two cases. Quantitatively, while the σ_2 values on the average do not differ significantly from those for kaolinite in distilled water, the log t_{50} values are in general higher, indicating relatively slower rates of deposition. Slower rates imply the presence of smaller floc sizes, which is in agreement with the observed difference in τ_{bmin} values between that for kaolinite in distilled water and that for

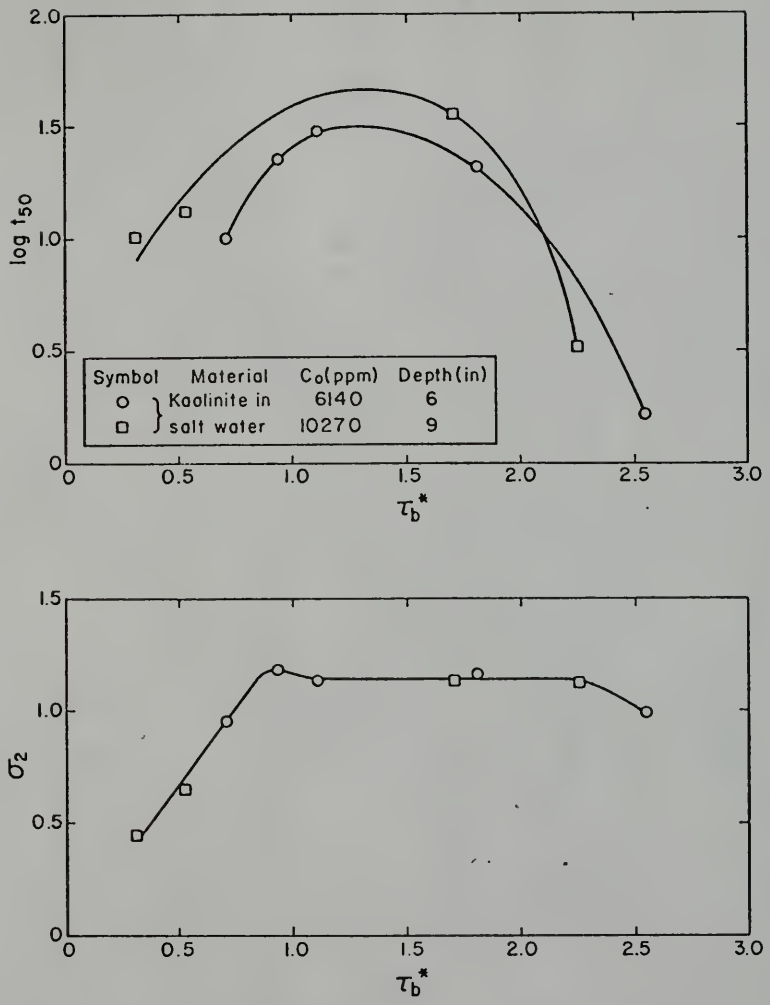

Fig. 4.2.43. Log t_{50} and σ_2 Versus τ_b^* for Kaolinite in Salt Water.

kaolinite in salt water, the latter being lower (1.50 dynes/cm^2) than the former (1.80 dynes/cm^2), which as mentioned in Section 4.2.1, correspondingly indicates smaller floc sizes.

4.2.3 Comparison with Results of Other Investigations

In order to compare the observed logarithmic-normal law for the rates of deposition as indicated by Eqs. (4.2-8) and (4.2-9), with results of other investigations, some of the data of Rosillon and Volkenborn (1964), Krone (1962) and Partheniades (1965) have been reanalyzed and plotted on logarithmic-normal coordinates. The experimental conditions for these investigations have been described in Section 2.2.2.

In Figs. 4.2.44 through 4.2.47, eight runs from the study of Rosillon and Volkenborn are plotted. The agreement with the logarithmic-normal law appears to be good both for τ_b^* values less than as well as greater than unity. The lowest τ_b^* value for which this law holds is 0.14 in Fig. 4.2.44. It should be pointed out that some of the runs corresponding to τ_b^* greater than unity could not be analyzed, because they were not carried out for long enough periods for the establishment of an equilibrium concentration, since the value of the latter is required for obtaining C^*.

The parameters σ_2 and t_{50} for these measurements are plotted against τ_b^* in Fig. 4.2.48. The plot of log t_{50} versus τ_b^* follows the general trend (except for one data point corresponding to τ_b^* of 1.14) for the suspensions of kaolinite. Thus at about $\tau_b^* = 1$, the curve indicates a maximum corresponding to the highest

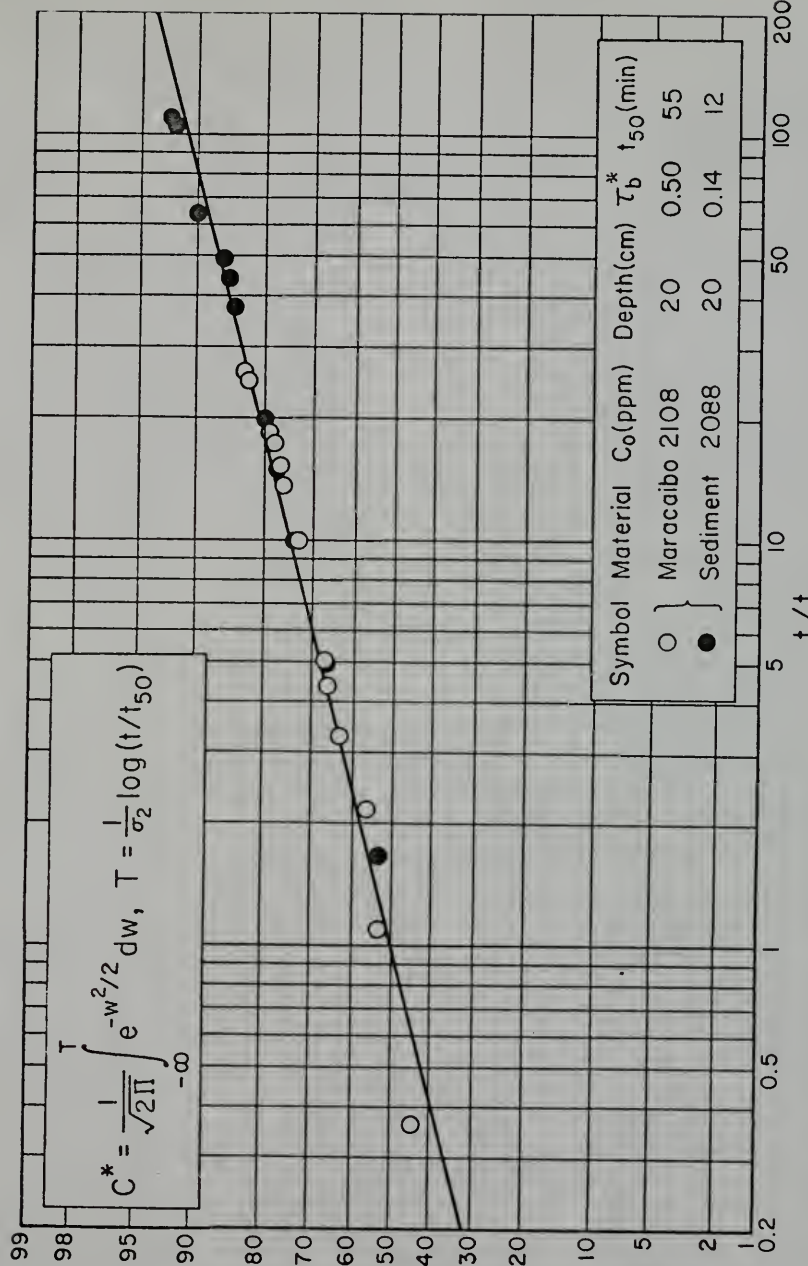

Fig. 4.2.44. Fraction of Depositable Sediment Concentration C^* Deposited at Time t, in Percent, Versus Time Parameter t/t_{50} for Maracaibo Sediment.

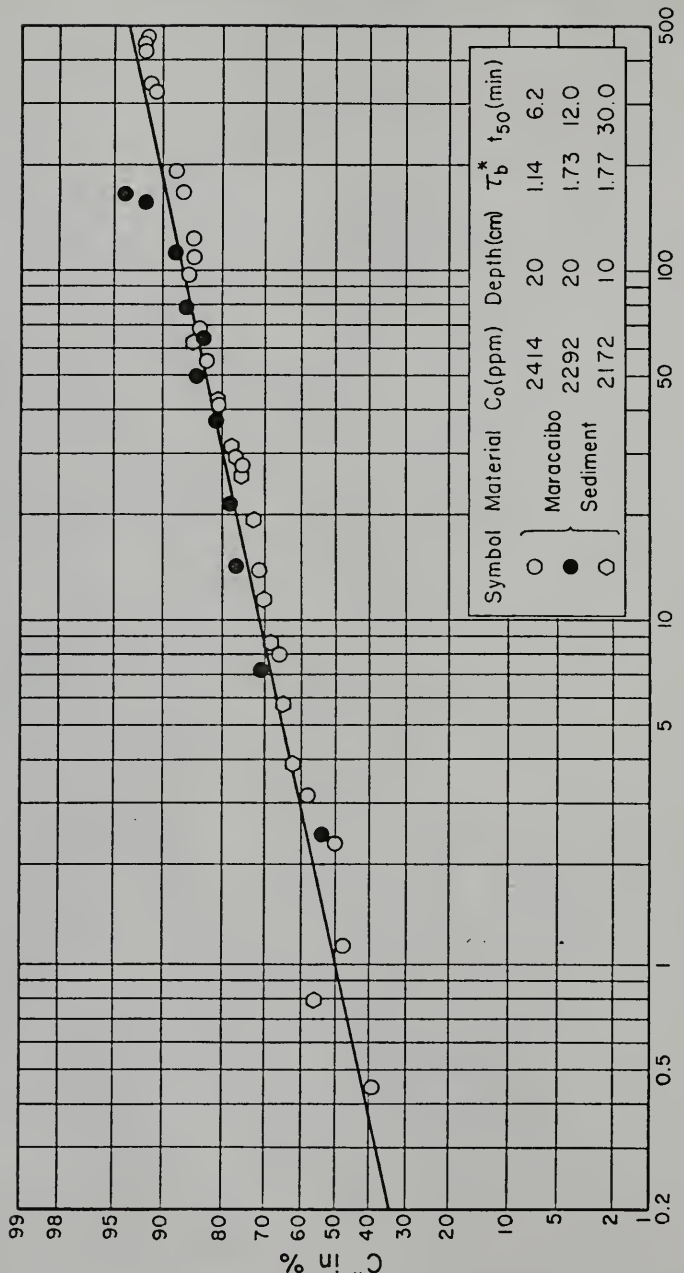

Fig. 4.2.45. C^* in Percent Versus t/t_{50} for Maracaibo Sediment.

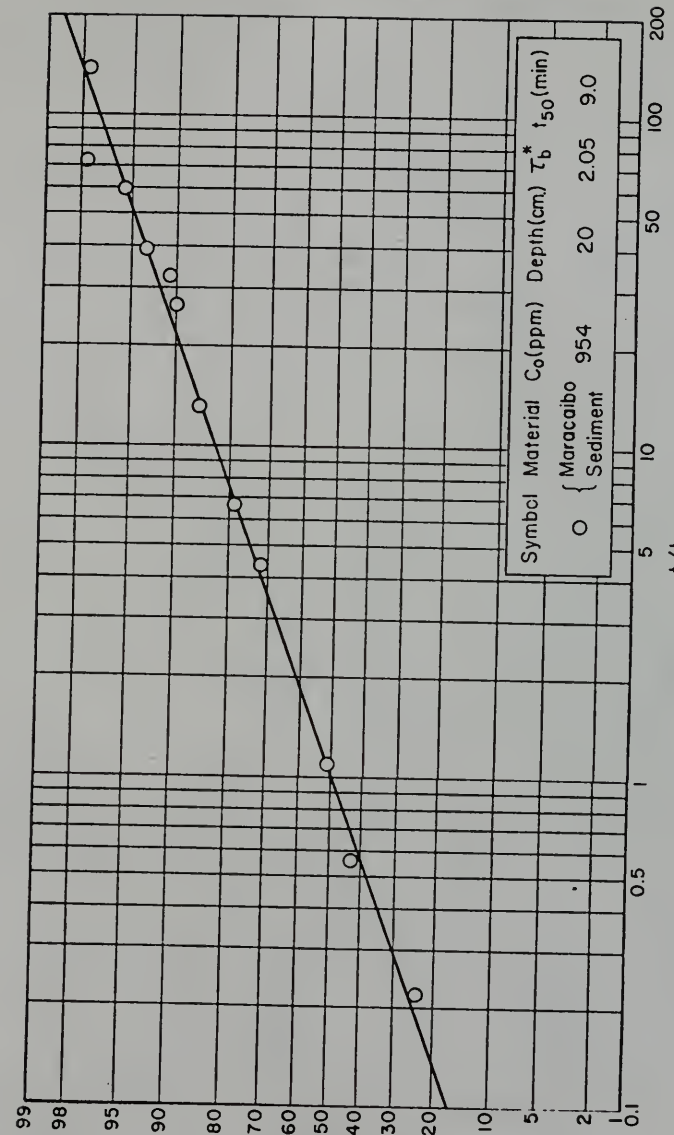

Fig. 4.2.46. C^* in Percent Versus t/t_{50} for Maracaibo Sediment.

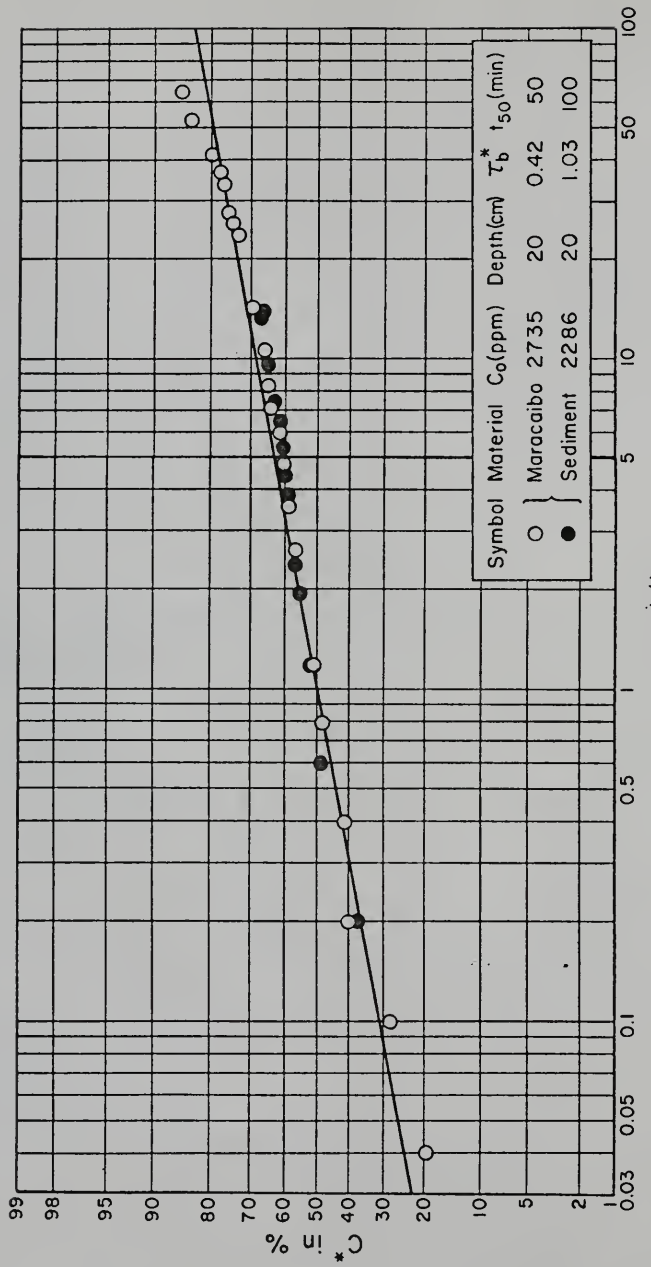

Fig. 4.2.47. C^* in Percent Versus t/t_{50} for Maracaibo Sediment.

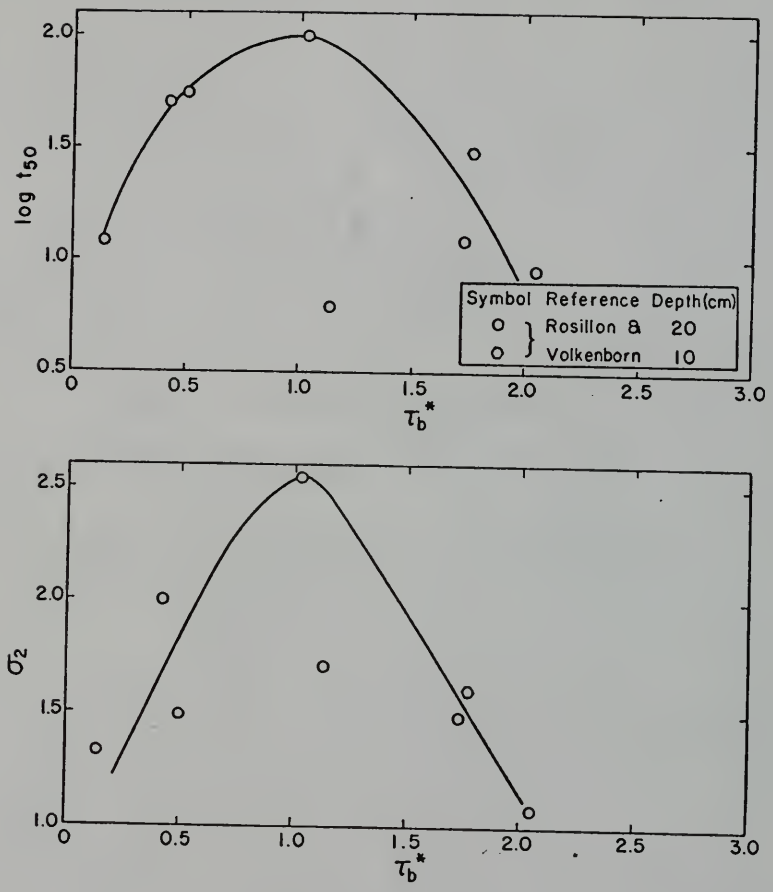

Fig. 4.2.48. Log t_{50} and σ_2 Versus τ_b^* for Maracaibo Sediment.

value of t_{50} of nearly 100 minutes. The effect of depth however is not noticeable because there is only one data point for the 10 cm depth. It should be noted that except for the data point at τ_b^* of 2.05, which corresponds to a C_o of 954 ppm shown in Fig. 4.2.46, the remaining data are for a C_o with a relatively narrow range of 2088 to 2735 ppm, with a mean value of 2210 ppm. Values of t_{50} are somewhat higher than those for the kaolinite suspension, partly because of the slower process of deposition, which is a characteristic of straight flumes, as discussed in Section 2.2.2. The plot of σ_2 versus τ_b^* also qualitatively resembles the corresponding plots for the kaolinite suspensions, for τ_b^* approximately less than unity, but for increasing value of τ_b^* above unity, σ_2 begins to decrease, unlike its behavior for the kaolinite suspension in salt water, where it becomes nearly independent of τ_b^*. Moreover, the σ_2 value is observed to be as high as 2.5, as compared to a value which is a little above unity for the kaolinite suspension, which once again indicates much slower rates of deposition in the tests of Rosillon and Volkenborn.

In Figs. 4.2.49 and 4.2.50, some of the runs of Krone and of Partheniades are described. These are grouped together because although the two investigators employed different flumes, both used Bay mud in salt water in their experiments. Once again the logarithmic-normal law is observed. It should be mentioned that the bed shear stress values for Krone's measurements were obtained from the corresponding mean flow velocity values based on a bed roughness of 0.0015 ft. derived from measurements by Partheniades, and discussed in Section 2.2.2. The value of $\tau_{bmin} = 0.65$ dynes/cm^2 assumed for Krone's data

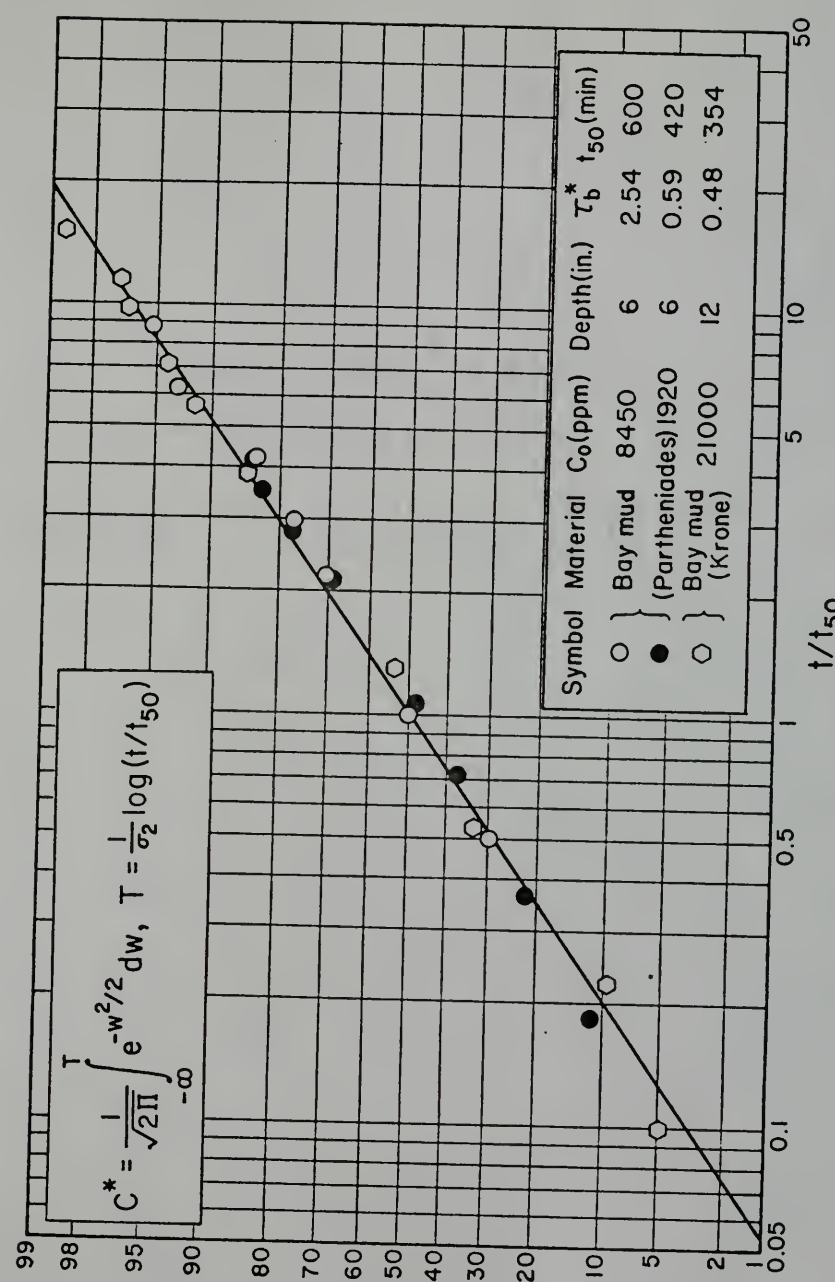

Fig. 4.2.49. Fraction of Depositable Sediment Concentration C^* Deposited at Time t, in Percent, Versus Time Parameter t/t_{50} for Bay Mud.

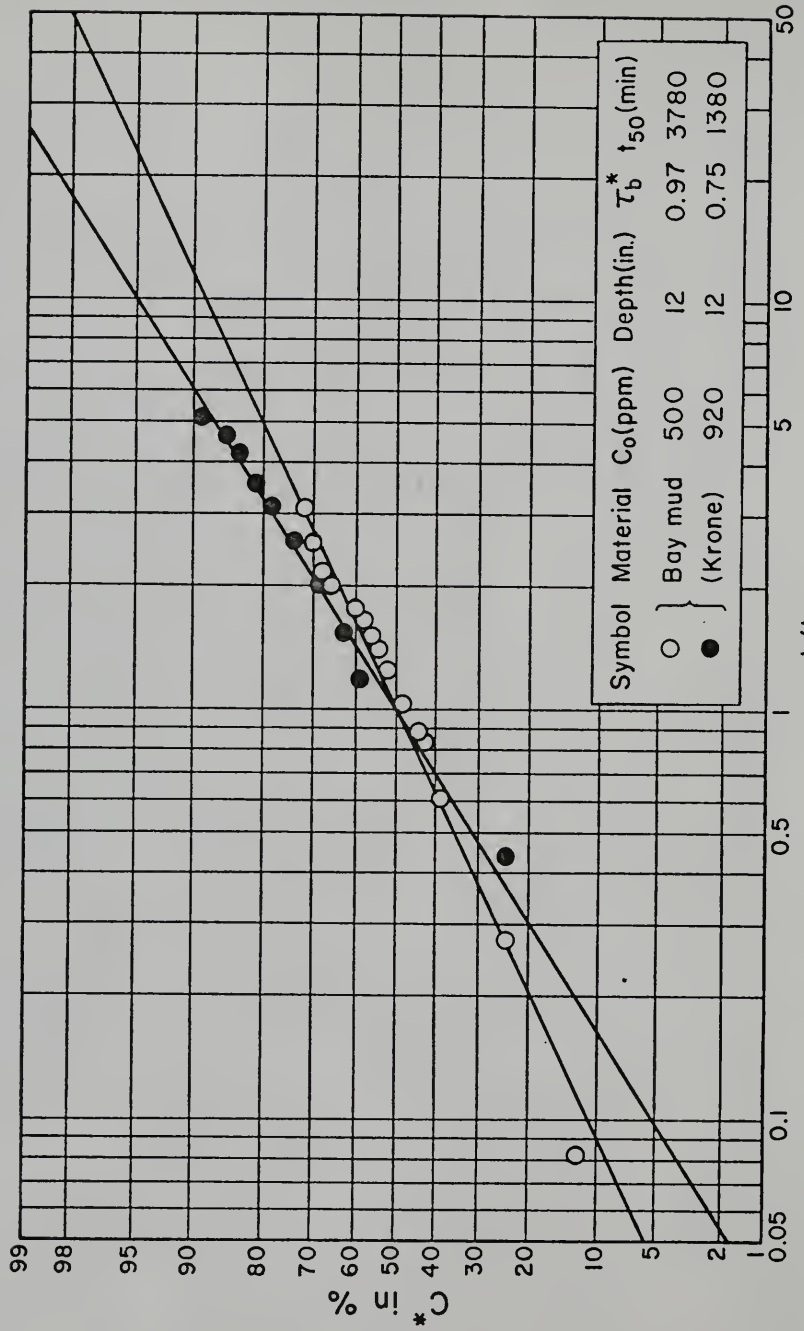

Fig. 4.2.50. C^* in Percent Versus t/t_{50} for Bay Mud.

is also taken from Partheniades' measurements. All of Krone's measurements were for bed shear stresses less than τ_{bmin}, i.e., τ_b^* less than unity.

Since the data points are relatively few, the plots of σ_2 and log t_{50} versus τ_b^* shown in Fig. 4.2.51 are tentative, although it appears that they may indicate trends which are similar to those of the previously discussed suspensions. It is noteworthy that log t_{50} values are on the average nearly twice as large as those for the suspension of kaolinite in salt water, and are also larger in general than those for Maracaibo sediment. For example, at a $\tau_b^* = 1$, a log t_{50} value of 1.5 may be taken as representative of the kaolinite suspension in salt water, whereas the corresponding value in Fig. 4.2.51 is nearly 3.2, i.e., the corresponding t_{50} values are of the order of 32 min and 1600 min, respectively. Thus although the suspensions are different, these numbers, which indicate the amount of time taken for a 50% deposition of the depositable material, give an approximate idea of the slowness with which settling occurs in straight flumes.

An interesting comparison of deposition rates for the indicated C_o and τ_b^* values and sediment suspensions is made in Fig. 4.2.52. Significant portions of these runs may be described by the logarithmic-normal law, but the upper ends of these curves deviate from this law and indicate in each case, much faster rates than would be suggested by the law. In Fig. 4.2.53, these runs are plotted on a semi-logarithmic plot. It appears that in each case, below the concentrations corresponding to the indicated horizontal dashed lines, the

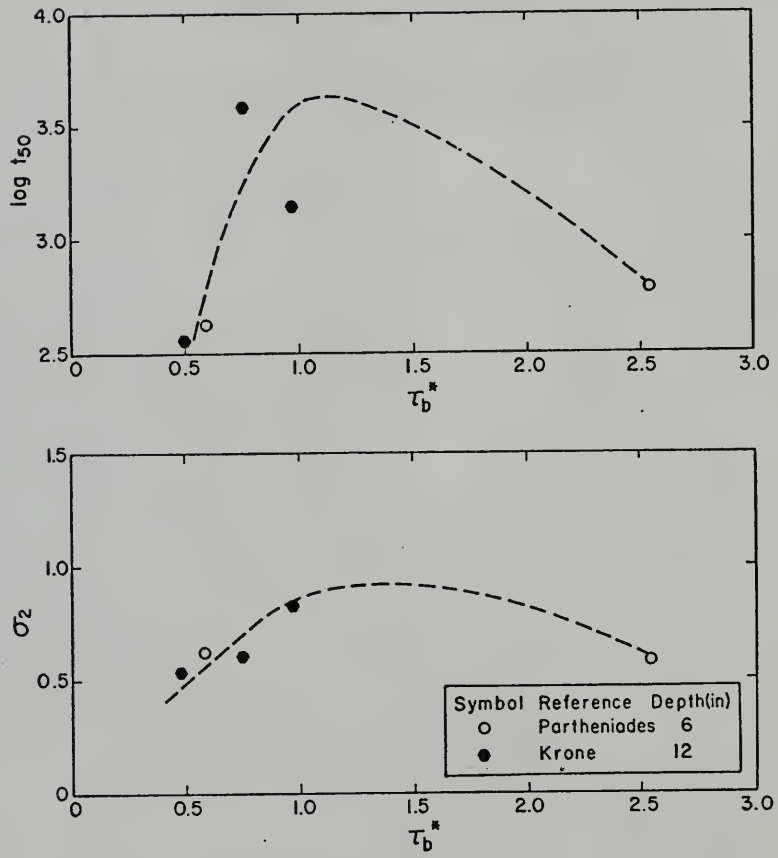

Fig. 4.2.51. $\log t_{50}$ and σ_2 Versus τ_b^* for Bay Mud.

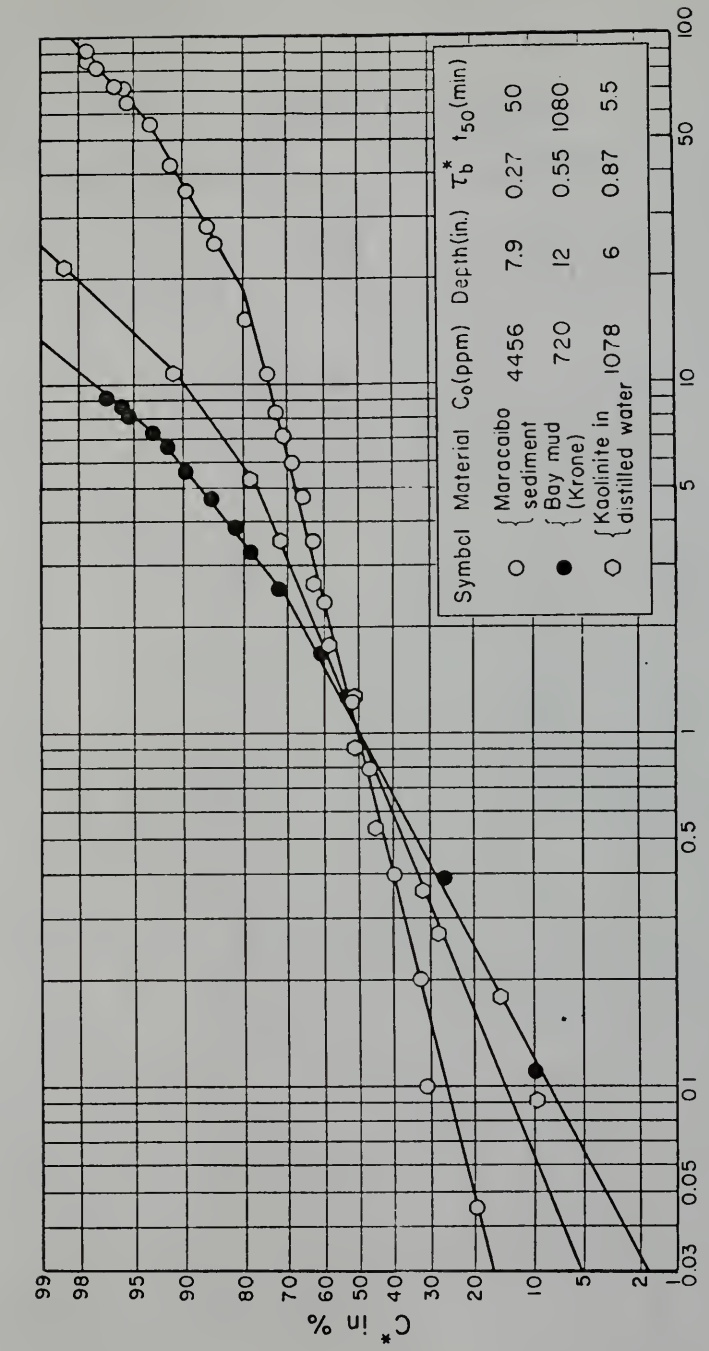

Fig. 4.2.52. Fraction of Depositable Sediment Concentration C^* Deposited at Time t, in Percent, Versus Time Parameter t/t_{50} for Three Different Suspensions.

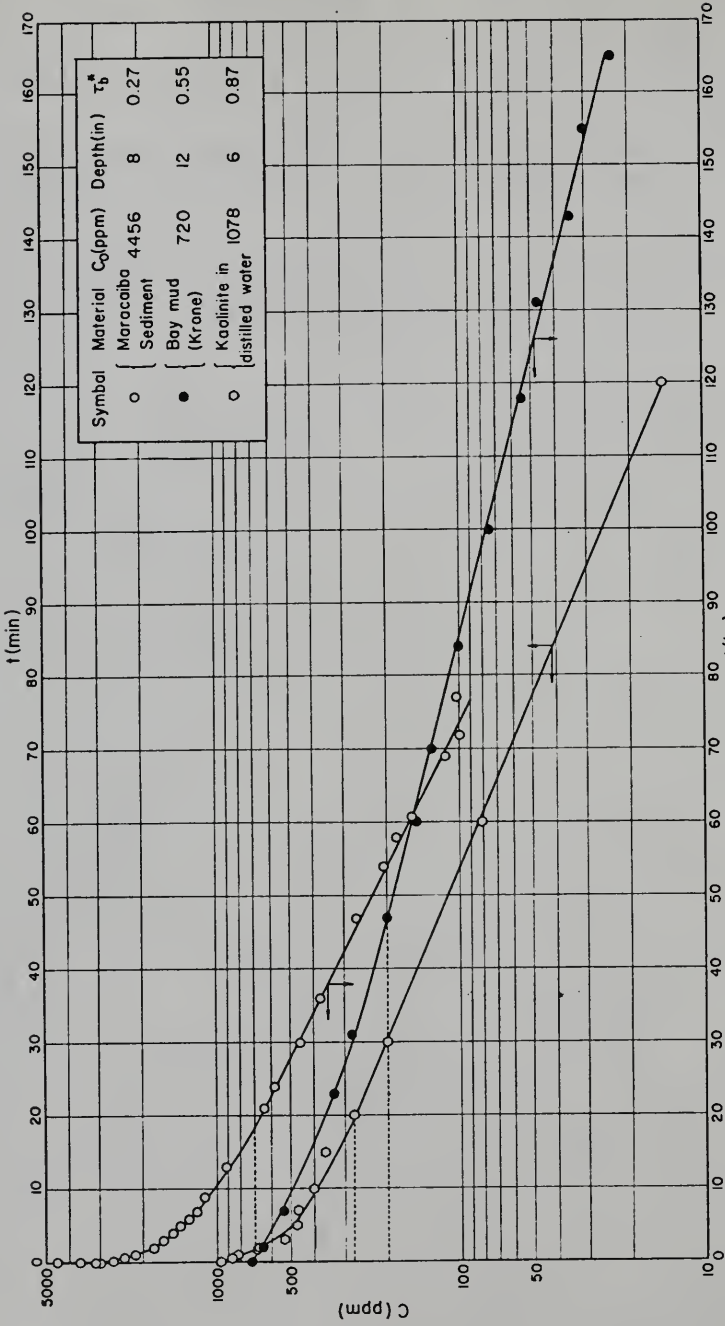

Fig. 4.2.53. Suspended Sediment Concentration C Versus Time t for Three Different Suspensions.

concentration decreases exponentially with time according to Eq. (2.2-2) suggested by Krone (1962). In Table 4.2.1, the ratios C/C_o are computed from Fig. 4.2.52 corresponding to the limit beyond which the logarithmic-normal law cannot reasonably approximate the data in each case, and also from Fig. 4.2.53 corresponding to the limit below which the data can be approximated by the exponential law of Eq. (2.2-2). A comparison of the ratios for each case shows a close agreement, and suggests that the portion of the curve that cannot be described by the exponential law in fact can be represented by the logarithmic-normal relationship. In his experiments, Krone observed that for concentrations below approximately 300 ppm, the exponential law of Eq. (2.2-2) holds. However, from the plots of Fig. 4.2.53 and the ratios C/C_o of Table 4.2.1 it appears that the level of suspended concentration below which Eq. (2.2-2) is valid is likely to be dependent on the type of sediment suspension, τ_b^*, depth of flow and C_o. Further the ratios C/C_o Table 4.2.1 suggest that at least for the runs of Fig. 4.2.53, the exponential law is valid only for the deposition of nearly the last one-fifth of the initial amount of sediment. Krone (1962) however found in his experiments that for extremely low τ_b^* values and C_o of the order of 100 to 200 ppm, the entire amount of sediment deposits according to the exponential law.

The run for kaolinite in distilled water plotted in Figs. 4.2.52 and 4.2.53 was the only measurement in the annular channel in which the last relatively small fraction of the suspended sediment deposited according to the exponential law. The range of validity of this law cannot be determined from one set of data. Further

investigation is therefore necessary to determine the applicability of the law at low sediment concentrations and bed shear stresses.

TABLE 4.2.1

Material	C_o (ppm)	Depth (in.)	τ_b^*	C/C_o in % from Fig. 4.2.52	C/C_o in % from Fig. 4.2.53
Maracaibo Sediment	4456	8	0.27	20.0	15.7
Bay Mud (Krone)	720	12	0.55	29.0	27.8
Kaolinite in Distilled Water	1078	6	0.87	22.0	25.5

4.2.4 Depth-Concentration Profiles

In order to examine the concentration gradients in the channel, tests for the measurements of deposition rates were carried out for the kaolinite suspension in distilled water, at a flow depth of 13 in. At this depth, it was possible to use all the four sample taps, which are located at heights y from the bottom of 1-9/16, 5, 8-3/4 and 12-1/8 in., respectively, as noted in Section 3.1.2. The tests conducted were for a C_o of 7680 ppm, and also for a C_o of 16900 ppm. Results from one of the tests for τ_b of 2.95 dynes/cm^2 are shown in Fig. 4.2.54. Measurements from all four taps indicate that the concentration in each case, approaches an equilibrium value, after

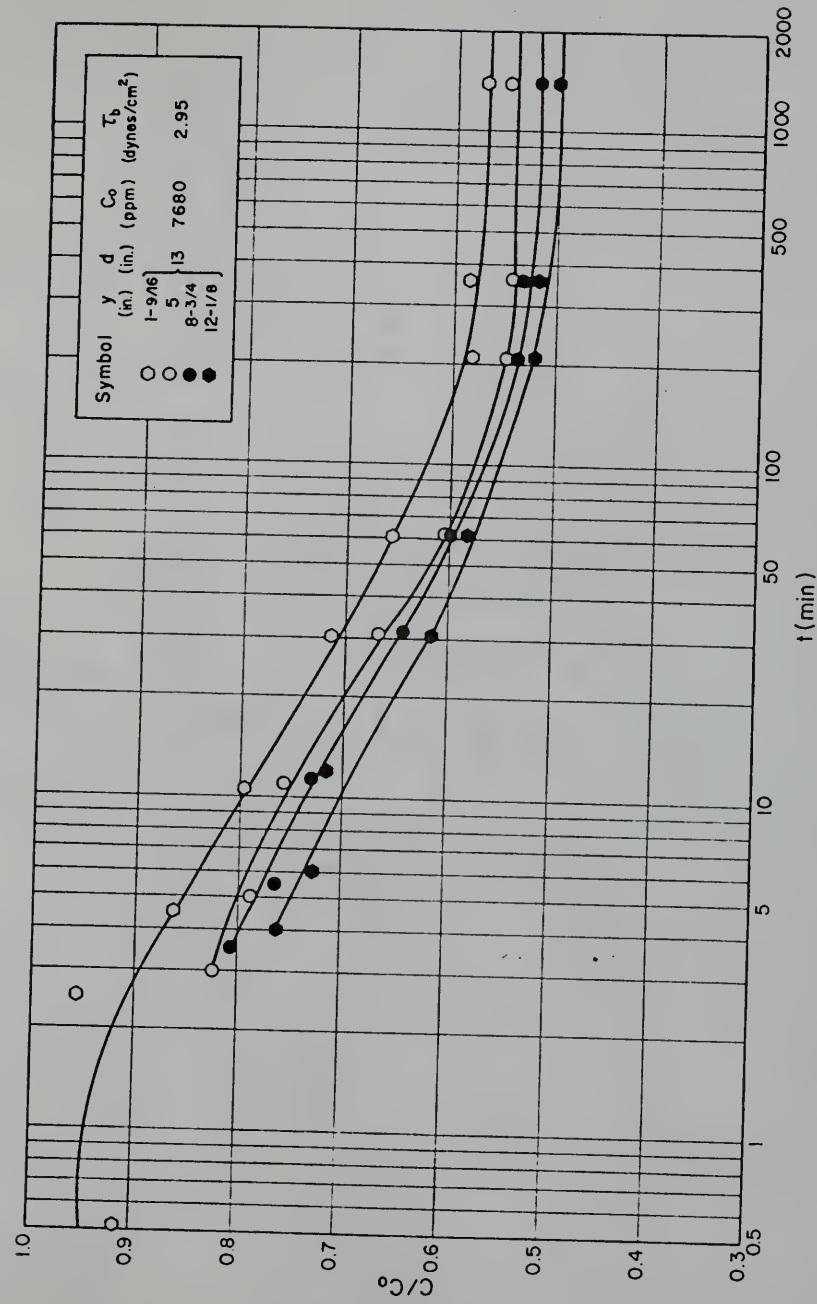

Fig. 4.2.54. Depth-Concentration Profiles Versus Time t for Kaolinite in Distilled Water for τ_b = 2.95 (dynes/cm^2).

almost a 1000 min period of deposition. In addition, the profiles indicate that the concentration gradients are relatively small. Thus, for example, at 5 min after the beginning of deposition, the highest concentration at y = 1-9/16 in. is higher than the lowest at y = 12-1/8 in. by about 12% only, and at 1400 min from the beginning of deposition, this difference is approximately 16%.

Fig. 4.2.55 shows measured profiles for C_o of 7680 ppm and τ_b of 1.10 dynes/cm^2, or τ_b^* of 1.10/1.80 = 0.61, which corresponds to a case of complete deposition of all the sediment. Thus, at 80 min, the suspended sediment is already only about 5% of the initial value. The concentration gradients appear to be relatively steep in the beginning, but after only about 15 min, they can be observed as becoming small.

It should be noted that the bed shear stresses computed for measurements at 13 in. depth could not be obtained directly from false bottom measurements, because out of the total channel depth of 18 in., only 13 in. could be used for false bottom measurements, as the latter itself was at an elevation of 5 in. from the channel bottom. However, in order to utilize the entire 13 in. of depth, water would have had to be filled up to the brim of the channel, which would then have resulted in spilling, when the ring was rotated over the water surface. For this reason, the bed shear stresses for 13 in. depth were obtained by extrapolation of the measurements given in Fig. 4.1.2.

In all measurements on the deposition rates described in Section 4.2.2, for each depth of flow, only one sample tap was

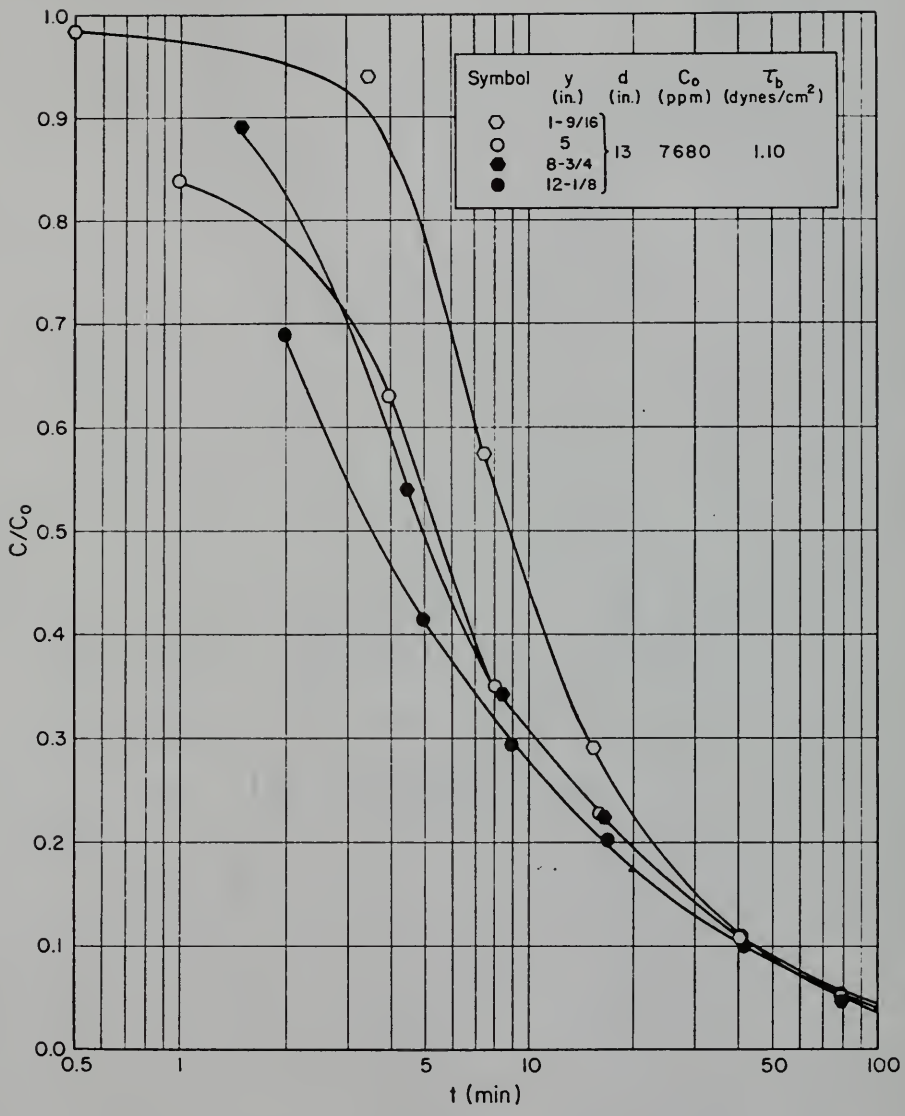

Fig. 4.2.55. Depth-Concentration Profiles Versus Time t for Kaolinite in Distilled Water for τ_b = 1.10 (dynes/cm^2).

used to determine the concentrations. Table 4.2.2 gives the flow depths d, the tap elevation y and the ratio y/d.

TABLE 4.2.2

Depth d (in.)	y (in.)	y/d
6	5	0.83
9	5	0.56
12	8-3/4	0.73
13	8-3/4	0.67

Measurements close to y/d = 0.50 would probably give values of the concentrations close to the values averaged over the depth of flow. Table 4.2.2 indicates that such is approximately the case only for 9 in. depth, the y/d values for other depths being relatively much higher. It should however be noted that strictly speaking y in this situation should be measured from the deposited bed surface, rather than the channel bottom, and this would accordingly reduce the y/d ratios. Further as mentioned earlier the observed concentration gradients are relatively small, so that the measured concentrations are not likely to be significantly different from the mean value. For this reason, measurements described in Section 4.2.2, and even those of other experimenters in Section 4.2.3, may be considered as depth-averaged values.

Under a steady state situation, when the equilibrium concentration of the suspended sediment is attained, the downward flux $W_s C$

due to gravitational settling of the flocs, where W_s is the terminal settling velocity and C is the sediment concentration, is balanced by the upward diffusive flux due to turbulence $\varepsilon_y(dC/dy)$, where ε_y is the turbulent diffusivity in the y direction. So that, according to this balance,

$$-W_s C = \varepsilon_y \frac{dC}{dy} \tag{4.2-15}$$

Now according to the velocity profile measurements described in Section 4.1.3, in the middle zone of flow nearly between 1 in. below the ring and 1 in. above the bed, the turbulence appears to be very nearly homogeneous, which implies that ε_y in this zone may be considered to be nearly independent of elevation y. This independence allows Eq. (4.2-15) to be integrated to yield

$$\frac{C}{C_a} = e^{-\frac{W_s}{\varepsilon}(y-a)} \tag{4.2-16}$$

where ε is a diffusivity independent of y, and C_a is a reference concentration at an elevation a from the bed. Eq. (4.2-16) has been investigated by Rouse (1961). It may be alternatively expressed as

$$\log\left(\frac{C}{C_a}\right) = -\frac{W_s}{(2.3)\varepsilon}(y - a) \tag{4.2-17}$$

Since the concentration profiles described in this section were measured approximately in the zone of homogeneous turbulence, as indicated by the sample tap elevations, the validity of Eq. (4.2-17) was examined by plotting $\log(C/C_a)$ versus y - a for three different profiles, after the attainment of equilibrium concentration, as indicated in Figs. 4.2.56 and 4.2.57, where C_a is the concentration

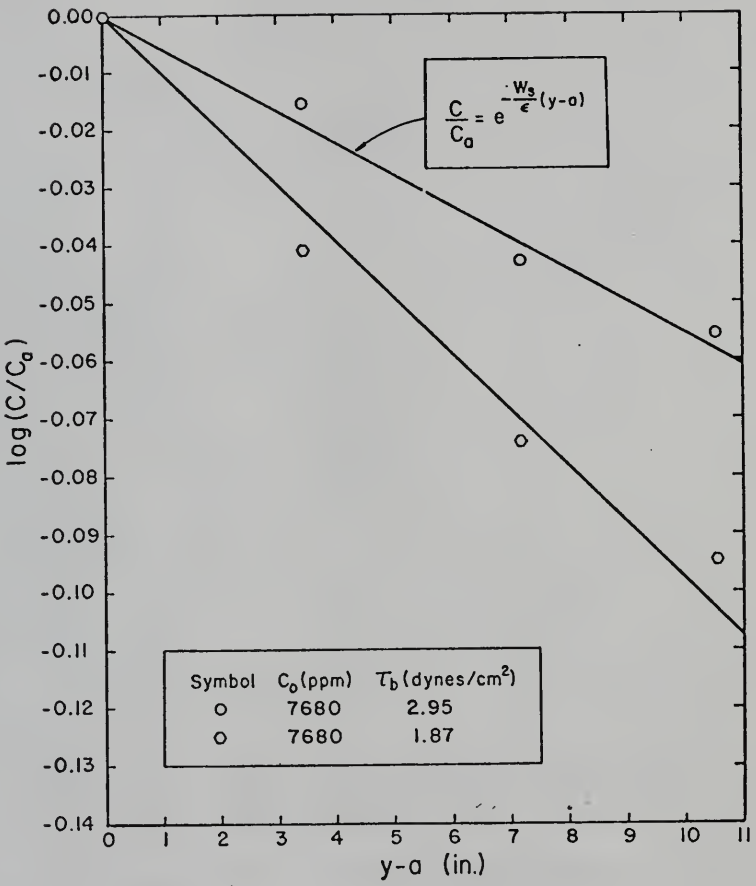

Fig. 4.2.56. Depth-Concentration Profiles at Equilibrium Concentration.

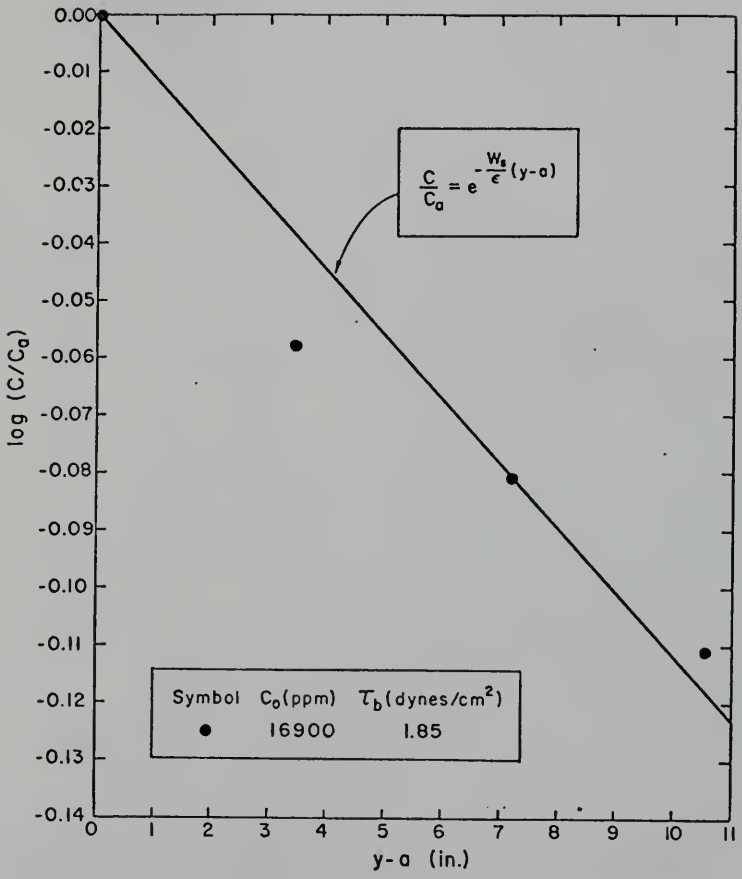

Fig. 4.2.57. Depth-Concentration Profile at Equilibrium Concentration.

at a = 1-9/16 in. The data points do indicate linear relationships predicted by Eq. (4.2-17), with slopes of $-W_s/(2.3)\varepsilon$. The agreement must be considered good especially in view of the fact that the $\log(C/C_a)$ axis is particularly sensitive to variations in C/C_a, and therefore also to errors in experimental measurements. For example, in Fig. 4.2.57, at y - a of 3.44 in., $\log(C/C_a)$ is plotted at -0.058, which corresponds to C/C_a of 0.874. On the other hand, if the same data point were to fall on the indicated straight line, $\log(C/C_a)$ would be -0.039, or C/C_a of 0.914, which is higher than the measured value by less than 6%.

Data corresponding to the straight lines of Figs. 4.2.56 and 4.2.57 are given in Table 4.2.3, where the values W_s/ε are obtained from the slopes.

TABLE 4.2.3

C_o (ppm)	τ_b (dynes/cm^2)	u_* (in/sec)	W_s/ε (in.)$^{-1}$
7680	2.95	0.68	0.013
7680	1.87	0.54	0.022
16900	1.85	0.54	0.026

The eddy diffusivity ε is in general expected to depend on u_* and C, so that

$$\varepsilon = \varepsilon(u_*, C) \qquad (4.2\text{-}18)$$

However, since the exact form of this general functional relationship

is not known a priori, absolute values of the settling velocities W_s cannot be obtained from the values of W_s/ε given in Table 4.2.3.

Partheniades (1962) measured velocity profiles in cohesive sediment laden flows in an open straight flume, with the help of a specially designed pitot tube, and observed that the profiles were not affected by the presence of suspended sediment to any significant extent. Such an observation suggests that the eddy diffusivity ε does not depend on the amount of the suspended material. Comparing the second and third set of data in Table 4.2.3, which correspond to the same value of u_* of 0.54 in./sec, it may be observed that despite almost doubling the initial concentration from 7680 to 16900 ppm, which also correspond to an increase in the equilibrium concentration by the same factor, the ratio W_s/ε is not affected significantly in relation to the error in estimating the value of this ratio, from the measured data. If it is therefore assumed as a first approximation that even in the present situation, ε is unaffected by the indicated change in suspended sediment concentration, then it may be inferred that the constancy of the ratio W_s/ε for the same u_* value indicates that the settling velocity W_s is also unaffected by the amount of suspended material in the case considered.

4.3 Discussion of Results

4.3.1 Near-bed Processes

The depositional behavior of sediment flocs in a turbulent flow field is controlled primarily by the dynamics of interaction between two kinds of stochastic physical processes occurring just above

the sediment bed. One of these is related to the kinetics of inter-floc collisions, and the other is related to the probability that a floc of a given size and shear strength may deposit on the bed itself. The inter-floc collision frequency is highest in the near-bed region of the flow, because the prevailing shear stresses are also of highest magnitude in this zone. In that region, under the growth-promoting influence of large numbers of collisions, and the growth-limiting influence of local shear, a floc will attain an optimum size.

The near-bed zone may be assumed to have a thickness ℓ_b of a few floc diameters, such that in general

$$\ell_b = \alpha_o d_s \qquad (4.3\text{-}1)$$

where d_s is the floc diameter and α_o is a proportionality coefficient. This assumed definition of ℓ_b requires some explanation. Since the floc diameter d_s is itself a function of the shear stresses acting within the near-bed zone, the thickness of this layer will vary with these stresses. As noted in Section 4.2.1, the bed shear stress in the measurements was varied from nearly 0.4 to 11 dynes/cm^2. Considering the deposition of Bay mud, for which a bed roughness k_s = 0.0015 ft. was derived, the wall Reynolds number $u_* k_s/\nu$ corresponding to this range of bed shear stress varies from nearly 3 to 16. Here, $\nu = 10^5$ ft.^{2}/sec is the kinematic viscosity of water. Christensen (1969) has modified the Prandtl mixing length hypothesis by introducing a hypothetical laminar mixing length, and this modification results in a more consistent description of the laminar sublayer. Using his results, which relate the variation of the laminar

sublayer thickness δ with $u_* k_s/\nu$, the range of δ for the present case may be found to be 0.0036 to 0.0022 ft., or a range of nearly 1200 to 730 microns. δ is thus observed to decrease with increasing bed shear stress which is expected. As a rough estimate, according to the results of Krone (1962) discussed in Section 2.2.2, a Bay mud floc may attain a size of approximately 45 microns at a τ_b of 0.4 dynes/cm^2. It is thus seen that δ at this shear stress is almost 27 diameters thick. Krone's measurements do not extend beyond τ_b greater than 0.6 dynes/cm^2, but from the observed estimate at 0.4 dynes/cm^2, it may be concluded that the floc size will in general not be of the same order of magnitude as the thickness of the laminar sublayer, even at higher shear stresses. According to the experimental measurements in the annular channel, kaolinite flocs have been observed to be somewhat larger than the Bay mud flocs, but the above derived conclusions regarding the floc size in comparison with the thickness of the laminar sublayer may be expected to hold even for kaolinite flocs. The near-bed layer ℓ_b may thus be generally considered, as a consequence of these conclusions, as one which is less than the laminar sublayer thickness in order of magnitude, i.e., the proportionality coefficient α_o will be less than unity.

The overall process of deposition may be elaborated by considering the formation of a sediment floc of a given size, as a result of one or more collisions, anywhere in the zone of thickness ℓ_b of the suspension just above the sediment bed. If this floc is sufficiently large, it will be able to descend towards the bed surface by countering the upward momentum flux due to turbulent

diffusion. When the floc approaches close enough to the bed surface, it is subjected to highest drag and hydrodynamic lift forces. These two forces at a given location and instant of time are proportional to each other, and their variation with time about their mean values is of a stochastic nature. Therefore, if the shear strength of the floc is of a sufficient magnitude to be able to withstand the high shear stresses acting on it, it will ultimately touch the bed and become part of it by attaching itself to its neighbors by cohesive bonds. If, however, the floc is composed of units held together by relatively weak forces, then the existing shear will rupture the descending floc at some plane or planes of failure, and the resulting smaller units, as a result of the rotation induced hydrodynamic lift, will be re-entrained into suspension. This situation is depicted schematically in Fig. 4.3.1, where τ_i is the local instantaneous shear stress acting on the floc.

Considering these processes, the probability that a floc may deposit is in general less than unity. As discussed below, this probability for a given sediment suspension is expected to depend on the flow condition as well as properties of the floc.

The instantaneous hydrodynamic lift force L may be expressed as the sum of the mean $\overline{L}$ and fluctuating L' components as

$$L = \overline{L} + L' \tag{4.3-2}$$

If τ_{bi} is the instantaneous value of the bed shear stress, then L and τ_{bi} may be expressed in terms of the instantaneous velocity u_t just above a floc as

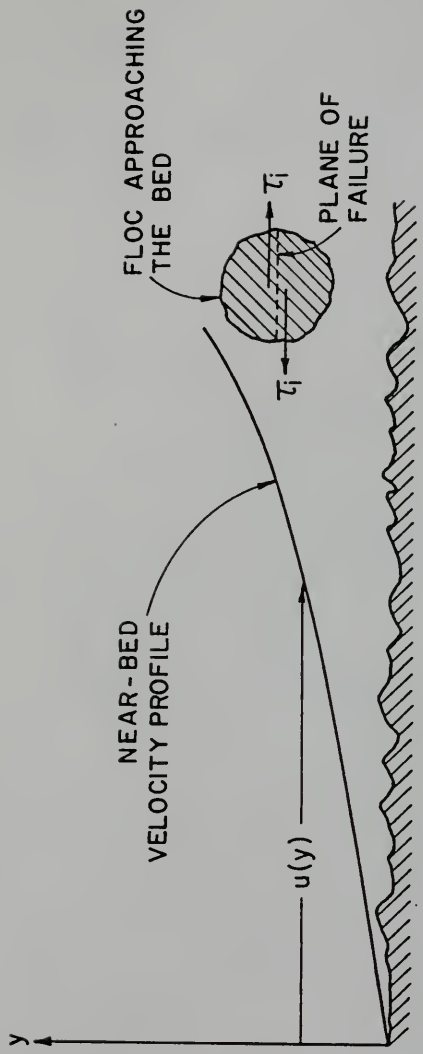

Fig. 4.3.1. Near-bed Effect of Shear Stress on Flocs.

$$L = C_L \alpha_1 d_s^2 \gamma \frac{u_t^2}{2g} \tag{4.3-3}$$

$$\tau_{bi} = C_\tau \gamma \frac{u_t^2}{2g} \tag{4.3-4}$$

where C_L and C_τ are the lift and drag coefficients, respectively, α_1 is an area shape factor, γ the specific weight of water and g the acceleration due to gravity. The coefficients C_L and C_τ in general depend on the flow conditions. Thus, at any given instant of time, L and τ_{bi} are related according to

$$\tau_{bi} = \frac{C_\tau}{C_L \alpha_1 d_s^2} L \tag{4.3-5}$$

So that any process described in terms of the lift force L can be equivalently described by the corresponding τ_{bi} through Eq. (4.3-5). Eq. (4.3-2) may be written as

$$L = \bar{L}(1 + \eta) \tag{4.3-6}$$

where $\eta = L'/\bar{L}$ is a random variable with a mean of zero. In Fig. 4.3.2, τ_{bi} and L are plotted according to Eq. (4.3-5), where, the fact that a negative bed shear stress, i.e., one whose direction is opposite to the direction of flow, can also give rise to an upward (positive) lift is taken into consideration. Also indicated therein is a frequency distribution $\phi(\eta)$ for η and the corresponding cumulative probability distribution P such that

$$P = P_r\left\{ \frac{L}{\bar{L}} - 1 \leq \eta \right\} \tag{4.3-7}$$

and

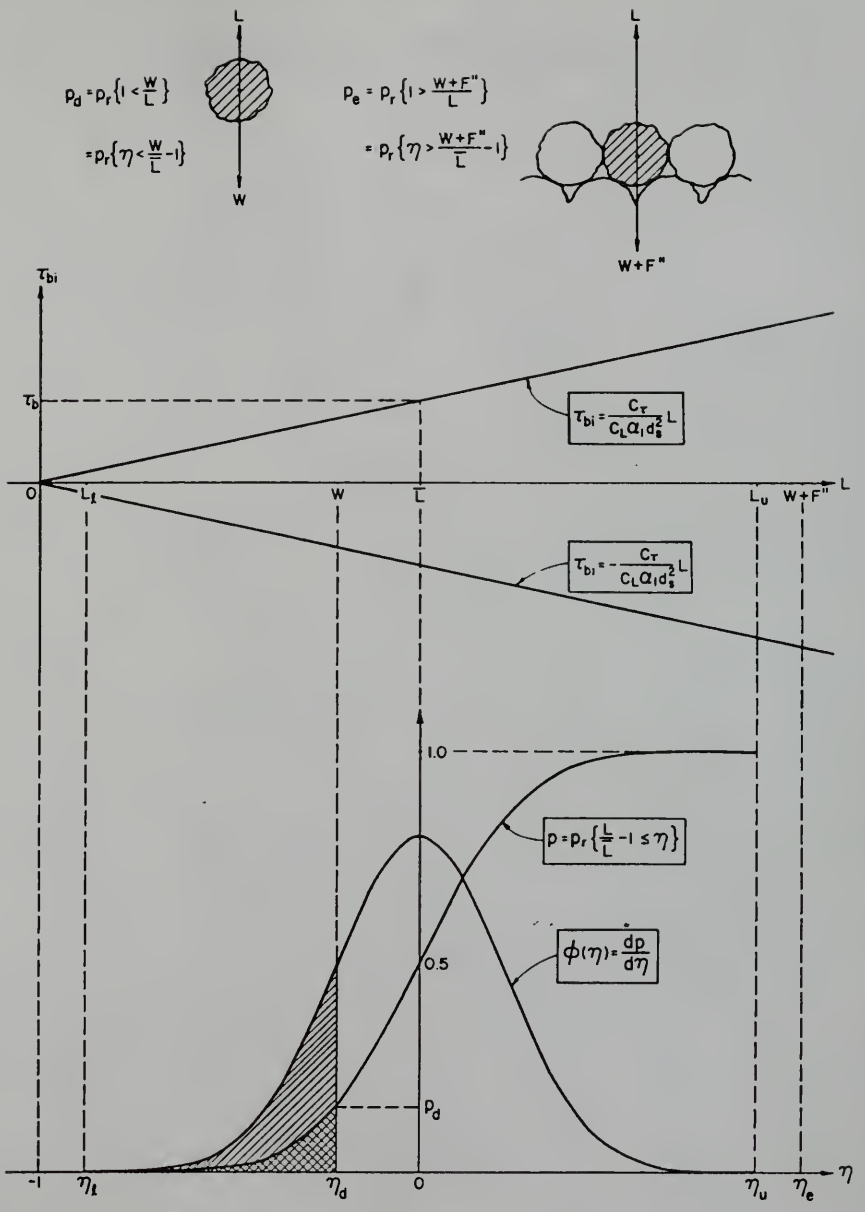

Fig. 4.3.2. Probabilities of Erosion and Deposition for Cohesive Sediments.

$$\phi(\eta) = \frac{dp}{d\eta} \tag{4.3-8}$$

Since real variables, by their very nature, can only have values of finite magnitude, it is assumed here that for any given situation, L will fluctuate between two finite values L_ℓ and L_u, as indicated in Fig. 4.3.2. This concept of a finite range $L_u - L_\ell$ for fluctuations of L has been used by Partheniades (1973) to develop a new definition of the wash load in channels in equilibrium. In Fig. 4.3.2 corresponding to the range $L_u - L_\ell$, the range of fluctuation of η is $\eta_u - \eta_\ell$, where $\eta_u = L_u/\overline{L}$ and $\eta_\ell = L/\overline{L}$. Because of the need to deal with probability density distributions for finite ranges of a random variable, analytic forms for such functions have been developed. One such function has been proposed by Braswell and Manders (1970), which has two parameters, one of which determines the mean and the other is a measure of the spread, and is therefore related to the standard deviation.

With respect to the described nature of deposition and the finite range of variation of the lift force L, the probability of deposition, p_d, may be defined as

$$p_d = p_r\left\{1 < \frac{W}{L}\right\} \tag{4.3-9}$$

and

$$p_d = 0 \quad \text{for} \quad 1 > \frac{W}{L_\ell} \tag{4.3-10}$$

Here, W is the buoyant weight of the floc expressed as

$$W = \alpha_2 d_s^3(\gamma_s - \gamma) \tag{4.3-11}$$

where α_2 is a volume shape factor and γ_s is the specific weight of the floc. According to Eqs. (4.3-9) and (4.3-10), if at any instant, the buoyant weight of the floc W is greater than the hydrodynamic lift force L, then deposition of the floc will occur. Further, since L cannot be lower than L_ℓ, p_d is consequently zero for W equal to or less than L_ℓ. Eqs. (4.3-9) and (4.3-10) can also be expressed as

$$p_d = p_r\left\{\eta < \frac{W}{L} - 1\right\} \tag{4.3-12}$$

and

$$p_d = 0 \quad \text{for} \quad \eta_\ell \geq \frac{W}{L} - 1 \tag{4.3-13}$$

Substituting Eqs. (4.3-5) and (4.3-11) into Eq. (4.3-12) gives

$$p_d = p_r\left\{\eta < \frac{\alpha_2 d_s^3(\gamma_s - \gamma)}{\frac{C_L \alpha_1 d_s^2}{C_\tau} \cdot \tau_b} - 1\right\} \tag{4.3-14}$$

where τ_b is the mean value of τ_{bi}. Thus for a given sediment suspension under a given flow condition if it is assumed that $\gamma_s - \gamma$ is constant, then p_d is shown by Eq. (4.3-14) to be dependent on the floc diameter d_s and the mean bed shear stress τ_b. If η_d is the value of η corresponding to a condition of equality within the brackets on the right-hand side of Eq. (4.3-14), then in general

$$p_d = p_r\left\{\eta_\ell \leq \frac{W}{L} - 1 < \eta_d\right\} \tag{4.3-15}$$

This condition is shown by the hatched regions in Fig. 4.3.2.

4.3.2 Nature of Equilibrium Concentration

The observation that for a given bed shear stress τ_b the relative equilibrium concentration $C^*_{eq} = C_{eq}/C_o$ remains independent of C_o is particularly significant from the point of inferring the nature of the equilibrium concentration C_{eq}, which in turn reflects the properties of the sediment floc themselves. In cohesionless sediment (e.g., sand) transport, the bed material load transport of such a material under a "steady state" condition has been explained (Einstein, 1950) in terms of a condition of equilibrium between the rates of sediment depositing and the rates of sediment eroding from the bed. In other words, the number of particles depositing per unit bed area per unit time is equated to the number of particles eroding per unit bed area per unit time. Recently, Chiu (1972) has extended this concept of bed load transport of sand, based on the same principle of equilibrium between eroding and depositing fluxes, to include the total transport of bed material load over the entire depth of flow, both in air and in water. This type of transport phenomenon implies that if in a channel in equilibrium additional amount of material of the same kind as that already present in the bed is added to the flow, then the concentration of the load will reduce to its previous equilibrium value, and the rates of erosion and deposition per unit bed area will attain the same values as before the addition, because they are determined, for a given sediment type, by the flow conditions alone. The rate of transport of the material at equilibrium will therefore remain unaffected.

In cohesive sediment transport, a similar explanation based on a process of simultaneous erosion and deposition of bed material resulting in equal rates for both does not hold, because the constancy of the ratio C_{eq}/C_o for a given flow condition implies that the initial concentration C_o rather than the flow condition determines the transport load. Thus, for example, if for a given flow condition, C_o is doubled, C_{eq} will double, and if C_o is halved, then C_{eq} will correspondingly be halved. It should be pointed out that this effect of C_o on C_{eq} was found, in the experiments on kaolinite in distilled water, to hold up to a C_o of nearly 26000 ppm. Since this limit is well above the highest fine sediment concentrations found in natural watercourses (Partheniades and Mehta, 1971), it may be concluded that the effect of C_o on C_{eq}, as explained here and generalized by Eqs. (4.2-1) and (4.2-2), can be expected to hold in the case of fine sediment transport in natural water bodies such as estuaries, rivers and canals.

Since the observed nature of the equilibrium concentration is not compatible with a process of simultaneous erosion and deposition of the sediment, and since the value of C_{eq} depends on the availability of an initial amount of suspended sediment, it may be inferred that for a given flow condition, once the equilibrium concentration is attained, neither erosion nor deposition of the sediment occurs. In other words, the flocculated bed, with its network-like structure (Partheniades, 1971), made of the deposited material, does not erode under the existing hydrodynamic lift and drag forces, and also that

the flocculated material in suspension consists of flocs that are unable to deposit under the prevailing conditions of upward diffusive flux due to turbulence and the stresses acting near the bed. This latter conclusion needs further explanation. Now even when the equilibrium concentration is attained, a large number of random collisions between the flocs constantly occur in the neighborhood of the sediment bed. Thus, it is quite likely that some of these collisions will result in the formation of flocs that are large enough to counter the upward diffusive flux due to turbulence and descend toward the bed surface, where the highest lift and drag forces prevail. However, the observation that ultimately the deposition of any such floc on the bed surface does not occur implies that such a large floc, as it approaches the bed, is disrupted by the stresses at the bed, and the resulting pieces are re-entrained by lift and drag forces into the bulk of the suspension. In other words, the shear strength of the floc is not sufficient for it to be able to resist the prevailing shear stress. In order to determine if any erosion of the bed occurs at equilibrium concentration, Partheniades, Cross and Ayora (1968) flushed out the suspended sediment at equilibrium concentration by replacing it with clear water. They found that no scouring of the deposited bed occurred.

The description of the behavior of a single floc, when extended to include the behavior of the entire amount of sediment in suspension at equilibrium concentration, leads to the following important general conclusions.

(1) The sediment constituting the equilibrium concentration is composed of sediment flocs which are too weak to produce, despite almost unending number of inter-floc collisions, flocs that have enough shear strength to be able to withstand the disruptive bed shear stresses and stick to the bed. Now in limited experiments by Partheniades et al. (1966), it was observed that the suspended flocculated sediment at equilibrium concentration contains the entire range of particle sizes present in the initially suspended sediment. This observation appears to indicate that the nature of the equilibrium concentration is not related to the individual particle sizes, and, therefore, that the behavior of the sediment in relation to the equilibrium concentration is associated entirely with the sediment flocs rather than the individual sediment particles. As a consequence, the incapability of the flocs at equilibrium concentration to be able to deposit on the bed must be associated with the weakness of the inter-floc rather than inter-particle bonds.

(2) By virtue of its ability to disrupt the flocs of relatively low shear strengths and re-entrain them into suspension, the bed shear stress, for a given sediment suspension, primarily controls the behavior of the equilibrium concentration. This is amply demonstrated by the results described in Section 4.2.1 and by Eqs. (4.2-1) and (4.2-2), which indicate C^*_{eq} to be uniquely dependent on τ_b (or equivalently $\tau^*_b = \tau_b/\tau_{bmin}$, with τ_{bmin} being a constant for a given sediment suspension). Further, despite the stochastic nature of the process of disruption of flocs near the bed associated with the random variations of the instantaneous bed

shear stress, as well as with the inter-floc collision frequently in the near-bed suspension itself, the net result of such a process for a given mean bed shear stress τ_b and a given sediment suspension is to divide an initial amount of sediment with concentration C_o into two parts, with the part represented by the concentration $C_{eq} = C^*_{eq} \cdot C_o$ being that which cannot deposit and the part represented by the concentration $C_o - C_{eq} = (1 - C^*_{eq})C_o$ being the one which deposits and forms a bed. It is shown in Section 4.2.1 that for a given τ_b, C^*_{eq} changes only if the sediment type or the water quality is changed. Figs. 4.2.3 through 4.2.6 and the accompanying discussion have shown that this variation of C^*_{eq} with the type of sediment suspension may be described in terms of the variation of the single parameter, τ_{bmin}. Finally, it appears that when the water quality is held constant, the cation exchange capacity (CEC) of the sediment is a parameter that is correlated to τ_{bmin}, so that the CEC may ultimately describe the variation of C^*_{eq} with the sediment type.

It is interesting to compare, for a given sediment suspension, the minimum shear stress for deposition τ_{bmin}, the critical shear stress for erosion τ_{be} and the maximum shear stress τ_{bmax} required to keep the entire amount of sediment in suspension. According to Eq. (4.2-1), theoretically, τ_{bmax} would have to be infinitely large for C^*_{eq} to be unity, which corresponds to a case when no deposition occurs. Therefore, for a reasonable estimate of τ_{bmax} if we assume $C^*_{eq} = 0.99$ as the point of near-complete suspension, then the corresponding τ_{bmax} may be obtained from Eq. (4.2-7) as

$$\tau_{bmax} = [13.9(\tau_b^* - 1)_{50} + 1]\tau_{bmin} \qquad (4.3\text{-}16)$$

Selecting the suspension of Bay mud in salt water in the annular channel, for which $\tau_{bmin} = 0.96$ dynes/cm^2 and $(\tau_b^* - 1)_{50} = 1.18$, $\tau_{bmax} = 16.9$ dynes/cm^2 is obtained from Eq. (4.3-16). In his experiments with a similar suspension of Bay mud, Partheniades found $\tau_{bmin} = 0.65$ dynes/cm^2 as mentioned in Section 2.2.2. Thus, the value of 0.96 dynes/cm^2 from the annular channel is 48% higher, but may be considered to be of the same order of magnitude, especially in view of the fact that the value of 0.65 dynes/cm^2 is an approximate estimate as noted in Section 2.2.2. Krone (1962) found the same value in the range of 0.60 to 0.78 dynes/cm^2, so that his highest value of 0.78 dynes/cm^2 is lower than 0.96 dynes/cm^2 by only 19%. Now a mean value of $\tau_{be} = 1.45$ dynes/cm^2 may be obtained from experiments of Partheniades (1965), and the above made comparison of τ_{bmin} values indicates that it may be reasonable to assume that τ_{be} in the annular channel would be of the same order of magnitude as that found from Partheniades' experiments. Alternatively, taking the ratio $\tau_{be}/\tau_{bmin} = 1.45/0.65 = 2.23$, for Partheniades' values and using the same ratio for the annular channel gives $\tau_{be} = (2.23) \cdot (0.96) = 2.14$ dynes/cm^2 for the annular channel. Comparing this value of τ_{be} with the τ_{bmax} value it is observed that the latter exceeds the former by a factor of $16.9/2.14 = 7.9$. This implies that the critical shear stress for erosion is considerably lower than the maximum shear stress required to keep an initially suspended material from depositing. In other words, even when in the

experiment on deposition, τ_b is between τ_{be} and τ_{bmax}, deposition of the suspended material occurs, despite the fact that scouring bed shear stresses, such as may scour a previously deposited bed, are present. Moreover, since an equilibrium concentration is attained even at such high shear stresses, it may be concluded as before that only the strongest flocs which can withstand the high bed shear stresses are deposited and that the bed formed of such flocs is not scoured under the existing shear stresses.

With reference to the described nature of the equilibrium concentration, the probability of deposition when equilibrium concentration is attained is zero, i.e., η_d is less than η_ℓ for this case. This in essence implies that the diameter d_s of any floc under such a condition is not large enough to satisfy the criterion defined by Eq. (4.3-14), or in other words, the shear strength of any large floc formed is not sufficient to resist the shear stresses just above the bed with the result that such a large floc is disrupted before reaching close enough to the bed, for it to be able to deposit. By virtue of the observed behavior of equilibrium concentration, any erosion of the bed material has also been precluded. The probability of erosion may be defined as

$$P_e = P_r \left\{ 1 > \frac{W + F''}{L} \right\} \tag{4.3-17}$$

and

$$P_e = 0 \quad \text{for} \quad 1 \leq \frac{W + F''}{L_u} \tag{4.3-18}$$

Here, F'' is the force with which a floc is held in place on the bed, and therefore for erosion to occur the lift force acting on the floc

is required to be equal to or greater than the sum of the weight of the floc W and F". F" is in fact the resultant of the cohesive forces with which the floc is bound to the bed by the neighboring flocs, and in addition, it includes the effect of any interlocking frictional force acting between the floc and its neighbors. However, since the exact mode by which a floc may be torn from the bed is of a somewhat complex nature, the effects of cohesive forces and frictional interlocking are combined together and represented by the resultant force F". Since erosion of the floc will occur as a result of the combined action of lift as well as drag force, the resultant of these two forces will in general be such that erosion will occur for a lift force lower than if the action of lift force alone were considered, as noted by Christensen and Bush (1971). However, this effect of the drag on the floc depends on the interlocking provided by the neighboring flocs, and it is therefore essentially included in the term F". Eqs. (4.3-17) and (4.3-18) may be written as

$$P_e = P_r\left\{ \eta > \frac{W + F''}{\bar{L}} - 1 \right\} \tag{4.3-19}$$

and

$$P_e = 0 \quad \text{for} \quad \eta_u \leq \frac{W + F''}{\bar{L}} - 1 \tag{4.3-20}$$

Therefore, if η_e is the value of η for an equlity condition within the brackets on the right-hand side of Eq. (4.3-19), then

$$P_e = P_r\left\{ \eta_e < \frac{W + F''}{\bar{L}} - 1 \leq \eta_u \right\} \tag{4.3-21}$$

The absence of erosion at equilibrium concentration implies that F" is so large that η_e is in fact greater than η_u, so that according to

Eq. (4.3-21), no erosion is possible. This situation is indicated in Fig. 4.3.2. The criteria, both for erosion and deposition, for an idealized individual floc are also described at the top of this figure.

Christensen (1965) has pointed out that from measurements of the lift force over a fixed bed by El-Samni (1949), it may be inferred that the instantaneous velocity u_t over the grains follows a normal distribution. Chiu (1972) has shown that the standard deviation corresponding to this normal distribution varies with the bed form and bed roughness, when measurements are taken on a movable cohesionless sediment bed. Extending this observation to the distribution of η in Fig. 4.3.1, it may be hypothesized that the limits η_u and η_ℓ will also depend on the bed form and bed roughness. They therefore may be assumed to be constant only for a particular bed.

In the light of the described nature of equilibrium concentration, it should be noted that the term "equilibrium" does not have the same meaning as in cohesionless sediment transport. The term was originally used (Partheniades, 1965), because it was believed that the nature of cohesive sediment transport was similar to cohesionless sediment transport. The present study has however shown that the equilibrium concentration must be understood as a steady state concentration.

4.3.3 Settling Velocities

The problems associated with integrating the diffusion

equation to describe the depositional behavior of cohesive sediments are pointed out in Appendix D, where it is mentioned that particularly the boundary condition at the sediment bed is difficult to describe, inasmuch as the terminal settling velocity W_s is an unknown function of the properties of the flow and sediment at this boundary. In this section, therefore, an attempt is made to determine the dependence of the settling velocity on the flow and sediment properties by taking a finite control volume approach to derive the sediment continuity equation, and using the logarithmic-normal law of deposition determined experimentally.

For settling under a turbulent condition, the settling velocity W_s is obtained by equating the buoyant weight W given by Eq. (4.3-11) to the drag force acting on the floc. So that

$$\alpha_2 d_s^3(\gamma_s - \gamma) = C_D \gamma \frac{W_s^2}{2g} \alpha_1 d_s^2 \qquad (4.3\text{-}22)$$

where C_D is the drag coefficient for an equivalent spherical floc of diameter d_s, and it is in general a function of the Reynolds number $W_s d_s/\nu$. Eq. (4.3-22) may be written as

$$W_s = K \cdot \sqrt{g \frac{(\gamma_s - \gamma)}{\gamma} d_s} \qquad (4.3\text{-}23)$$

where

$$K = \sqrt{\frac{2\alpha_2}{\alpha_1 C_D}} \qquad (4.3\text{-}24)$$

In Fig. 4.3.3, a finite control volume indicated by the dashed rectangle is selected for flow through any section of the annular channel. The length of the control volume is Δx, width is b, which

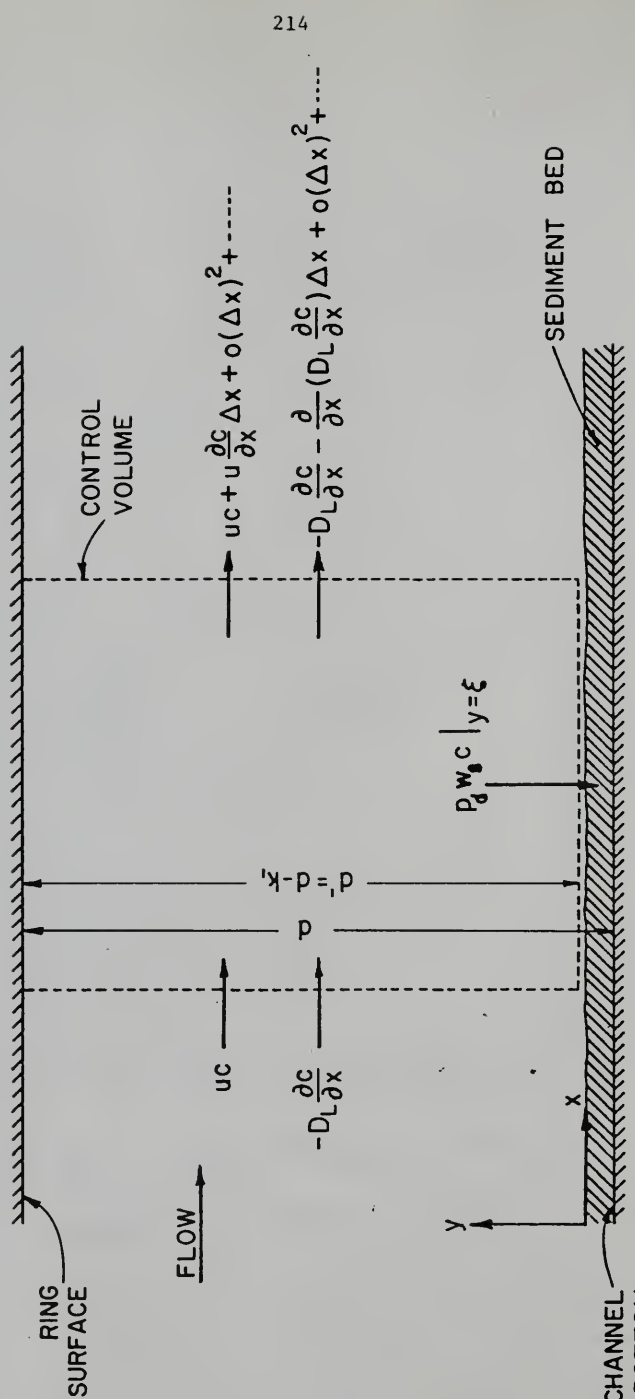

Fig. 4.3.3. Finite Control Volume for Sediment Continuity in Annular Channel.

is the same as the width of the channel, and the height is d'. The height d' is in fact measured from the surface of the bed to the surface of the ring at the top. However, in determining the bed shear stress in the experimental measurements, the depth d was considered as the distance measured from the channel bottom, rather than the bed surface. Thus d and $d' = d - k_1$ differ by k_1, which is the depth from the channel bottom the level $y = \xi$, where ξ is a small elevation above the theoretical bed surface at $y = 0$, and it is considered to be the bottom boundary for the control volume. As deposition progresses, up until in equilibrium concentration is attained, k_1 increases but its variation with time is associated with the complex process of formation and consolidation of the bed, and, therefore, its functional dependence on time must either be assumed or experimentally evaluated. d' will correspondingly decrease with time until equilibrium concentration is attained, beyond which point it will show no further variation. It should be pointed out that in actuality, the decrease in d' with time will have effect on the velocity profile as well as the mean bed shear stress, with the latter increasing in magnitude as time progresses.

The fluxes in and out of the control volume are as indicated. These include the convective flux involving the product uC, and the turbulent diffusive flux involving the term $D_L(\partial C/\partial x)$, where D_L is the longitudinal dispersion coefficient. The term $p_d W_s C\Big|_{y=\xi}$ is the downward sediment flux just above bed surface, where p_d is the probability of deposition defined by Eq. (4.3-14), W_s is the near-bed settling velocity given by Eq. (4.3-23), and $C\Big|_{y=\xi}$ is the near-bed sedi-

ment concentration. The small distance ξ where the near-bed flux is evaluated is not a well-defined parameter for a bed which is undergoing consolidation, but it may be considered to be of the order of a floc diameter d_s. For a small time interval Δt, equating the net amount of sediment into the volume to the increase within the volume according to Eq. (D-1) in Appendix D, and then allowing Δx and Δt to approach zero gives

$$bd' \frac{\partial C}{\partial t} dxdt + bd'u \frac{\partial C}{\partial x} dxdt = bd' \frac{\partial}{\partial x} \left(D_L \frac{\partial C}{\partial x} \right) dxdt - p_d W_s C \Big|_{y=\xi} bdxdt \tag{4.3-25}$$

or, dividing by bd'dxdt results in the expression

$$\frac{\partial C}{\partial t} + u \frac{\partial C}{\partial x} = \frac{\partial}{\partial x} \left(D_L \frac{\partial C}{\partial x} \right) - p_d W_s C \Big|_{y=\xi} \frac{1}{d'} \tag{4.3-26}$$

In the annular channel, $\partial C/\partial x = 0$, so that

$$\frac{dC}{dt} = -p_d W_s C \Big|_{y=\xi} \frac{1}{d'} \tag{4.3-27}$$

The product $p_d W_s$ defines an apparent settling velocity near the bed, and in general, it is smaller in magnitude than W_s, inasmuch as p_d is generally less than unity. If W_s' is this apparent settling velocity, then using the expressions for p_d and W_s from Eqs. (4.3-14) and (4.3-23) gives

$$W_s' = p_r \left\{ \eta < \frac{\alpha_2 d_s^3 (\gamma_s - \gamma)}{\frac{C_L \alpha_1 d_s^2}{C_\tau} \tau_b} - 1 \right\} \cdot K \cdot \sqrt{g \frac{(\gamma_s - \gamma)}{\gamma} d_s} \tag{4.3-28}$$

In terms of W_s', Eq. (4.3-27) may be written as

$$\frac{dC}{dt} = - W_s' C\Big|_{y=\xi} \frac{1}{d'} \tag{4.3-29}$$

Next we may assume that $C\Big|_{y=\xi}$ is related to the depth-averaged concentration C (depth-averaged value is assumed here, but is not specified by any additional symbol for convenience) within the suspension according to

$$C\Big|_{y=\xi} = k_2 C \tag{4.3-30}$$

where k_2 will in general be a function of the flow conditions as well as suspension properties. Now apparent settling velocities may only be associated with the depositable part of the sediment, since $p_d = 0$, once equilibrium concentration is attained, so that C in Eq. (4.3-29) must be construed as the depositable concentration $C - C_{eq} = (C_o - C_{eq})C^{**}$, and therefore Eq. (4.3-29) may be written as

$$\frac{dC^{**}}{dt} = - \frac{k_2 W_s'}{d'} C^{**} \tag{4.3-31}$$

where it is understood that W_s' is evaluated at $y=\xi$. Expressions for C^{**} and dC^{**}/dt may be substituted from Eqs. (4.2-11) and (4.2-14), and Eq. (4.3-31) can be written explicitly in terms of W_s' as

$$W_s' = \frac{\dfrac{(0.434)d'}{\sqrt{2\pi}\,\sigma_2 k_2} e^{-T^2/2} \dfrac{1}{t}}{\dfrac{1}{2}\,\mathrm{erfc}(T/\sqrt{2})} \tag{4.3-32}$$

where T is given by Eq. (4.2-9).

Assuming $k_1 = 1$, i.e., neglecting the effect of the sediment bed thickness on the flow parameters, and also considering $k_2 = 1$, i.e., assuming that the concentration at $y=\xi$ is equal to the mean sediment concentration, the apparent settling velocity W_s' is plotted

against time in Figs. 4.3.4, 4.3.5 and 4.3.6, for selected values of the initial concentration C_o, depth of flow and τ_b^*, for the different types of sediment suspensions tested or analyzed.

In Figs. 4.3.4 and 4.3.5, the data are for the kaolinite in distilled water suspension. Comparing the first three sets of curves in Fig. 4.2.4, which are for 9 in. depth and C_o of 1060 ppm, it is observed that increasing τ_b^* from 0.5 to 1.0 generally decreases the settling velocity, except for the first short period of 1-1/2 min of deposition during which a relatively higher velocity is indicated. However, when τ_b^* is increased from 1.0 to 1.5, relatively negligible effect on the curve is indicated, with only a slight increase in the settling velocity. These effects of τ_b^* may be explained by its effect on W_s' in the near-bed zone of thickness ℓ_b. If in Eq. (4.3-28) $\tau_b = \tau_b^* - \tau_{bmin}$ is substituted, then W_s' may be expressed as

$$W_s' = p_r \left\{ \eta \leq \alpha_3 \frac{d_s(\gamma_s - \gamma)}{\tau_b^*} - 1 \right\} \cdot K \sqrt{g \frac{(\gamma_s - \gamma)}{\gamma} d_s} \qquad (4.3\text{-}33)$$

where

$$\alpha_3 = \frac{\alpha_2 C_\tau}{\alpha_1 C_L \tau_{bmin}} \qquad (4.3\text{-}34)$$

It is thus observed that if α_3, K and $\gamma_s - \gamma$ are assumed to be constant, the magnitude of W_s' is determined by the opposing effects of d_s and of τ_b^*, according to Eq. (4.3-33). However, since d_s itself is determined by τ_b^*, the latter ultimately controls W_s'. Thus the decrease in W_s' as τ_b^* increases from 0.5 to 1.0 means that increasing τ_b^* results in a smaller floc diameter d_s due to the action

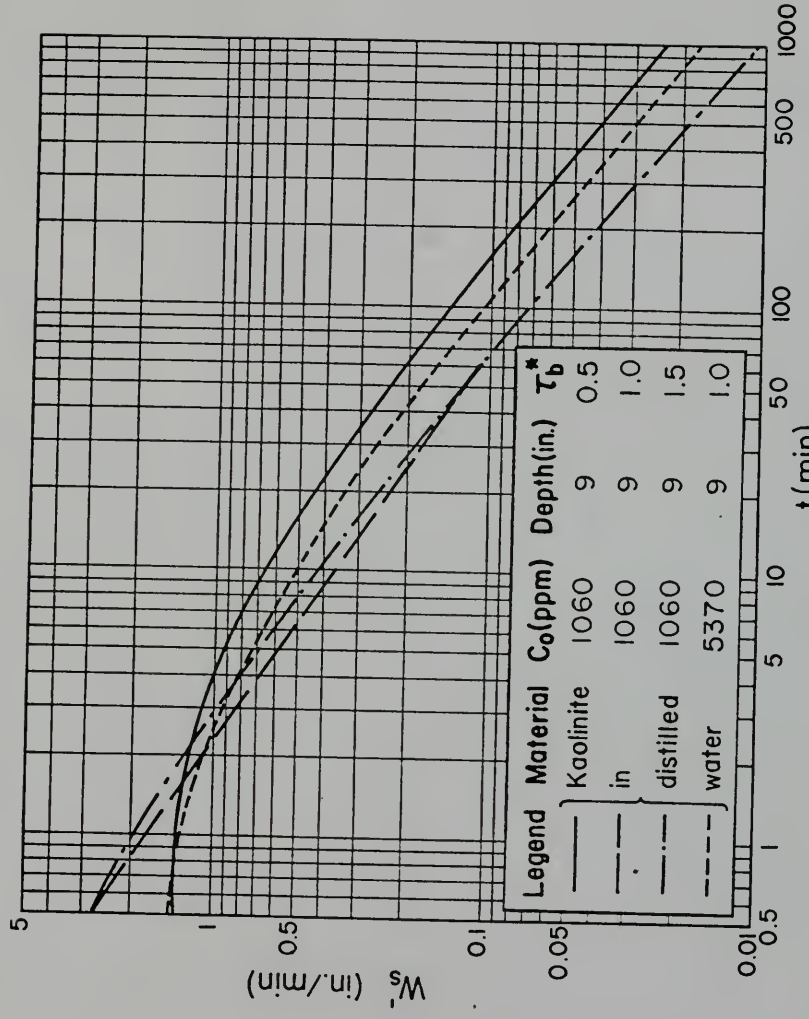

Fig. 4.3.4. Apparent Settling Velocity W' Versus Time t for Kaolinite in Distilled Water.

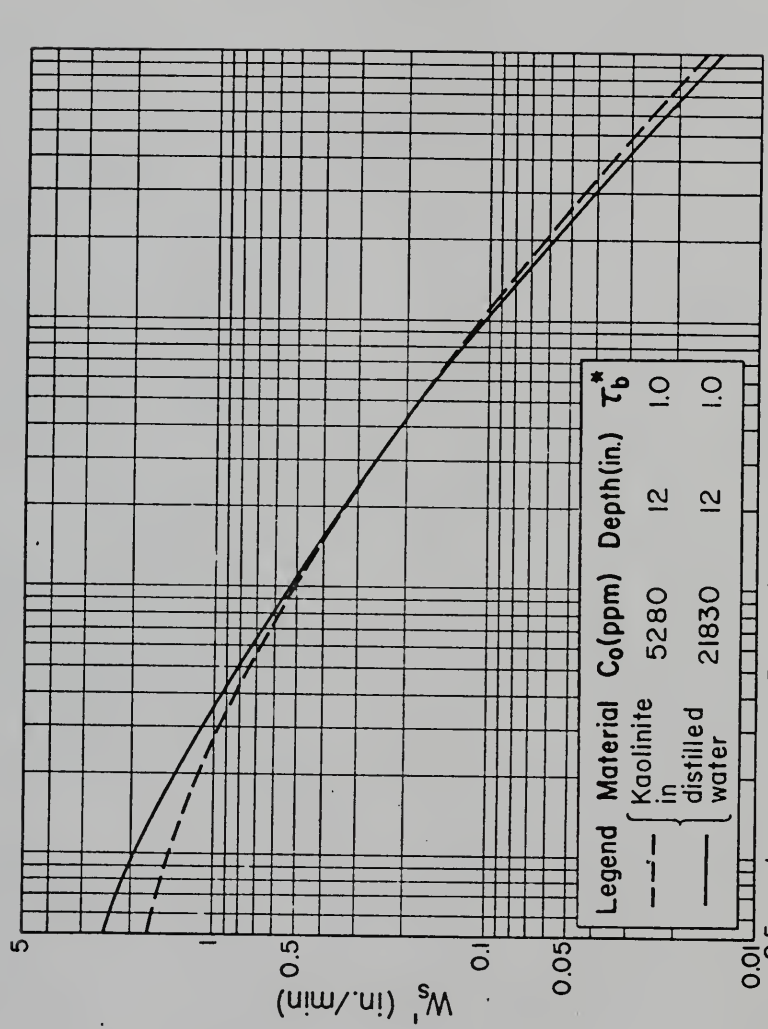

Fig. 4.3.5. Apparent Settling Velocity W_s' Versus Time t for Kaolinite in Distilled Water.

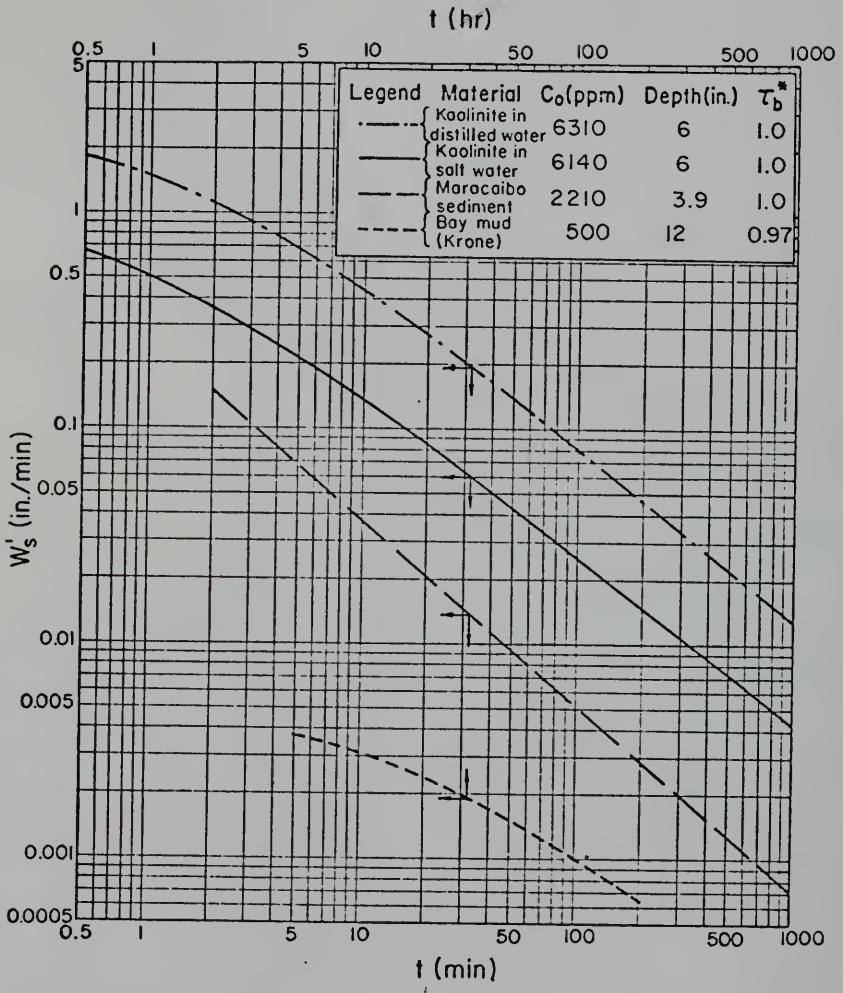

Fig. 4.3.6. Apparent Settling Velocity W_s' Versus Time t for Four Different Suspensions.

of increasing shear force. This reduces p_d (term within brackets), as well as the term under square root sign in Eq. (4.3-33), and consequently W_s' is lowered. The relatively small change in W_s' when τ_b^* is increased to 1.5 implies that relative to τ_b^* the effect due to d_s is increased in such a manner that there is no overall effect on W_s'. In other words it means that despite the increase in the shearing force acting on the flocs, the increased inter-floc collisions due to the higher bed shear stress cause the formation of relatively larger flocs so that d_s is larger, and this counter-balances the effect due to the increase in τ_b^*.

The fourth curve in Fig. 4.3.4 is for 9 in. depth and τ_b^* of unit, but with a C_o of 5370 ppm, and this curve may be compared with the second to determine the effect of C_o. It is observed that increasing C_o increases the settling velocity, except for the first relatively short period of four minutes during which decreased settling velocities are observed. The observed increase in W_s' with increasing C_o is attributed to the higher frequency of inter-floc collisions due to increased sediment concentration, which results in larger d_s and thus increases W_s'. A similar but less significant effect of C_o is evident in the two curves of Fig. 4.3.5 for the 12 in. depth.

The effect of depth may be considered by comparing the three curves for $\tau_b^* = 1.0$ and a relatively unchanging C_o of 6310, 5370 and 5280 ppm at depths of 6, 9 and 12 in. in Figs. 4.3.6, 4.3.4 and 4.3.5, respectively. Comparison does not reveal any significant or consistent trend in the effect of depth, and therefore it may be concluded that for these examined cases depth does not have a

significant effect on W_s'. In other words, for the selected value of τ_b^* and of C_o, the overall effect of depth on d_s is not significant, so that W_s' is not affected.

In Fig. 4.2.6, a settling velocity curve for kaolinite in distilled water is compared with curves obtained for kaolinite in salt water, the Maracaibo sediment (Rosillon and Volkenborn, 1964) and Bay mud (Krone, 1962). Strictly speaking the last two cannot be computed from Eq. (4.3-32), since in a straight flume a concentration gradient $\partial C/\partial x$ exists. However, it is assumed to be negligible in these cases. It should be pointed out in this connection that the exponential decrease of concentration at relatively low concentrations suggested by the data of Fig. 4.2.53 can be described by Eq. (4.3-31), if it is integrated for a constant W_s'. Hence, because Eq. (4.3-32) is valid for $\partial C/\partial x = 0$, it appears reasonable to assume the same for the data corresponding to the curves of Fig. 4.3.6. This argument is further strengthened by the fact that time-concentration runs from the annular channel as well as straight flumes have in general been described by the same general law in terms of a logarithmic-normal relationship. Table 4.3.1 gives an order of magnitude comparison for the four cases, where it is observed for example that at 1000 min, W_s' for Maracaibo sediment is lower than the corresponding value for kaolinite in distilled water by a factor of 1:17.6.

TABLE 4.3.1

Material	Time	W_s' (in./min)
Kaolinite in distilled water	1000 min	0.013
Kaolinite in salt water	1000 min	0.0043
Maracaibo Sediment (Rosillon and Volkenborn)	1000 min	0.00074
Bay mud (Krone)	1000 min	0.0026

It is interesting to note that with increasing time, in all cases, the curves of W_s' versus time begin to indicate a linear trend on the log-log coordinates, which may be expressed as

$$W_s' = a't^m \tag{4.3-35}$$

where the coefficients a' and m in general will be functions of C_o, depth and τ_b^* for a given sediment suspension. If Eq. (4.2-35) is substituted into Eq. (4.3-31) and the resulting expression integrated, the result is

$$\ln\left(\frac{C^{**}}{C_1^{**}}\right) = \frac{-a'}{d(m+1)}\left(t^{m+1} - t_1^{m+1}\right). \tag{4.3-36}$$

where C_1^{**} is the value of C^{**} at time t_1 beyond which the settling velocity curve may be approximated by Eq. (4.3-35). As an example, for the topmost curve of Fig. 4.2.6, Eq. (4.3-35) may be approximated for t greater than 10 min. So that for t_1 = 10 min, C_1^{**} = 0.245 may be obtained from Eq. (4.2-11). Also the depth d = 6 in. for this case

and $a' = 2.8$ in./min and $m = -0.77$ may be evaluated from the plot. Substituting these values in Eq. (4.3-36) gives

$$C^{**} = (0.245)e^{-2.03(t^{0.23} - 1.70)} \qquad (4.3\text{-}37)$$

Values of C^{**} computed from Eq. (4.3-37) for t between 10 min and 1000 min are found to be almost identical to those computed from Eq. (4.2-11).

CHAPTER 5

CONCLUSIONS AND RECOMMENDATIONS

5.1 Summary and Conclusions

From the standpoint of the depositional properties, a fine cohesive sediment exhibits a behavior which is distinctly different from that of a cohesionless or coarse sediment. This distinction arises primarily from the fact that fine sediment particles have specific surface areas that are relatively much larger than those of cohesionless grains. As a result, the physicochemical forces acting on fine particle surfaces are larger, by orders of magnitude, than the submerged weights of the individual particles. These surface forces therefore exert a dominating influence in controlling the depositional properties of fine sediments.

In natural watercourses such as estuaries, navigable channels and irrigation canals, where shoaling of fine sediments is often a significant problem, the presence of slight salinity or other ionic species results in the coagulation or flocculation of fine sediment particles, by virtue of the attractive surface forces acting between the particles. As a consequence, the flocs have diameters and therefore settling velocities which are orders of magnitude higher than those of the individual particles. The depositional behavior of fine sediments is therefore essentially associated with the settling properties of flocs.

In a turbulent flow field, the depositional behavior of fine sediment flocs depends on the flow variables as well as on the physico-

chemical properties of the flocculated suspension. As a consequence, the present experimental study of the depositional process was carried out essentially in two stages: (1) by keeping the sediment type and water quality constant, the depositional properties of a selected sediment suspension were related to the hydrodynamic parameters and (2) by using different types of suspensions, these hydrodynamic parameters, which describe the depositional behavior, were related to the physicochemical properties of the suspensions. The experiments in the specially designed annular apparatus and the important conclusions derived from the results are described below.

1. Since previous investigations had indicated that the bed shear stress is an important flow parameter in controlling the depositional behavior, the shear stress on the annular ring was measured for an indirect estimation of the bed shear stress. Later, the bed shear stress was directly measured by an annular false bottom. A comparison of the values obtained by direct and indirect methods showed a reasonable agreement, and indicated that the indirect estimation was based on assumptions which were basically sound.

2. Velocity profiles were measured for flow depths of 6-1/4 and 9 in. by small propeller probes. These profiles were found to have a qualitative resemblance to turbulent couette flows between infinite parallel plates, but the effects of the walls of the channel and the secondary currents caused these profiles to deviate distinctly from couette flow profiles. One characteristic feature was the presence of a middle zone of almost homogeneous turbulence, nearly 1 in. below the ring and 1 in. above the channel bottom. It was further found that

the profiles close to the bottom exhibited the logarithmic variation corresponding to a fully rough flow condition.

3. In order to investigate the role of flow variables in the depositional behavior, a large number of time-concentration runs were carried out using a commercial kaolinite in distilled water at flow depths of 6, 9 and 12 in. A few measurements were also carried out at a depth of 13 in. The initial suspended concentration C_o was varied from nearly 1000 to 26000 ppm, and the bed shear stress τ_b ranged from nearly 0.4 to 11 dynes/cm^2. An important observation from these measurements was that for a bed shear stress τ_b greater than a given minimum shear stress τ_{bmin}, the suspended sediment concentration C reaches, after a relatively short period of deposition, a steady state concentration C_{eq}, referred to as equilibrium concentration. For τ_b less than τ_{bmin}, C_{eq} is zero, so that τ_{bmin} is the minimum shear stress below which no amount of sediment may indefinitely remain in suspension. It was further found that irrespective of the depth of flow or the value of C_o between 1000 and 26000 ppm, the ratio C_{eq}/C_o is a function of the parameter $\tau_b^* = \tau_b/\tau_{bmin}$ only. In other words, since τ_{bmin} is a constant for a given sediment suspension, the ratio C_{eq}/C_o is determined uniquely by the bed shear stress τ_b. The ratio $C_{eq}^* = C_{eq}/C_o$ is called the relative equilibrium concentration, and $C_{eq}^{**} = 1 - C_{eq}^{**}$ is referred to as the degree of deposition.

The observed independence of C_{eq}^* from C_o implies that its value for any given flow condition depends on the availability of an initial amount of sediment of concentration C_o. Thus at steady state, any given initial amount of sediment of concentration C_o is apparently divided

into two parts, with the part represented by the concentration $C_{eq} = C_o \cdot C^*_{eq}$ which does not deposit, and the part represented by the concentration $C_o - C_{eq} = C_o \cdot C^{**}_{eq}$, which permanently deposits and forms a bed. This behavior, associated with the equilibrium concentration, is a fundamental characteristic of fine sediments, and it points out the distinct difference between cohesive and cohesionless sediment transport, since in the latter, the amount transported at steady state depends solely on the flow conditions, and not on the availability of the material for transport.

4. The relative equilibrium concentration C^*_{eq} is found to be logarithmic-normally distributed with the shear stress parameter $(\tau^*_b - 1)$, a standard deviation σ_1 and geometric mean $(\tau^*_b - 1)_{50}$. It was found that for the suspension of kaolinite in distilled water, $\tau_{bmin} = 1.80$ dynes/cm^2, $(\tau^*_b - 1)_{50} = 0.72$, and $\sigma_1 = 0.49$.

5. In order to investigate the effect of the physicochemical properties of sediment suspensions on C^*_{eq}, or equivalently on the degree of deposition C^{**}_{eq}, three types of suspensions other than that of kaolinite in distilled water were tested in the annular apparatus in salt water at 34000 ppm salinity. These were: (1) kaolinite, (2) Bay mud, (3) 50/50 mixture of kaolinite and Bay mud. In addition, previous results of Rosillon and Volkenborn (1964), Partheniades (1965) and Partheniades et al. (1966) were also reanalyzed. It was found that C^*_{eq} from all these experiments was dependent only on the parameter $(\tau^*_b - 1)/(\tau^*_b - 1)_{50}$. In other words, on a logarithmic-normal plot of C^*_{eq} versus $(\tau^*_b - 1)/(\tau^*_b - 1)_{50}$, all the data points

indicated a single straight line characterized by a constant value of $\sigma_1 = 0.49$.

6. A plot of $(\tau_b^* - 1)_{50}$ versus τ_{bmin} for suspensions in salt water showed that these two parameters are related to each other. It was therefore concluded that τ_{bmin} alone is sufficient to characterize the degree of deposition of fine sediment suspensions, when the ambient medium is of a constant quality.

7. It was further shown that τ_{bmin} values for suspensions in salt water are correlated to the cation exchange capacity (CEC) of the sediments. Since the CEC is a measure of the physicochemical surface forces on the clay particles, it may be considered to be a parameter that is representative of the interparticle forces within sediment flocs, and, therefore, indicative of the physicochemical properties of the flocculated suspension itself. The results indicate that since τ_{bmin} is related to CEC, the latter alone is sufficient to characterize the degree of deposition.

8. From measurements of deposition rates of suspension of kaolinite in distilled water as well as salt water, it is found that the fraction $C^* = (C_o - C)/(C_o - C_{eq})$ of the depositable concentration which is deposited at a given time is logarithmic-normally distributed with time t, with a standard deviation σ_2 and geometric mean t_{50}. It is further noted that σ_2 and the mean, log t_{50}, are functions of τ_b^*, depth of flow and C_o, for a given suspension.

The variation of σ_2 and log t_{50} with τ_b^* is such that for a particular τ_b^*, the rate of deposition reaches its lowest value. As τ_b^* decreases below this particular value, the rates become higher,

while as τ_b^* increases above this value, the rate also increases, but less significantly.

The effect of depth for τ_b^* less than unity is such that increasing the depth tends to increase the rate of deposition. For τ_b^* greater than unity, the effect is less significant and less distinct.

The effect of C_o is such that in general, increasing C_o decreases the rate of deposition.

9. Reanalyzed measurements of Krone (1962), Rosillon and Volkenborn (1964) and Partheniades (1965) also indicate that these measurements, which were obtained in straight flumes, agree well with the logarithmic-normal law for deposition. It is also found that although the rates of deposition in straight flumes are relatively much slower than in the annular apparatus by virtue of the geometric differences between the two types of apparatus, and these are reflected in the magnitudes of σ_2 and log t_{50}, the qualitative trends in variation of these parameters with τ_b^*, depth of flow and C_o are similar.

10. Measurements of suspended sediment concentration profiles for 13 in. depth at equilibrium concentration indicate a constant turbulent diffusivity in the middle depth zone nearly 1 in. below the ring and 1 in. above the bed. This result confirms the observation from velocity profile measurements that in the middle depth zone, a nearly homogeneous turbulence exists.

11. It is noted that the process of deposition is governed by the nature of processes within a small near-bed layer of a thickness of a few floc diameters, and that its thickness is generally smaller than the height of the laminar sublayer. Within this layer,

the kinetics of the stochastic processes related to the variations of instantaneous lift and drag forces, as well as those related to the inter-floc collision frequency are responsible for the settling behavior of flocs. Those flocs with shear strengths which are not sufficient to withstand the high prevailing shear stresses near the bed are disrupted and re-entrained into suspension by the lift forces. On the other hand, flocs which are strong enough to withstand the shear stresses are able to deposit and become part of the bed. This nature of selection of depositable flocs defines a probability of deposition. It is clear that at equilibrium concentration, the probability of deposition is zero. Further, since at this concentration no erosion of the bed material takes place, the probability of erosion is also zero.

12. Based on a finite control volume, a sediment continuity equation is derived for the annular channel. Then, substituting the logarithmic-normal law of deposition into this equation, an expression is obtained for the near-bed apparent settling velocity W_s' as a function of τ_b^*, depth of flow and C_o. A comparison with W_s' derived from straight flume measurements shows that the latter can be one to two orders of magnitude lower than W_s' derived from measurements in the annular channel. Finally, from the plots of W_s' versus time it appears that over significant portions of time during which deposition is occurring, W_s' decreases exponentially with time.

5.2 Recommendations for Further Research

The present study is primarily concerned with the dual effect

of flow parameters and the physicochemical properties of sediment suspensions on the degree of deposition and the depositional rates, in a turbulent flow field. The ultimate objective of such a study is to provide for research and engineering practice, correlations in terms of readily determinable hydrodynamic and physicochemical parameters that may be used to determine the degree and the rates of deposition, for any given cohesive sediment in a water of known quality. To this end, the present experimental work has thrown a considerable light on the hydrodynamic interaction of flow and sediment, and it has further shown that it is possible to relate,in certain cases, the physicochemical characteristics to terms of parameters such as the cation exchange capacity of sediments. Based on conclusions derived from this study, the following objectives and recommendations for future research are in order:

1. An important future objective is an investigation of the effect of bed roughness on the degree of deposition and on the deposition rates. The effect of roughness must be studied experimentally by inserting,in the channel, plexiglass false bottoms such as the one described in Section 3.1.2, with roughness elements glued on them. Three or four roughness sizes should be tested.

2. The dependence of the degree and rates of deposition on the bed shear stress raises the question as to whether the way in which turbulent momentum is transferred from the boundary to the fluid is also of importance in the settling behavior of flocs, inasmuch as the zone just above the sediment bed largely controls the depositional rate, as concluded in the present study. An investigation of this

question should involve detailed measurements of mean velocity profiles and turbulence intensities, with the help of a hot-film anemometer. The average bed shear stress should also be measured directly, as in the present study. These measurements would describe the nature of turbulence within the annular channel, and this would make it possible a comparison of the turbulence structure in the annular channel with that in open channel. Important information would also be obtained regarding turbulence near the bed. The experiments in this phase should be conducted at the operational speeds of the ring and the channel, so that the overall effect of the secondary currents is such that a uniform deposition of the sediment may occur. Although preliminary measurements at M.I.T. (Partheniades, Cross and Ayora, 1968) have indicated that the bed shear stress is constant across the width at operational speeds, the question regarding the effect of the secondary currents on the turbulence characteristics and the velocity distribution near the bed still remains to be answered. It is expected that the recommended measurements will provide a satisfactory answer, and will indicate how closely an endless straight conduit is approximated at the operational speeds.

3. Since temperature has a significant effect on the chemical bonds between atoms and molecules, the physicochemical forces between cohesive sediment particles are also expected to vary significantly with temperature. It is therefore necessary to study the effect of temperature on the deposition rates at different constant temperatures. A rule of thumb for chemical reactions is that their rates double for

every 10°C increase in temperature. A corresponding rule may therefore be discovered for the rates of deposition.

4. It is recommended that further experimental work be carried out to examine in detail the rates of deposition for relatively low bed shear stresses, where the logarithmic-normal law does not hold. Since, as noted in Section 4.2.2, difficulties were encountered in obtaining accurate measurements just after the beginning of deposition, as a result of the high settling rates associated with the large kaolinite flocs in distilled water, a sediment suspension with smaller floc sizes should be used. As the two natural sediments analyzed (Bay mud and Maracaibo sediment) were found to have comparatively small floc sizes, based on the values of the minimum shear stress τ_{bmin}, these sediments may be conveniently employed.

5. A systematic study of the effect of secondary motion on the distribution of the boundary shear and on the depositional characteristics should be conducted next. The first step of this phase would be a study of the transfer of momentum due to shear stress at the ring, from the surface of the ring to the channel bottom, for various relative speeds between the ring and the channel and depths of flow. The false bottom must be used to measure the average bed shear stress, and a triaxial array hot-film anemometer should be used to determine mean velocity profiles and turbulent intensities, since three-dimensional aspects of the flow are essentially involved.

The above recommendation is motivated by the following observations. It has already been noted that any deviation from the

operational speeds strongly affects the depositional characteristics. This observation suggests that the unbalanced secondary currents have a strong effect on deposition. It appears therefore that these currents affect the spacial distribution of turbulence intensities, especially in the zone near the bed, where the depositional characteristics are controlled. However, to date, no quantitative relationships describing these effects have been found. It is therefore the purpose of this phase of the recommended project to provide a relevant quantitative measure for the secondary current effect on the turbulence close to the boundary, and to investigate the relationship between the shear stress distribution and the velocity profiles near the bed.

6. Another recommendation is concerned with an investigation of parameters that may suitably describe the physicochemical characteristics of sediment suspensions. It is desired, that more experimental measurements using different sediment types, be carried out to examine the usefulness of the cation exchange capacity as a parameter. It has been pointed out, that this quantity can only be used to compare two sediment suspensions if their water quality is the same. On the other hand it is not possible to compare in this way, two sediment suspensions in which the water quality changes, as for example a suspension of kaolinite in salt water and one with kaolinite in distilled water. In both cases the CEC is the same, but their depositional properties have been found to be different. It is therefore recommended that other parameters, which also may be used as measures of the cohesive forces, may be investigated. One parameter that may be investigated for such a purpose is the viscosity

of a sediment suspension at a given concentration and applied shear, which may be measured in a Brookfield type viscometer.

7. A detailed measurement of the particle size distribution of the suspended sediment is suggested. This would throw more light on the observation made by Partheniades et al. (1966) that the nature of the equilibrium concentration is not related to the characteristics of the particle size distribution. The necessary system to collect the suspension for this purpose has already been designed for the present annular channel, as described in Section 3.1.2.

8. An important future objective of applied research related to the present study should deal with the application of the results on deposition, as well as erosion, in determining the space and time history of suspended sediment in an estuarine system. The basic modelling method for this has been described in Appendix E. After developing a numerical model for a simple idealized estuary, this method can be extended to describe the effects of wind and tides on cohesive sediment transport in an estuarine system with a relatively complex geometry.

APPENDICES

APPENDIX A

BED DEPTH MEASUREMENT

The procedure for the measurement of the depth of deposited bed of the flocculated sediment at the end of a deposition test is described briefly in Section 3.2.2. In Fig. A.1 two such typical measurements are plotted for the indicated depth and initial concentrations. Measurements closest to the walls had to be 5/8 in. away from the walls because the measuring gage could not be positioned closer to the wall than this distance. For the measurements at 9 in. depth, the mean bed depth is 1.89 cm, and the highest and the lowest values are 1.93 and 1.85 cm, which respectively correspond to deviations of +2.1% and -2.1% from the mean. For the 12 in. depth measurements, the mean bed depth is 1.26 cm, and the highest value of 1.40 cm and the lowest of 1.10 cm, respectively, correspond to deviations of +11.1% and -12.7% from the mean.

Mean depth values obtained from measurements such as those shown in Fig. A.1 are plotted in Fig. A.2 as functions of the initial concentration C_o in ppm, for the indicated depths of flow. Though the data points are scarce, it may be observed that the data for each depth, for C_o ayproximately above 10000 ppm, appear to increase linearly with the initial concentration. This observation is in agreement with that of Krone (1962), who noted a similar linear trend for C_o above 10000 ppm when he measured the depths of deposited flocculated beds of Bay mud in a 1000 ml cylinder, for C_o ranging up to 100000 ppm under quiescent conditions. The linear trend of increasing

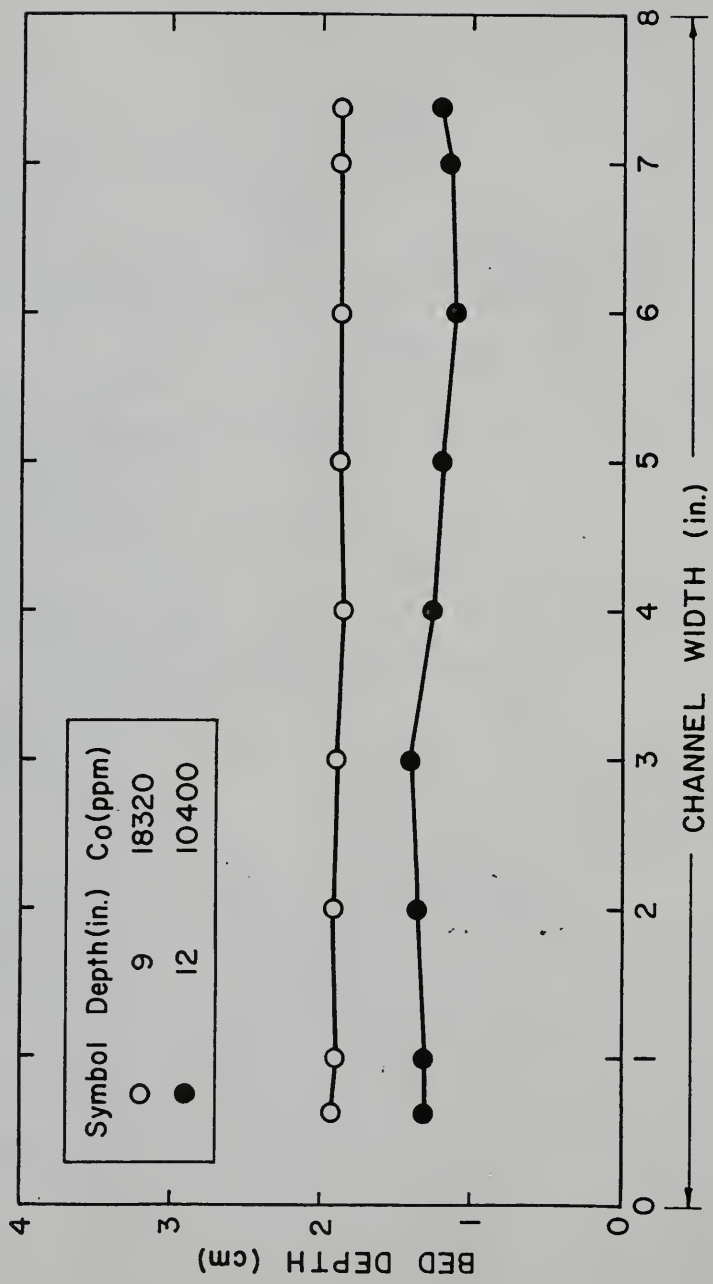

Fig. A.1. Measurement of Sediment Bed Depth Across Channel Width.

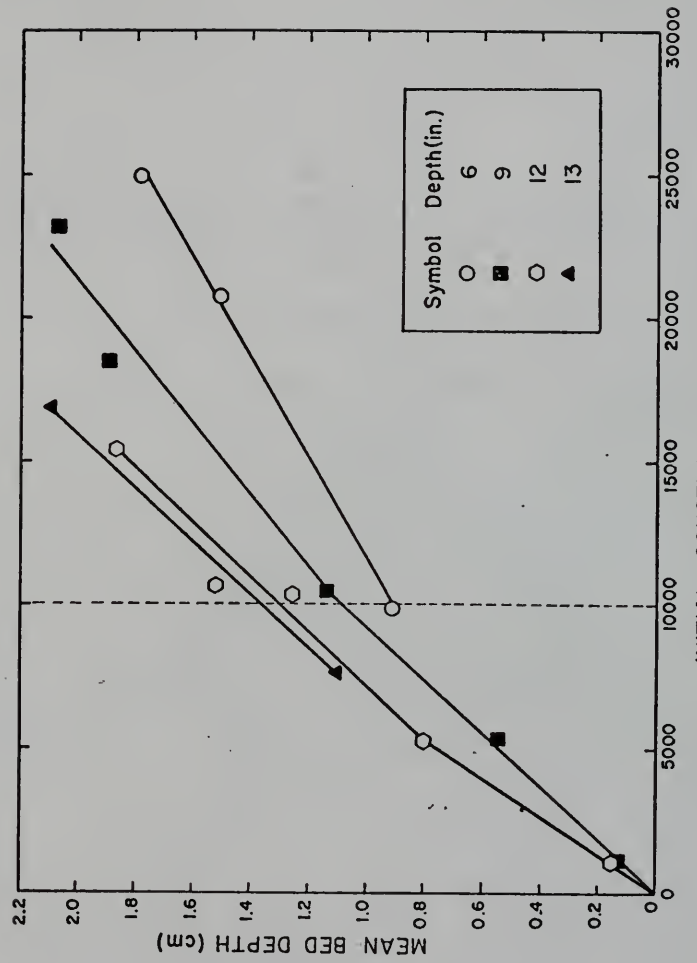

Fig. A.2. Mean Bed Depth Versus Initial Concentration C_o.

bed depth with increasing C_o above 10000 ppm implies that the structure of the bed remains unchanged above this concentration, i.e., any further consolidation of the lattice formed by the interconnected flocs does not take place, so that the addition of a given constant amount of the sediment material increases the bed depth by a corresponding constant amount. Thus, it may be noted from Fig. A.2 that increasing C_o from 10000 ppm to 15000 ppm increases the bed depth for 6 in. flow depth by 2.9 cm, and the corresponding increase for 12 in. flow depth is 5.4 cm, which is nearly twice the value for 6 in. depth. This increase is consistent because the amount of sediment added to increase C_o from 10000 ppm to 15000 ppm is twice at 12 in. depth as compared to that at 6 in. depth.

APPENDIX B

METHOD OF LEAST SQUARES FOR LINEAR RELATIONSHIPS ON LOGARITHMIC-NORMAL PLOTS

In general, the probability P of a normal N(0,1) distribution with an upper integral limit x_a may be expressed as

$$P = \frac{1}{\sqrt{2\pi}} \int_{-\infty}^{x_a} e^{-w^2/2}\, dw \qquad \text{(B-1)}$$

where w is a dummy variable. Then if P_{mi} is the measured value and P_{ti} is the true value of the probability at a given value of $x_a = x_{ai}$, the sum of the square of the error (s.s.e.), $P_{ti} - P_{mi}$, for n measurements would be

$$\text{s.s.e.} = \sum_{i=1}^{n} (P_{ti} - P_{mi})^2 \qquad \text{(B-2)}$$

Now consider

$$x_a = \frac{1}{\sigma} \log(x''_i/x''_{50}) \qquad \text{(B-3)}$$

where x" is a logarithmic-normally distributed variable, x''_{50} is its geometric mean and σ the standard deviation. Eq. (B-3) can be written as

$$x_a = \frac{\log x'' - M}{\sigma} \qquad \text{(B-4)}$$

where the mean $M = \log x''_{50}$. Thus we have from Eq. (B-1)

$$P_t(\sigma,M) = \frac{1}{\sqrt{2\pi}} \int_{-\infty}^{\frac{\log x''-M}{\sigma}} e^{-w^2/2}\, dw \qquad \text{(B-5)}$$

By the method of least squares values of σ and M must be found that give the best straight line fit from Eq. (B-5) for the n data points of P_{mi} versus x_i' plotted on logarithmic-normal coordinates. By Taylor Series expansion of $P_t(\sigma,M)$ for increments $\Delta\sigma$ and ΔM, we have

$$P_t(\sigma + \Delta\sigma,\ M + \Delta M) = P_t(\sigma,M) + \left(\frac{\partial P_t}{\partial \sigma}\right)\Delta\sigma + \left(\frac{\partial P_t}{\partial M}\right)\Delta M + (0)^2 + \ldots. \tag{B-6}$$

Then substituting Eq. (B-6) in Eq. (B-2) gives

$$\text{s.s.e.} = \sum_{i=1}^{n} \left(P_{ti}(\sigma,M) + \left(\frac{\partial P_t}{\partial \sigma}\right)_i \Delta\sigma + \left(\frac{\partial P_t}{\partial M}\right)_i \Delta M + (0)^2 + \ldots. - P_{mi}\right)^2 \tag{B-7}$$

The method of least squares involves minimizing the s.s.e. with respect to the variables $\Delta\sigma$ and ΔM. Thus, the conditions for a minimum are

$$\frac{\partial (\text{s.s.e.})^2}{\partial \Delta\sigma} = 0 \tag{B-8}$$

and

$$\frac{\partial (\text{s.s.e.})^2}{\partial \Delta M} = 0 \tag{B-9}$$

Eqs. (B-8) and (B-9) must be solved simultaneously for certain $\Delta\sigma_o$ and ΔM_o for given initial values σ_o and M_o. These obtained values of the increments are then added algebraically to σ_o and M_o to give new values σ_1 and M_1, and the process is repeated by solving Eqs. (B-8) and (B-9) once again for new values of the increments $\Delta\sigma_1$ and ΔM_1. Thus the repeated iteration ultimately converges σ and M to values which minimize the s.s.e., with $\Delta\sigma$ and ΔM approaching zero with successive iterations. As a result, the Taylor Series expansion of

Eq. (B-6) approaches the chain rule for differentiation, and therefore, we may neglect the higher than first order terms involving $\Delta\sigma$ and ΔM in Eq. (B-6).

Substituting Eq. (B-7), after neglecting terms of second and higher orders, into Eqs. (B-8) and (B-9) gives

$$\sum_{i=1}^{n} 2(P_{ti} + \left(\frac{\partial P_t}{\partial \sigma}\right)_i \Delta\sigma + \left(\frac{\partial P_t}{\partial M}\right)_i \Delta M - P_{mi})\left(\frac{\partial P_t}{\partial \sigma}\right)_i = 0 \tag{B-10}$$

and

$$\sum_{i=1}^{n} 2(P_{ti} + \left(\frac{\partial P_t}{\partial \sigma}\right)_i \Delta\sigma + \left(\frac{\partial P_t}{\partial M}\right)_i \Delta M - P_{mi})\left(\frac{\partial P_t}{\partial M}\right)_i = 0 \tag{B-11}$$

which may be simplified to give

$$\sum_{i=1}^{n} (P_{ti} - P_{mi})\left(\frac{\partial P_t}{\partial \sigma}\right)_i + \left(\frac{\partial P_t}{\partial \sigma}\right)_i^2 \Delta\sigma + \left(\frac{\partial P_t}{\partial M}\right)_i \left(\frac{\partial P_t}{\partial \sigma}\right)_i \Delta M = 0 \tag{B-12}$$

and

$$\sum_{i=1}^{n} (P_{ti} - P_{mi})\left(\frac{\partial P_t}{\partial M}\right)_i + \left(\frac{\partial P_t}{\partial M}\right)_i \left(\frac{\partial P_t}{\partial \sigma}\right)_i \Delta\sigma + \left(\frac{\partial P_t}{\partial M}\right)_i^2 \Delta M = 0 \tag{B-13}$$

Solving Eqs. (B-12) and (B-13) simultaneously for $\Delta\sigma$ and ΔM gives

$$\Delta\sigma = \frac{S_2 S_5 - S_3 S_4}{S_2^2 - S_1 S_3} \tag{B-14}$$

$$\Delta M = \frac{S_2 S_4 - S_1 S_5}{S_2^2 - S_1 S_3} \tag{B-15}$$

where

$$S_1 = \sum_{i=1}^{n} \left(\frac{\partial P_t}{\partial \sigma}\right)_i^2 \tag{B-16}$$

$$S_2 = \sum_{i=1}^{n} \left(\frac{\partial P_t}{\partial M} \right)_i \left(\frac{\partial P_t}{\partial \sigma} \right)_i \tag{B-17}$$

$$S_3 = \sum_{i=1}^{n} \left(\frac{\partial P_t}{\partial M} \right)_i^2 \tag{B-18}$$

$$S_4 = \sum_{i=1}^{n} (P_{mi} - P_{ti}) \left(\frac{\partial P_t}{\partial \sigma} \right)_i \tag{B-19}$$

and

$$S_5 = \sum_{i=1}^{n} (P_{mi} - P_{ti}) \left(\frac{\partial P_t}{\partial M} \right)_i \tag{B-20}$$

$(\partial P_t/\partial \sigma)_i$ and $(\partial P_t/\partial M)_i$ may be obtained from Eq. (B-1) as

$$\left(\frac{\partial P_t}{\partial \sigma} \right)_i = \frac{-x_{ai}}{\sqrt{2\pi}\,\sigma} e^{-x_{ai}^2/2} \tag{B-21}$$

$$\left(\frac{\partial P_t}{\partial M} \right)_i = -\frac{1}{\sqrt{2\pi}\,\sigma} e^{-x_{ai}^2/2} \tag{B-22}$$

where x_{ai} is given by Eq. (B-4).

It should be noted that for the relative equilibrium concentration plots, $P_m = C^*_{eq}$, $x'' = (\tau_b^* - 1)$, $x''_{50} = (\tau_b^* - 1)_{50}$ and $\sigma = \sigma_1$. For the deposition rate plots, $P_m = C^*$, $x'' = t$, $x''_{50} = t_{50}$ and $\sigma = \sigma_2$.

For any σ_j and M_j where $j = 0,1,2,\ldots$, Eqs. (B-14) and (B-15) may be written as

$$(\Delta\sigma)_j = \frac{(S_2)_j (S_5)_j - (S_3)_j (S_4)_j}{(S_2)_j^2 - (S_1)_j (S_3)_j} \tag{B-23}$$

and

$$(\Delta M)_j = \frac{(S_2)_j (S_4)_j - (S_1)_j (S_5)_j}{(S_2)_j^2 - (S_1)_j (S_3)_j} \tag{B-24}$$

and the new values are

$$\sigma_{j+1} = \sigma_j + (\Delta\sigma)_j \tag{B-25}$$

and

$$M_{j+1} = M_j + (\Delta M)_j \tag{B-26}$$

In all cases the initial values of $\sigma_o = 1$ and $M_o = 1$ were chosen. The criterion for convergence used was

$$|(s.s.e.)_j| = \left|\left\{ \sum_{i=1}^{n} (P_{ti} - P_{mi})^2 \right\}_j\right| < 10^{-6} \tag{B-27}$$

The equations were programmed on an IBM 360 computer at the University of Florida. Values of P_t were computed from a program of IBM's Scientific Subroutine Package. In all cases, convergence was rapid and did not give rise to any significant instability. In no case were more than six iterations required.

APPENDIX C

ANALYSIS OF MARACAIBO SEDIMENT

In order to determine the nature of the sediment from the Maracaibo estuary, three samples were collected from the bottom of the Inner Maracaibo Channel at locations E-32, T-35 and T-41 indicated in Fig. C.1. Particle size distributions of these samples are given in Fig. C.2. All the samples contained sand, some gravel, and shell fragments, in addition to silt and clay. In Table C.1, the percentage of gravel, sand, silt and clay are given. Also indicated therein are the depths at which the samples were collected.

TABLE C.1

Location	Depth (ft.)	% Gravel	% Sand	% Silt	% Clay
E-32	42.5	0.5	21.5	51.0	27.0
T-35	45.0	1.0	26.0	53.0	20.0
T-41	45.0	5.0	32.0	46.0	17.0

The sand grain size distribution was determined by sieve analysis, and the silt and clay fractions were analyzed by the standard method of sample withdrawals by a pipette, of the deflocculated material, at various times. It should be noted that in the determination of the fine grain size distribution, the sample was not dried initially for obtaining the total dry weight of the material used in the test. This was done in accordance with the

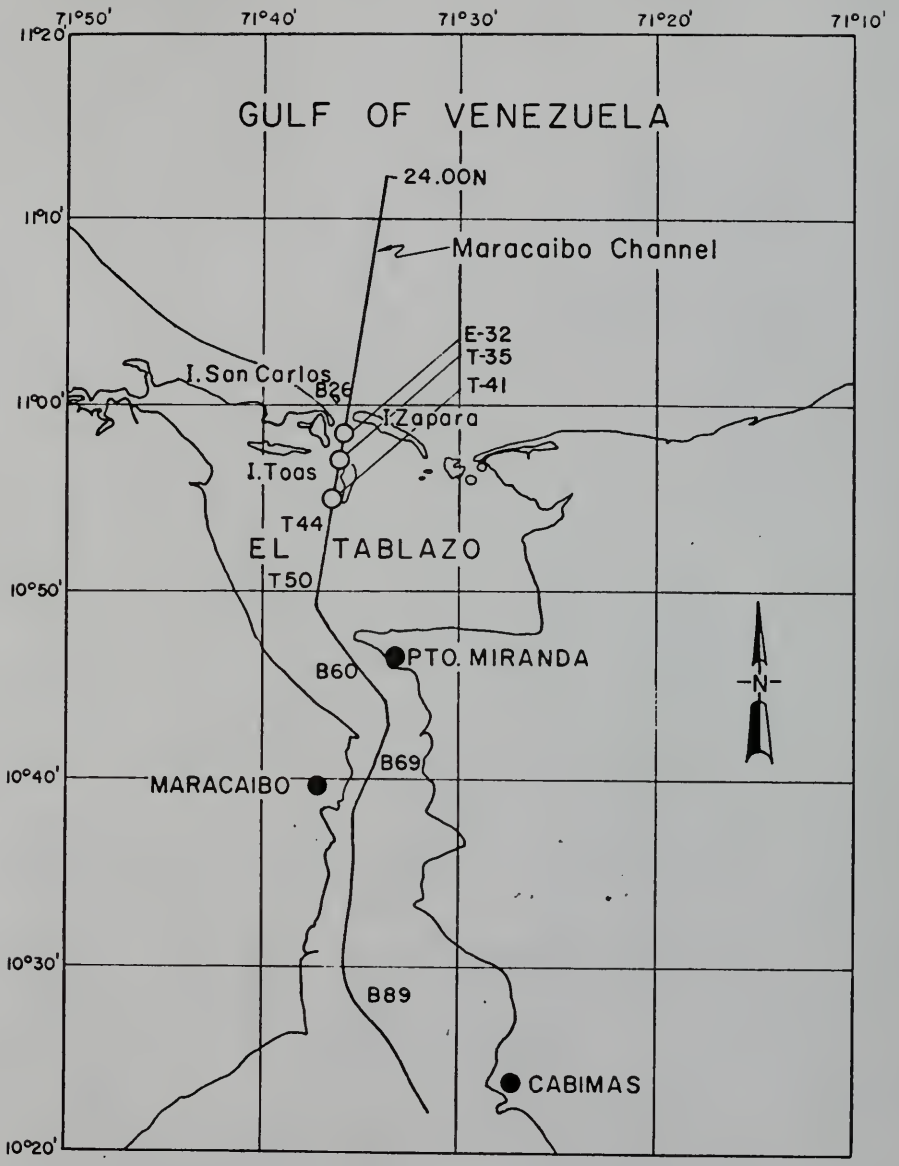

Fig. C.1. Geographic Location of Maracaibo Channel.

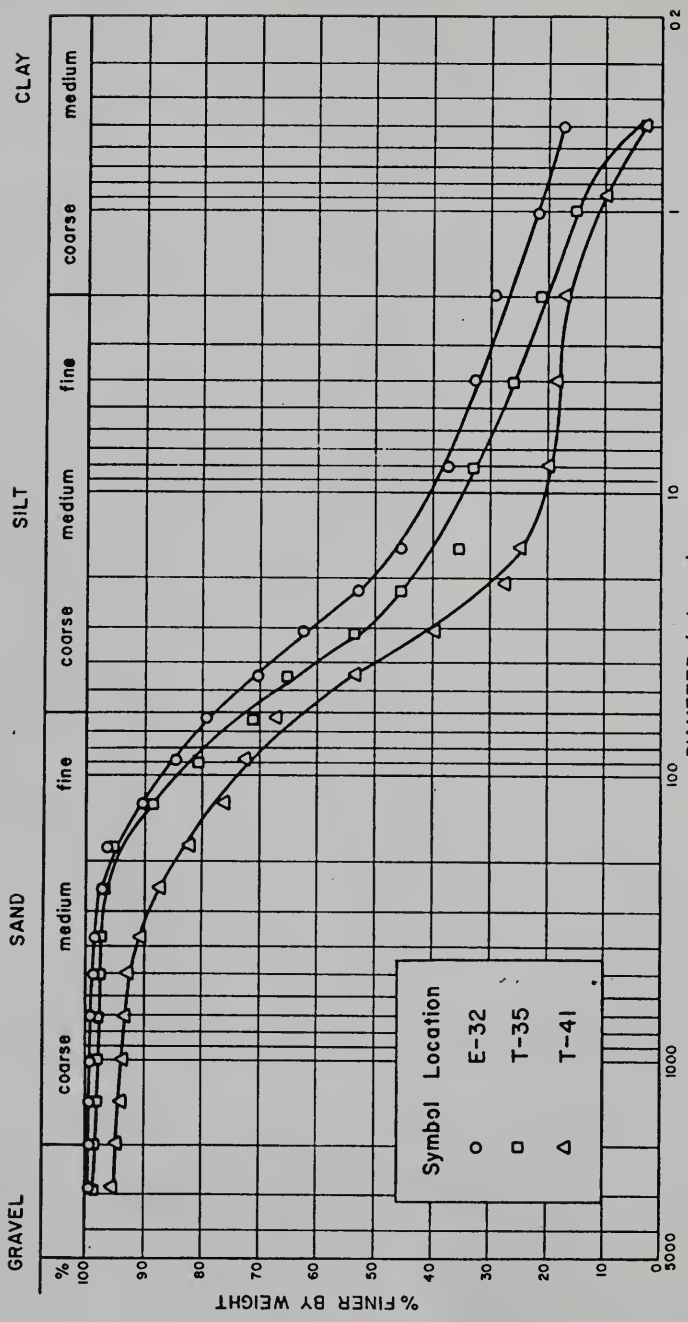

Fig. C.2. Particle Size Distributions of Sediment Samples from Maracaibo Channel.

observation made by Krone (1962) that if the sediment sample is dried, it is likely that it will not redisperse completely in water, with the result that the subsequently measured size distribution will indicate larger particle sizes as compared to those obtained by using the original wet sample. For this reason, the total dry weight of the material was obtained at the end of the test.

In Table C.2, the amounts of gravel, sand and silt are computed, relative to the amount of clay in each case. It is observed that from location E-32 to T-41, there is a consistent increase in the amounts of gravel, sand and silt, per unit amount of clay. This is also clearly seen from Fig. C.2.

TABLE C.2

Location	Gravel/Clay	Sand/Clay	Silt/Clay	Clay/Clay
E-32	0.02	0.80	1.89	1
T-35	0.05	1.30	2.65	1
T-41	0.29	1.88	2.71	1

The material dredged from the bottom of the channel is grey in color. If, however, some of it is thoroughly mixed in water in a tall glass cylinder, its color changes to brown. If allowed to stand in the cylinder, the deposited material once again changes from brown to greenish grey and finally back to grey. This behavior of the sediment is similar to that of Bay mud, described in Section 3.1.3. As explained there, these color changes indicate

the presence of iron sulphide in the sediment, as well as of bacteria which are capable of reducing the ferric ion to ferrous ion.

X-ray diffraction patterns with copper (Cu) Kα radiation of the three samples were nearly identical. Fig. C.3 shows the pattern for sample T-41 obtained from a smear slide of the less than 62 micron fraction, which essentially contains silt and clay. An abundance of quartz is present, and a calcite peak is also observed. The clay mineral peaks are relatively weak, because the samples contain relatively low amounts of clay as compared to silt, and also because a smear slide does not enhance the clay mineral peak intensities as compared to those for the non-clay constituents, as much as a sediment slide does. Methods for preparation of such slides have been described by Gibbs (1971).

In Fig. C.4, a pattern is shown for the less than 2 micron clay fraction on a sediment slide. Intense peaks for the (00ℓ) basal reflections are observed for kaolinite and illite. Since the slide was treated with ethylene glycol, the montmorillonite peak has shifted to 17 Å, and a small chlorite peak is observed at 14.2 Å. Quartz is also present.

Using a method described by Griffin (1971), the following approximate percentages of the different clay minerals were obtained: illite 45%, kaolinite 22%, montmorillonite 19%, and chlorite 13%. The predominant clay mineral constituent therefore is illite.

Since the silt and clay constitutents of the three samples were found to be almost identical in composition, as indicated by their X-ray patterns, the cation exchange capacity was determined from

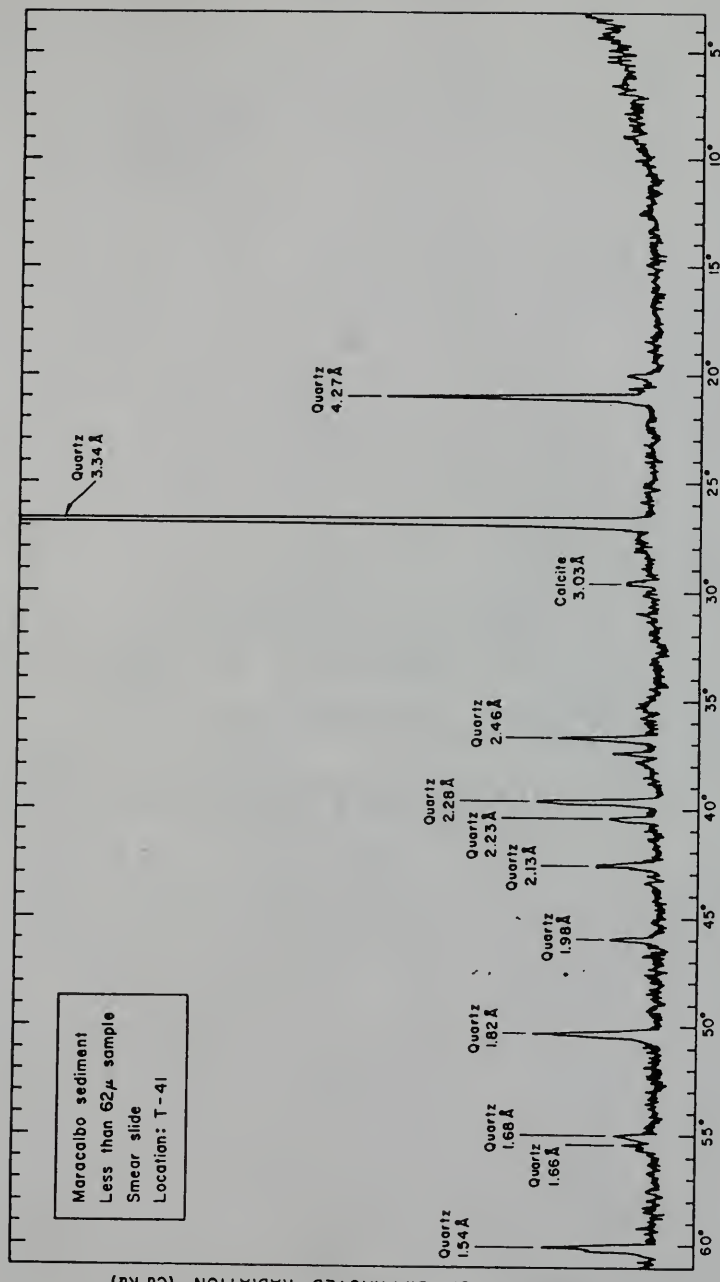

Fig. C.3. X-ray Diffraction Pattern for Maracaibo Sediment for Less than 62 Micron Fraction.

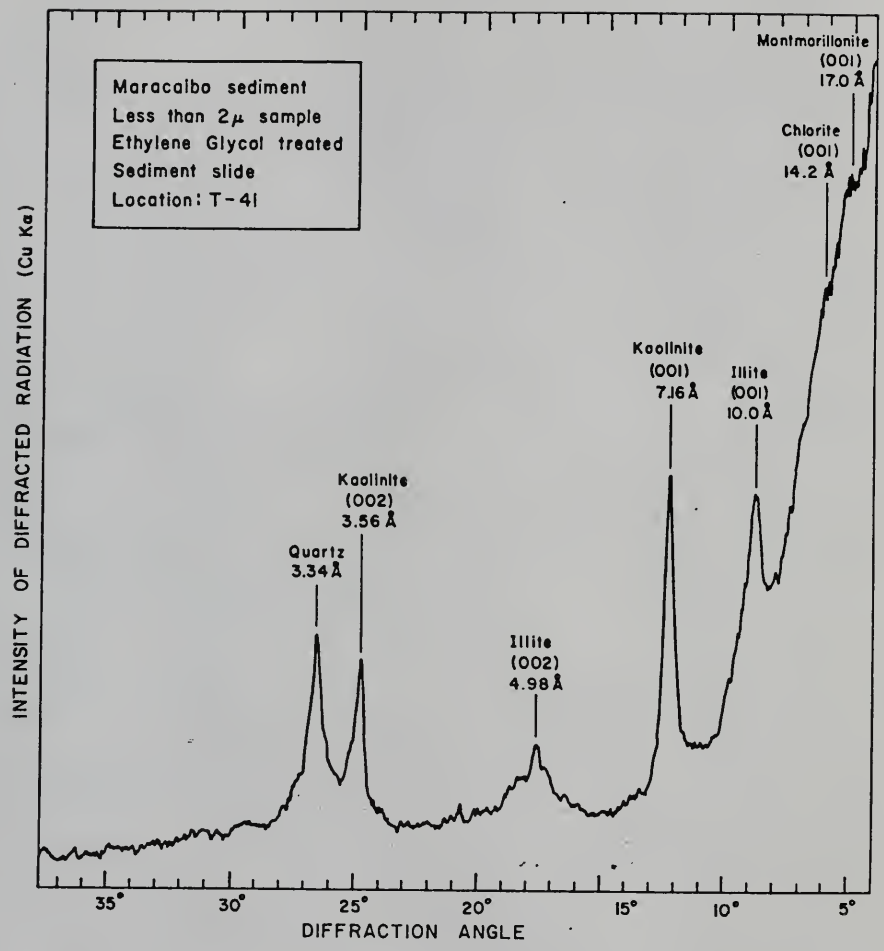

Fig. C.4. X-ray Diffraction Pattern for Maracaibo Sediment for Less than 2 Micron Fraction.

a sample which itself was obtained by mixing the three samples together. The mean cation exchange capacity was thus found to be equal to 39 milliequivalents per hundred grams. In order to determine if this value is compatible with the contributions to it made by each of the clay constitutents present in the material, the exact CEC of each of these constituents must be known. However, since these are not known, values given by Grim (1968) were selected for an approximate estimation. The ranges of these values of CEC in milliequivalents per hundred grams are given as follows: illite 10 to 40, kaolinite 3 to 15, montmorillonite (smectite) 80 to 150, and chlorite 10 to 40. The mean values corresponding to these ranges are illite 25, kaolinite 9, montmorillonite 115 and chlorite 25 milliequivalents per hundred grams. Adding these values in proportion to the percentages of each of the constituent present gives a CEC of 38 milliequivalents per hundred grams, which is in remarkably good agreement with the measured value.

APPENDIX D

ANALYTIC FORMULATION OF DEPOSITIONAL PROCESS

The equation of continuity for a sediment in a fluid under turbulent flow conditions can be written for a small element of fluid with dimensions dx, dy, dz shown in Fig. D.1. There, ρ' is the density of the suspension (mass of suspension/volume of suspension), C is the instantaneous sediment concentration (mass of sediment/mass of suspension) and u, v, ω are the instantaneous fluid velocity components in the x, y, z directions, respectively. W_s is the terminal settling velocity of the particles or flocs, so that $\rho W_s C$ is the corresponding downward flux of the sediment. It should be pointed out that since particles or flocs of various sizes are present in the sediment, the product $W_s C$ is the sum of the fluxes corresponding to each of the sizes present. The convective fluxes into and out of the volume element are shown in Fig. D.1, where the molecular diffusive fluxes are neglected and therefore are not indicated. The continuity principle can be expressed as:

$$\left\{\begin{array}{l}\text{net flux of sediment}\\ \text{into the volume element}\end{array}\right\} = \left\{\begin{array}{l}\text{rate of increase of}\\ \text{sediment within the}\\ \text{volume element}\end{array}\right\} \qquad \text{(D-1)}$$

where it is assumed that, despite the continuous process of formation and destruction of the flocs occurring within the volume element due to interparticle collisions, the overall size distribution remains invariant, so that there is no net generation or destruction of the flocs of any particular size. Therefore adding all the flux terms

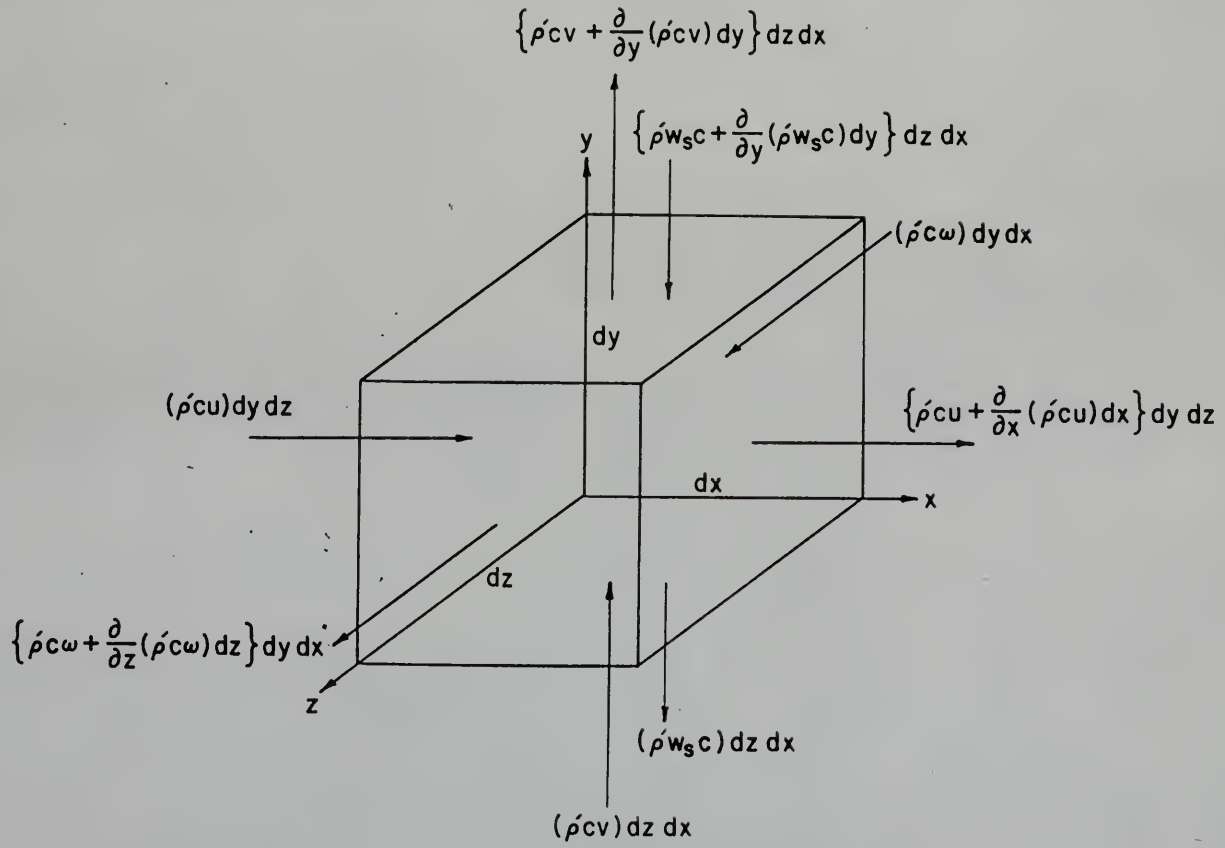

Fig. D.1. Sediment Continuity for an Elemental Volume.

shown in Fig. D.1 algebraically, equating them to the rate of increase of sediment mass within the volume, and then dividing the equation by the volume dxdydz, we get from Eq. (D-1)

$$-\frac{\partial}{\partial x}(\rho' Cu) - \frac{\partial}{\partial y}(\rho' Cv) - \frac{\partial}{\partial z}(\rho' C\omega) + \frac{\partial}{\partial y}(\rho' W_s C) = \frac{\partial}{\partial t}(\rho' C) \tag{D-2}$$

Next, the instantaneous velocities and concentration of Eq. (D-2) may be expressed, in terms of a time-average term (denoted by a bar) and fluctuating term (denoted by a prime), as

$$u = \bar{u} + u' \tag{D-3}$$

$$v = \bar{v} + v' \tag{D-4}$$

$$\omega = \bar{\omega} + \omega' \tag{D-5}$$

$$C = \bar{C} + C' \tag{D-6}$$

Substituting Eqs. (D-3) through (D-6) in Eq. (D-2) and averaging each term with respect to time results in the equation

$$\frac{\partial \bar{C}}{\partial t} + \bar{u}\frac{\partial \bar{C}}{\partial x} + \bar{v}\frac{\partial \bar{C}}{\partial y} + \bar{\omega}\frac{\partial \bar{C}}{\partial z} - \frac{\partial}{\partial y}(W_s \bar{C}) = -\frac{\partial}{\partial x}(u'C') - \frac{\partial}{\partial y}(v'C') - \frac{\partial}{\partial z}(\omega'C') \tag{D-7}$$

where use is made of the continuity equation

$$\frac{\partial \bar{u}}{\partial x} + \frac{\partial \bar{v}}{\partial y} + \frac{\partial \bar{\omega}}{\partial z} = 0 \tag{D-8}$$

The cross-product terms such as $\overline{u'C'}$, which represent the turbulent diffusion fluxes may be expressed, in terms of the mean concentration gradients, by analogy with Fick's law of diffusion, as

$$\overline{u'C'} = - \varepsilon_x \frac{\partial \bar{C}}{\partial x} \tag{D-9}$$

$$\overline{v'C'} = - \varepsilon_y \frac{\partial \bar{C}}{\partial y} \tag{D-10}$$

$$\overline{\omega'C'} = - \varepsilon_z \frac{\partial \bar{C}}{\partial z} \tag{D-11}$$

where ε_x, ε_y and ε_z are the turbulent diffusivities in the x, y and z directions, respectively. It should be noted here again that these fluxes are summed over the contributions made by particles or flocs of each size present. Substituting Eqs. (D-9), (D-10) and (D-11) into Eq. (D-7) and expanding the terms yields

$$\frac{\partial \bar{C}}{\partial t} + \bar{u} \frac{\partial \bar{C}}{\partial x} + \bar{v} \frac{\partial \bar{C}}{\partial y} + \bar{\omega} \frac{\partial \bar{C}}{\partial z} = \left(\frac{\partial \varepsilon_x}{\partial x} \frac{\partial \bar{C}}{\partial x} + \varepsilon_x \frac{\partial^2 \bar{C}}{\partial x^2} \right) + \left(\frac{\partial \varepsilon_y}{\partial y} \frac{\partial \bar{C}}{\partial y} + \frac{\partial}{\partial y} (W_s \bar{C}) \right.$$

$$\left. + \varepsilon_y \frac{\partial^2 \bar{C}}{\partial y^2} \right) + \left(\frac{\partial \varepsilon_z}{\partial z} \frac{\partial \bar{C}}{\partial z} + \varepsilon_z \frac{\partial^2 \bar{C}}{\partial z^2} \right) \tag{D-12}$$

Eq. (D-12) was derived by McLaughlin (1961) and has been discussed by Partheniades (1971).

Case a. Open flume: If Eq. (D-12) is to be applied to a two-dimensional case approximating an open channel flow in a flume, then $v = \omega = 0$, $\partial C/\partial z = 0$ and $u = u(y)$ only, so that

$$\frac{\partial \bar{C}}{\partial t} + u \frac{\partial \bar{C}}{\partial x} = \frac{\partial \varepsilon_x}{\partial x} \frac{\partial \bar{C}}{\partial x} + \varepsilon_x \frac{\partial^2 \bar{C}}{\partial x^2} + \frac{\partial \varepsilon_y}{\partial y} \frac{\partial \bar{C}}{\partial y} (W_s \bar{C}) + \varepsilon_y \frac{\partial^2 \bar{C}}{\partial y^2} \tag{D-13}$$

If the flow is close to uniform, then the diffusivities are independent of x, for no sediment. This may also be assumed to be the case for relatively low sediment concentrations (Partheniades, 1971), so that

$$\frac{\partial C}{\partial t} + u \frac{\partial C}{\partial x} = \varepsilon_x \frac{\partial^2 C}{\partial x^2} + \frac{\partial \varepsilon_y}{\partial y} \frac{\partial C}{\partial y} + \frac{\partial}{\partial y} (W_s C) + \varepsilon_y \frac{\partial^2 C}{\partial y^2} \qquad \text{(D-14)}$$

where the bars over C have been dropped for convenience, although their presence is implied. Next, considering the similarity in the law of deposition in the annular channel and in straight flumes, it may be assumed that $\partial C/\partial x$ is negligible in the latter case, as discussed in Section 4.3.3. Eq. (D-14) therefore reduces to

$$\frac{\partial C}{\partial t} = \frac{\partial}{\partial y} (W_s C) + \frac{\partial \varepsilon_y}{\partial y} \frac{\partial C}{\partial y} + \varepsilon_y \frac{\partial^2 C}{\partial y^2} \qquad \text{(D-15)}$$

In order to solve Eq. (D-15), the following initial and boundary conditions must be specified.

1. Initial condition:

$$C(y)\Big|_{t=0} = C_o \qquad \text{(D-16)}$$

which assumes a thorough mixing of the sediment at the beginning of the deposition process, and is a reasonable description of the initial condition in the straight flume.

2. Free surface boundary condition:

$$W_s C(t)\Big|_{y=d} = - \varepsilon_y \frac{\partial C(t)}{\partial y}\Big|_{y=d} \qquad \text{(D-17)}$$

i.e., there is no net rate of transport in the y direction across the free surface.

3. Bottom boundary condition:

$$(1 - p_d)\, W_s C(t)\Big|_{y=\xi} = -\varepsilon_y \frac{\partial C(t)}{\partial y}\Bigg|_{y=\xi} \qquad \text{(D-18)}$$

where p_d is the probability of deposition discussed in Section 4.3.1. ξ is a small distance above the theoretical bed ($y = 0$) where the bottom boundary condition is effectively applicable, since at $y = 0$, $\varepsilon_y = 0$ according to Eq. (D-19), so that no diffusive flux would occur at that level, and therefore the boundary condition cannot be applied there. This boundary condition assumes that while the sediment is depositing, no erosion of the bed material is taking place.

For comparatively low sediment concentrations, we may assume for an open channel flow

$$\varepsilon_y = \kappa u_* y\left(1 - \frac{y}{d}\right) \qquad \text{(D-19)}$$

where κ is the Karman constant and d is the total depth of flow. Substituting Eq. (D-19) into Eq. (D-15) gives

$$\frac{\partial C}{\partial t} = W_s \frac{\partial C}{\partial y} + \kappa u_*\left(1 - \frac{2y}{d}\right)\frac{\partial C}{\partial y} + \kappa u_* y\left(1 - \frac{y}{d}\right)\frac{\partial^2 C}{\partial y^2} \qquad \text{(D-20)}$$

where a further assumption is made that for relatively low concentrations, W_s is constant. The initial and boundary conditions for the solution of Eq. (D-20) are given by Eqs. (D-16), (D-17) and (D-18). However, boundary conditions of Eqs. (D-17) and (D-18) cannot be used to solve Eq. (D-20) unless the values of W_s, C and $\partial C/\partial y$ at $y = d$ and $y = \xi$ are known, as well as the value of the probability of deposition p_d. The conditions at the bottom boundary are especially difficult to determine because the structure of turbulence, and the exact nature

of the interaction of the flocs and the flow just above the bed surface, are the unknown factors.

It is interesting to integrate Eq. (D-20) and examine the resultant indefinite integral involving certain constants to be determined from the boundary conditions. Assuming a solution of the form:

$$C(y,t) = \overline{Y}(y)\overline{T}(t) \tag{D-21}$$

Eq. (D-20) can be solved by separating the variables involving y and t to yield

$$\frac{d\overline{T}}{dt} + \alpha\overline{T} = 0 \tag{D-22}$$

and

$$\kappa u_* y\left(1 - \frac{y}{d}\right)\frac{d^2\overline{Y}}{dy^2} + \left[W_s + \kappa u_*\left(1 - \frac{2y}{d}\right)\right]\frac{d\overline{Y}}{dy} + \alpha\overline{Y} = 0 \tag{D-23}$$

where α is a constant. The solution of Eq. (D-22) is

$$\overline{T} = A_1 e^{-\alpha t} \tag{D-24}$$

where A_1 is a constant of integration. Eq. (D-23) can be reduced to the following form (with $x' = y/d$)

$$x'(1 - x')\frac{d^2\overline{Y}}{dx'^2} + \left(\frac{W_s}{\kappa u_*} + 1\right) - 2x'\frac{d\overline{Y}}{dx'} + \frac{\alpha d}{\kappa u_*}\overline{Y} = 0 \tag{D-25}$$

which has the form of Gauss's hypergeometric equation

$$x'(1 - x')\frac{d^2\overline{Y}}{dx'^2} + [m' - (n' + q' + 1)x']\frac{d\overline{Y}}{dx'} - n'q'\overline{Y} = 0 \tag{D-26}$$

so that

$$m' = \frac{W_s}{\kappa u_*} + 1 \tag{D-27}$$

$$n' = \frac{1}{2} \pm \sqrt{\frac{1}{4} - \frac{\alpha d}{\kappa u_*}} \tag{D-28}$$

$$q' = \frac{1}{2} \mp \sqrt{\frac{1}{4} - \frac{\alpha d}{\kappa u_*}} \tag{D-29}$$

Solutions of Eq. (D-25) can be obtained for different values of α, d, κ and u_* as hypergeometric series, by the Frobenius method, and in general may be expressed as

$$\overline{Y} = F(m', n', q', x') \tag{D-30}$$

so that combining Eqs. (D-24) and (D-30) according to Eq. (D-21) to

$$C = F(m', n', q', y/d)A_1 e^{-\alpha t} \tag{D-31}$$

Averaging Eq. (D-31) over the depth d changes Eq. (D-31) to

$$C = \overline{F}A_1 e^{-\alpha t} \tag{D-32}$$

where the bar over F implies y-averaged value. Eq. (D-32) indicates an exponential decrease of suspended sediment concentration with time, at low sediment concentrations in open flumes. This is indeed observed to be the case as suggested by the data shown in Fig. 4.2.53 and discussed in Section 4.2.3.

When high sediment concentrations are present, both W_s and ε_y are likely to depend on concentration and therefore also on time, since the former changes with the latter. In such situations, the law of Eq. (D-32) cannot be valid. This is observed to be the case in experiments of Krone (1962), Partheniades (1965) and Rosillon and Volkenburn (1964) as discussed in Section 4.2.3, where it is noted

that in such cases, the logarithmic-normal law of Eq. (4.2-8) appears to hold. However, since the functional dependence of W_s and ε_y on concentration or time are not known, it is not possible to solve Eq. (D-14) for high sediment concentrations. It should be noted that if one is considering the case $\tau_b^* > 1$, then C must be replaced by the depositable concentration $C - C_{eq}$, so that Eq. (D-15) may be written in terms of $C^{**} = (C - C_{eq})/(C_o - C_{eq})$ as

$$\frac{\partial C^{**}}{\partial t} = \frac{\partial}{\partial y}(W_s C^{**}) + \frac{\partial \varepsilon_y}{\partial y}\frac{\partial C^{**}}{\partial y} + \varepsilon_y \frac{\partial^2 C^{**}}{\partial y^2} \qquad \text{(D-33)}$$

Eq. (D-33) holds both for τ_b^* greater than as well as less than unity, in the latter case C_{eq} being equal to zero.

Case b. Annular channel: Strictly speaking, the sediment continuity equation for the annular channel must be derived in polar coordinates, with r and θ replacing z and x, respectively. However, because the flow in the annular channel approximates an endless straight flume, only the y coordinate ultimately remains in the equation and therefore such a derivation is not warranted.

In the annular channel, by virtue of its geometry, there is no gradient of concentration along the flow direction, so that Eq. (D-13) and consequently Eq. (D-33) hold exactly. The boundary conditions are given by Eqs. (D-16), (D-17) and (D-18). The dependence of ε_y on depth or concentration is however not known and the same holds for W_s. However, for low concentrations ε_y may be assumed to be independent of C, so that, irrespective of its functional dependence on y, an exponential law similar to Eq. (D-32) may be derived if W_s

is assumed to be constant. The data from the annular channel shown in Fig. 4.2.53 indicate such an exponential decrease of concentration with time. However, the evidence is not conclusive because certain other runs described in Section 4.2.2 indicate different depositional behavior. It is possible that to assume W_s as constant may not be valid in such situations. Further investigation is therefore necessary.

For high sediment concentrations the unknown dependence of W_s and ε_y on depth, concentration and time prohibits integration of Eq. (D-33). The reasoning here is similar to that cited for the similar situation in open flumes.

APPENDIX E

APPLICATION OF RESULTS

An application of the results on deposition, as well as the previously investigated results on erosion, is described here for the simple case of cohesive sediment transport in a straight rectangular channel, in which the suspended sediment is fully mixed in the vertical direction, and in which tidal flow is primarily responsible for the scouring and deposition of the sediment. For the purpose of determining the time history of sediment concentration, the channel, may be divided into n sections, which may or may not be of equal lengths. In a zone where more detailed description of the sediment variation is required, smaller length sections may be selected. A channel cross section is shown in the inset of Fig. E.1, where A is the cross-sectional area, B the width and η' the water surface elevation measured from a selected datum. In order to determine numerically the variation of sediment concentration with time and space, the following basic equations and initial and boundary conditions are required:

a. Hydrodynamic equations: Before dealing with the problem of sediment transport, the time and space history of the flow within the channel sections must be known. For this, the equation of motion

$$\frac{\partial u}{\partial t} + u \frac{\partial u}{\partial x} = - ku|u| - g \frac{\partial \eta'}{\partial x} \qquad \text{(E-1)}$$

and continuity

$$\frac{\partial \eta'}{\partial t} = - \frac{1}{B} \frac{\partial}{\partial x} (uA) \qquad \text{(E-2)}$$

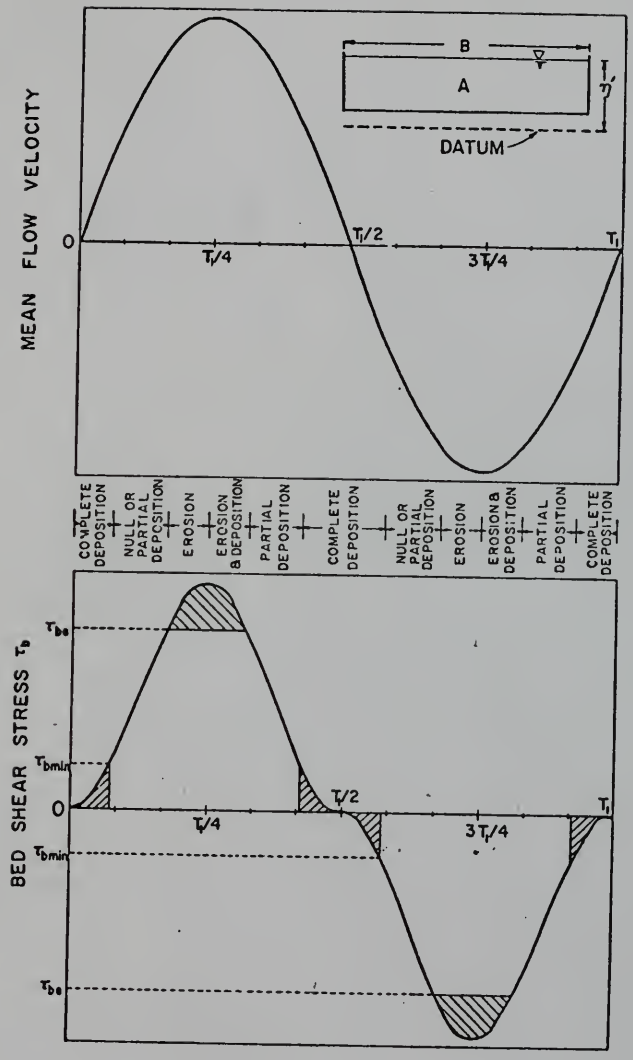

Fig. E.1. Periods of Erosion and Deposition in a Tidal Cycle.

must be solved numerically. Here, k is the coefficient of frictional resistance, g is the acceleration due to gravity and it is assumed that the flow velocity u is uniform over the cross section. In order to solve Eqs. (E-1) and (E-2), the time variations of u and η' at the beginning of the first channel section and at the end of the nth section must also either be known or assumed. Shubinski et al. (1965) have developed such a hydrodynamic model for the San Francisco Bay system.

b. Diffusion equation: The diffusion expression given by Eq. (D-13) may be written for the vertically (y-direction) mixed case as

$$\frac{\partial C}{\partial t} + u \frac{\partial C}{\partial x} = \frac{1}{A} \frac{\partial}{\partial x} \left(A D_L \frac{\partial C}{\partial x} \right) + \tilde{R} \qquad \text{(E-3)}$$

where D_L is the dispersion coefficient in the x-direction, which replaces ε_x in Eq. (D-13), and it accounts for the fact that the flow velocity is not uniform over the cross section, and consequently, as shown by Taylor (1954) the effective dispersion of sediment in the x-direction is much larger than that predicted by ε_x, which is the diffusivity in the x-direction for a uniform flow velocity. The variation of the cross-sectional area $A = B \cdot \eta'$ is taken into account in the diffusion term. The additional term $\tilde{R}$ is a source or sink term which accounts for the erosion and deposition of the sediment. These phenomena actually occur at the bottom boundary of the channel, but in effect they cause a variation of the sediment concentration within the bulk of the suspension with time. Eq. (E-3) may be written as

$$\frac{\partial C}{\partial t} + u \frac{\partial C}{\partial x} = \frac{1}{A} \frac{\partial}{\partial x} \left(AD_L \frac{\partial C}{\partial x} \right) + R_d + R_e \qquad \text{(E-4)}$$

where R_d and R_e are the sink and source for deposition and erosion, respectively. Since in the annular channel, $\partial C/\partial x$ is zero, R_d may be obtained directly from Eq. (4.2-14) as

$$R_d = \left(\frac{dC}{dt} \right)_{\substack{\text{annular} \\ \text{channel}}} = - \frac{(C_o - C_{eq})}{\sqrt{2\pi}\, \sigma_2} e^{-T^2/2} \cdot \frac{(0.434)}{t} \qquad \text{(E-5)}$$

where T is defined by Eq. (4.2-9). Similarly, R_e may be obtained from the erosion experiments of Partheniades (1962). Here again, based on arguments similar to those used in Section 4.3.3 in describing the process of deposition in straight flumes, it may be assumed that $\partial C/\partial x$ is negligible in erosion measurements, so that from the results of Partheniades,

$$R_e = \left(\frac{dC}{dt} \right)_{\substack{\text{open} \\ \text{flume}}} = \left(\frac{dC}{dt} \right)_{2e} \left(\frac{\tau_b}{\tau_{be}} - 1 \right) \qquad \text{(E-6)}$$

where τ_{be} is the critical shear stress for initiation of erosion, and $(dC/dt)_{2e}$ is the rate of concentration increase at twice the critical shear stress τ_{be}. In general, for a given sediment type in a given ambient water quality, the parameters D_L, τ_{be} and $(dC/dt)_{2e}$ must be known. In addition, the dependence of σ_2 and t_{50} which are implicit in the definition of T according to Eq. (4.2-9) on the flow conditions must also be known. Eq. (E-4) along with Eqs. (E-5) and (E-6) can then be numerically integrated in conjunction with Eqs.

(E-1) and (E-2) to yield the time and space history of the sediment concentration.

Fig. E.1 shows a hypothetical mean (over the cross section) tidal velocity profile, and the corresponding curve for the bed shear stress τ_b, for one tidal cycle. The purpose here is to indicate the time periods over which erosion and/or deposition of the sediment material may take place, depending on the values of τ_{bmin} and τ_{be}. Starting with $\tau_b = 0$ at $t = 0$ up to the point at which $\tau_b = \tau_{bmin}$, a complete deposition of the sediment may occur. A particularly favorable situation for this is at low tide ($t = 0$) when no flow is present. If all the sediment is deposited by the time $\tau_b = \tau_{bmin}$, then in the next time period between $\tau_b = \tau_{bmin}$ and $\tau_b = \tau_{be}$, neither deposition nor erosion can occur. If, on the other hand, some of the sediment is still in suspension, part of it will deposit depending on the value of τ_b, since for $\tau_b > \tau_{bmin}$, the depositable fraction of the sediment is in general less than unity. As τ_b increases above τ_{be}, scouring of the bed material will begin, and it may be assumed that during the period when $\tau_b = \tau_{bmin}$ and up to $t = T/4$, deposition of the remaining small amount of the material in suspension is negligible. However, beyond $t = T/4$, and up to the time at which τ_b is reduced to τ_{be}, while erosion continues at slower and slower rates, the decelerating flow causes some deposition of the material suspended as a result of scouring. When τ_b reaches below τ_{be}, erosion ceases, but partial deposition continues until τ_b becomes lower than τ_{bmin}, at which point the entire sediment begins to deposit. A similar sequence of events is then repeated after

$t = T_I/2$, but with the flow in the opposite direction. It should be pointed out that the case described here corresponds to a situation where even the peak value of τ_b is less than that required to keep any initially suspended material from depositing. This shear stress τ_{bmax}, as noted in Section 4.2.1, may be an order of magnitude higher than τ_{bmin}. Therefore in the present case, deposition of the sediment can occur over the entire tidal cycle, although it is assumed that there exists a period (between $\tau_b = \tau_{be}$ and the peak value of τ_b at $t = T_I/4$) during which erosion only is occurring because most of the depositable sediment has already deposited in the previous part of the cycle. Another point that should be mentioned is that the examined case is one where the flow is generally either accelerating or decelerating, and therefore it is non-uniform, whereas the results of erosion and deposition are derived from tests made under uniform flow conditions, so that caution is warranted in the application of these results. Thus, for using the results, for each time step chosen for numerical integration, and each section of the channel, some mean values of flow velocity must be used in order for the derived laws of deposition and erosion to hold. In this context it should be noted that the quantity C_o for a given time step corresponds to the suspended concentration at the end of the previous time step.

REFERENCES

Bird, R. B., Stewart, W. E., and Lightfoot, E. N., Transport Phenomena, John Wiley & Sons, Inc., 1960.

Braswell, R. N., and Manders, C. F., "A New Finite Range Probability Distribution Function (FRPDF) with Parameters -Nomogram and Tables," Rep. Stat. Appl. Res., JUSE, Vol. 17, No. 2, p. 11, 1970.

Chiu, T. Y., "Sand Transport by Air or Water," Ph.D. Dissertation, Univ. of Florida, Gainesville, 1972.

Christensen, B. A., Discussion of "Erosion and Deposition of Cohesive Soils," by Partheniades, E., J. Hydr. Div., Proc. ASCE, Vol. 91, No. HY5, p. 301, September, 1965.

Christensen, B. A., Sediment Transport Class Notes, Univ. of Florida, Gainesville, 1969.

Christensen, B. A., and Bush, P. W., "Statistically Based Determination of Depth and Width Ratios in Alluvial Watercourses," Proc. International Symposium on Stochastic Hydraulics, Pittsburgh, May, 1971.

Corps of Engineers, U. S. Army, "Typical Major Tidal Hydraulic Problems in the United States and Research Sponsored by the Corps of Engineers, Committee on Tidal Hydraulics," Tech. Bull. No. 6, June, 1963.

Dunn, I. S., "Tractive Resistance of Cohesive Channels," J. Soil Mech. and Foundation Div., Proc. ASCE, Vol. 85, No. SM3, Proc. paper 2062, June, 1959.

Dwight, H. B., Tables of Integrals and Other Mathematical Data, Fourth Edition, The Macmillan Co., 1965.

Einstein, H. A., "The Bed-Load Function for Sediment Transportation in Open Channel Flows," Tech. Bull, No. 1026, U. S. Dept. of Agriculture, Soil Conservation Service, Washington, D.C., September, 1950.

El-Samni, E. A., "Hydrodynamic Forces Acting on the Surface Particles of a Stream Bed," Ph.D. Dissertation, Univ. of California, Berkeley, 1949.

Epsey, W. H., Jr., "A New Test to Measure the Scour of Cohesive Sediment," Hydr. Engr. Lab., Dept. of Civil Engr., Tech. Rep. HYD01-6301, Univ. of Texas, Austin, April, 1963.

Etter, R. J. and Hoyer, R. P., Partheniades, E. and Kennedy, J. F., "Depositional Behavior of Kaolinite in Turbulent Flow," J. Hydr. Div., Proc. ASCE, Vol. 94, No. HY6, Proc. paper 6242, November, 1968.

Gibbs, R. J., "X-ray Diffraction Mounts," Chapter 23, in Procedures in Sedimentary Petrology, Edited by R. E. Carver, Interscience (Wiley), 1971.

Gole, C. V., Tarapore, Z. S., and Brahme, S. B., "Prediction of Siltation in Harbour Basins and Channels," Proc. 14th Congress of Int. Assoc. for Hydr. Res., Vol. 4, p. 33, Paris, August, 1971.

Griffin, G. M., "Interpretation of X-ray Diffraction Data," Chapter 24 in Procedures in Sedimentary Petrology, Edited by R. E. Carver, Interscience (Wiley), 1971.

Grim, R. E., Clay Mineralogy, McGraw-Hill Book Co., 1968.

Grissinger, E. H., "Resistance of Selected Clay Systems to Erosion by Water," Water Resources Research, Vol. 2, No. 1, p. 131, 1966.

Harrison, A. J. M., and Owen, M. W., "Siltation of Fine Sediments in Estuaries," Proc. 14th Congress of Int. Assoc. for Hydr. Res., Vol. 4, p. 1, Paris, August, 1971.

Krone, R. B., "First Annual Progress Report on the Silt Transport Studies Utilizing Radioisotopes," Hydr. Engr. Lab. and Sanitary Engr. Res. Lab., Univ. of California, Berkeley, December, 1957.

Krone, R. B., "Flume Studies of the Transport of Sediment in Estuarial Shoaling Processes," Final Rep. Hydr. Engr. Lab. and Sanitary Engr. Res. Lab., Univ. of California, Berkeley, June, 1962.

Krone, R. B., "Predicted Suspended Sediment Inflows to the San Francisco Bay System," Prepared for Central Pacific River Basins Comprehensive Water Pollution Project, Federal Water Pollution Control Administration, Southwest Region, September, 1966.

Leliavsky, S., An Introduction to Flurial Hydraulics, Constable and Co., Ltd., 1959.

McLaughlin, R. T., "Settling Properties of Suspension," Trans. ASCE, Part I, Vol. 126, p. 1734, 1961.

Mehta, A. J. and Partheniades, E., "Effect of Physico-chemical Properties of Fine Suspended Sediment on the Degree of Deposition," Proc. Int. Symp. on River Mech., Int. Assoc. for Hydr. Res., Vol. 1, p. 465, Bankok, January, 1973.

Moore, W. L., and Masch, F. D., Jr., "Experiments on the Scour Resistance of Cohesive Sediments," J. Geophys. Res., Vol. 67, No. 4, p. 1437, 1962.

Owen, M. W., "The Effect of Turbulence on the Settling Velocities of Silt Flocs," Proc. 14th Congress of Int. Assoc. for Hydr. Res., Vol. 4, p. 27, Paris, August, 1971.

Partheniades, E., "A Study of Erosion and Deposition of Cohesive Soils in Salt Water," Ph.D. Dissertation, Univ. of California, Berkeley, 1962.

Partheniades, E., "The Present State of Knowledge of the Behavior of Fine Sediments in Estuaries," Tech. Note No. 8, Hydrodynamics Lab., M.I.T., Cambridge, June, 1964.

Partheniades, E., "Erosion and Deposition of Cohesive Soils," J. Hydr. Div., Proc. ASCE, Vol. 91, No. HY1, Proc. paper 4204, January, 1965.

Partheniades, E., "Field Investigations to Determine Sediment Sources and Salinity Intrusion in the Maracaibo Estuary, Venezuela," Rep. No. 94, Hydrodynamics Lab., M.I.T., Cambridge, June, 1966.

Partheniades, E., Kennedy, J. F., Etter, R. J. and Hoyer, R. P., "Investigations of the Depositional Behavior of Fine Cohesive Sediments in an Annular Rotating Channel," Rep. No. 96, Hydrodynamics Lab., M.I.T., Cambridge, June, 1966.

Partheniades, E., Cross, R. H., and Ayora, A., "Further Results on the Deposition of Cohesive Sediments," Proc. 11th Conf. on Coastal Engr., Vol. 1, Ch. 47, p. 723, London, September, 1968.

Partheniades, E. and Paaswell, R. E., "Erodibility of Channels with Cohesive Boundary," J. Hydr. Div., Proc. ASCE, Vol. 96, No. HY3, Proc. paper 7156, March, 1970.

Partheniades, E., "Erosion and Deposition of Cohesive Materials," Chapter 25, in River Mechanics,Edited by H. W. Shen, Colorado State Univ., Fort Collins, 1971.

Partheniades, E., "Salinity Intrusion and Its Effect on Shoaling," Chapter 26, in River Mechanics, Edited by H. W. Shen, Colorado State Univ., Fort Collins, 1971.

Partheniades, E., and Mehta, A. J., "Deposition of Fine Sediments in Turbulent Flows," Rep. No. 16050 ERS, Water Pollution Control Series, U. S. Environmental Protection Agency, August, 1971.

Partheniades, E., "On the Concept of the Wash Load," Proc. Int. Symp. on River Mech., Int. Assoc. for Hydr. Res., Vol. 1, p. 573, Bankok, January, 1973.

Rosillon, R. and Volkenborn, C., "Sedimentación de Material Cohesivo en Agua Salada," Thesis, Univ. of Zulia, Maracaibo, Venezuela, November, 1964.

Rouse, H., Fluid Mechanics for Hydraulic Engineers, Dover Publications, Inc., 1961.

Schlichting, H., Boundary Layer Theory, Sixth Edition, McGraw-Hill Book Co., 1968.

Shubinski, R. P., McCarty, J. C., and Lindorf, M. R., "Computer Simulation of Estuarial Networks," J. Hydr. Div., Proc. ASCE, Vol. 91, No. HY5, Proc. paper 4470, September, 1965.

Shubinski, R. P. and Krone, R. B., "A Proposed Model for Sediment Processes in Estuaries," Presented at ASCE Conference on Water Resources in the Seventies, Memphis, January, 1970.

Smerdon, E. T. and Beasely, R. P., "The Tractive Force Theory Applied to Stability of Open Channels in Cohesive Soils," Res. Bull. 715, Univ. of Missouri, College of Agriculture, Agr. Expt. Station, October, 1959.

Strain Gage Bulletin 100/101, Issued by Baldwin Lima Hamilton, Inc., Waltham, Mass., 1967.

Strain Instruments Catalog, Product Data 602-3, Issued by Baldwin Lima Hamilton, Inc., Waltham, Mass., 1968.

Task Committee on Preparation of Sedimentation Manual, Committee on Sedimentation of the Hydraulics Division, "Chapter V, Sediment Control Methods: C. Control of Sediment in Canals," J. Hydr. Div., Proc. ASCE, Vol. 98, No. HY9, Proc. paper 9177, September, 1972.

Taylor, G. I., "Dispersion of Matter in Turbulent Flow Through a Pipe," Proc. Roy. Soc. London (A), Vol. 223, 1954.

Technical Data Sheet, Bulletin No. 80, Issued by R. T. Vanderbilt Co., Inc., New York, 1970.

Terzaghi, K. and Peck, R. B., Soil Mechanics in Engineering Practice, Second Edition, John Wiley & Sons, Inc., 1967.

Van Olphen, H., An Introduction to Clay Colloid Chemistry, Interscience (Wiley), 1963.

BIOGRAPHICAL SKETCH

Ashish J. Mehta was born in Bombay, India, on July 15, 1944. He graduated from Fellowship High School, Bombay, in June, 1960.

From June, 1960 to June, 1964, he attended the University of Bombay, where he received the degree of Bachelor of Science in Chemistry. From September, 1964 to December, 1966, he studied in the University of California at Berkeley, where he received the degree of Bachelor of Science, with a major in Chemical Engineering.

In January, 1967, he entered the University of Florida, where he pursued graduate studies leading to the degree of Master of Science in Engineering in the Department of Chemical Engineering, in March, 1969. Since that time, Mr. Mehta has been studying in the Department of Civil and Coastal Engineering towards the degree of Doctor of Philosophy.

I certify that I have read this study and that in my opinion it conforms to acceptable standards of scholarly presentation and is fully adequate, in scope and quality, as a dissertation for the degree of Doctor of Philosophy.

Emmanuel Partheniades, Chairman
Professor of Civil and Coastal Engineering

I certify that I have read this study and that in my opinion it conforms to acceptable standards of scholarly presentation and is fully adequate, in scope and quality, as a dissertation for the degree of Doctor of Philosophy.

Robert G. Dean
Professor of Civil and Coastal Engineering

I certify that I have read this study and that in my opinion it conforms to acceptable standards of scholarly presentation and is fully adequate, in scope and quality, as a dissertation for the degree of Doctor of Philosophy.

Bent A. Christensen
Professor of Civil and Coastal Engineering

I certify that I have read this study and that in my opinion it conforms to acceptable standards of scholarly presentation and is fully adequate, in scope and quality, as a dissertation for the degree of Doctor of Philosophy.

George M. Griffin, Jr.
Professor of Geology

This dissertation was submitted to the Dean of the College of Engineering and to the Graduate Council, and was accepted as partial fulfillment of the requirements for the degree of Doctor of Philosophy.

March, 1973

Robert E Uhrig

Dean, College of Engineering

Dean, Graduate School